Optimisation of Racing Car Suspensions featuring Inerters

by

Jose Daniel Pardo Barcelo

The Department of Mechanical Engineering and Mathematical Sciences

Oxford Brookes University

A thesis submitted in partial fulfilment of the requirements of

Oxford Brookes University for the degree of

Doctor of Philosophy

November 2012

Acknowledgements

The research stage towards earning this PhD degree has been one of the most intellectually inspiring experiences of my life. It has allowed me to grow as a person and as an engineer. I would like to take this opportunity to thank the people who have helped me to get to the finish line. First, I would like to thank my Director of Studies, Dr. James Balkwill, who has played a key role in my success as a doctoral candidate. I am grateful for your support and guidance throughout my PhD.

I would also like to thank the members of my supervisory committee: Dr. Denise Morrey and Nick Bowler. I would like to give a very special thanks to Dr. Denise Morrey for your invaluable help and active support in preparing and writing this thesis. Without your help, insight, and guidance this work would not have been possible. I am thankful to Nick Bowler for your feedback in the development of a lap-time simulator. I would also like to show my deep appreciation to my research Tutors, Dr. Khaled Hayatleh and Dr. Rob Beale.

I would also like to thank all the members of the OBU Workshop, Kieron, Warwick and Tony. I really appreciate all the effort and patience you put into having the test car built. I am thankful to John and Ian who always assisted me with the logistics involved in my research.

To my fellow members of the MEMS Research Team: Luke Bennett, Tulay Ibicek, Marco Cecotti, David Rodrigues and Dr. Nikos Vrellos. I would like to say thank you for all the good moments we had together. I will always remember the important role you played in this journey.

At this point, I would like to thank all of my close friends here: Santi, Dioni, Broja, Esteban, Marte, Carlos Bravo, Silvia. Guys, you have always given me a huge moral support. You always stood by my side in times of need and you celebrated my success.

Last but certainly not least, I would like to give an enormous “Thank you” to my parents, Pepe and Africa, my brother, Nacho, and my Italian family, Nicola, Eliana, Simo. Even if we are miles away, I always received your love and support as if you were next to me. Finally, I would like to give a huge “Thank you” and a very big kiss to my girlfriend, Veronica. We started this journey together and you have always given me the strength, support and love I needed to complete it. We made it!

Abstract

Racing car suspensions are a critical system in the overall performance of the vehicle. They must be able to accurately control ride dynamics as well as influencing the handling characteristics of the vehicle and providing stability under the action of external forces.

This work is a research study on the design and optimisation of high performance vehicle suspensions using inerters. The starting point is a theoretical investigation of the dynamics of a system fitted with an ideal inerter. This sets the foundation for developing a more complex and novel vehicle suspension model incorporating real inerters. The accuracy and predictability of this model has been assessed and validated against experimental data from 4-post rig testing.

In order to maximise overall vehicle performance, a race car suspension must meet a large number of conflicting objectives. Hence, suspension design and optimisation is a complex task where a compromised solution among a set of objectives needs to be adopted. The first task in this process is to define a set of performance based objective functions. The approach taken was to relate the ride dynamic behaviour of the suspension to the overall performance of the race car. The second task of the optimisation process is to develop an efficient and robust optimisation methodology. To address this, a multi-stage optimisation algorithm has been developed. The algorithm is based on two stages, a hybrid surrogate model based multi-objective evolutionary algorithm to obtain a set of non-dominated optimal suspension solutions and a transient lap-time simulation tool to incorporate external factors to the decision process and provide a final optimal solution.

A transient lap-time simulation tool has been developed. The minimum time manoeuvring problem has been defined as an Optimal Control problem. A novel solution method based on a multi-level algorithm and a closed-loop driver steering control has been proposed to find the optimal lap time.

The results obtained suggest that performance gains can be obtained by incorporating inerters into the suspension system. The work suggests that the use of inerters provides the car with an optimised aerodynamic platform and the overall stability of the vehicle is improved.

Nomenclature

OBU – Oxford Brookes University

FE – Finite Element

F1 – Formula One

FiA – *Fédération Internationale de l'Automobile*

PMEM – Permanent Magnet Electric Motor

CAD – Computer-Aided Design

ANN – Artificial Neural Network

CFD – Computational Fluid Dynamics

MIMO – Multiple Input, Multiple Output

3D – Three Dimensional

2D – Two Dimensional

EOM – Equations of Motion

CPU – Central Processing Unit

MOO – Multi-Objective Optimization

MOOP – Multi-Objective Optimization Problem

SQP – Sequential Quadratic Programming

LMI – Linear Matrix Inequality

LMIP – Linear Matrix Inequality Problem

EA – Evolutionary Algorithm

MOEA – Multi-Objective Evolutionary Algorithm

GA – Genetic Algorithm

PSA – Pattern Search Algorithm

NSGA-II – Fast Non-Dominated Sorting Genetic Algorithm

DOF – Degree of Freedom

SDOF – Single-Degree-Of-Freedom

n-DOF – n-Degree-Of-Freedom

DACE – Design and Analysis of Computer Experiments

DoE – Design of Experiments

OA – Orthogonal Array

LHS – Latin Hypercube Sampling

PR – Polynomial Regression

KRG – Kriging model

RBF – Radial Basis Functions

MAE – Maximum Absolute Error

AAE – Average Absolute Error

RMSE – Root Mean Square Error

HBVP – Hamiltonian Boundary-Value Problem

MBD – Multi-Body Dynamics

IR – Installation Ratio

CPV – Constant Peak Velocity

FRF – Frequency Response Function

SISO – Single-Input, Single-Output

LSB – Low-Speed Bump

HSB – High-Speed Bump

LSR – Low-Speed Rebound

HSR – High-Speed Rebound

FWM – Flywheel Mount

LTS – Lap-time Simulation

QSS – Quasi Steady-State

OC – Optimal Control

RHC – Receding Horizon Control

MPC – Model Predictive Control

RWD – Rear Wheel Drive

CoG – Centre of Gravity

MTM – Minimum Time Manoeuvring

MLOA – Multilevel Optimisation Algorithm

IWN – Integrated White Noise

List of Figures

List of Tables

Table of Contents

1. Introduction

1.1. Introduction

Racing cars are complex systems whose ultimate performance depends on the design and optimisation of several interacting subsystems such as the chassis, powertrain, bodywork, electronics, steering, suspensions and tyres. This research work focuses on the design and optimisation of one these systems: the vehicle suspension system. Race car suspensions are a critical system in the overall performance of the vehicle. They must be able to accurately control ride dynamics as well as influence the handling characteristics of the vehicle and provide stability under the action of external forces.

Different suspension layouts and technologies have been used over the years in order to improve the capabilities of a racing car suspension. With the development of electronic technology and the use of complex controls methods, fully active suspensions systems for racing applications were successfully developed in the early 1990s. The use of active systems led to important performance gains over conventional passive systems. A clear example of this success was the Williams FW14 and FW14B Formula 1 cars (see Figure 1-1).

Figure 1-1: 1992 FW14B Williams Formula 1 car equipped with fully active suspension

However, these types of suspensions were banned in most of the racing series due to the increasing safety concerns of the corresponding governing bodies. The need for improved suspension capabilities without the use of electronic aids has led to a recent development in

passive suspension technology. Dr. Malcolm C. Smith (2002) introduced a new passive mechanical device that could have potential performance benefits in passive vehicle suspensions, called an inertial damper, or as it is most commonly known nowadays, an inerter. An ideal inerter was defined as a massless linear two-terminal, one-port device in which the force applied to the terminals is proportional to the relative acceleration between these terminals (Smith, 2002). The first physical prototype inerter reported in literature was created at Cambridge University (Figure 1-2).

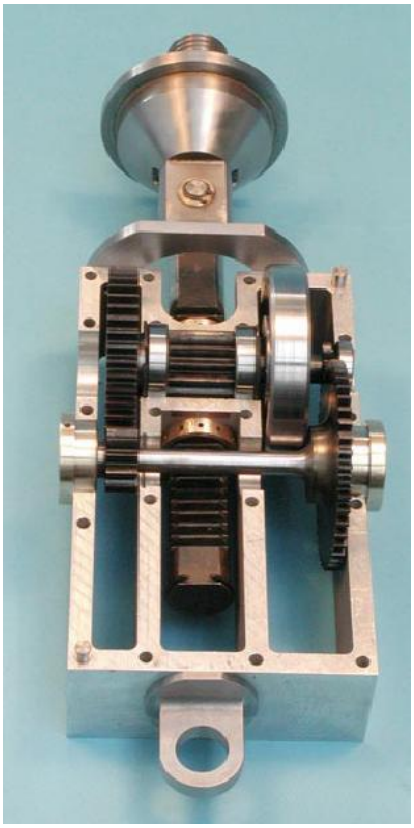

Figure 1-2: Prototype inerter designed at Cambridge University (Smith, 2003)

According to this work (Smith, 2002), inerters could be used to create suspension layouts that could potentially provide enhanced suspension capabilities. In theoretical work presented in literature (Smith & Wang, 2004), the introduction of inerters into the suspension required all suspension components to be tuned appropriately if performance benefits are to be obtained.

Moreover, in order to design a winning race car, all of the systems must be designed to maximise the performance of the vehicle. In the particular case of the suspension system, the main functions or goals that a racing car suspension must achieve in order to optimise vehicle performance are:

- To keep the tyres in contact with race track.
- To resist the chassis motions induced by external forces (inertial and aerodynamic forces).
- To control the handling characteristics of the vehicle in dynamic situations.

All these suspension objective functions need to be optimised simultaneously if race car performance is to be maximised. Multi-objective optimisation algorithms allow designers to find optimal suspension solutions considering all of the defined objective functions simultaneously. However, the fact that some objectives may conflict with each other prevents from obtaining a unique optimal solution. Instead of this, a trade-off or compromise solutions are often obtained. This means that if a unique optimal suspension is to be obtained, additional information is required in order to transform the underdetermined suspension optimisation problem into a determined one. No reported literature has been found that investigates objective methods of acquiring, managing and utilising this additional information in order to provide a final optimised suspension solution.

Several tools are nowadays available to engineers in order to design and analyse racing cars in a virtual environment. Among the different virtual tools (CAD/CAM, CFD, FEA, etc.) available to race teams and car manufacturers, lap time simulators are powerful tools for the analysis of the performance of a race car. Lap-time simulation tools allow users to evaluate the impact that certain design parameters may have on the overall performance of a race car and quantify the performance gains obtained from varying those parameters. Most of the work related to lap-time simulators found in literature neglects the impact of suspension components in the behaviour of the racing car. This is often due to the high computational requirements associated with the simulation of a fully dynamic race car model. Moreover, no reported literature investigates the interaction of suspension ride dynamics with the optimisation of vehicle performance.

1.2. Aims of the Research

The overall aim of the research work is to develop a novel method to determine an optimised Grand Prix racing car suspension featuring inerters through the use of optimisation algorithms and a vehicle model validated against data obtained from experimental testing.

This objective will include a number of tasks which are to:

- Carry out a critical review of the published material with regard to inerters, suspension design, modelling and optimisation, vehicle experimental testing methods and lap time simulation.
- Investigate and characterise the effects of ideal inerters in mechanical vibratory systems.
- Develop and validate experimentally a novel race car suspension model incorporating real inerters.
- Extend the suspension parameter estimation method in order to identify the parameters of suspensions fitted with inerters.
- Develop a novel transient lap time simulation tool.
- Investigate the effects of suspension parameters in the overall performance of the race car and define representative performance based objective functions.
- Develop a robust and efficient optimisation methodology based on hybrid multi-objective evolutionary algorithms, surrogate modelling and lap-time simulation.

1.3. Thesis Outline

This thesis has been organised into 8 chapters, the first of which presents an introduction of the work carried out and outlines the overall aim and objectives of this research thesis. The rest of chapters are organised as follows.

Chapter 2 focuses on the review of relevant literature related to design, analysis and applications of inerters; ride dynamic analysis; methods for experimental suspension design and testing; development and application of multi-objective optimisation algorithms and development of transient lap-time simulation tools.

Chapter 3 presents a theoretical study of ideal inerters in simple vibratory systems. In this investigation, the effect of ideal inerters in simple vibratory systems has been characterised. A single degree-of-freedom (SDOF) system featuring inerters has been analysed under un-damped and damped conditions. Analytical expressions that represent the dynamic behaviour of the system have been proposed for both cases. Dynamic behaviour of both systems under forced excitation has been studied in the frequency domain. The transient response of the damped system has been analysed in the time domain. An extended transient analysis has been carried out in the damped case. The conclusions drawn from this theoretical study have been used as the foundation for the analysis of more complex vehicle suspension models featuring real inerters.

Chapter 4 is devoted to the design and description of the experimental apparatus. The first part of this chapter describes design process required to produce an experimental test car featuring physical inerters. This process includes the specification of design requirements, concept design of different alternatives, final design selection and detailed design. Furthermore, the experimental testing facilities involved in this research have been described and the calibration and data acquisition procedure has been explained. In the last part of chapter 4, the current method for estimating suspension parameter from experimental data developed by a fellow research student has been explained and extensions in order to account for real inerters and other nonlinear effects have been proposed.

In chapter 5, an experimentally validated vehicle model for vertical dynamics has been developed. The chapter presents a study of suitability of different dynamic modelling commercial packages. Moreover, model complexity has been analysed with respect to the requirements of the present thesis. In this chapter, a novel experimentally validated vehicle

suspension model that includes a real inerter and a nonlinear vertical tyre model has been developed and accuracy has been discussed.

Chapter 6 is dedicated to the development of a transient lap time simulation tool. In this chapter, the problem of lap time minimisation has been stated as a minimum time manoeuvring (MTM) Optimal Control problem. A novel solution methodology based on multi-level optimisation and a closed-loop steering control has been developed and discussed. Furthermore, a vehicle model that includes the validated suspension model developed in Chapter 5 has been constructed. Equations of motion of this vehicle have been derived using the Lagrange Energy Method. The last section of chapter 6 presents a case study that analyses the performance of the solution method in finding the minimum lap time.

Chapter 7 is devoted to the development of a suspension optimisation method. The suspension optimisation problem has been defined as a multi-objective optimisation problem (MOOP). A set of novel performance based suspension objective functions has been developed. A novel optimisation methodology has been developed in order to obtain an optimal suspension configuration including inerters. The optimisation methodology has been based on surrogate model based hybrid multi-objective optimisation, as the main search engine, and the lap-time simulator developed in Chapter 6 as final decision maker. In the last section of the chapter, the optimisation method has been applied to obtain an optimal suspension configuration for a conventional suspension and a suspension featuring inerters. Results for both case studies have been discussed and the impact of inerters in the performance of a racing car has been analysed.

In chapter 8, a summary of the major conclusions drawn from this research work has been presented followed by the proposition of potential recommendations for future work in this research area.

2. Literature Review

2.1. Introduction

Chapter 2 presents a comprehensive review of the literature related to the present research project. Relevant work undertaken in the field of suspension design and optimisation has been reviewed and discussed in order to set a foundation of knowledge in the subject and to formulate the scope of the present research work.

First, a historical background of race car suspensions has been presented. Evolution from the tyre/chassis era to aerodynamics dominance is discussed. The introduction of active suspensions, their advantages with respect to conventional suspension systems and their subsequent ban are briefly reviewed.

Inerter technology is introduced as an alternative to regain the loss of suspension performance due to the ban of active systems. The concept of the inerter is introduced and its potential applications are discussed. Previous work in the field of suspension design with inerters is analysed. Furthermore, the design and experimental testing of physical inerters and their impact in vehicle suspension performance is reviewed.

Discussions on experimental testing and suspension simulation are also introduced. The use of test facilities in order to analyse the dynamics of a suspension, to estimate dynamic parameters and to optimise suspension settings is presented and discussed. Moreover, different suspension models in simulation are introduced. The utility of these models in suspension design and optimisation is presented.

Section 2.6 focuses on optimisation algorithms. The key factors of a successful suspension optimisation process are presented. First, a review of previous studies related to the definition of objective functions used for race car suspension optimisation is carried out. Moreover, a review of optimisation algorithms for complex problems as well as techniques for enhanced efficiency and robustness is discussed.

Finally, the last section of this chapter is dedicated to lap-time simulation technology. The basic strategies for lap-time simulation are reviewed. Critical review of previous published material with regard to the development of the solution methods of the time optimal control

problem and the development of vehicle models is carried out. Different methods for solving Optimal Control problems are discussed.

2.2. Race Car Suspension Historical Background

The main goal in motor racing is to design a vehicle that is able to complete a race track in the quickest time possible (Milliken & Milliken, 1995). In order to maximize performance, racing cars must be designed so that maximum longitudinal and lateral forces can be generated from tyre contact patches without exceeding the road-holding capabilities of the vehicle. Since the only intended linkage between tyres and chassis is the suspension, its design and optimisation plays an important role in determining the maximum available grip at any point on the race track. Moreover, race car suspensions control chassis motions and weight transfer and provide stability and feedback from the track to the driver. The design of a race car suspension must account for all these factors, making the task of suspension optimisation highly complex.

The introduction of aerodynamics into motor racing offered improved vehicle performance capabilities, especially after the introduction of ground effects in the late 1970s (Wright, 1982). As downforce induced by aerodynamics increases normal load on the tyres, higher cornering and braking forces can be generated by the tyres (Dominy & Dominy, 1984). However, race car aerodynamics is highly sensitive to changes in ride height and pitch attitude (Floyd & Law, 1994). This affects the suspension design process, since designers not only need to optimise suspensions for optimal tyre/chassis interaction but also for optimal aerodynamic performance.

In order to optimise suspension performance, during the 1980s and early 1990s advanced electronic technology was introduced into race car suspension design. Semi-active suspensions (Dominy & Bullman, 1995) and fully-active suspensions (Purdy & Bullman, 1997) were developed in Grand Prix race cars offering remarkable enhanced capabilities with respect to passive system (Sharp, et al., 1987). However, in 1994 FiA (governing body) decided to ban the use of active suspension in motor racing due to the economic costs involved in the design of this technology and safety concerns derived from the alarming corner speeds that race cars were reaching.

Ever since the ban of active suspension technology, suspension designers have focused on the research and development of advanced passive suspension technologies that could help to

regain lost performance with respect to active suspension. An example of this is the Tuned Mass Damper system used by Renault F1 Team during 2005 season. The system operated as a vibrator absorber, so that vibrations at the tyre mode could be absorbed. This provided a stable front platform for braking. In 2006, this system was deemed illegal by the governing body.

2.3. Inerter Technology

In (Smith, 2002), the concept of inertial damper (or abbreviated inerter) was introduced. Smith defined an ideal inerter as a "mechanical two terminal, one port device with the property that the equal and opposite force applied at the nodes is proportional to the relative acceleration between the nodes". The behaviour of an ideal inerter can be represented by equation (2.1):

$$F = b \cdot (a_2 - a_1) \tag{2.1}$$

Where b represents the inertance and is expressed in kg in SI units; a_1 and a_2 represent the acceleration of the inerter terminals; and F represents the force created by an ideal inerter.

This publication claims that the concept of an inerter could be used to complete the classical mechanical – electrical analogy. In this classical analogy, the main components that integrate a network are variables and ports. For an ideal translational mechanical system, the main variables are force and velocity. Force equates to electrical current and translational velocity equates to electrical voltage. Ports can be defined as "a pair of nodes (or terminals) in a mechanical system to which an equal and opposite force is applied and which experience a relative velocity" (Smith, 2002). The main ports for mechanical systems are springs, dampers and masses. In this classical analogy, springs equate to inductors, dampers to resistors and masses to grounded capacitors (upper diagram in Figure 2-1). This classical analogy was restricted in its realization since no mechanical element could represent a true two-terminal capacitor. However, inerters can replace masses in the analogy since these ports represent true two- terminal capacitors (lower diagram in Figure 2-1). In this revised analogy, a mass port could be considered as a special case of inerter in which one of the terminals is grounded. Moreover, the most important implication of this new mechanical-electrical analogy resides in the fact that all network synthesis and analysis techniques developed for decades in Electrical Engineering could be theoretically applied without any restrictions.

Figure 2-1: Mechanical – Electrical analogy: Classical (upper) and Revised with inerter (lower) (Smith, 2002)

Three applications were proposed by Smith (2002): an alternative to classical vibrator absorbers without the need for additional tuned masses; the design of strut suspensions using a classical electrical network synthesis approach; and the use of inerters to create simulated masses in experimental studies. Furthermore, the concept of the inerter soon gained the attention of the research community. Potential applications of the inerter idea were exploited, especially in the field of suspension design and optimisation, where the inerter concept arose as a solution to regain the loss of suspension performance caused by the ban of active suspensions in the Motorsport industry.

2.3.1. Physical realisation of Inerters

Several physical inerter configurations have been reported in the literature over the years. Although the inerter concept was first introduced by Smith in 2002, there are a number of US

patents that reveal the development of mechanical inerters. The design of the first physical inerter dates back to the beginning of 20th Century (Watres, 1908). Although, the mechanism presented in this patent was not named as an inerter at that time, the working principle and construction corresponds nowadays to what we now understand as an inerter. The aim of this device was to provide a shock absorbing action in early automotive carriages. Several modifications of this early inerter design were made in the coming years. King (1912) developed a ballscrew mechanism coupled with an internal spring in order to provide suspension effects between the carriage and the axle. Tauscher (1928) conceived a double-spring ballscrew inerter mechanism to absorb shocks in a rear axle motor vehicle suspension. A variant of this early spring-inerter mechanism was also applied to absorb vibrations in door spring hinges (Seqveland, 1933). More complex designs were subsequently developed in following years (Bleakney, et al., 1949; Gies & Rumsey, 1962). Those mechanisms were intended to control the vibrations produced in aircraft wings and other truss structures.

The first design patent that refers to what we now understand as an inerter dates from 2009 (Wang, et al., 2009). Different variants of a ballscrew inerter were proposed. An alternative to the ballscrew inerter, Smith (2002) was on a rack-and-pinion mechanism. In both designs, the working principle is very similar: the relative translational movement between terminals is transformed by some means (ballscrew or rack-and-pinion mechanism) into a rotational movement in a flywheel. With the ballscrew design solution, the inertance is characterised by inertia of the flywheel and the lead of the screw whereas, with the rack-and-pinion solution, the inertance characteristic depends on inertia of the flywheel and gear ratio between rack and pinion. A slightly different approach was proposed by Wang *et al.* (2011). In this design, fluid inside a hydraulic system is used to generate differential pressures in a hydraulic motor which, at the same time, induces a rotational acceleration in a flywheel. Results of experimental testing of the hydraulic inerter show significant deviations from theoretical ideal inerter behaviour. A more complex configuration was developed by Wang and Chan (2008). In this work, a semi-active inerter is developed as a Permanent Magnet Electric Motor (PMEM) is coupled with a passive mechanical ballscrew inerter. Wang suggested that virtually any mechanical network could be synthesized with the use of mechatronic inerters.

2.3.2. Inerter Technology applied to Vehicle Suspension Dynamics

Shortly after his first publication, Smith (2003) focused his attention on the application of inerters into vehicle suspensions as an alternative to active suspensions. The article focused

on the realization of passive mechanical networks to obtain optimised suspension configurations. Moreover, in a research paper published by Smith and Wang (2004), an extensive theoretical investigation was carried out in order to study the potential benefits of inerters in vehicle suspensions. Several suspension layouts incorporating inerters were proposed and suspension parameters were optimised with respect to some prescribed objective functions. The study was carried out for a quarter-car vehicle model and for a full car vehicle model. In both studies, experimental data for a real inerter was briefly presented but no actual validated vehicle models were developed.

Papageorgiou and Smith (2005) were the first to publish research work related to experimental testing of inerters. In this work, experimental rack-and-pinion and ballscrew inerters were designed and tested on a rig test facility. Experimental data was provided but no real inerter model is obtained. Wang and Su (2008) presented an extension of previous experimental work done in the field. Using the same inerter device, a validated nonlinear inerter model was proposed. The experiments carried out in these articles, analyse the inerter in isolation. Results showed that the model provided a good agreement between simulation and experimental data. This nonlinear inerter model was then used to optimise a theoretical quarter-car vehicle suspension model. The effects of inerter nonlinearities in suspension performance were analysed. Results of this analysis showed that, according to the objective functions defined by the authors, nonlinearities reduced the efficiency of the inerter in suspension optimisation.

2.3.3. Inerter Technology applied to other Engineering fields

The inerter concept has been also applied to other engineering fields. Wang *et al.* (2006) studied the application of inerters in train suspension systems in order to improve passenger comfort and train stability. Evangelou *et al.* (2007) carried out a theoretical study for the design of passive mechanical steering compensator for high performance motorcycles. Investigations showed that potential improved dynamic motorcycle responses in wobble and weave vibration modes could be obtained simultaneously with the use of inerters. Papageorgiou *et al.* (2007) extended this research work and proposed the design of an experimental passive mechanical steering compensator for motorcycle. The device was designed as a damper in series with an inerter and tested on a purpose-built test bench. A comprehensive nonlinear validated model was obtained from experimental testing. Inerter technology has also been studied in Structural Engineering. Several studies analysed the

potential improvement of building vibration isolation performance with inerters. Wang *et al.* (2007) carried out a theoretical optimisation using three different elastic foundations for different building structures. Performance gains were obtained by the use of inerters in all cases. Wang *et al.* (2010) extended previous research work. This work included an additional building foundation layout. Experimental testing was carried out in a purpose-built test bench but the behaviour of the real inerter was briefly discussed.

All experimental studies reported in literature are limited to the analysis of a real inerter device in isolation. There are no reported studies in the literature that suggest an integrated analysis of real inerters into vehicle suspensions. Several suspension models have been used in literature in order to study the potential benefits of inerters in vehicle suspensions. However, none of these models have been validated against suspension experimental data coming from four or seven post rig facilities.

2.4. Experimental Testing on Vehicle Suspensions

Experimental testing provides a method of tuning and analysing different suspension options according to specific objectives. The main ways a vehicle suspension can be tested are: track testing and laboratory rig testing.

Laboratory testing offers a much more cost-effective and controlled environment than physical testing on the track. The main aim of a suspension test rig is twofold: on one hand, rigs are used to apply fundamental inputs in order to characterise and estimate parameters; and, on the other hand, they use controlled actuators to recreate external dynamic actions applied to the vehicle suspension. Suspension test rigs can be classified according to the number of actuators used: quarter-car test rigs, four-post test rigs and seven-post test rigs are the most common ones, although eight-post test rigs have also been developed (Southward & Boggs, 2008).

Quarter-car test rigs are designed to study the fundamental dynamics of a suspension without the need of having a full vehicle or prototype present on the test. In these rigs, the sprung mass is limited to move only vertically relative to the reference frame, while the suspension and tyre coupling can be designed in different ways depending on the nature of the study carried out. Figure 2-2 shows an example of the quarter-car test rig used in Virginia Polytechnic Institute (Andersen, 2007).

Figure 2-2: Quarter-Car test rig (Andersen, 2007)

In this work, the test rig was used to develop and validate a nonlinear McPherson Strut suspension model. The same rig was also used by Ziegenmeyer (2007) to estimate the disturbance inputs of a quarter-car suspension model and to develop a real-time observer to the tyre coupled quarter-car suspension test rig. A similar quarter-car test rig was used by Boggs *et al.* (2008) in order to obtain suspension sensitivity information and to construct a validated quarter-car computer model. In this work, the rig was built to be as similar to a lumped 2DOF model as possible. Yildirim and Eski (2009) designed an experimental quarter-car rig test in order to study the performance of Artificial Neural Networks in the control of active suspensions. The rig was equipped with an experimental active suspension system and featured with a rotating tyre.

Multiple-post test rigs are experimental facilities that allow the simulation and recreation of external actions applied to the vehicle (*e.g.*, road inputs, inertial forces or aerodynamic forces) in a controlled and repeatable environment. Four-post test rigs are composed by four independently controlled servo-hydraulic actuators (one for each wheel) capable of recreating, to some extent, any road input a vehicle may experience under driving conditions. Inputs can be obtained from previously recorded actual track data or can be fundamental

mathematical functions (e.g. sine waves or step inputs). Measurement systems are fitted to the test vehicle so that dynamic characteristics of the vehicle, suspensions and tyres can be determined and suspension setup changes can be assessed and optimized (Kowalczyk, 2002; Cambiaghi, et al., 1998; Maher, 2011). Four-post rigs are often provided with additional non-controlled (one or two) pneumatic actuators. These actuators can only provide static forces that are normally used to set vehicle suspension within the normal operating range. As opposed to four-post rigs, seven-post rig facilities incorporate three additional controllable actuators connected to the chassis (conventionally referred to them as 'aeroloaders') that allow the combined analysis of road excitation with aerodynamic and inertial effects (Kelly, et al., 2002). Eight-post rigs are composed by four road excitation actuators and four 'aeroloaders'. These rigs offer the added capability of analysing the dynamic warp stiffness of the vehicle more accurately than seven-post rigs (Southward & Boggs, 2008). In general, more actuators offer added value to the tests performed. However, multi–post test rigs are multiple input/multiple output (MIMO) systems which require high levels of control (Fricke & Hogg, 2010). Hence, more actuators require the development of more complex control algorithms.

Examples of racing car suspension characterisation and optimisation in test rig facilities are very sparse in literature. Boggs *et al.* (2009) used experimental data from 7-post rig testing to produce an efficient vehicle parameter identification method. Miller (2002) tested a Formula SAE car on a 7-post rig in order to optimise anti-roll bar and damper settings. A case study of ChampCar damper optimisation was presented by Kowalczyk (2002). Results show that, when using multiple criteria for optimising a suspension, trade-off among objectives functions is obtained. However, no reported studies in literature investigate the use of a 4-post rig test facility to analyse vehicle suspensions incorporating real inerters.

2.5. Virtual Suspension Simulation

Vehicle suspension models are commonly used in dynamic analysis. They are powerful tools for virtual suspension design and optimisation. These models allow the analysis of the impact of different suspension settings on the performance of the vehicle in a cost and time efficient way (Soliman, et al., 2001; Rakheja & Ahmed, 1991; Barak, et al., 2004; Soliman, et al., 2008). Vehicle suspension models can also be used in optimisation in order to determine optimal suspension configurations with respect to some prescribed objective functions

(Metwalli, 1986; Alkhatib, et al., 2004; Georgiou, et al., 2007; Verros, et al., 2005; Kuo, et al., 2008).

While simple suspension models are useful for gaining a general understanding of the system, more comprehensive models are required for accurate description of suspension dynamic behaviour and for efficient suspension optimisation. The complexity of these models depends on the number of DOF considered and the design of the particular suspension components (e.g. passive, semi-active or fully active suspensions, design of nonlinearities or modelling of parasitic effects). The following sections review the most relevant vehicle suspension models that can be found in reported literature.

2.5.1. Modelling of vehicle equations of motion

The simplest suspension model is a single degree-of-freedom (SDOF) system. This simplistic system assumes that the vehicle can be modelled as a point mass that moves along the vertical axis and that the tyres can be modelled as an equivalent massless linear spring. The use of this type of model is very rare in suspension analysis due to its crude representation of the behaviour of the physical vehicle. Storey *et al.* (2006) used a SDOF model to investigate the performance of different active and semi-active suspension systems. Alkhatib *et al.* (2004) used a linear SDOF to obtain optimal spring and damper rates with the aid of a Genetic Algorithm (GA). A more complex model includes the effect of unsprung mass in the dynamic response of the vehicle. This is the so-called quarter-car vehicle model or 2-DOF vehicle model. The use of quarter-car models has been widely reported in literature due to its simplicity and yet its relative accuracy in simulating the main vibration modes of the vehicle (body and hub vibration modes). Several authors used quarter-car models in order to carry out suspension analysis (Rakheja & Ahmed, 1991; Soliman, et al., 2001; Jazar, et al., 2006), and suspension optimisation (Metwalli, 1986; Alkhatib, et al., 2004; Georgiou, et al., 2007; Verros, et al., 2005; Gobbi, et al., 2006; Chi, et al., 2008). The next step in vehicle suspension modelling complexity is the so-called half-car model. Half-car models are common in literature. These models assume that the main body (sprung mass) presents two predominant motions: a translational (vertical) motion as well as a rotation around either roll or pitch axis. Sun *et al.* (2002) used a 4-DOF system to represent a half-car vehicle model. In this work, the model was used to analyse the effect of suspension parameters on the transient response of the vehicle. Soliman *et al.* (2008) used half-car models in roll and pitch planes in order to analyse the impact of the main suspension parameters in the dynamic response of the vehicle.

Extended half-car models that consider aerodynamic effects have been developed in order to analyse the interaction between aerodynamics and ride dynamics (Floyd & Law, 1994; Abdelhady, 2002). Kuo *et al.* (2008) and Sun and Chen (2003) used a half-car 4-DOF model in order to perform suspension optimisation. An improvement of the previous model is the extension to 7DOF suspension models. These models allow the simulation of the vertical ride dynamics of a full car as well as all the rotational modes simultaneously (pitch, roll and warp). Barak *et al.* (2004) developed a full-car vehicle model in order to analyse the dynamic behaviour of a full suspension. Abdelhady and Crolla (1989) used a 7-DOF vehicle model in order to investigate the theoretical performance benefits of active suspensions with respect to passive systems. In *Wang et al.* (2006), Shannan and Vanderploeg (1989) and Lu and DePoyster (2002), full-car vehicle models were also developed to study the performance of active suspensions in combined ride and handling manoeuvres. More complex models are less frequent in suspension modelling literature. These complex models often incorporate additional degrees of freedom in order to improve accuracy and reliability. Shirahatt *et al.* (2008) and Del Castillo *et al.* (1990) produced vehicle models with an additional DOF for the vertical movement of a driver. Graf and Kosuch (2008) introduced an extended full-car model. This model presented an additional DOF which accounts for compliance in the chassis. The chassis was modelled as two rigid bodies connected by a torsional spring.

2.5.2. Modelling of individual suspension components

Suspension model complexity also depends on the details with which suspension features are modelled. Many studies in literature model a suspension as a linear combination of a spring in parallel with a damper (and an additional force in the case of active suspensions) regardless of whether these components present linear or nonlinear characteristics. (Deshpande, et al., 2006) modelled a secondary suspension system coupled to the main suspension system to investigate the effect of jump avoidance. In (Stamatov, et al., 2007), parasitic effects were modelled as part of the suspension strut. Elastic compliance due to bushings and damper friction effects are also included in this model. Other models include suspension kinematics in the dynamic model (Balike, 2010; Andersen, 2007; Al-Holou, et al., 2002). In the past few years, different vehicle suspension models featuring inerters have also been proposed in order to evaluate the potential benefits of inerters in suspension optimisation (Smith & Wang, 2004; Scheibe & Smith, 2009). However, these vehicle suspension models were proposed from a theoretical point of view but they were never validated against experimental data. No reported works that validate vehicle suspension

models incorporating inerters against experimental suspension data have been found in literature.

In addition to suspension components, tyres must also be modeled. Captain *et al.* (1979) presented four different vertical tyre models. In this study, guidelines for the selection of the most suitable tyre model were provided. However, over the years, most of vertical suspension models reported in literature consider a linear single contact point tyre model. In its most basic configuration, this tyre can be modeled as a linear spring that represents the flexibility characteristic of a tyre (Williams & Haddad, 1997; Williams, 1997; Sharp, et al., 1987). This model can be extended in order to account for tyre energy dissipation effects. This term is commonly modeled as a damping effect (Akcay & Turkay, 2009; Graf & Kosuch, 2008). Although this tyre model is widespread in the field of Suspension Dynamics due to its simplicity, no reported literature has been found that correlates this model against experimental data. A more complex nonlinear semi-empirical vertical tyre model was developed by Pacjeka (2006). Experimental data obtained from tyre rig testing was used to create this semi-empirical model. However, the main drawback of this model is that it requires the tyre to be tested experimentally to be able to integrate the model into simulation. No reported studies that use this vertical tyre model for suspension simulation have been found.

2.6. Suspension Optimisation

Suspension optimisation has been a topic of growing interest for research in the last decades. The development of suspension models allows the use of different optimisation algorithms to search through the design space for an optimal suspension setting according to some predefined objective functions in a robust and efficient way (Gobbi, et al., 1999; Chi, et al., 2008; Shirahatt, et al., 2008; Verros, et al., 2005). In current motor racing, where cost reduction is of paramount concern, computer algorithms can be quite useful for efficient suspension design and optimisation. The use of virtual optimisation tools reduces the time of track testing and provides a better understanding of the vehicle suspension. The ultimate goal of this optimisation process is to obtain a suspension setting that optimises the overall performance of the car. In mathematical terms, a general minimisation problem can be expressed as follows (Antoniou & Lu, 2007):

$$\begin{cases} Given\ a\ funtion\ f: \boldsymbol{S} \rightarrow \mathbb{R} \\ Find\ a\ solution\ \boldsymbol{x_0}\ in\ \boldsymbol{S}\ so\ that\ f(\boldsymbol{x_0}) \leq f(\boldsymbol{x})\ for\ all\ \boldsymbol{x}\ in\ \boldsymbol{S} \end{cases} \tag{2.2}$$

Where *S* represents a set of tunable parameters (or "search space") and *f* represents the function to be minimised (or "cost function").

According to this definition, the success in achieving this goal depends largely on two key factors:

- Selection of objective functions *f*.
- Development of a robust and efficient optimisation methodology.

A review of the literature is provided in the following sections with regard to the selection of objective function for suspension optimisation and the development of a suspension optimisation method.

2.6.1. Performance Objective Functions for Suspension Systems

The selection of these objective functions is a paramount concern in suspension design and optimisation. As expressed in eq. (2.2), the outcome of an optimisation problem is a set of parameters S that minimises the value of an objective function *f*. Hence, objective functions must be chosen so that they accurately represent the goals a suspension designer is trying to achieve. Furthermore, the performance of an optimisation algorithm depends largely on the configuration of the cost function, i.e. cost functions must be created in such a way that the optimiser can efficiently extract useful information from them to continue with the search. Most of the work found in literature is related to the definition of objective indexes for production car suspension optimisation (Sharp, et al., 1987; Georgiou, et al., 2007; Gobbi, et al., 2006; Li & Kuo, 2000).

In suspension analysis, vehicle comfort is commonly defined as the amount of vertical acceleration transmitted from road to the sprung mass and ultimately, to the driver and passengers. The most common mathematical function selected to express comfort is root-mean-square (RMS) due to the intrinsic continuity and differentiability of this mathematical function. (Jazar, et al., 2006; Hegazy & Sandy, 2009; Sun & Chen, 2003; Gobbi, et al., 2006; Georgiou, et al., 2007; Sun, et al., 2010; Thompson, 1973). A more complex comfort index was introduced by Johnson *et al.* (2010). In this research work, different objective functions were presented and their performance was discussed.

Vehicle safety is defined as tyre/road holding. It is well reported that the fluctuations in vertical loads applied to the tyres influence strongly their ability to produce longitudinal and

lateral forces (Gillespie, 1992; Milliken & Milliken, 1995; Pacjeka, 2006). Thus, reduction of tyre load fluctuations can then provide a more robust and closely controlled vehicle response. As with ride comfort index, the function chosen in literature to express vehicle safety (or control) is the RMS of the dynamic tyre load fluctuation (Verros, et al., 2005; Georgiou, et al., 2007; Cooke, et al., 1997; Thompson, 1983).

Rattle space or suspension working space has also been considered as an objective function in road car suspension optimisation. Suspension travel defines vehicle suspension packaging, suspension kinematics characteristics and suspended body minimum ride heights, so controlling its magnitude is important for suspension design. An RMS of suspension stroke is used as well (Verros, et al., 2005; Molina-Cristobal, et al., 2007; Georgiou & Natsiavas, 2009).

All these suspension objectives focus on the ride performance of the vehicle, and little attention is paid to the effects of suspension on the handling characteristics of the vehicle. Moreover, given the competitive nature of motorsport industry, objective functions related to vehicle performance rarely enter the public domain. It was demonstrated that the control of suspension parameters have an important effect on handling characteristics (Wang, et al., 2006; Cooke, et al., 1997; Shim & Margolis, 2005; Blank & Margolis, 1996; Miura, et al., 2004). Only a few studies are found to measure handling as well as ride functions (Gobbi, et al., 1999; Benedetti, et al., 2006). However, in these studies, the handling functions were limited to prescribed manoeuvres, and the direct relationship between suspension parameters and the impact of suspension dynamics on overall vehicle performance was not discussed. Moreover, these suspension cost functions have been mostly developed from quarter-car studies, where only vertical motion is considered. Very little literature can be found on the definition of objective functions accounting for rotational vibration modes as well as translational (vertical) modes. Most of these studies proposed a sum of the weighted terms where weighting terms were selected arbitrarily (Hrovat, 1997). Furthermore, these indices have been mainly applied to studies for production road cars that operate well inside the limits of adhesion. However, in motor racing, race cars are constantly operating at the limits of tyre adhesion. In this situation, handling characteristics are highly coupled with ride performance of the suspension (Mashadi & Crolla, 2005). In this study, it was demonstrated that the understeer characteristics of a vehicle at relatively high lateral accelerations (~ 1g) can vary sharply due to the effect of suspension dynamics. However, this study did not propose objective functions to deal with this behaviour. Blank and Margolis (1996) proposed

functions that related lateral and vertical dynamics for a quarter-car model but no relationship to overall vehicle performance was discussed. In current Formula 1 (F1) cars, aerodynamics is a key factor in the overall performance of the vehicle. There are studies in literature that highlighted the coupling between aerodynamics and suspension dynamics (Floyd & Law, 1994; Aschwanden, et al., 2006; Aschwanden, et al., 2008). However, none of these studies developed objectives functions for suspension optimisation accounting for aerodynamic performance. Moreover, there are no reported studies in literature that investigate the effect of coupled ride and handling dynamics on the overall performance of a race car through lap-time simulation (LTS) or physical track testing.

2.6.2. Multi-objective Optimisation Algorithm

Suspension systems are a critical part of a racing vehicle because they are the only physical linkage between tyres and chassis. Moreover, from a purely dynamic point of view, the main goals of a vehicle suspension are (Gillespie, 1992):

- To keep the tyres in contact with race track.
- To resist chassis motions induced by external forces (inertial and aerodynamic forces).
- To control the weight balance across all four tyres under dynamic situations.

In order to achieve these goals and therefore maximise vehicle performance, suspension design must be translated into an optimisation problem (see equation (2.2)). A vast variety of general mathematical optimisation algorithms is available in literature (Venkatamaran, 2002; Antoniou & Lu, 2007; Weise, 2011). In this section, only the most relevant algorithms applied to suspension design and optimisation have been reviewed.

Many reported studies dealing with suspension optimisation can be found in literature. Thoresson *et al.* (2009) and (2009b) successfully applied a Dynamic-Q gradient-based algorithm to single-objective suspension optimisation problem. Els *et al.* (2006) compared the performance of two gradient-based single-objective optimisation methods: a Sequential Quadratic Programming (SQP) and a Dynamic-Q method. The study suggested that the SQP method was more efficient and robust. Chi *et al.* (2008) ran a comparative study of three optimisation algorithms: Evolutionary Algorithm (EA), Pattern Search Algorithm (PSA) and Sequential Quadratic Program (SQP). Results showed that gradient-based algorithms provided strong and efficient local convergence. The number of function evaluations was

lower, therefore making them very computationally efficient. However, these methods required gradient and Hessian information of the objective function, which could be either provided by the user or sorted by the software itself using finite differences approximation method, meaning that this approach would be poor when dealing with systems with discontinuities, nonlinearities or discrete functions. Furthermore, gradient-based approaches do not guarantee to find the global optimum of the problem. Alternatively, non gradient-based algorithms such as EAs and PSA use meta-heuristic methods for searching optimal solutions through the design space. Optimal solutions are evolved from generation to generation in a stochastic, discrete and nonlinear process (Man, et al., 1996). No gradient information is required so they are more powerful in finding a near global optimum. However, EAs present some disadvantages with respect to local gradient-based search techniques: due to the population based search approach of EAs, the optimisation process is computationally expensive and simulation times are often high. Another drawback is that the efficiency and the reliability of the algorithm depend largely on the parameters used to set the optimisation problem (e.g. population size, crossover probability, mutation probability, percentage of elistist individuals). Baumal *et al*. (1998) used a single-objective Genetic Algorithm (GA) in order to optimise ride comfort with an active suspension. Li and Kuo (2000) successfully applied an EA to single-objective passive suspension optimisation. A different optimisation approach was proposed by Sun and Chen (2003) and Papageorgiou and Smith (2006). In this approach, linear matrix inequalities (LMIs) were used to synthesise optimised suspension layouts.

All previous studies considered the optimisation of a single suspension objective function. However, as mentioned at the beginning of the section, optimal suspension design requires the optimisation of several objective functions simultaneously. Therefore, the suspension optimisation problem must be considered as a general multi-objective optimisation problem (MOOP). A general MOOP can be mathematically expressed as follows (Deb, 2001):

$$\begin{aligned} \min \quad & F(\boldsymbol{x}) = \{f_1(\boldsymbol{x}), f_2(\boldsymbol{x}), \dots, f_m(\boldsymbol{x})\} \\ subjected\ to \quad & G(\boldsymbol{x}) = \{g_1(\boldsymbol{x}), g_2(\boldsymbol{x}), \dots, g_j(\boldsymbol{x})\} \geq 0 \\ & H(\boldsymbol{x}) = \{h_1(\boldsymbol{x}), h_2(\boldsymbol{x}), \dots, h_k(\boldsymbol{x})\} = 0 \\ & x_{iL} \leq x_i \leq x_{iU} \quad , \quad i = 1, \dots, n \end{aligned} \tag{2.3}$$

Where $\boldsymbol{x}=\{x_1, x_2, \ldots, x_n\}$ is the vector of n decision variables

$F(x)$ is the vector of m objective functions

$G(x)$ is the vector of j inequality constraints

$H(x)$ is the vector of k equality constraints

x_{iL}, x_{iU} are the limits of the search space for the *i-th* decision variable

Traditional gradient-based optimisation techniques present an important limitation: the MOOP must be re-formulated into a single-objective optimisation problem so that objective function gradient information can be acquired. This means that interactions between objective functions cannot be studied independently. Alternatively, the meta-heuristic nature and the population-based approach of EAs make them well-suited to solve real MOOPs (Deb, 2001; Sbalzarini, et al., 2000). However, due to the diversity of the MOOPs, it is rarely possible to use the standard EA, instead, over the years, several variants and modifications have been developed to try to cope with the singularities of each problem. Several EA comparative studies can be found in literature (Zitzler, et al., 2000; Konak, et al., 2006; Fonseca & Fleming, 1995). These studies analyse the performance and robustness of different EAs under different test problems. Results from these studies show that elitist EAs offer enhanced performance capabilities with respect to non-elitist EAs. In particular, the elitist non-dominated sorting genetic algorithm (NSGA-II) outperforms other contemporary EAs in terms of convergence to near-true Pareto-optimal sets (Deb, et al., 2002). Moreover, EAs can be coupled with local gradient-based search algorithms to improve the efficiency of the optimisation algorithm and to ensure that the true Pareto optimal set is obtained (Deb & Goel, 2001). Several approaches using multi-objective EAs have been applied to suspension design. Cheli *et al.* (2007) applied a multi-objective EA to optimise the kinematic characteristics of an active suspension. Loyer and Jézéquel (2009) used an EA to obtain a Pareto optimal set of a passive quarter car linear suspension. Molina-Cristobal *et al.* (2007) applied a multi-objective EA to obtain an optimised ideal suspension mechanical network featuring inerters.

2.6.3. Surrogate Model Based Optimisation

EAs are well-suited for solving true multi-objective optimisation problems due to their population-based searching approach. However, in order to find the true Pareto optimal set,

the computational effort require is high. Real-life engineering problems usually involve simulation of high-fidelity and complex virtual models, where large search spaces and multiple objective functions need to be optimised. Moreover, in these optimisation problems, every time the objective function is evaluated, the solution of the dynamic system must be computed via numerical integration techniques. This means that the sole use of EAs can become computationally very intensive. Alternatively, metamodelling techniques can be used in combination with an EA in order to enhance the computational efficiency of the optimisation method (Bramanti, et al., 2001). Surrogate models, or metamodels, are compact analytic models that approximate the dynamic behaviour of complex systems. Surrogate models are constructed through data obtained from a limited set of simulations of the original model (Forrester, et al., 2008). The input/output nature of surrogate provides direct and fast relationships between performance objectives and design variables (Queipo, et al., 2005). Surrogate model based optimisation has been successfully applied to different engineering fields: Bouazizi *et al.* (2009), applied this approach to structural design; Chung and Alonso (2004) used a surrogate model in combination with a hybrid EA to design the external profile of a low-boom supersonic business jet; Vaidyanathan *et al.* (2004) and Goel *et al.* (2007) created an approximate model of a model of a single-element rocket injector in order to efficiently optimise the performance of the injector; Lyu *et al.* (2006) used the surrogate-based approach to optimise the torsion beam in a vehicle suspension system; and Cappelleri *et al.* (2002) applied a metamodel-based approach to design a piezoelectric bimorph actuator.

Examples of metamodelling studies can also be found in the field of Vehicle Dynamics. Butz *et al.* (2010) created a metamodel of a vehicle multi-body dynamic system in order to estimate suspension parameters. Chen *et al.* (1999) used a surrogate model based approach to improve the handling characteristics of a vehicle. Gobbi *et al.* (1999) and Benedetti *et al.* (2006) used a metamodel based optimisation method in order to determine a suspension setting for optimal handling characteristics. Yang and Huang (2009) and Wentao *et al.* (2011) used the same approach to improve ride comfort and safety of a road car.

A formal process of surrogate model based multi-objective optimisation was established by Wilson *et al.* (2001) and it can be summarised in the following diagram:

Figure 2-3: Process of MOO using Surrogate Approximations (Wilson, et al., 2001)

The first step in this process is to sample a set of construction points in the design space. These sampling points set the structure above which the surrogate model is constructed. The quality of the surrogate model is highly dependent on the distribution of the construction points across the design space. According to this, a design of experiments (DoE) approach must be used to ensure a representative spread of construction points. Wang and Shan (2007) offered an overview of the most commonly used DoE techniques. Furthermore, Simpson *et at.* (2001) proposed some preferential relationships between DoE and surrogate model choice (see Figure 2-4). These construction points are then fed into the original model and cost functions are evaluated, so that a map that directly relates inputs (design space) to outputs (objective functions) can be created. This map is then required to interpolate some mathematical metamodeling function.

Figure 2-4: Techniques for Metamodelling (Simpson, et al., 2001)

Several surrogate modelling techniques have been reported in literature: polynomial regression (PR), Kriging modelling (KRG) and Radial Basis functions (RBF) are the most widely used methods (Jin, 2005). Several studies were carried out in order to investigate the performance of each metamodelling technique (Simpson, 1998; Simpson, et al., 2001; Jin, et al., 2000; Fang, et al., 2005; Shihani, et al., 2006). Metamodelling techniques were evaluated in order to test different capabilities such as model creation simplicity, model response accuracy and computational effort (measured as simulation time). These studies suggested that a Kriging metamodelling technique offers a good compromise among all the features tested. Kriging methods have their origins in mining and geostatistical applications. This method is a combined model that can be defined as follows:

$$y(\boldsymbol{x}) = f(\boldsymbol{x}) + Z(\boldsymbol{x}) \qquad (2.4)$$

Where $f(\boldsymbol{x})$ represents a global approximation of the original function and it is expressed as a polynomial model and $Z(\boldsymbol{x})$ is expressed as a stochastic function that represents localised deviations in between data samples (Simpson, et al., 2001).

The following step is to validate the predictive capabilities of the approximate model. A new set of random sampling points is generated and used to evaluate the quality of the

approximate model with respect to the original model. The most common statistical metrics used to evaluate the accuracy and predictability of the surrogate model are the root mean square error (RMSE) and maximum absolute error (MAE) (Wang & Shan, 2007). Alternatively, more exhaustive comparative studies present more complex statistical metrics such as R2, relative average absolute error (RAAE), or relative maximum absolute error (RMAE) (Jin, et al., 2000). Once the metamodel has been validated, it can be used in substitution of the original computationally expensive model as the input of the optimisation process.

2.7. Lap-Time Simulation

The use of lap-time simulation (LTS) tools is important in the design and development of race cars. LTS packages simulate a vehicle model negotiating a race track. LTS tools can provide significant advantages to race teams since different designs and settings can be virtually tested without the need of building a prototype and of track testing. Thus, a LTS package is more cost and time effective than physical track testing and allows modifications on fundamental parameters of the vehicle design.

LTS packages simulate a vehicle completing a lap on race track in the minimum time possible. In order to do so, equations of motion (EOMs) of the vehicle system must be solved to find the on-limit adhesion conditions. According to this, LTS tools can be classified into three categories depending on the strategy used to solve these EOMs (Siegler, et al., 2000):

- Static or Steady-State Strategy.
- Quasi-static or Quasi-Steady-State Strategy (QSS).
- Transient Strategy.

In a Steady-State strategy, the race track is divided into straights and constant radius corners. Longitudinal and lateral motions are completely decoupled and all the time-dependent terms are neglected. Only lateral acceleration due to circular motion is accounted for in this strategy. This strategy is barely used for accurate LTS studies due to its simplicity.

A QSS strategy represents an extension of the previous strategy. In this approach corners are divided into a set of constant radius turns. Each of these segments will be of different corner radius, i.e. decreasing corner radius up to corner apex and increasing from it.

At each segment, a balance in the forces applied to the vehicle exists. The vehicle is assumed to be moving from one state to the immediate next state in a steady fashion. Lateral acceleration is obtained from equations derived for a constant radius motion and a tyre model is then used to obtain the lateral force needed to maintain this lateral acceleration. The longitudinal tyre forces used to accelerate the vehicle longitudinally can then be calculated from either a combined tyre model such as Pacejka Magic Formula (Pacjeka, 2006) or from a tyre friction circle approach (Milliken & Milliken, 1995). The accuracy of this strategy depends on the length of the corner segment used in simulation. Examples of this QSS strategy can be found in (Brayshaw, 2004; Braghin, et al., 2008).

The most important limitation found in the previous two strategies is that no transient effects are accounted for in the simulation. The third strategy is used to overcome this limitation. In a transient strategy, the fully transient solution of the dynamic system is obtained. Since the objective of the present research work is to study and optimise the dynamics of a race car suspension, attention is focused on the discussion of transient LTS in the following sections.

2.7.1. Previous work on Transient Lap-Time Simulation

Transient LTSs carry out the non-steady simulation of a vehicle around a race track. In this strategy, numerical integration of fully dynamic EOMs of the vehicle for each instant of time is carried out. Due to the competitive nature of Motorsport, only a few studies with regard to the design and development of transient LTS have been reported in literature. The first attempt at developing a transient optimal LTS dates from late 1980s. Metz and Williams (1989) used a simple 3-DOF planar vehicle model to estimate the minimum time in a prescribed short distance manoeuvre. Fujioka and Kimura (1992) proposed a similar method in order to carry out an analysis of steering and powertrain systems. A different solution method was proposed by Hendrikx *et al.* (1996): the lap-time simulation time problem was solved in the distance domain rather than in the time domain. In these works, transient LTS was solved as a minimum time manoeuvring (MTM) problem. Optimal control inputs were then obtained to solve the MTM problem via OC solution methods (see section 2.7.2).

The first complete lap transient LTS was developed by Casanova (2000). Casanova developed a method for solving the MTM problem based on Optimal Control (OC) theory. In his work, the LTS problem was proposed as a time Optimal Control problem. The OC was then transcribed to a Non-linear Programming (NLP) problem via a parallel shooting direct method. Casanova identified two limitations in this procedure: computational effort to solve

the OC problem and sensitivity of objectives and constraints stability with respect to early controls. Automatic differentiation (AD) was proposed in his research work as a method to increase the computation efficiency. In order to reduce the sensitivity to early control inputs, the race track was split into shorter sections where optimal control problem was solved independently and then re-attached to the global solution. Several studies resulted from this work: a study of the significance of yaw inertia in the performance of the car (Casanova, et al., 2000), a sensitivity study of the significance of vehicle mass (Casanova, et al., 2001), and a study of the impact in lap time of longitudinal CoG location (Casanova, et al., 2002) were successfully carried out by using this LTS. Kelly (2008) developed an alternative OC algorithm for obtaining the optimal lap time based on Receding Horizon Control/ Model Predictive Control (RHC/MPC) theory. This work was based on a previous publication by Velenis and Tsiotras (2005). The use of MPC algorithms solved the dependency of final convergence to initial control input guesses. However, this algorithm was computationally very expensive.

In both methods proposed by Casanova and Kelly, driver control inputs were modelled as open-loop controls. Current investigations propose a close-loop driver model coupled with MPC to find the optimal racing line at constant forward speed (Timings & Cole, 2010; Timings & Cole, 2011). Although these studies are in an experimental stage, they suggest that both limitations could be reduced by the use of close-loop input controls.

2.7.2. Lap Time Simulation as an Optimal Control Problem

The problem of finding the minimum time manoeuvring (MTM) can be expressed as a time Optimal Control (OC) problem (Casanova, 2000). In general terms, the OC problem can be defined as to find a control u^* that minimises a performance index J (Kirk, 2004). This can be expressed mathematically as:

$$
\begin{aligned}
\min_{u} \quad & J = h\left(x\left(t_f\right), t_f\right) + \int_{t_0}^{t_f} g(x(t), u(t), t)dt \\
subject\ to \quad & \dot{x}(t) = f(x(t), u(t), t) \quad with \quad x(t_o) = x_0 \\
& C_{in}(x(t), u(t), t) \leq 0 \\
& C_{eq}(x(t), u(t), t) = 0 \\
& u_{min} \leq u(t) \leq u_{max}
\end{aligned} \tag{2.5}
$$

$for\ all\ t \in [t_0, t_f]$

Except for very simple engineering problems, most optimal control problems cannot be solved analytically. Instead, numerical methods must be used to find optimal controls u^*. Hence, in this section attention is paid to numerical methods for solving OC problems. Numerical methods for solving optimal control problems can be classified into two general categories:

- Indirect methods
- Direct methods

In indirect methods, Calculus of Variations is applied to obtain first-order necessary conditions for optimality. These necessary conditions transform the OC problem into a Hamiltonian boundary-value problem (HBVP) by application of Pontryagin's minimum principle (Kirk, 2004). The solution of this HBVP is then obtained by applying a numerical solution technique. Different numerical solution techniques can be found in classical OC literature. The most common methods are shooting, multiple shooting, finite difference and collocation. The main advantages of the use of indirect methods for solving OC problems are a high accuracy in the solution and the proximity of the final solution to the true optimal control law. However, indirect methods have several disadvantages. Firstly, deriving first-order necessary conditions for optimality is a non-trivial procedure, since these conditions must be derived analytically. Secondly, a good initial guess of the unknown boundary conditions is required, because indirect methods typically have small radii of convergence. Some indirect methods also require an accurate initial guess of the co-state variables which, due to its non-intuitive and non-physical nature, is often difficult to obtain. Finally, for problems with active path constraints, a-priori knowledge of the constrained and unconstrained arcs or switching structure must be known (Huntington, 2007).

In a direct method, the continuous-time optimal control problem is approximated to a finite-dimensional nonlinear programming problem (NLP) (Betts, 2010). In this method, derivation of a set of optimality conditions is not required. The resulting NLP can be solved by well-developed algorithms for numerical optimisation (Nocedal & Wright, 2006; Gill, et al., 2002; Biegler & Zavala, 2008). Direct methods offer a series of advantages with respect to indirect methods: necessary conditions for optimality need not to be derived; the impact of initial guesses in final convergence is not as important as in indirect methods, because of a larger radii of convergence; no initial guess for the co-state vector is required; the structure of the problem can be modified more easily. However, the main disadvantage of these methods is the reduced accuracy in the solution with respect to indirect methods. Moreover, more work is required to check optimality, as direct methods often provide inaccurate co-state information or no information at all.

Many different direct methods for solving OC problems have been reported in literature depending on the way the OC problem is converted into a nonlinear programming problem (NLP) (Benson, 2005). The main methods for direct transcription are direct shooting and collocation methods. Direct shooting methods discretise only the control variable *u(t)*, and the dynamics of the system are obtained by explicit numerical integration. This method is useful for problems where the number of discretised input control points is limited. However, the efficiency of a direct shooting method decreases as the number of control points increases, due to the sensitivity of final convergence to early inputs. Direct multiple-shooting methods overcome this problem. In multiple shooting methods, the time interval is split into sub-intervals where a direct shooting method is then applied. A state continuity condition is enforced at the interface between intervals. The most important drawback of these transcription methods is the high computational effort required to integrate the dynamic system numerically.

2.7.3. Full Vehicle Model

A vehicle model is an important factor in the development of accurate lap time simulators. Vehicle modelling requires the idealisation of an actual vehicle system into a set of dynamic equations of motion (EOM). In general terms, a vehicle model can be expressed mathematically as a set of first-order ordinary differential equations (ODEs) (Close & K., 1995):

$$\frac{dx(t)}{dt} = f(x(t), u(t), t) \qquad (2.6)$$

Where *x(t)* represents a vector of the state variables of the system, *u(t)* represents the vector of external inputs, *t* represents time and *f* is a vector value function that computes the derivatives of the state variable vector.

The selection of an appropriate vehicle model is a compromise between model complexity, accuracy and efficiency (Allen & Rosenthal, 1994). A more complex model will offer more accurate results. However, a more comprehensive model will require a larger number of ODEs to be solved per evaluation, leading to a more computationally expensive model. Furthermore, the number of parameters required to simulate a vehicle model increases with model sophistication.

Several vehicle models have been reported in literature. The simplest full vehicle model can be represented as a mass point where lateral and longitudinal forces are assumed to be directly controllable (Velenis & Tsiotras, 2005; MÜhlmeier & Müller, 2002). However, this model does not account for fundamental vehicle under/oversteering characteristics. A better suited model is the so-called 'bicycle model' (see Figure 2-5).

This is a planar vehicle model and consists of 3 DOFs: longitudinal and lateral displacement and rotation around CoG. This model is useful to analyse the general handling characteristics in a conceptual design stage where very little vehicle parameters are available (Milliken & Milliken, 1995). Several examples of the use of a bicycle model have been reported in literature (Hendrikx, et al., 1996; Velenis & Tsiotras, 2005; Schmitt, et al., 2008; Fujioka & Kimura, 1992; Metz & Williams, 1989). In these models, longitudinal forces applied to the tyres are assumed to be controllable inputs. An evolution of the previous model is a vehicle model that includes tyre spin as additional DOFs (Prokop, 2001).

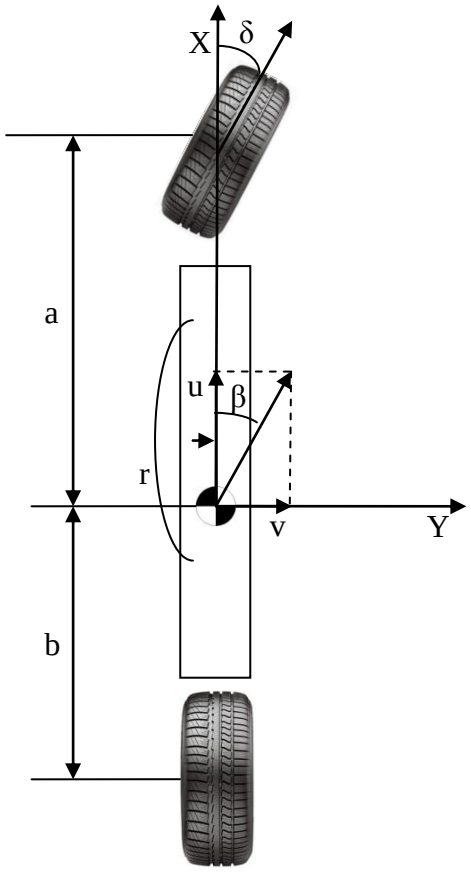

Figure 2-5: 3-DOF Bicycle Model

Bicycle models do not account for effects such as lateral transfer or roll motion. Full vehicle models are then required to study such effects. Casanova (2000) used a two-track model with rotating wheels in the lap time simulation tool. The model is planar and weight transfer is approximated as a steady-state load variation. Whitehead *et al.* (2004) produced a bicycle model that also accounted for roll motion. Stone and Demetriou (2000) developed a 6-DOF model that included chassis translational and rotational motions in all three axes, but unsprung mass and tyre motions were neglected. Kelly (2008) presented an extension of Casanova's vehicle model. The vehicle model had additional vertical and rolling DOFs, but the model neglected the vertical dynamics of unsprung masses.

More complex 3D vehicle models are required for comprehensive studies of vehicle ride and handling dynamics. Ghike and Shim (2008) used an 8-DOF model in order to develop an integrated active chassis control scheme. In this model, body pitch and heave motions as well as unsprung mass vertical motions are neglected. A 14-DOF system provides the simplest

representation of a full-car vehicle model (March & Shim, 2007). Such a model account includes translational and rotational body motions (6 DOFs) and vertical and rotational motion at each wheel (two additional DOFs per wheel). Shim and Ghike (2007) presented a comparative study of the accuracy of different vehicle models. In this work, a comprehensive nonlinear 14-DOF full vehicle model was developed first and simplifying assumptions were then gradually introduced into the model. Differences among vehicle models were analysed in order to compare the impact of modelling simplifications in the dynamic response of the vehicle.

2.7.4. Lap Time Simulation as part of Suspension Optimisation Algorithm

As mentioned in the previous section, the outcome of a suspension multi-objective optimisation is a set of non-dominated optimal solutions (Deb, 2001). In motor racing, since only passive suspensions are allowed by the governing body, one single solution from the optimal set must be selected. Higher order information is required to select the specific solution that will suit a particular situation. So, in order to choose among the Pareto-optimal solution set, a decision-maker tool is required. In vehicle suspension design and optimisation, a decision-maker is composed of a set of performance metrics that will weight the different objective functions so that a final solution can be obtained. In Motorsport, the ultimate goal of vehicle system is to obtain a configuration such that the time taken to complete a lap around a race track could be minimised. Modifications in suspension settings have an important impact on the performance of the car and, ultimately, on its lap time. According to this, higher order information will come from the study of the impact of suspension changes in the overall performance of a race car. The higher order information could be obtained from two different approaches: on-track testing and lap-time simulation. Due to the competitive nature of Motorsport, no relevant data have been published with regard to the impact of suspension changes in the actual on-track performance of a race car. Moreover, developing a decision maker based on track testing would involve the construction of a fully operative race car prototype. Although information obtained from this type of testing is invaluable, the costs involved and the limited number of tests allowed by governing body make this option unviable in most cases. A much more cost-effective option for the development of a decision maker tool can be found in the analysis of suspensions in the overall vehicle performance via lap-time simulation.

Although it has been already stated that changes in the suspension will have an impact on vehicle handling characteristics and on overall vehicle performance (Benedetti, et al., 2006; Blank & Margolis, 1996; Floyd & Law, 1994), only a few reported studies have been found in literature with regard to the analysis of the impact of a race car suspensions on one-lap performance. Kelly (2008) presented a study of a race car transient cornering manoeuvres. In this study, an idealised vehicle suspension with decoupled heave and roll modes was proposed, and the effect of heave and roll stiffness and damping was analysed for different corner layouts. However, there are no reported studies in literature that make use of lap-time simulators as higher order information decision makers in the suspension optimisation process.

2.8. Summary

A review of the significant literature for this research work has been presented in this chapter. The first section introduces the importance of suspension in racing cars. A brief historical background of the evolution of race car suspension technology has been reviewed and the importance of suspension design and optimisation has been highlighted.

The inerter concept and its potential applications have been presented. The definition of an ideal inerter has been introduced and the different design solutions available in literature have been discussed. Moreover, reported studies of potential benefits in field of ground vehicle suspensions, motorcycle steering systems and building technology have been discussed. Experimental inerter studies have been also covered. The review presented on this area revealed that experimental inerters have only been tested in isolation to other suspension components.

In section 2.4, experimental testing techniques for the dynamic analysis of vehicle suspension have been discussed. The main characteristics of post rig test facilities have been discussed, and examples of their use in literature have been provided. No reported studies consider the analysis of suspension featuring inerters using these facilities.

A section dedicated to reviewing virtual suspension modelling and simulation has also been covered. A review of different suspension models has been carried out. Model complexity and applications in simulation and optimisation have been discussed. Although research studies devoted to modelling and validation of individual inerters devices have been found,

no literature that proposes a complete and validated vehicle suspension model that includes real inerters has been reported.

Suspension optimisation is a key factor in vehicle performance. Section 2.6 covered different aspects in suspension optimisation. Firstly, a review of suspension objectives reported in literature has been carried out. Secondly, different optimisation algorithms applied to suspension technology have been presented. Optimisation methods have been reviewed with respect to the requirements for suspension optimisation. Finally, methods for increasing the efficiency and robustness of optimisation algorithms have been described. However, no studies have been found in literature that produced an objective performance-based suspension optimisation methodology that reflects the impact of ride dynamics on handling characteristic and on the performance of a race car.

The last section of chapter 2 was dedicated to lap-time simulation. The concept and importance of lap-time simulation in motor racing has been presented. Different lap time simulation strategies have been described and the most relevant work in this field has been critically reviewed. Furthermore, a review of vehicle models for simulation has been carried out. Different full vehicle models have been discussed. No reported studies that use lap-time simulation as a decision maker in a suspension optimisation problem have been found.

Chapter 2 sets out the state-of-the art of engineering and technology in the research areas related to the work developed in this thesis and it highlights the gaps in existing work related to optimisation of racing car suspensions featuring inerters.

3. Theoretical Analysis of Ideal Inerters in Vibratory Systems

3.1. Introduction

The simplest model in the analysis of dynamic vibratory systems can be described as a single degree-of-freedom (SDOF) rigid mass, elastically connected to a base or some form of excitation. The system is termed SDOF because the mass is only allowed to move in one direction.

SDOF models can provide relevant information about the system regardless of their simplicity. Furthermore, due to this simplicity, these models have been widely used in many applications such as bridges, buildings, aerospace structures, mechanical engineering and so on. The results obtained from the analysis of a SDOF system can be used as the foundation for the development of more complex models.

The study and analysis of these models has been widely covered in literature and Dynamics textbooks. However, there is no record in the literature that characterises and analyses the effect of inertial damping in the dynamic behaviour of such systems. First of all, an ideal inerter can be defined as a mechanical device in which the force applied to its terminals is proportional to the relative acceleration between these nodes (Smith, 2002). According to this definition, the characteristic equation of an (ideal) inerter, as described in section 2.3, is:

$$F = b \cdot (a_2 - a_1) \tag{3.1}$$

Where F is the equal and opposite force applied at each terminal, a_i represents the absolute acceleration at the ith node and b represents inertance and has units of kilograms in SI.

In this chapter, the property of an ideal ball screw inerter has been defined. Furthermore, an ideal inerter modelled as a SDOF is analysed for un-damped and damped cases. Equations of motion of the system are derived and analytical solutions are given in free and forced vibration situations. The effect of inerters and its interaction with other elastic components are analysed. Results of this analysis set the foundation for the development of more complex vibratory systems.

3.2. Definition of the properties of an ideal inerter

As discussed in Chapter 2, ideal inerters are only characterised by the inertance property *b* (see equation (3.1)). The calculation of the inertance *b* depends on the design solution adopted to build a physical inerter. In the present research work, a ball screw inerter has been adopted as design solution[1]. Figure 3-1 shows the conceptual design of a ball screw inerter.

Figure 3-1: Conceptual design of a ball screw inerter (Smith, 2006)

The basic working principle of an ideal inerter such as the one shown in Figure 3-1 is as follows: the reciprocating movement between inerter terminals 1 and 2 induces a rotational motion in a rotating nut via a ball screw mechanism. This ball screw mechanism also transforms the linear force applied between terminals 1 and 2 into a torque in the rotating nut. The rotating nut is solidly connected to a flywheel. Hence, motion and torques are transferred completely from the nut to the flywheel. According to this, applying Newton's Second law of motion for rotational systems to a free-body diagram of the flywheel:

$$\sum M_{ext} = I_{fw} \cdot \ddot{\theta} \qquad (3.2)$$

Where M_{ext} represent the sum of all external moments applied to the flywheel, I_{fw} represents the moment of inertia of the flywheel and $\ddot{\theta}$ represents the angular acceleration of the flywheel.

[1] Detailed description of the design process is presented in Chapter 4.

Due to the coupling between translational and rotational movement, translational force at the device terminals, *F*, and torque transmitted to the flywheel, *T*, are related by the following expression:

$$T = \frac{F \cdot l}{2\pi} \tag{3.3}$$

Where *l* represents the lead of the screw, *F* represents the translational force at the device terminals.

In the same way as above, translational relative displacement of the device terminals (*x(t)*) is related to the angular rotation of the flywheel, θ, as follows:

$$x = \frac{\theta \cdot l}{2\pi} \quad \rightarrow \quad \frac{d^2}{dt^2} \quad \rightarrow \quad \ddot{x} = \frac{\ddot{\theta} \cdot l}{2\pi} \tag{3.4}$$

Introducing equations (3.3) and (3.4) into equation (3.2), the following expression is obtained:

$$F = I_{fw} \cdot \left(\frac{2\pi}{l}\right)^2 \cdot \ddot{x} \tag{3.5}$$

Recalling that the representation of an ideal inerter is $F = b \cdot a_{rel}$ (see equation (3.1)), the inertance of a ball screw mechanism can be obtained as:

$$b = I_{fw} \cdot \left(\frac{2\pi}{l}\right)^2 \tag{3.6}$$

Where *b* represents the inertance of the inerter expressed in kg and a_{rel} represents the translational relative acceleration between inerter terminals.

3.3. Analysis of an un-damped Inerter modelled as a SDOF

The simplest model in engineering vibration is a single degree-of-freedom (SDOF) system that does not account for damping effects – un-damped case. Such a model is depicted in Figure 3-2.

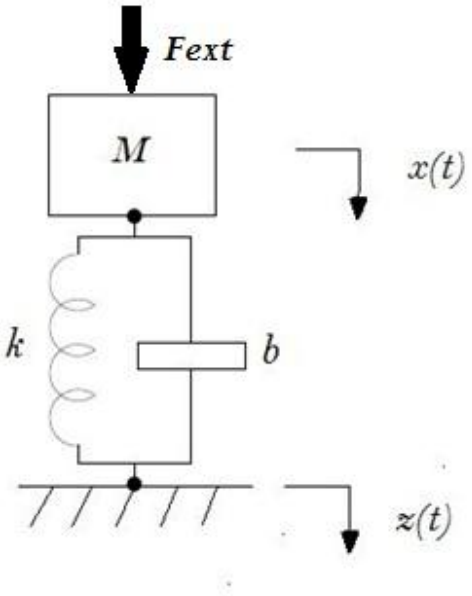

Figure 3-2: Un-damped SDOF system with inerter

In the conventional SDOF model, the solid-rigid mass is connected elastically via an ideal spring to a base or excitation. Only translational motion in vertical direction has been considered as a degree of freedom. In this study, an ideal inerter is connected in parallel with the spring. In order to obtain the equation of motion of the system depicted in Figure 3-2, Newton's Second law of Mechanics has been applied to the free-body diagram of this system.

$$\Sigma F = m \cdot a \quad \rightarrow \quad m \cdot g + F_{ext} + k \cdot (z - x) + b \cdot (\ddot{z} - \ddot{x}) = M \cdot \ddot{x} \qquad (3.7)$$

Equation (3.7) represents the motion of the mass *M* subjected to the force of the spring and the inerter, gravity and external forces applied to the mass; *x(t)* and its derivatives represent the movement (displacement, velocity and acceleration) of the mass *M* and *z(t)* and its derivatives represents the movement of the base. Note that, for simplicity in the notation, *x(t)=x*.

Assuming that the system at *t=0* is in equilibrium and no external forces are applied to the mass, equation (3.7) can be rearranged as follows:

$$(M + b) \cdot \ddot{x} + k \cdot x = b \cdot \ddot{z} + k \cdot z \quad \rightarrow \quad \ddot{x} + \frac{k}{M+b} x = \frac{b}{M+b} \ddot{z} + \frac{k}{M+b} z \qquad (3.8)$$

Where (3.8) is a second-order ordinary differential equation (ODE). Assuming that, the input of the base excitation is a sinusoidal waveform (forced excitation), equation (3.8) can be solved by applying Laplace transform to both sides of the equation:

$$\mathcal{L}(\ddot{x} + \frac{k}{M+b}x = \frac{b}{M+b}\ddot{z} + \frac{k}{M+b}z) \rightarrow$$

$$s^2X(s) - sx(0) - v(0) + \frac{k}{M+b}X(s) = \frac{b}{M+b}s^2Z(s) + \frac{k}{M+b}Z(s) \quad (3.9)$$

Where *s* represents the Laplace operator. In systems subjected to sinusoidal inputs $s=j\omega$, where *j* is the imaginary number and ω is the angular frequency and *x(0)* and *v(0)* represent the initial conditions (displacement and velocity) of the system.

Note that, by applying the Laplace transform to the equation (3.8), the resulting equation (3.9) is now second-order algebraic equation that can be solved easily.

For simplicity in the solution, the initial conditions of mass *M* have been set equal to 0. According to this, the transmissibility function of the system *G(s)*, i.e. the ratio between the output and the input, has been defined as:

$$G(s) = \frac{X(s)}{Z(s)} = \frac{bs^2 + k}{(M+b)s^2 + k} \quad (3.10)$$

Or in terms of angular frequency:

$$G(s) = G(j\omega) = \frac{k - b\omega^2}{k - (M+b)\omega^2} \quad (3.11)$$

Eq. (3.11) represents the frequency response function (FRF) of an un-damped SDOF system fitted with an inerter. This equation represents the frequency domain of a system under forced vibration.

In addition to this, a non-dimensional parameter χ can be defined in order to express the inertance *b* in terms of the mass of the system *M*:

$$\chi = \frac{b}{M} \quad (3.12)$$

By introducing expression (3.12) into equation (3.11), the following expression has been obtained:

$$G(s) = G(j\omega) = \frac{k - b\omega^2}{k - (1+\chi)M\omega^2} \quad (3.13)$$

Note that, even though, due to the nature of the system, no imaginary part exists, equation (3.13) can still be expressed in complex notation $z=a+bj$, where a is the real part, b is the imaginary part and j is the imaginary number. According to this, the magnitude and phase of a complex number can be obtained as follows:

$$|z| = \sqrt{a^2 + b^2} \tag{3.14}$$

$$\varphi = \text{atan}\left(\frac{b}{a}\right) \tag{3.15}$$

According to this, the amplitude and phase angle response for an un-damped single DOF with inerter can be expressed as follows:

$$A(\omega) = |G(j\omega)| = \frac{k - b\omega^2}{k - (1+\chi)M\omega^2} \tag{3.16}$$

$$\varphi(\omega) = atan\left(\frac{0}{\frac{k - b\omega^2}{k - (1+\chi)M\omega^2}}\right) = 0 \; or \; \pi \tag{3.17}$$

Equations (3.16) and (3.17) can be therefore used to determine the response of the system and to analyse the impact of the inerters in this response. A set of mechanical properties must be set in order to obtain the analytical solution of the system. Table 3-1 shows the mechanical parameters selected in this study.

These mechanical parameters have been introduced into equations (3.16) and (3.17), so that the effect of inerters in the amplitude ratio and phase responses of the SDOF system can be analysed. Figure 3-3 depicts the response of an un-damped SDOF system for different values of inertance.

Mass (M)	100 kg
Spring stiffness (k)	20000 N/m
Inertance tuning range (b)	[0-120] kg
Frequency range (f)	[0-20] Hz

Table 3-1: Mechanical properties of the un-damped SDOF system

Note that, although the frequency range of study is from 0 to 20 Hz, the plot only shows the first 10 Hz for clarity. The y-axis has been limited due to the fact that, at the natural

frequency of system, the amplitude ratio in resonance tends to ∞ because of the lack of the energy dissipation term.

In Figure 3-3, the blue trace represents the response of a conventional un-damped single DOF system. Meanwhile, red and green traces represent the response of a system fitted with medium and high level of inertance respectively.

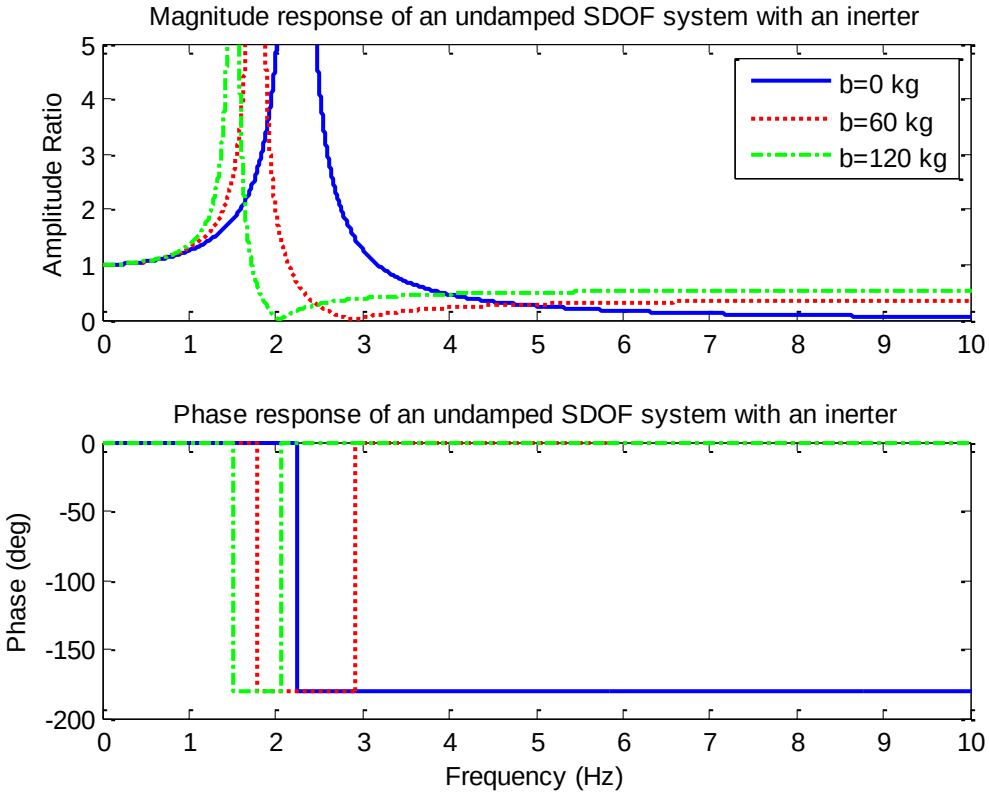

Figure 3-3: Steady-state response of an un-damped SDOF system. Amplitude ratio response (upper graph) and phase response (lower graph)

According to this, a number of conclusions can be drawn:

- At $\omega = \sqrt{\frac{k}{(1+\chi)M}}$, the value of the amplitude ratio becomes ∞, meaning that the system will exhibit an unstable vibration mode. This effect is known as resonance and the frequency at which the resonance takes place is known as natural frequency (ω_n). The natural frequency of the system decreases with increased inertance. The denominator of the natural frequency expression represents the dynamic effective mass of the system, i.e. $M_{eff} = (1 + \chi)M$. According to this definition, higher values of inertance will increase the dynamic effective mass of the system and this will reduce the frequency at which the resonant peak takes place. Note that, with no inerter

fitted ($\chi=0$), the effective mass of the system equals its real mass and the natural frequency corresponds to the classical expression $\omega = \sqrt{\frac{k}{M}}$.

- At $\omega = \sqrt{\frac{k}{b}}$, the value of amplitude ratio is 0, meaning that the system will exhibit no vibration at all regardless of the input excitation. This effect is known as vibration absorption and the frequency at which the vibration absorption takes place has been defined as absorption frequency (ω_{abs}). At this point, the inerter operates as a vibration absorber. Moreover, the definition of the absorption frequency suggests that, as the value of inertance increases, the absorption frequency decreases. Note that, for $b=0$ (no inerter fitted to the system), there is no point of full vibration absorption. This is equal to saying that, for an un-damped SDOF without inerters, the vibration absorption can only be achieved for $\omega=\infty$.

- The lack of damping in the system causes sharp changes in phase angle response. As expected from classical dynamics theory, the phase of the conventional system lags from 0 to 180 degrees at the resonance peak. Inerters introduce an effect of phase lead (Smith, 2002). This phase compensation effect can be noticed Figure 3-3 – lower graph: as the mass reaches the natural frequency, the phase lags by 180 degrees and when the mass reaches the absorption frequency, the phase response goes back to 0 degrees lag.

- It is also important to notice that, as the inertance increases, the natural and the absorption frequencies get closer together. This is due to the fact that, as inertance b increases, χ becomes the predominant term in the definition of the effective mass M_{eff}, i.e.

$$For\ b \uparrow\uparrow \quad \rightarrow \quad (1+\chi)M \approx \chi M = b \quad \rightarrow \quad \omega_n \approx \omega_{abs}$$

3.4. Analysis of a Damped Inerter modelled as a SDOF

The analysis of the un-damped case has been helpful in understanding the basics of the inerter behaviour. However, in most real-life engineering applications a certain level of energy dissipation must be assumed. For fundamental vibration analysis, an ideal damper can be assumed to model this energy dissipation term. In this section, damping effects have been included in the study of the inerters in vibratory systems. Therefore, the SDOF presented in the previous section has been extended in order to account for the damping component. Figure 3-4 shows a schematic representation of a damped SDOF system fitted with inerters.

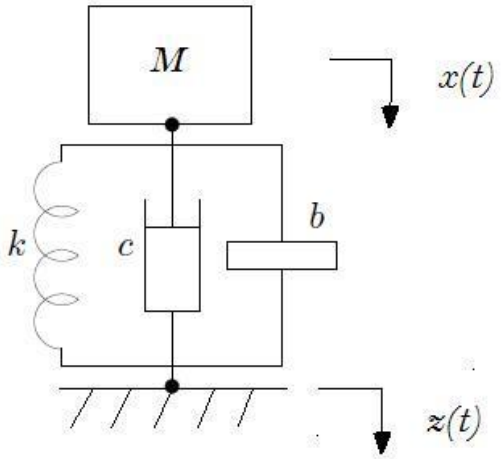

Figure 3-4: Damped SDOF system with inerter

Following the same procedure as in the previous section, the equation of motion of the system has been derived by applying Newton 2nd Law of Mechanics to the free-body diagram of the system:

$$m \cdot g + F_{ext} + k \cdot (z - x) + c \cdot (\dot{z} - \dot{x}) + b \cdot (\ddot{z} - \ddot{x}) = M \cdot \ddot{x} \qquad (3.18)$$

Assuming that the system is in equilibrium at the beginning of the motion and no external forces have been applied to the mass, the previous equation of motion can be re-arranged into the following second-order ordinary differential equation:

$$\ddot{x} + \frac{c}{M+b}\dot{x} + \frac{k}{M+b}x = \frac{b}{M+b}\ddot{z} + \frac{c}{M+b}\dot{z} + \frac{k}{M+b}z \qquad (3.19)$$

Equation (3.19) has been translated into an algebraic equation by using the Laplace transform as follows:

$$s^2X(s) - sx(0) - v(0) + \frac{c}{M+b}[sX(s) - x(0)] + \frac{k}{M+b}X(s) = \frac{b}{M+b}s^2Z(s) + \frac{c}{M+b}sZ(s) + \frac{k}{M+b}Z(s) \qquad (3.20)$$

Equation (3.20) represents the behaviour of a general single DOF system that accounts for both damping and inertial effects expressed in terms of the Laplace operator. From this equation, both the steady-state and transient responses of the system have been derived.

In the following sections of this chapter, the steady-state amplitude ratio and the phase angle response subjected to a forced excitation has been analysed in the frequency domain. Furthermore, the transient response of the system has been studied by obtaining the analytical expression of mass displacement *x(t)* in the time domain.

3.4.1. Analysis in the frequency domain

As in section 3.3, initial conditions of displacement and velocity have been considered to be 0, so equation (3.20) can be rewritten as follows:

$$[(M+b)s^2 + cs + k]X(s) = [bs^2 + cs + k]Z(s) \quad \rightarrow$$

$$G(s) = \frac{X(s)}{Z(s)} = \frac{bs^2 + cs + k}{(M+b)s^2 + cs + k} \qquad (3.21)$$

Laplace operator *s* has been substituted by the frequency term in order to obtain *G(w)*. By applying equations (3.14) and (3.15) to *G(w)*, amplitude ratio and phase angle frequency domain responses have been obtained:

$$A(\omega) = \sqrt{\frac{(k - b\omega^2)^2 + (c\omega)^2}{(k - (M+b)\omega^2)^2 + (c\omega)^2}} \qquad (3.22)$$

$$\varphi(\omega) = atan\left(\frac{-cM\omega^3}{b(M+b)\omega^4 + [c^2 - k(M+2b)]\omega^2 + k^2}\right) \qquad (3.23)$$

As discussed in section 3.3, a set of mechanical parameters must be provided in order to obtain the amplitude ratio and phase angle response of the system (see Table 3-2).

Mass (M)	100 kg
Spring stiffness (k)	20000 N/m
Damping Ratio Range	[0.1-1]
Inertance tuning range (b)	[0-120] kg
Frequency range (f)	[0-20] Hz

Table 3-2: Mechanical properties of the damped SDOF system

Introducing the values of Table 3-2 into equations (3.22) and (3.23), the steady-state response of the system has been obtained. The following figures represent the effect of inertance in the response of the SDOF for different damping levels.

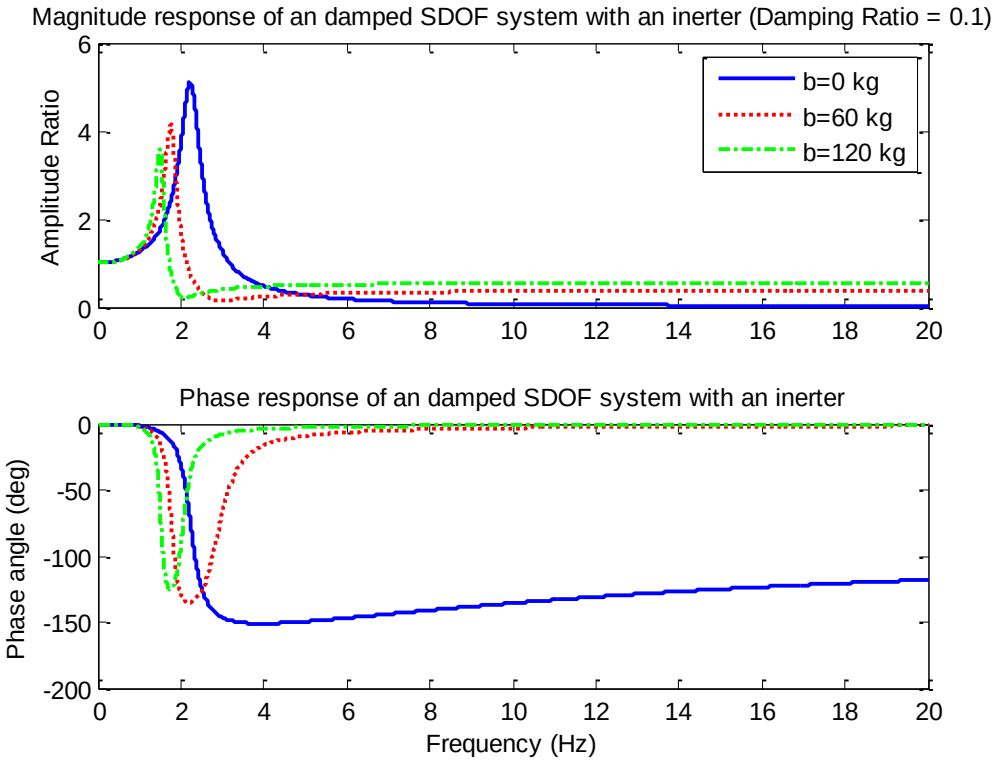

Figure 3-5: Steady-state response of damped SDOF system (Damping Ratio = 0.1). Amplitude ratio response (upper graph) and phase response (lower graph)

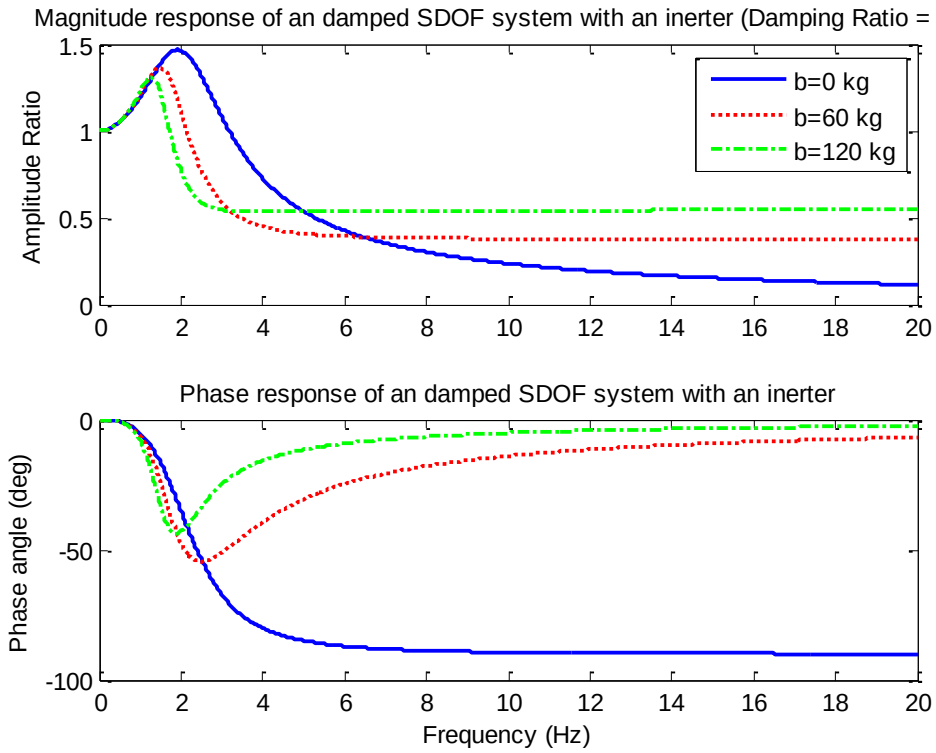

Figure 3-6: Steady-state response of damped SDOF system (Damping Ratio = 0.5). Amplitude ratio response (upper graph) and phase response (lower graph)

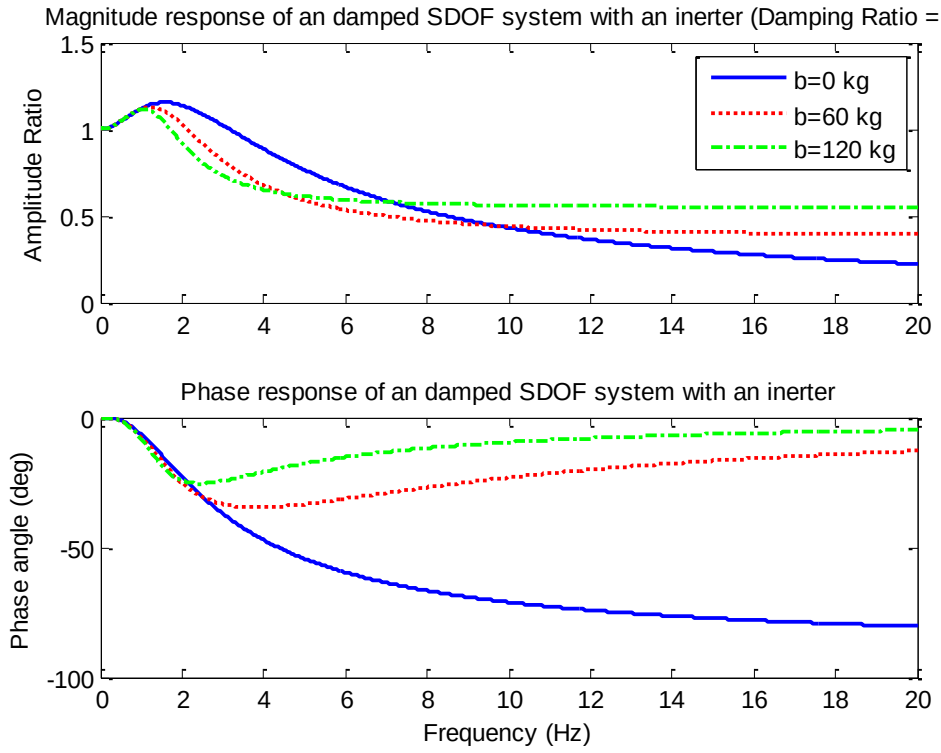

Figure 3-7: Steady-state response of damped SDOF system (Damping Ratio = 1). Amplitude ratio response (upper graph) and phase response (lower graph)

Firstly, Figure 3-5 to Figure 3-7 show that the effect of an inerter in a SDOF system is similar regardless of the level of damping of the system. More inertance translates into an increase in the dynamic effective mass of the system, which, in turn, reduces both the natural frequency and the amplitude of the resonant peak. As expected, increasing damping helps to smooth the steady-state response of the system. Higher levels of damping contribute to a better controlled resonant mode, i.e. lower values of amplitude ratio around the natural frequency.

As in the un-damped case, the inerter acts as a vibration absorber. However, in this case, the damping term causes a reduction this absorption effect. Note that, with a damping ratio of 0.1 (see Figure 3-5), the decrease of the amplitude ratio at ω_{abs} is quite noticeable. However, the vibration absorption effect can be barely noticed for higher damping ratios (see Figure 3-6 and Figure 3-7). This is due to fact that increases in damping reduce the relative motion of the suspension ("locking-up" effect).

Moreover, at high frequencies, the amplitude ratio tends to $\frac{b}{M+b}$ regardless of the level of damping of the system. This effect is caused because the inerter is connected to both the input (base) and the output (mass). As shown in the un-damped case, inerters introduce a phase lead on the system. This phase lead causes the mass to catch up with the input excitation back again after initial phase lag. Phase angle response plots show that the phase compensation is more effective for higher values of inertance. This, in turn, allows the output to match more effectively the input, hence, the amplitude ratio at higher frequencies gets closer to 1. In the limit, very high levels of inertance, phase compensation would be 100% effective, leading to a perfect match between input and output signals, i.e. an amplitude ratio equals to 1. On the other hand, higher levels of damping contribute to slowing down this phase compensation (see Figure 3-7), reducing the effectiveness of the output to catch up with the input.

Some conclusions can be drawn from this frequency domain analysis: on one hand, higher inertance values could be beneficial at low frequencies ($\omega \approx \omega_n$) due to the fact that, for the same spring value *k*, the effective frequency response corresponds to the one of a softer system, i.e. lower amplitude at the body mode and lower natural frequency. Lower transmissibility at low frequencies improves body control. However, on the other hand, at high frequencies ($\omega > \omega_n$), lower values of inertance could be more beneficial, due to the increased transmissibility caused by high inerter values. Therefore, high inertance will cause poorer vibration isolation at frequencies over the natural frequency ω_n. This suggests that a

compromise may need to be met between body control and vibration isolation when selecting the optimal value of inertance *b*.

3.4.2. Analysis in the time domain

Apart from the frequency domain response of the system under a force excitation, it is also important to analyse how a SDOF system with an inerter settles down back to the equilibrium state when pulled away from it. A time domain transient analysis has been carried out in this section. The analytical expression that describes the motion of the mass *x(t)* has been derived and the transient response of the system when pulled away from the equilibrium condition has been analysed.

According to this, assuming that no input has been applied to the system, i.e. *z=0*, equation (3.19) has been rewritten as:

$$\ddot{x} + \frac{c}{(1+\chi)M}\dot{x} + \frac{k}{(1+\chi)M}x = 0 \tag{3.24}$$

And defining the natural frequency and the damping ratio as,

$$\omega_n = \sqrt{\frac{k}{(1+\chi)M}} \tag{3.25}$$

$$\xi = \frac{c}{C_c} = \frac{c}{2\sqrt{(1+\chi)Mk}} \tag{3.26}$$

Where C_c represents critical damping and can be defined as the amount of viscous damping that result in a displaced system returning to its original position without oscillation.

Expressions (3.25) and (3.26) have been introduced into equation (3.24), so that the following equation has been obtained:

$$\ddot{x} + 2\xi\omega_n\dot{x} + {\omega_n}^2 x = 0 \tag{3.27}$$

Equation (3.27) represents a second-order ordinary differential equation. As in previous sections, this equation has been rewritten in terms of Laplace operator:

$$s^2X(s) - sx(0) - v(0) + 2\xi\omega_n[sX(s) - x(0)] + {\omega_n}^2X(s) = 0$$

And re-arranging the previous equation, the following expression has been obtained:

$$X(s) = \frac{v(0) + (s + 2\xi\omega_n)x(0)}{s^2 + 2\xi\omega_n s + {\omega_n}^2} \tag{3.28}$$

In order to obtain the analytical solution of the transient response of the SDOF, the roots of the denominator equation (also known as characteristic equation) can be obtained and equation (3.28) can be re-arranged according to the value of the roots of this characteristic equation. Moreover, the value of these roots depends on the value of the damping ratio ξ. According to this, three different cases can be distinguished: under-damped, critically damped and over-damped cases. For each of these cases, equation (3.28) can be re-arranged into a different expression. These re-arranged equations can then be solved by means of Inverse Laplace transform.

Under-damped case ($0 < \xi < 1$)*:*

The denominator of eq. (3.28) can be rewritten as follows:

$$s^2 + 2\xi\omega_n s + {\omega_n}^2 = (s + \xi\omega_n)^2 + {\omega_n}^2 - (\xi\omega_n)^2 = (s + \xi\omega_n)^2 + {\omega_n}^2(1 - \xi^2)$$
$$\Longrightarrow (s + \xi\omega_n)^2 + {\omega_d}^2$$

Where $\omega_d = \omega_n\sqrt{1 - \xi^2}$ is the damped natural frequency.

If the new expression for the denominator is introduced in equation (3.28) and some re-arrangements are made to the equation, the following expression can be obtained:

$$X(s) = \frac{(s + \xi\omega_n)x(0)}{(s + \xi\omega_n)^2 + {\omega_d}^2} + \frac{\left(\frac{v(0) + \xi\omega_n x(0)}{\omega_d}\right)\omega_d}{(s + \xi\omega_n)^2 + {\omega_d}^2} \tag{3.29}$$

And by applying inverse Laplace transform to equation (3.29), the analytical expression for mass displacement can be obtained as:

$$x(t) = e^{-\xi\omega_n t}\left[x(0)\cos(\omega_d t) + \frac{v(0) + \xi\omega_n x(0)}{\omega_d}\sin(\omega_d t)\right] \tag{3.30}$$

Equation (3.30) represents an oscillatory system, due to the sinusoidal terms, with a logarithmic decrement in the amplitude of vibration. Note that, expressions for mass velocity and acceleration with respect to time can be readily derived from equation (3.30) by using common time differentiation.

Critically damped case ($\xi = 1$)*:*

In this special case, the damped natural frequency ω_d is equal to 0 and equation (3.29) can be rewritten as follows:

$$X(s) = \frac{x(0)}{s + \omega_n} + \frac{v(0) + \omega_n x(0)}{(s + \omega_n)^2} \tag{3.31}$$

By applying again inverse Laplace transform to the equation (3.31), the analytical solution for a critically damped case can be obtained as follows:

$$x(t) = e^{-\omega_n t}[x(0) + (v(0) + \omega_n x(0))t] \tag{3.32}$$

Expression (3.32) shows that the response of the system does not present an oscillatory behaviour due to the lack of sinusoidal terms. Instead, the response of the system to free-vibration non-zero initial condition would logarithmically decay to the equilibrium point.

Over-damped case ($\xi > 1$)*:*

The solution process for this case is much longer and tedious than in the other two cases. So, for brevity and clarity of the section, only the final time-domain expression for displacement has been presented.

$$x(t) = \frac{1}{2\omega_n\sqrt{\xi^2 - 1}}\left[Ae^{\left(-\xi + \sqrt{\xi^2 - 1}\right)\omega_n t} + Be^{\left(-\xi - \sqrt{\xi^2 - 1}\right)\omega_n t}\right] \tag{3.33}$$

Where $A = v(0) + \omega_n x(0)[\xi + \sqrt{\xi^2 - 1}]$

$B = -v(0) + \omega_n x(0)[-\xi + \sqrt{\xi^2 - 1}]$

As in the previous case, equation (3.33) represents an exponential decay to the equilibrium condition. However in this case, the decay is slower than in a critically damped system due to the $-\xi + \sqrt{\xi^2 - 1}$ factor added to the exponential function.

Equations (3.30), (3.32) and (3.33) represent the transient response of a damped SDOF system incorporating an ideal inerter subject to a non-zero initial condition. In this section, the initial conditions considered to run the study are presented in the following table:

Initial displacement x(0)	0.2 m
Initial velocity v(0)	0 m/s

Table 3-3: Initial conditions for transient analysis

By setting these initial conditions, a system being subjected to a step input of amplitude 20 cm at t=0 sec can be simulated.

Two different tests have been run: the first one, in the under-damped region; and the second one, in the transition from over-damped to under-damped region. In order to do so, two different values of damping coefficient have been set.

Test	**Damping Coefficient**
Under-damped	1000 N/m/s
Transition	3465 N/m/s

Table 3-4: Damping coefficients used in simulation

For each of these tests, three different levels of inertance have been applied to study the effect of inerters in the transient behaviour of the system. Figure 3-8 and Figure 3-9 show the transient response for an under-damped and a near critically damped system respectively.

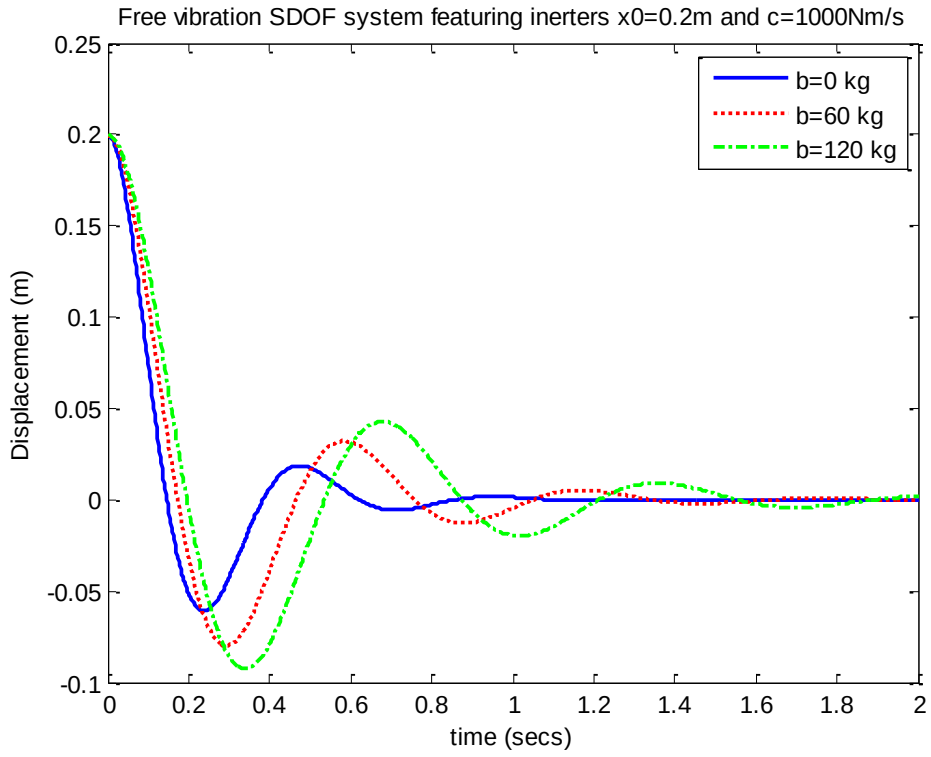

Figure 3-8: Transient response of the system in the under-damped region

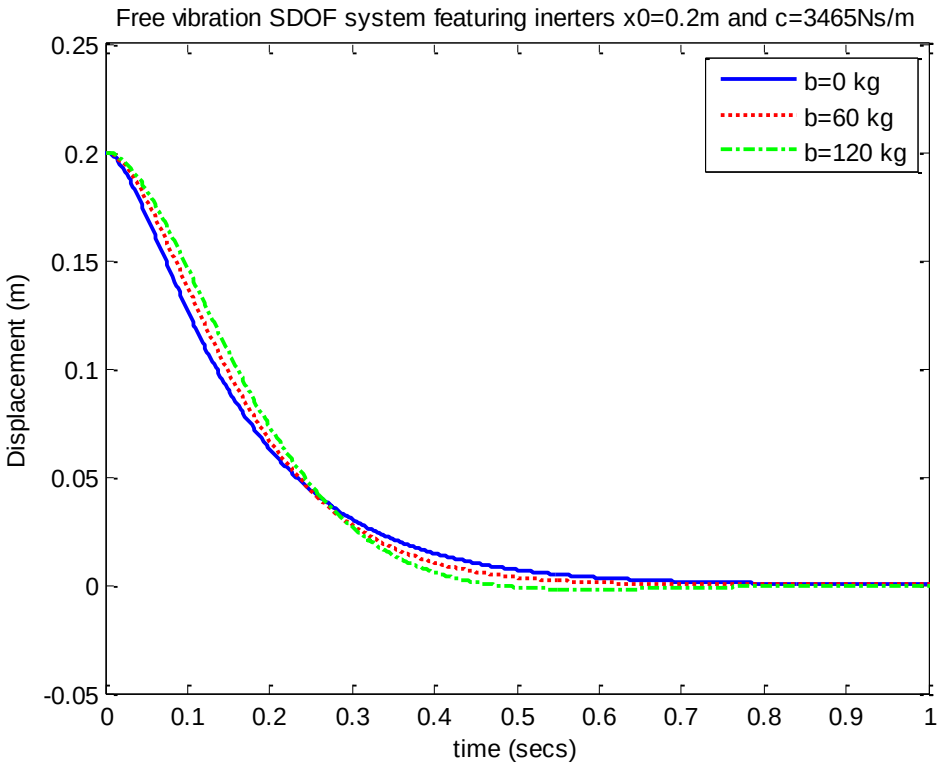

Figure 3-9: Transient response of the system in the transition region

Furthermore, Table 3-5 summarises the changes in natural frequency ω_n, damping ratio ξ and settling time τ_s for the three different inerter settings, where settling time can be defined for an under-damped system as follows:

$$\tau_s = \frac{\ln(0.02)}{\xi \omega_n} \tag{3.34}$$

Results in Table 3-5 show that, according to the results obtained from the frequency domain analysis, an increase in inertance *b* causes a decrease of the natural frequency. This increase of inertance *b* also induces a reduction of the overall damping ratio of the system which leads to a more oscillatory transient response (see Figure 3-8). The increase of inertance *b* also causes an increase in the settling time meaning that the response of the system will be slower.

	b= 0 kg	**b= 60 kg**	**b= 120 kg**
Natural Frequency (ω_n)	14.14 rad/sec	11.18 rad/sec	9.53 rad/sec
Damping Ratio (ξ)	0.35	0.28	0.24
Settling Time (τ_s)	0.782 sec	1.252 sec	1.721 sec

Table 3-5: Results of the transient response with c = 1000 Ns/m

Table 3-6 summarises the changes in natural frequency ω_n, damping ratio ξ and for the three different inerter settings in the near critically damped case study. Results from Figure 3-9 and Table 3-6 show that, as in the previous case study, both natural frequency ω_n and damping ratio ξ decrease as inertance b increases. In this case, additional inertance on the system has changed the over-damped response to an under-damped response.

	b= 0 kg	**b= 60 kg**	**b= 120 kg**
Natural Frequency (ω_n)	14.14 rad/sec	11.18 rad/sec	9.53 rad/sec
Damping Ratio (ξ)	1.22	0.97	0.83

Table 3-6: Results of the transient response with c = 3465 Ns/m

3.4.3. Study of sensitivity

The final part of this section has been devoted to studying the behaviour between an inerter and a damper. In order to do so, sensitivity study has been carried out. The variable of study in the sensitivity analysis is the overall damping ratio of the system. The nominal parameters used in this study are presented in Table 3-7.

Mass (M)	100 kg
Spring stiffness (k)	20000 N/m
Damping Coefficient (c)	3465 N/m/s
Inertance (b)	50 kg

Table 3-7: Parameters used for sensitivity analysis

The parameters from Table 3-7 have been chosen so that the initial damping ratio is equal to 1. Damping and inertance values have been swept in a range of ±50% from their nominal values and overall damping ratio has been obtained.

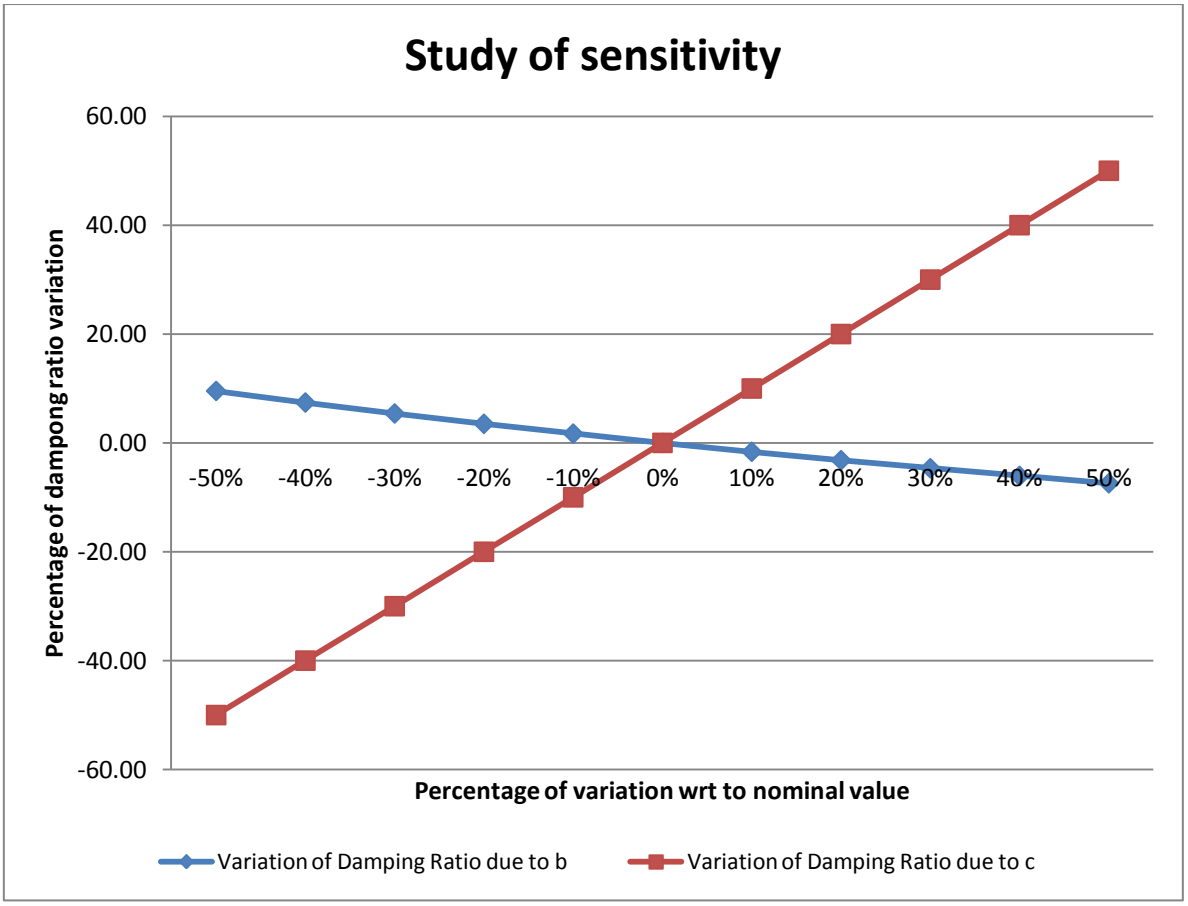

Figure 3-10: Study of damping ratio sensitivity against damping coefficient and inertance

As expected from previous analyses, the modification of damping and inertance has opposite consequences in the variation of damping ratio. Figure 3-10 shows that the influence of the damping coefficient *c* in the variation of the damping ratio of the system is much higher than the influence of the inertance *b*.

This relationship between these two parameters can be very useful in the design of mechanical vibratory systems. The variation of the damping coefficient could be considered as a coarse adjustment of damping ratio of the system; while the fine adjustment would come from the variation of the inertance value.

3.5. Summary

The aim of this chapter was to study and analyse the effect of ideal inerters in simple vibratory mechanical systems, prior to considering how these can be realised and how they behave in practical systems. Section 3.2 defined the inertance characteristics of an ideal ball screw mechanical inerter. Section 3.3 introduced the equations of motion for an un-damped SDOF system fitted with inerters under forced vibration situation and a steady-state analysis has been carried out in order to outline the basic properties of an ideal inerter in simple vibratory systems. In section 3.4, this study has been generalised for a system that accounted for damping effects. Steady-state and transient responses have been analysed for a range of damping and inertance values. Finally, a sensitivity analysis has been carried out in order to study the relative impact of inerters in the overall damping ratio of a vibratory system.

Several conclusions can be drawn from this chapter:

- Increasing the value of inertance causes a decrease in both the natural frequency of the system ω_n and the amplitude $A(\omega)$ at the resonant peak. This is due to an increase in the dynamic effective mass $M_{eff}=M+b$ of the system.

- The addition of an ideal inerter in an un-damped system causes a phenomenon of vibration absorption. The frequency at which this phenomenon takes place is known as the absorption frequency ω_{abs}. In the damped case, this phenomenon still persists. However, higher values of damping lead to a decrease of the vibration absorption effectiveness.

- Phase lead is an important characteristic introduced by the use of inerters. This characteristic helps to compensate the phase lag experienced by the system as it reaches its resonant frequency. Higher values of inertance increase the effectiveness of the phase compensation.

- Frequency domain analysis suggests that a higher value of inertance is beneficial at low frequencies (around the ω_n) and can be desirable because it offers an enhanced body mode control and, to some extent, depending on damping, a vibration absorption effect. However, at high frequencies (far away from the ω_n), lower values of inertance would be more beneficial. Low inertance values will promote better vibration isolation at high frequencies.

- Transient analysis suggests that increased inertance values reduce the effective damping ratio of the system. This study suggests that inerters could be used to fine tune the transient characteristics of a system.

- Sensitivity studies reveal that tuning the damping coefficient and the inertance value have opposing consequences in the damping ratio. The impact of damping variation in the effective damping ratio is larger than the impact of inertance variations.

This chapter has characterised the behaviour of simple ideal dynamic systems fitted with inerters. The characteristic response in frequency and time domain of a SDOF system with and without damping effects has been obtained. The study carried out in this chapter sets the foundation above which a novel vehicle suspension model incorporating real mechanical inerters has been developed.

4. Experimental Design

4.1. Introduction

The theoretical study carried out in the chapter 3 showed that potential benefits can be obtained from the use of ideal inerters in dynamic systems. The next step in this suspension design and optimisation process is to construct a physical vehicle suspension fitted with mechanical inerters that will allow experiments to be carried out in order to investigate suspension performance capabilities.

Regardless of the product being designed, a generic design process for the development of mechanical components and assemblies can be composed of six general steps (Ullman, 1997). In each phase, a number of tasks need to be accomplished before moving to the next stage. Figure 4-1 shows a typical representation of a generic design process. Although the process has been depicted as a linear sequence, design is often an iterative process where outcomes from one stage feed information into the previous ones.

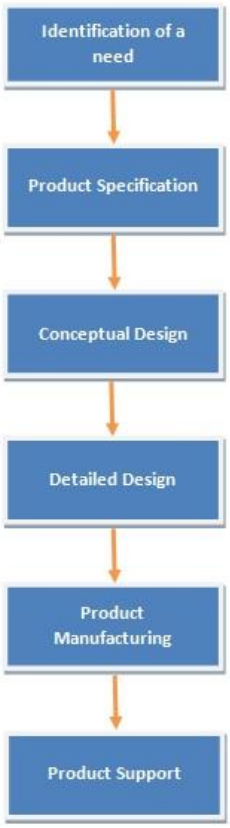

Figure 4-1: Generic mechanical design process

The first part of this chapter has been devoted to the design of the experimental apparatus according to the mechanical design process depicted in Figure 4-1. The design process consists of two parts: firstly, design and manufacturing of mechanical inerters; and, secondly, re-design and modification of a former Formula Student steel space-frame chassis in order to accommodate the changes to the suspension and layout.

In the second part of the chapter, the experimental test facilities used in the present research work have been described. The working principle of the Multimatic 4-post rig test facility has been presented. Furthermore, this chapter describes the rig test instrumentation system and calibration procedure required to acquire robust, reliable experimental data. The last part of this chapter has been devoted to describing the method used to analyse raw data obtained from the data acquisition system and to estimate vehicle suspension experimental parameters.

4.2. Design of Racing Car Suspension incorporating Real Inerters

The design process shown in Figure 4-1 focuses on the design and development of commercial products. However, most of this process is still valid for the design of research experimental components. According to this design process, the first stage is the identification of a need. In this thesis, the design and manufacture of a test car incorporating real inerters for experimental investigation represents this need. This design consists of two parts:

- Design and manufacture of real inerters
- Design and manufacture of a test vehicle capable of accommodating the inerter alongside the conventional suspension devices.

Due to the nature of the research work, the output of the design process is a prototype chassis incorporating real inerters. According to this, the last stage in the generic process depicted in Figure 4-1 does not apply to this thesis.

4.2.1. Design of a Mechanical Inerter

The process followed to design a physical inerter is summarised in the following figure:

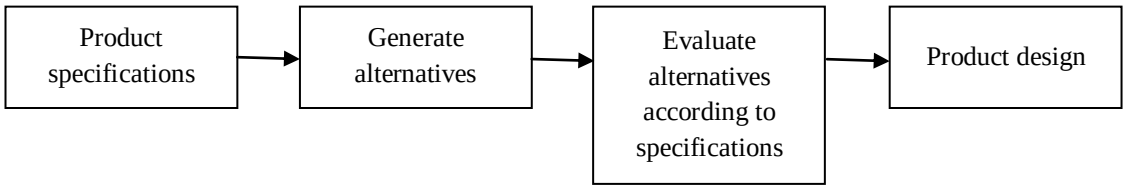

Figure 4-2: Specific design process of a physical inerter

The first stage of this design process is to define a set of engineering specifications, which will be used as decision criteria in the selection of the most suitable alternative concept. The following design specifications are critical for the design of a physical inerter:

- Design simplicity
- Weight
- Packaging
- Reliability
- Maintenance
- Adjustability
- Interchangeability
- Potential parasitic effects

An ideal inerter is defined as "a mechanical one-port device such that the equal and opposite force applied at the nodes is proportional to the relative acceleration between the nodes" Smith (2002). In order to generate a force proportional to the acceleration between terminals several design solutions have been proposed:

- Rack-and-pinion-type inerter
- Ball-screw-type inerter
- Hydraulic-type inerter

In order to select the most suitable design solution, these design alternatives must be evaluated according to the design criteria identified. The inerter mechanism must be simple. This simplicity would be translated into fewer mechanical components and a leaner manufacturing process. The mechanical complexity of ball-screw inerters is low due to the

small amount of mechanical components making up the device. Rack-and-pinion inerters are more complex than ball-screws inerters because gearing systems need to be designed and manufactured in order to translate the relative translational motion between inerter' terminals into rotational motion of the flywheel. Hydraulic inerters are the most complex option. The design of hydraulic inerters must include the selection of a proper working fluid, design of hydraulic lines and valves, and selection of a hydraulic pump and reservoir.

In racing applications, weight and packaging are important design variables in order to maximise the performance of the vehicle. Due to the amount of components required on a rack-and-pinion inerter, this option would not be well-suited in terms of packaging and weight requirements. Hydraulic inerters offer high inertance-to-weight ratios provided a proper hydraulic circuit design; therefore they are the best option for weight and spatial savings. Ball-screw inerters present a compromise solution compared to the other two options. The design is compact but the fact that they need to run flywheels in order to generate the inertance characteristic (see equation (3.6)) increases its weight.

Although the inerters designed in this research work are prototypes, reliability and maintenance are important specifications since the devices are meant to be tested under cyclic dynamic suspension loads. All three options present similar profiles in terms of reliability and maintenance, with the hydraulic option being the best one. Rack-and-pinion and ballscrew inerters require periodic lubrication in order to avoid wear and excessive friction.

Another important design factor is adjustability and interchangeability. During a racing season, GP cars need to race under different track layouts, environmental conditions, etc. Race car systems must be able to provide a range of adjustability so that maximum performance can be achieved regardless of these changing conditions. Moreover, components must be designed so that minimum time is spent during the replacement of components. Hence, the ability to tune the characteristic property of the device and the possibility of replacing it efficiently are then desirable. All options offer potentially good adjustability either by modifying the gear ratio, changing the inertia of the flywheel or redistributing the flow around a hydraulic pump.

Another aspect to take into consideration is the deviation of a real inerter from its ideal behaviour. Parasitic effects such as backlash, gear-play, friction, compliance, hydraulic pressure losses and/or fluid compressibility contribute to this deviation from ideal behaviour. Rack-and-pinion systems often suffer from gear-play. Tight manufacturing tolerances will

help to reduce this effect. Ball-screw mechanisms present friction and backlash problems, although, in this case, backlash can be solved by preloading the balls of the screw. Furthermore, lubricants create a protective film between two moving parts that allows two solid surfaces to be separated and therefore friction can be minimised. Finally, hydraulic inerters have been deemed to produce a large deviation from ideal behaviour (Wang, et al., 2011).

A decision matrix for the selection of the inerter design solutions has been produced taking into consideration all the above criteria (see Table 4-1). In this decision matrix, weighting factors have been set in order to rank the different contribution of design criteria towards the selection of the final design solution. Moreover, scores have been given to each design solution according to their individual contribution towards the accomplishment of the criteria.

Criterion	**Weighting factor (%)**	**Physical inerter design solutions**					
		Rack-and-pinion		**Ball-screw**		**Hydraulic**	
		Raw	**Weighted**	**Raw**	**Weighted**	**Raw**	**Weighted**
Design simplicity	20	50	10	90	18	20	4
Weight	15	20	3	50	7.5	60	9
Packaging	15	10	1.5	70	10.5	90	13.5
Reliability	10	65	6.5	75	7.5	80	8
Maintenance	10	35	3.5	30	3	90	9
Adjustability	15	70	10.5	80	12	90	13.5
Interchangeability	10	40	4	60	6	80	8
Potential parasitic effects	5	60	3	90	4.5	20	1
TOTAL	**100%**		**42%**		**69%**		**66%**

Table 4-1: Decision matrix for physical inerter design solutions

According to this decision matrix, the highest overall score corresponds to a ball-screw-type inerter. Once the appropriate mechanism has been selected, the next step of the design process is to proceed with the conceptual design (see Figure 4-1). At this stage, the general basic component layout has been drafted following the designs proposed in Wang *et al.* (2009). From this concept design, the main components of the inerter device have been identified. Moreover, recalling the definition of the working principle of a ball-screw inerter carried out in Chapter 3, the characteristic inertance b depends on the inertia of the flywheel I_{fw} and the lead of the screw l (see equation (3.6)). Hence, adjustments in inertance

characteristic b can be carried out by adjusting either inertia of the flywheel I_{fw} or the lead of the screw l. Since the lead of the screw cannot be modified once it has been manufactured, the inertia of the flywheel I_{fw} becomes the only parameter capable of adjusting the inertance characteristic b.

The next step is then to continue with the detailed mechanical design of the inerter components. The most complex part in the design of the inerter in terms of manufacturing complexity is the ball-screw mechanism itself. Furthermore, this component requires precision machining, special surface shaft treatments and ball preloading. Due to this manufacturing complexity, the ball-screw mechanism was decided to be purchased from THK, a manufacturing company specialised in linear guide and ball-screw mechanisms (THK Co., Ltd., 2012). Therefore, components of the ball-screw mechanism have been designed following the dimensioning procedure provided by specialist manufacturer THK (THK Co., Ltd., 2012). In addition to this, a set of design requirements must be defined in order to proceed with this dimensioning procedure. In the present research work, three basic requirements have been identified in order to design a real inerter:

- Maximum relative displacement between inerter terminals x_{strutD}.
- Maximum relative velocity between inerter terminals v_{strutD}.
- Maximum relative acceleration between inerter terminals a_{strutD}.

Design values for these requirements have been obtained from Bahrain GP race track profile data available. In order to select those values, it has been assumed that inputs from race track are applied directly to the suspension (worst case scenario). According to this, x_{strutD} has been obtained from maximum track elevation difference. v_{strutD} has been calculated from maximum track elevation gradient assuming a car travelling at v_x=90 m/s (324 kph)[2]. In a similar way, maximum race track elevation acceleration has been used to obtain a_{strutD}. In addition to this, a safety factor has been applied to all three design requirements. Table 4-2 shows the design requirements used to design the ball-screw mechanism.

[2] This forward velocity represents standard top speed recorded for current F1 cars **Fuente especificada no válida.**.

Max. Strut displacement	100 mm
Max. Strut velocity	1 m/s
Max. Strut acceleration	10g

Table 4-2: Ball-screw mechanism design requirements

The result of this dimensioning process is the selection of a ball-screw mechanism that meets the requirements expressed in Table 4-2. The manufacturer's product code for the mechanism selected in this research work is BLR1616-3.6. Table 4-3 summarises the main characteristics of this product.

Shaft outer diameter $ø_{shaft}$	16 mm
Lead of screw l	16 mm
Nut characteristic	Double-ring precision nut

Table 4-3: Ball-screw mechanism specfications

Next, the flywheel has been designed as a set of interchangeable steel disks that can be added or removed from the inerter device. A special flywheel mount disk was also designed to attach the flywheel disks to the rotating ring of the nut. An aluminium casing was designed to provide one of the terminals of the inerter. The other terminal was located on the opposite side of the shaft. Both terminals were designed as spherical rod end joints.

Two different sets of flywheel disks are designed in order to provide full range of adjustment: thin disks (2-mm thickness) for fine adjustability and thick disks (4-mm thickness) for coarse adjustability. By using equation (3.6), Table 4-4 provides the calculated mass and inertia properties for each type of disk.

Disk type	**Disk thickness (mm)**	**Total inertia ($kgcm^2$)**	**Inertance (kg)**	**Total mass (gr)**
1	2	0.63	**8.6**	74.0
2	4	1.26	**19.4**	148.0

Table 4-4: Range of adjustability of ball-screw inerter

Note that, at full capacity, the inerter weights 2.2 kgs. and is capable of providing 238 kgs. of inertance.

All components discussed earlier have been modelled in Solidworks 2009 (Dassault Systems Solidworks Corp., 2012). The final 3D CAD assembly of the inerter is shown in Figure 4-3.

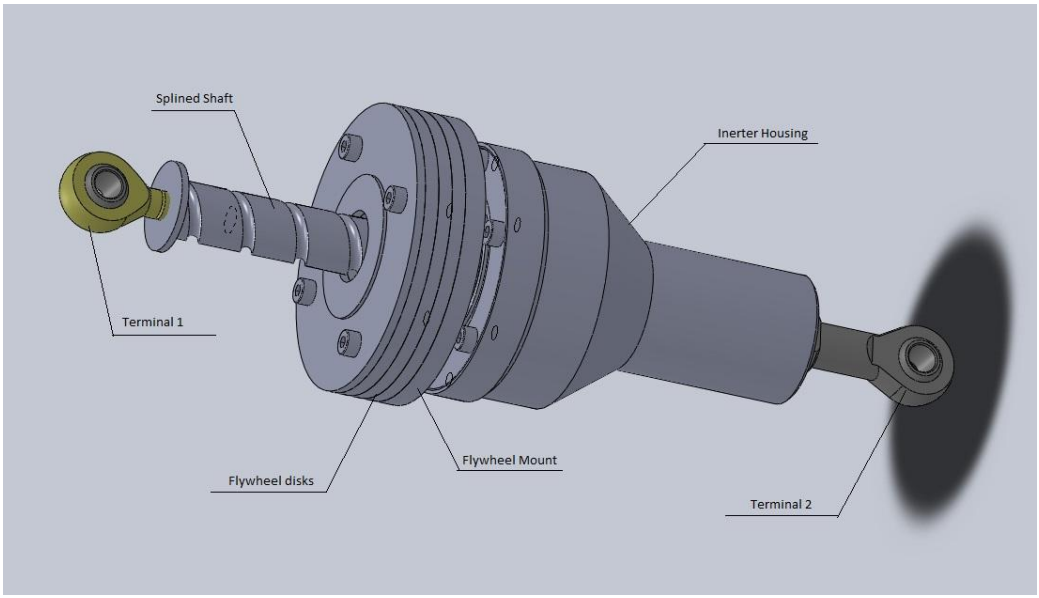

Figure 4-3: Detailed 3D CAD design of a ball-screw inerter

Once the detailed design was finished, 2D drawings of each component were produced, and manufactured. The result was a prototype of a ball-screw inerter, as shown in Figure 4-4.

Figure 4-4: Photograph of a prototype inerter: a) Inerter assembly and b) Principal components

4.2.2. Design of a prototype test car

A design process similar to the one explained in the previous section has been followed here. A test car must be designed and manufactured in order to test the interaction of real inerters with other suspension elements. In order to minimise the costs attributed to the design and manufacturing a specific chassis, suspension arms and racing tyres, the new suspension has been designed around an existing OBU Formula Student car. The original chassis was a steel tubular space-frame equipped with independent double wishbone suspension and inboard

spring-dampers at all four corners. The car was also provided with used racing tyres. No engine, power-train or steering systems were required, since the present thesis focuses on the analysis of ride dynamics.

The main focus in this section is the re-design of the suspension geometry and layout in order to accommodate the new components. This re-design includes the definition of all suspension components excluding suspension arm hard-points as well as the design of new pullrods (front) and pushrods (rear), rockers, bracket mounting, anti-roll bars (ARBs) and heave spring-dampers.

The design of the new suspension system can be then split into two areas: kinematic and dynamic design. In both cases, the major specifications to be taken into consideration in order to carry out the design process of the new suspension are simplicity, adjustability and reliability. Suspension components have been designed to be as simple as possible to facilitate manufacturing and reduce costs. Adjustability is important to allow flexibility in the study of suspension optimisation. And finally, all components have been designed and manufactured to endure the loading cycles the test facility will subject them to.

The first step of the detailed design process has been to modify the chassis. Following the principle of simplicity, only minimal structural modifications of the chassis have been applied. Cross bars have been added in the cockpit space in order to increase the torsional stiffness of the chassis. The weight of the driver has been recreated by using sand bags strapped to the chassis as ballast. The weight of the engine, gearbox and differential has been replicated by pieces of solid steel attached to the chassis in order to keep the fore/aft balance of the car as close to 50/50 weight distribution as possible.

The next step in the design process has been to design the kinematics of the suspension. This includes the definition of a new suspension layout. A new suspension geometry is required in order to accommodate and package all the suspension components in the space available. The new suspension layout must account for the following considerations:

- Each corner of the car is equipped with an inboard spring-damper unit.
- Anti-roll bars are used on both axles. The ARB design consists of a solid torsion bar connected to each of the rockers via a lever arm and a drop link on each side.

- A 3rd spring-damper unit can also be added to the suspension in order to control heave axle excitations at both ends of the car. These devices are connected between rockers.

- Front axles are equipped with two inerters connected from the rocker to the chassis; meanwhile the rear axle is equipped with one axle inerter connected between rockers

According to this, both front and rear rockers have been completely re-designed in order to accommodate all the new components mentioned previously. Rear rockers have also been placed in a new location with respect to the previous design for better packaging.

Furthermore, following the principle of adjustability, rockers have been designed so that different suspension characteristics can be obtained. All rockers present 3 different pull-rod/push-rod joint points, so that, by changing this position, different motion ratios can be induced, therefore modifying the spring and damper rates experienced at the tyre contact patch. Since no steering system was provided, steering links have been welded to the front wishbones in order to avoid undesired tyre steering vibrations.

3D kinematic models of front and rear suspensions have been created in the multibody dynamics (MBD) software MSC.Adams R3 (MSC Software, 2012). Figure 4-5 and Figure 4-6 show the layout of the new front and rear suspension respectively. Components have been colour-coded to facilitate their identification within the model (see Table 4-5).

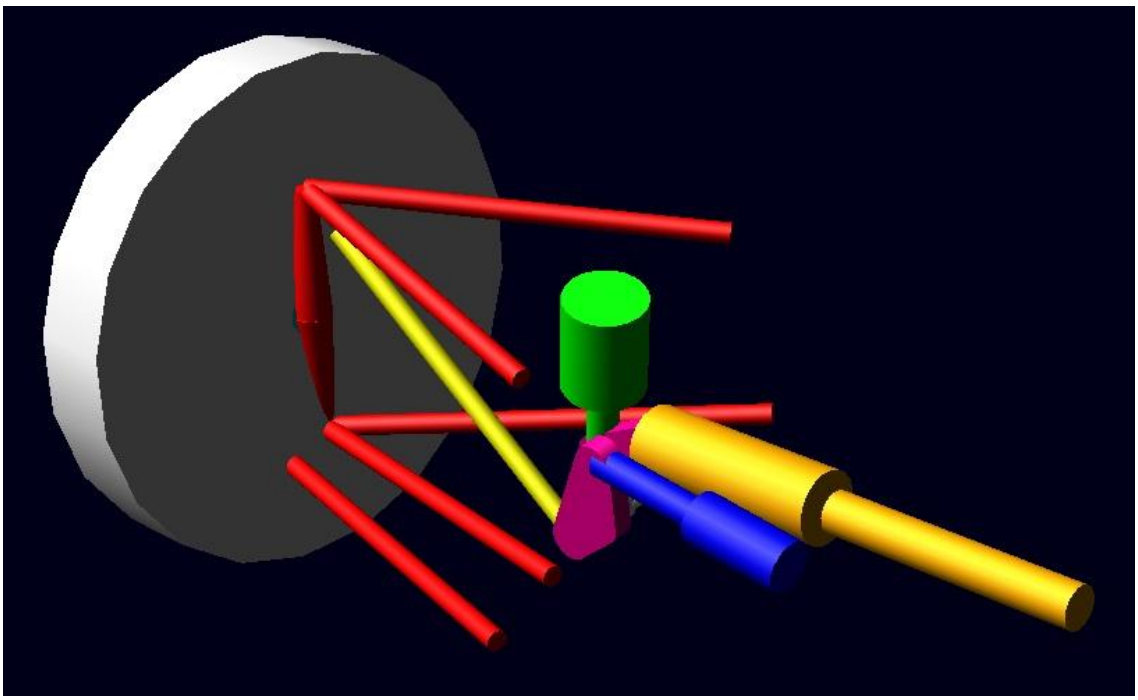

Figure 4-5: 3D MBD kinematic model of re-designed front suspension

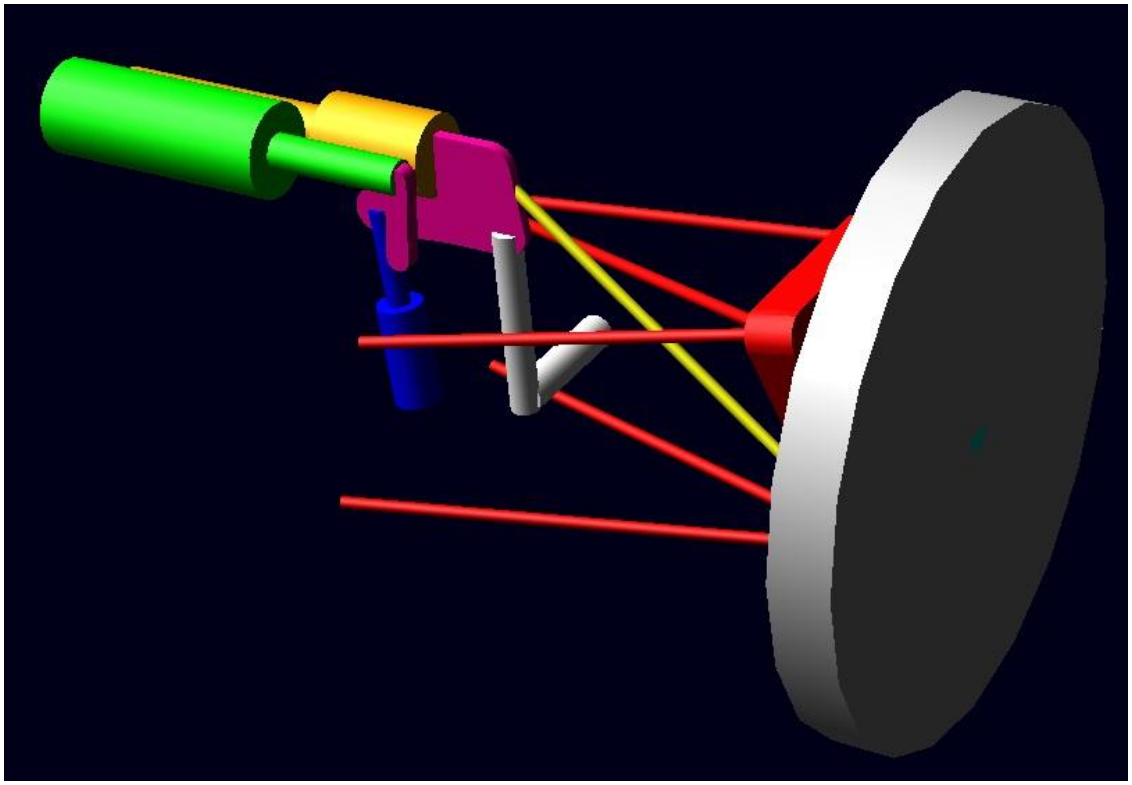

Figure 4-6: 3D MBD kinematic model of re-designed rear suspension

Colour	Suspension Component
Silver	Wheel and tyre assembly
Red	Suspension arms and upright
Yellow	Pull-rod (front) and push-rod (rear)
Magenta	Rocker
Blue	Corner spring-damper unit
Green	Inerter
Orange	Axle spring-damper unit
White	ARB drop link and lever arm

Table 4-5: Colour-coded key table for MBD suspension models

The main purpose of these models was to evaluate the packaging and the kinematic movement of the suspension. Accordingly, these kinematic MBD models have been used to define the suspension layout and the location of the attachment positions of the new suspension components to the rocker, on one end, and to the chassis, on the other end. These hard points have been designed to provide a near constant installation ratio (IR) between wheel vertical travel and suspension components along the suspension movement range due

to the fact that it will facilitate future suspension modelling and analysis since the IR can be considered a constant value.

Once the kinematic model was finished, a 3D CAD model of the re-designed vehicle was produced. All components were designed and assembled into the chassis in Solidworks 2009 (Dassault Systems Solidworks Corp., 2012).

The final stage of the design process was devoted to the design of the suspension from a dynamic point of view. In this phase, spring stiffnesses of elastic components and damping rates have been defined. The main specification has been adjustability. The suspension has been designed so that it was possible to achieve a stiffness range from a relative softly sprung car (ride frequency of about 1.5 Hz) up to a heavily sprung car (ride frequency over 6 Hz). These limits would correspond to suspensions for production sports cars for the lower bound of the ride frequency range and to suspensions for high performance competition cars with aerodynamic effects, such as Formula 1 cars, for the upper bound. Table 4-6 shows a summary of the design spring stiffness required to achieve a particular suspension ride frequency for one of the rear corners.

Four sets of springs have been selected: 100 (17.5), 200 (35), 350 (61.3) and 500 (87.6) lb/in (N/mm)[3]. This range covers a ride frequency from 1.5 to 4 Hz (see Table 4-6). Ride frequency could be further increased by adding a 3rd spring to the axle. A similar table could be produced in order to select the appropriate ride frequency for the axle spring. Two sets of axle springs were selected: 900 (157.6) and 1100 (192.6) lb/in (N/mm).

[3] Spring manufacturers typically provide spring stiffness specifications in imperial units

		Spring Rate (N/mm)			Spring Rate (lb/in)		
		Installation Ratio			Installation Ratio		
Ride frequency (Hz)	Wheel Rate (N/mm)	1.5	1.67	1.89	1.5	1.67	1.89
1.5	5.6	12.5	15.5	19.9	71.4	88.5	113.4
1.6	6.3	14.3	17.7	22.6	81.2	100.7	129.0
1.7	7.2	16.1	20.0	25.6	91.7	113.7	145.6
1.8	8.0	18.1	22.4	28.7	102.8	127.4	163.2
1.9	8.9	20.1	24.9	31.9	114.6	142.0	181.9
2	9.9	22.3	27.6	35.4	126.9	157.3	201.5
2.1	10.9	24.6	30.5	39.0	140.0	173.5	222.2
2.2	12.0	27.0	33.4	42.8	153.6	190.4	243.8
2.3	13.1	29.5	36.5	46.8	167.9	208.1	266.5
2.4	14.3	32.1	39.8	50.9	182.8	226.6	290.2
2.5	15.5	34.8	43.2	55.3	198.3	245.8	314.9
2.6	16.7	37.7	46.7	59.8	214.5	265.9	340.6
2.7	18.1	40.6	50.3	64.5	231.3	286.8	367.3
2.8	19.4	43.7	54.1	69.3	248.8	308.4	395.0
2.9	20.8	46.9	58.1	74.4	266.9	330.8	423.7
3	22.3	50.1	62.2	79.6	285.6	354.0	453.4
3.2	25.4	57.0	70.7	90.6	325.6	402.8	515.9
3.5	30.3	68.2	84.6	108.3	388.8	481.9	617.2
4	39.6	89.1	110.5	141.5	507.8	629.4	806.1
4.5	50.1	112.8	139.8	179.1	642.6	796.5	1020.2
5	61.9	139.3	172.6	221.1	793.4	983.4	1259.6
5.5	74.9	168.5	208.9	267.6	960.0	1189.9	1524.1
6	89.1	200.6	248.6	318.4	1142.5	1416.1	1813.8

Table 4-6: Spring Stiffness design matrix for rear suspension

The next step was to select appropriate damping rates for the full range of ride frequencies. Dampers have been selected so that they were capable of producing appropriate damping characteristics for the full range of spring stiffness settings. According to this design premise, 4-way adjustable Cane Creek Double Barrel dampers (Cane Creek, 2012) were the option selected in this design because they were the only option found that could provide a wide range of damping characteristics. Furthermore, additional 3rd axle dampers could be added if additional damping was required. In order to reduce the cost of the experimental apparatus, 3-way adjustable Öhlins dampers from the Formula Renault owned by Oxford Brookes University have been used.

The anti-roll bars were also designed following the same principle of adjustability. Three sets of torsion bars were designed: Ø8 mm, Ø10 mm and Ø14 mm. Moreover, the lever arms have 3 different drop link connections. These lever arms have 3 different drop-link connections. This way, changing the torsion bars will provide a coarse roll stiffness adjustment, while fine tuning will come from changing the lever arm length.

Figure 4-7 to Figure 4-9 show 3D CAD models of the whole new test car assembly, the detail of the front suspension assembly, and the detail of the rear suspension assembly respectively.

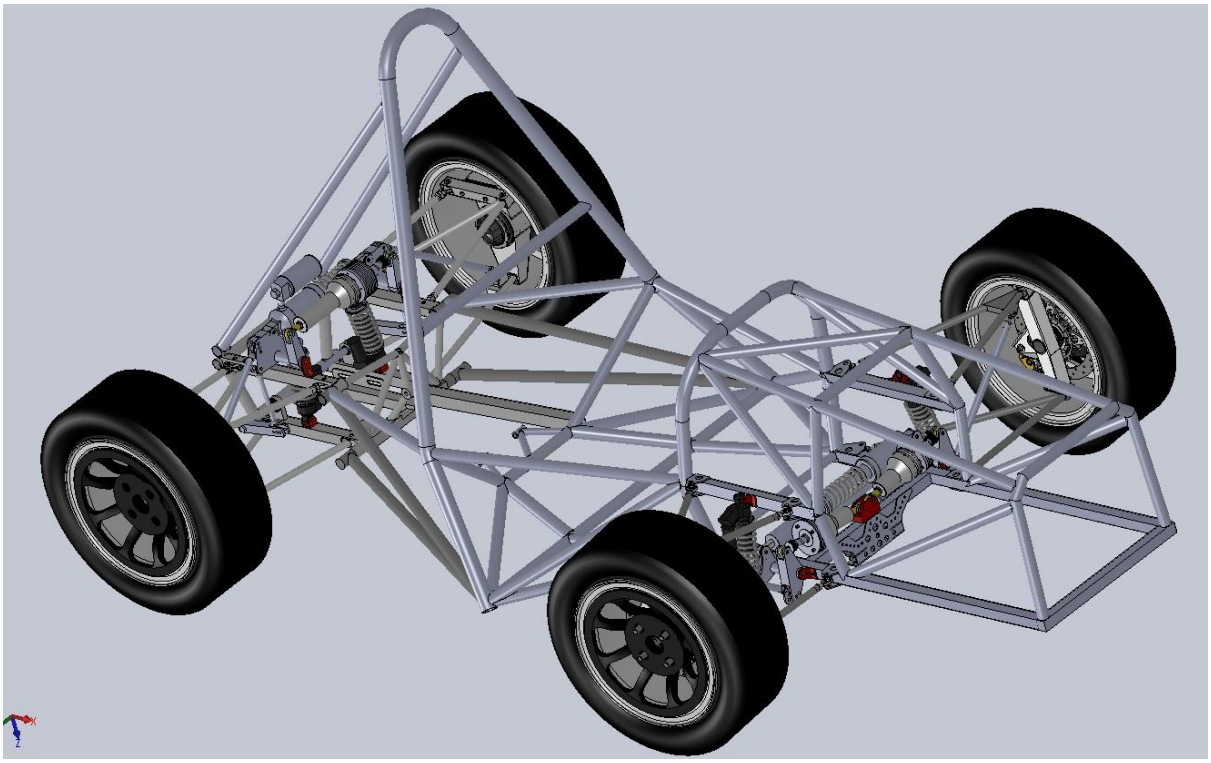

Figure 4-7: 3D CAD design of the new test car

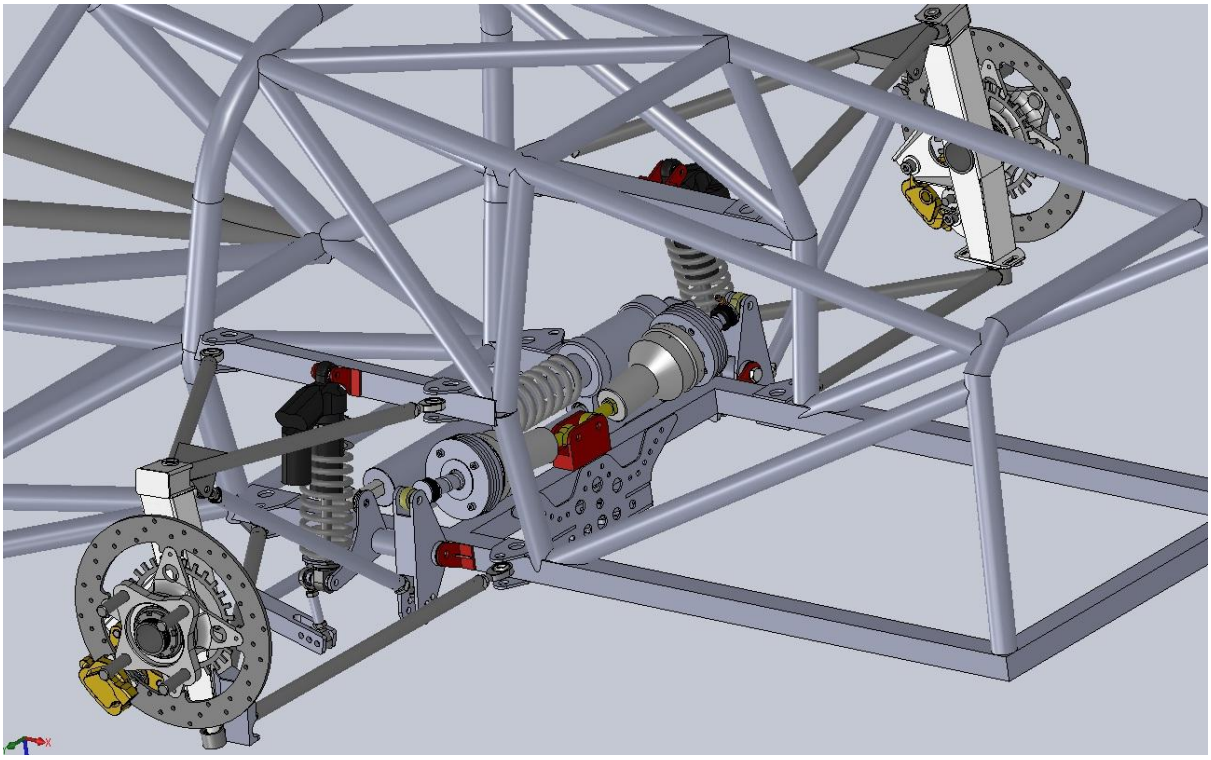

Figure 4-8: 3D CAD detailed design of the new front suspension incorporating inerter

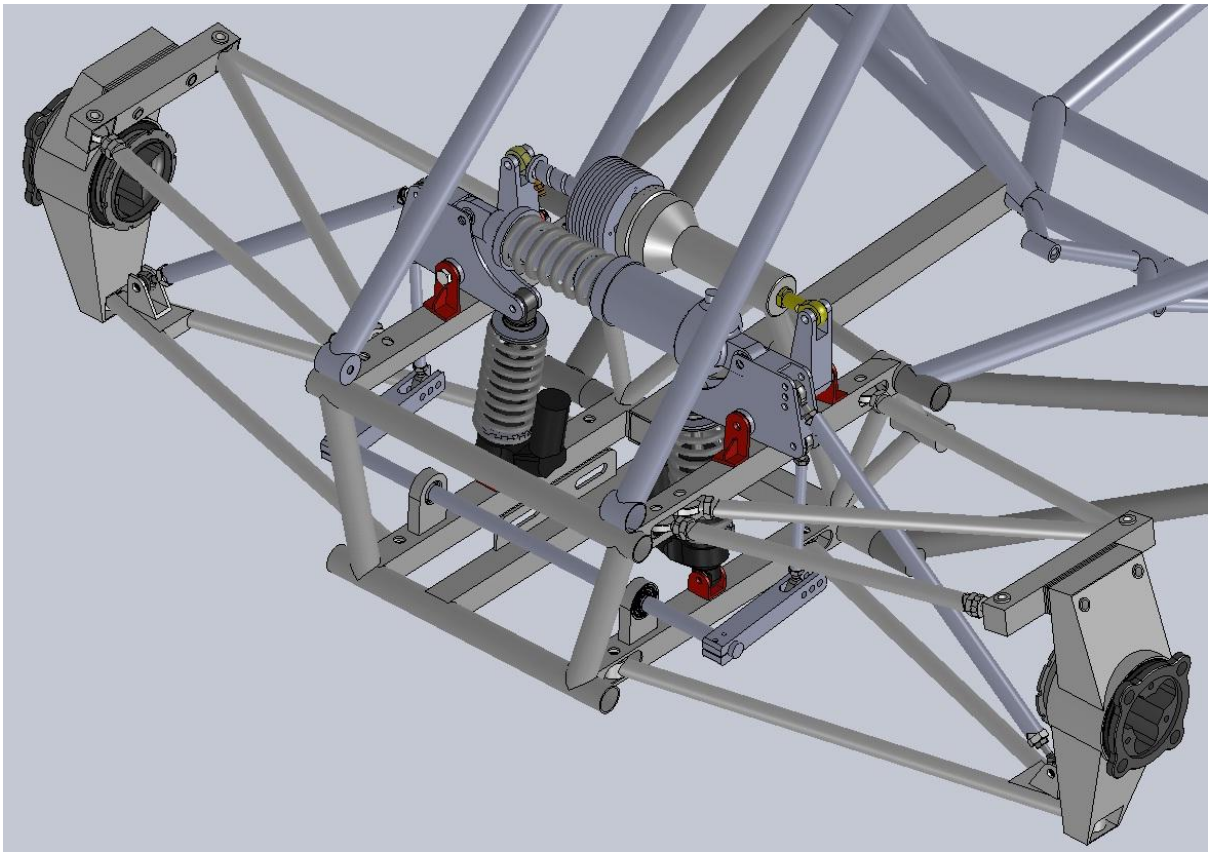

Figure 4-9: 3D CAD detailed design of the new rear suspension incorporating inerter

Finally, 2D CAD drawings for suspension components and assemblies were produced from the previous 3D models and manufactured in the OBU workshop. The final result is a reconditioned test car with inerters as shown in Figure 4-10 to Figure 4-12.

Figure 4-10: General view of the redesigned test vehicle

Figure 4-11: Test car front suspension view

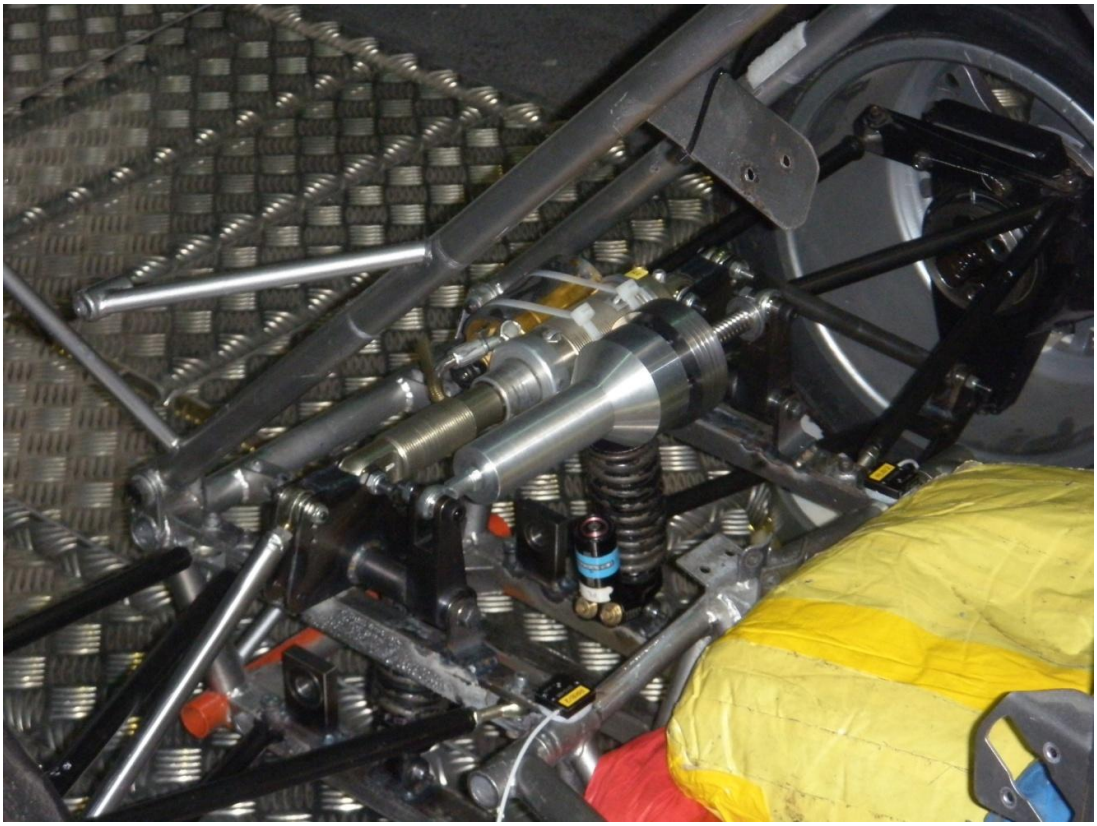

Figure 4-12: Test car rear suspension view

4.3. Experimental Test System Description

The experimental test facility used in this research work was the Multimatic four-post rig facility at Oxford Brookes University. This facility has been custom designed and installed by Multimatic Technical Centre Europe (Multimatic Technical Centre, 2011). Figure 4-13 and Figure 4-14 show the four-post rig test facility.

Figure 4-13: Upper view of OBU Four-post rig test facility

Figure 4-14: Lower view of OBU Four-post rig test facility

The four-post rig consists of three main subsystems:

- Actuation system
- Measurement and control system
- User rig computer software

A schematic representation of the components of the OBU Four-post rig has been shown in Figure 4-15.

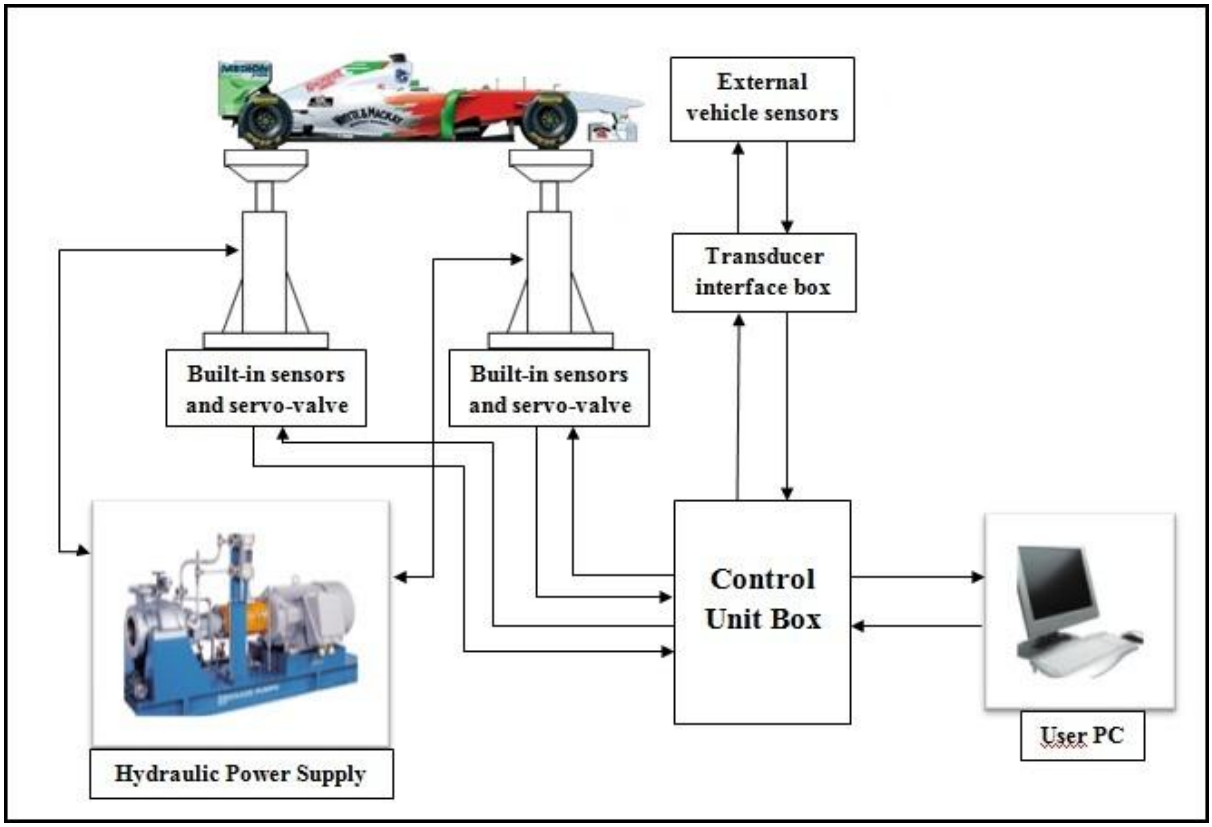

Figure 4-15: Schematic representation of 4-post rig

The actuation system is composed of four independently controlled servo-hydraulic actuators used to input forces and displacements at the tyre contact patches. An additional pneumatic actuator was provided. This pneumatic actuator is capable of producing a static downward force on the chassis. Pressure into the hydraulic system is supplied via two 210-bar fluid supply pumps.

These pumps are installed in a separate building that also contains a fluid storage reservoir, the fluid cooling system and a pump control box. There is an additional pump control box located next to user rig computer. The two pumps are variable angle swash plate pumps. Each pump is powered by electric motors capable of generating 45 kW at 415 V. Special 3-phase

electrical supplies are required to run the motors. Each pump can supply up to 210 bar pressure and 100 l/min flow rate. The pumps are arranged in parallel so they would be able to supply a maximum flow rate of 200 l/min.

The measurement and control system comprises of an electronic controller, sensor interface boxes and transducers. There are two types of transducers: 'built-in' or internal transducers and external transducers. Internal transducers are built in to the actuators. Each actuator incorporates internal transducers for measuring contact patch load and acceleration and relative actuator displacement. Readings from the internal actuator displacement transducer are fed to the control unit in close-loop control so that the controller identifies the exact position of the post and actuates the servo-control valves to produce the desired post displacement according to the target signal (road input) selected by the user. These transducers are directly connected to the electronic controller. External transducers are those related to the vehicle movement, typically body and hub accelerometers and suspension displacement potentiometers. These transducers are connected to a sensor interface box which, in turn, sends the electrical signals of these external transducers to the main control unit. The main purpose of this interface box is to act as an extension lead from the control unit. Each actuator has its own interface box. Each interface box provides connection for up to 7 different channels per corner. Figure 4-16 shows one of the transducer interface boxes.

Figure 4-16: Transducer interface box

During four-post rig operation, all the measurements (internal and externals) are sent to the electronic control unit. The functions of this unit are to control the position of the actuators and to store data from transducers. The electronic controller acts as the main interface between the rig user computer, the actuators and the measurement system. Both electronic

control unit and the actuation system are expensive pieces of equipment. By decoupling the host computer from the control and actuation systems, these systems can be protected from potential external risks associated to the user PC such as viruses or software corruption which could ultimately damage the testing equipment.

The last component of the test rig is the user software. This software is called Dynosoft MX and it is used to operate and display test data. This software is connected via a USB link to the control unit. A view of the command window is shown in Figure 4-17.

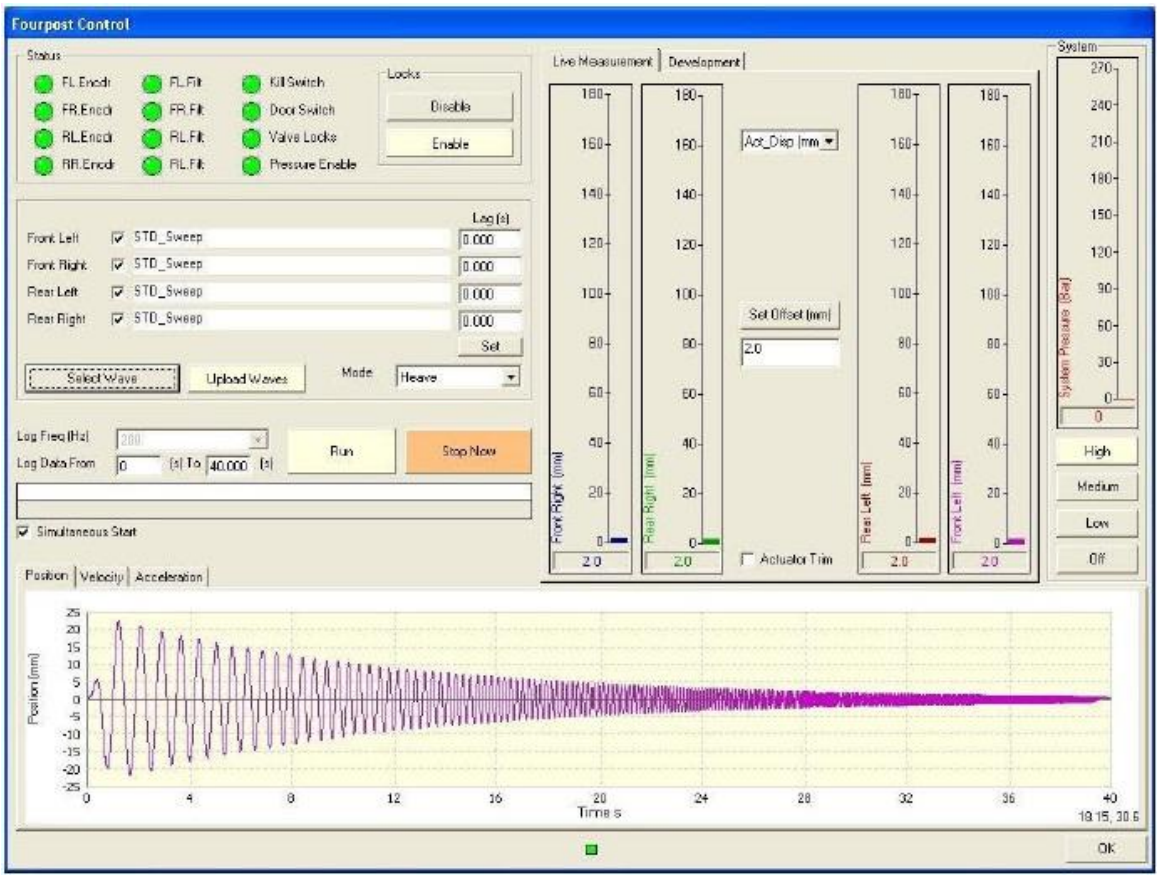

Figure 4-17: Four-post rig main command window

The main features of the software are:

- Calibration of measurement channels
- Definition and control of input waveforms, sampling rates, vibration modes
- Data acquisition, storage and export of all transducers measurements
- Display of data as a function of time and ‘XY’ plots
- Calculation of math channels and simple data processing operations

For detailed specifications, operational and a more in-depth description of the working principle of the rig, the reader is referred to the *Multimatic Four Post Technical Specification and Operating Manual* (Multimatic Technical Centre, 2011).

4.4. System calibration Procedure

Initial calibration of the Four-post Rig was carried out when the rig was commissioned in August 2008. This calibration was carried out by the Multimatic technicians and a certificate of calibration was presented. Furthermore, certified annual calibrations have been carried out during each annual service by Multimatic. The last service dates from October 2011. A copy of the certificate has been included in Appendix A. This process includes the calibration of the actuator load cells, accelerometer and displacement potentiometer as well as the calibration of the body and hub accelerometers and strut displacement string potentiometers.

In addition to this annual calibration, strut displacement string potentiometers and body and hub accelerometers calibration settings are checked regularly in order to ensure that the output data is fully reliable. Dynosoft MX software allows calibration settings monitoring and manipulation.

For suspension displacement potentiometers, the calibration check is carried out by measuring the displacement of the sensor with a vernier calliper and recording the voltage measured by the software. This process is repeated for two different displacements and calibration is obtained as the gradient of displacement to voltage. An additional intermediate displacement is used to check that the sensor has been properly calibrated.

In the case of accelerometers, the calibration check is done both dynamically and statically. Dynamically, body and hub accelerometers of each corner are fixed to their respective actuator with the PTFE pads removed. A sinusoidal input wave is applied. Measured acceleration values are then compared against the actuator pad acceleration in a XY plot. If the difference in the accelerometer outputs is more than 1% RMS then the hub and/or body accelerometer calibration settings are modified to match the slopes. This process does not offer an absolute calibration of the system; as this method is conditioned by pad acceleration. If the pad acceleration was incorrect, then the rest of calibration would be incorrect as well.

In order to overcome this limitation, an additional static accelerometer calibration is also carried out. Body and hub accelerometers are placed on a flat surface in upright position. A calibrated accelerometer should read 1g of vertical acceleration (gravity action).

Accelerometers are then turned upside down and they should read -1g. If a deviation of more than 1% from these values occurs, a scaling factor is applied to the gradient of acceleration over voltage.

An additional benefit of a combined static and dynamic method for accelerometer calibration is that it could detect potential errors of calibration in the pad accelerometers.

4.5. Parameter Determination Method

The main aims of a four-post rig can be described as:

- Estimation of suspension and vehicle parameters
- Optimisation of suspension performance
- General chassis diagnostics

In this section, special attention has been paid to the first of these objectives. Acquired parameters from experimental testing present a series of benefits: they can be used to compare experimental measurements against design variables and identify potential improvements in design (iterative design process); they can also be used to develop vehicle models in simulation. If properly validated, these models can accurately represent the real behaviour of the vehicle and could then be used to run off-line computer suspension optimisation. One of the main benefits of this process is that it produces important savings in cost, because fewer components need to be manufactured at the prototyping stage, and time for optimisation is reduced, as optimisation algorithms are capable of sweeping through hundreds of suspension set-ups in a reduced amount of time.

In this section, the operating process of the rig has been explained. Furthermore, the method for parameter estimation developed by a research student in the Department of Mechanical Engineering at Oxford Brookes University has been briefly described (Bennett, 2012). This method has been then extended so that parameters related to real inerters and nonlinear tyres can be also determined.

4.5.1. Set of parameters required

A four-post rig recreates road inputs experienced by a vehicle whilst driving on a road and/or race track. These road inputs can be typically decomposed into 4 independent vibration modes:

- Heave mode: all 4 wheel are in phase
- Pitch mode: front and rear wheels out of phase by 180º
- Roll mode: left and right wheels out of phase by 180º
- Warp or articulation mode: cross diagonal wheels out of phase by 180º

According to this, in order to simulate the response of a vehicle to all these vibration modes on a test rig, the simplest model that could be used is a simplified 7-DOF system (see Figure 4-18).

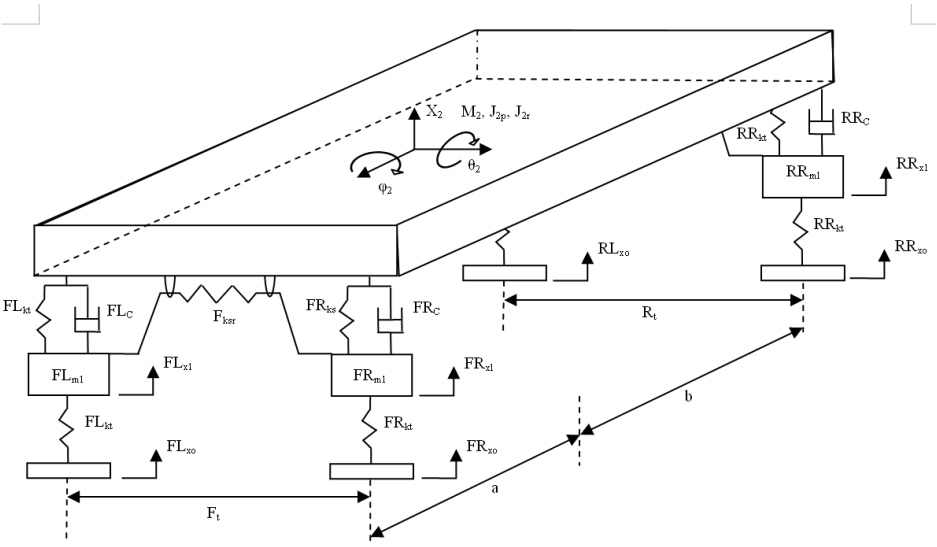

Figure 4-18: Simplified 7-DOF vehicle suspension model (Bennett, 2012)

The set of vehicle parameters required for simulating a validated model that can be estimated from experimental testing include overall vehicle dimensions, mass properties for all bodies (sprung and unsprung masses), suspension characteristics and tyre parameters.

Overall vehicle dimensions such as wheelbase *wb*, front track t_f and rear track t_r can be directly measured. All four corner weights W_{FL}, W_{FR}, W_{RL} and W_{RR} can be measured from the actuator load cells when the car is standing still (no dynamic inputs applied). The overall mass of the vehicle W_{Tot} can then be obtained by adding all four corner weights (see eq. (4.1)).

$$W_{Tot} = W_{FL} + W_{FR} + W_{RL} + W_{RR} \tag{4.1}$$

Furthermore, longitudinal weight distribution *Long_WDist*, lateral weight distribution *Lat_WDist*, diagonal weight distribution *Diag_WDist* and distances from CoG to front axle *a* and to rear axle *b* can also be calculated from corner weights using equations (4.2) to (4.6).

$$Long\_WDist(\%) = \frac{W_{FL} + W_{FR}}{W_{Tot}} \cdot 100 \tag{4.2}$$

$$Lat\_WDist(\%) = \frac{W_{FL} + W_{RL}}{W_{Tot}} \cdot 100 \tag{4.3}$$

$$Diag\_WDist(\%) = \frac{W_{FL} + W_{RR}}{W_{Tot}} \cdot 100 \tag{4.4}$$

$$b = \left(1 - \frac{Long\_WDist}{100}\right) \cdot wb \tag{4.5}$$

$$a = wb - b \tag{4.6}$$

Note that, distances a and b have been obtained from the overall longitudinal weight distribution of the vehicle. Once front and rear unsprung masses have been estimated, longitudinal sprung weight distribution *Long_WDist_Sprung* could be obtained and a and b re-calculated.

Unsprung masses, chassis inertias and suspension and tyre characteristics will require the use of dynamic inputs in order to be estimated.

4.5.2. Vehicle Instrumentation Procedure

The vehicle is instrumented with 12 external transducers arranged as follows:

- 4 Body accelerometers (1 per corner)
- 4 Hub accelerometers (1 per corner)
- 4 Strut displacement potentiometers (1 per corner)

Accelerometers are attached to the components using a thin layer of 'blu-tac'. In this way, the accelerometers can be easily removed and replaced at any other location. 'Blu-tac' also provides a flexible mounting that allows the sensors to be placed in non-horizontal surfaces. Accelerometers are aligned to the gravity field using a spirit level. In addition to this, 'blu-tac' acts as a natural high-pass filter. It filters out very high frequency contents (>50 Hz) associated with noise.

Body accelerometers have been fitted to each of the corners of the chassis. The ideal location of the accelerometers is in a stiff part of the chassis as close as possible to the vertical axis directly above the wheel centre. In this way the measurements are taken at the same points as

where accelerations are modelled in a lumped-mass dynamic vehicle model. However, due to the space-frame chassis construction, accelerometers cannot be placed exactly in this position. Instead, they are placed as close as possible to the axle centreline and as far away as possible from each other. Relative positions of all the accelerometers with respect to the wheels have then been measured. Figure 4-19 and Figure 4-20 show the location of the body accelerometers at all the corners.

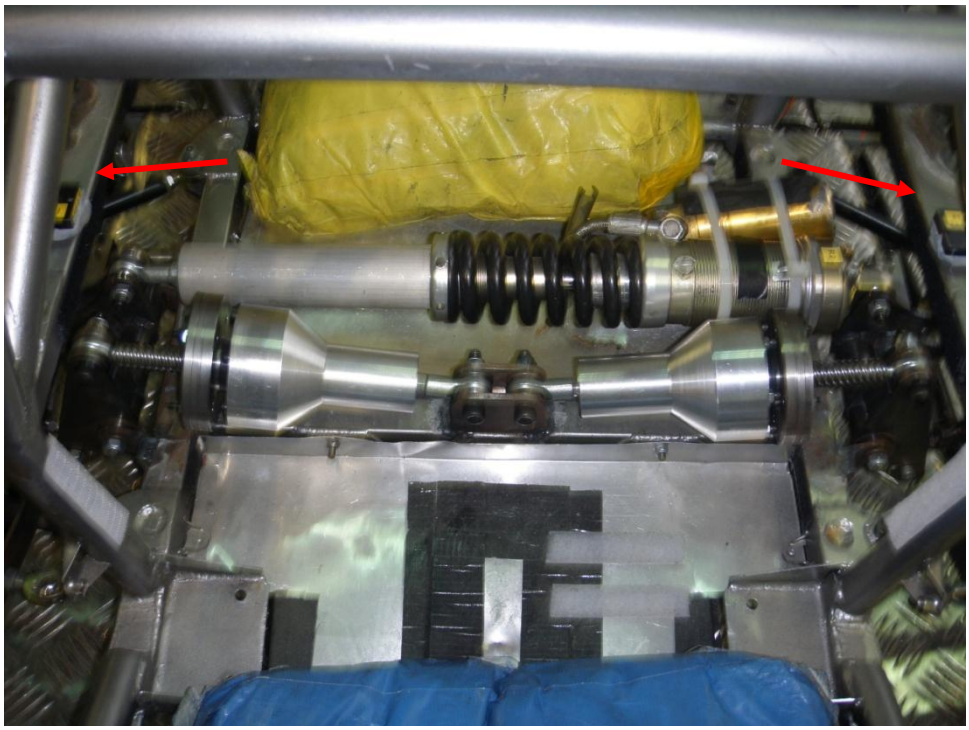

Figure 4-19: Front body accelerometer location

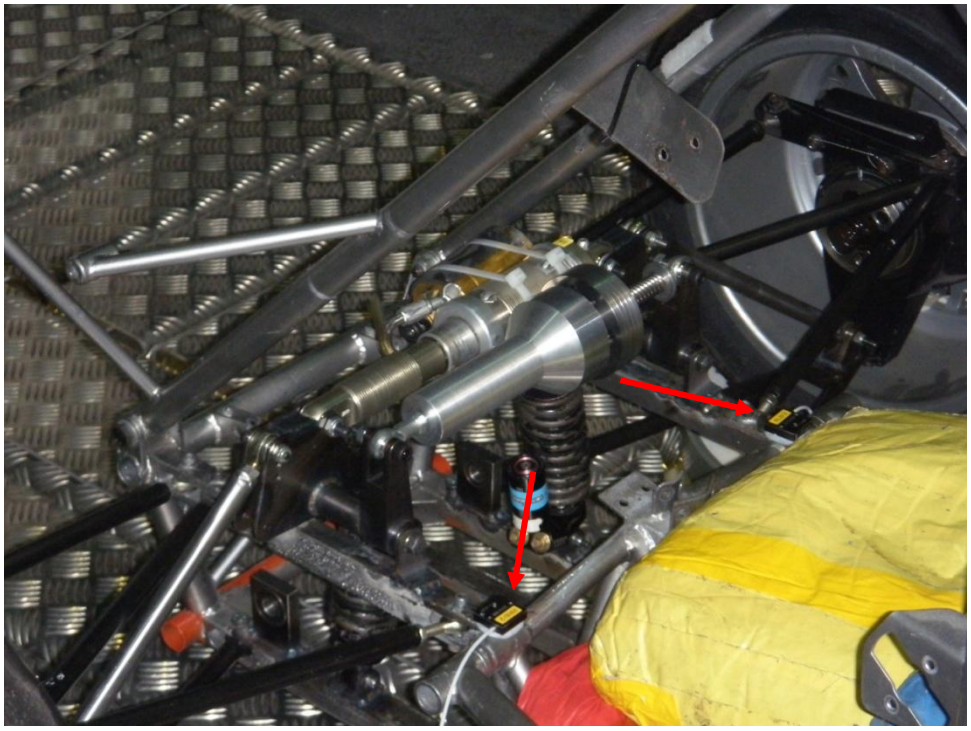

Figure 4-20: Rear body accelerometer location

Hub accelerometers have been placed into the uprights. Ideally, they should be placed as close to the vertical axis from contact patch centreline as possible. Figure 4-21 and Figure 4-22 show the position of front and rear hub accelerometers in this research work.

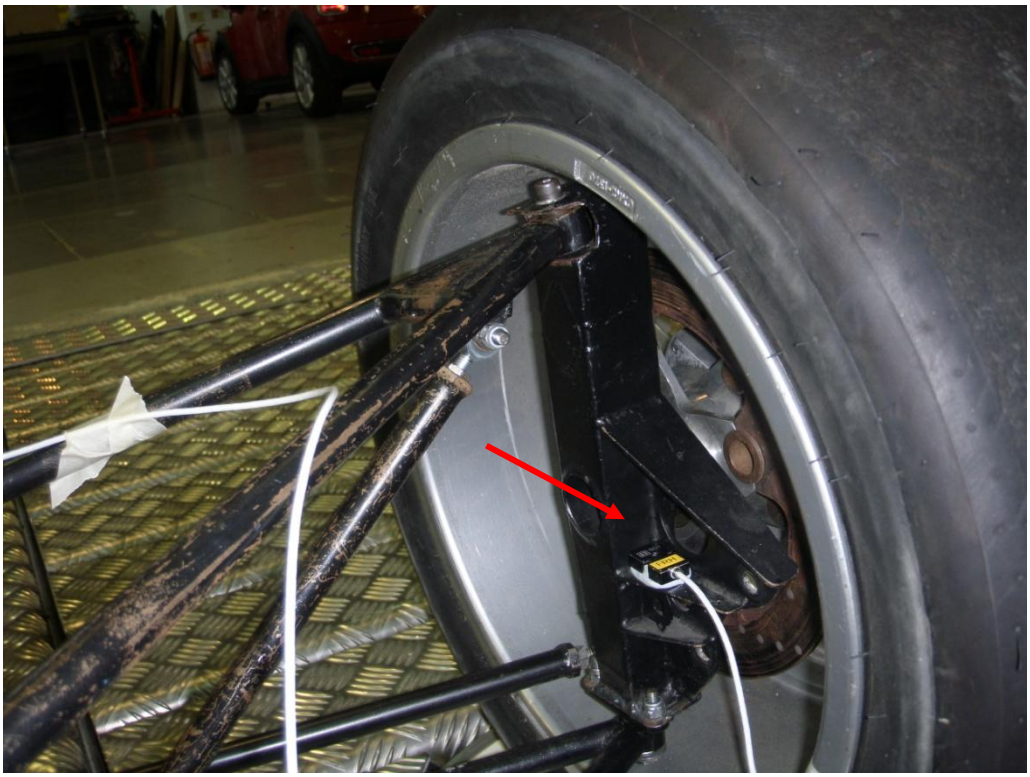

Figure 4-21: Front hub accelerometer position

Figure 4-22: Rear hub accelerometer position

Finally, strut displacement spring potentiometers have been placed. As with the accelerometers, to most closely replicate the lumped-mass vehicle model, the ideal position of the displacement potentiometers would be from the wheel CoG to a stiff vertical location above this point on the body. However, since there is no chassis or bodywork directly above the wheel, spring potentiometers have to be located along the damper line of action. Bespoke aluminium brackets were designed and manufactured to place the potentiometer box as close to the chassis-to-damper terminal as possible. The other terminal was directly attached to the damper-to-rocker joints and secured with tape to avoid detachment. Figure 4-23 and Figure 4-24 show the aluminium brackets and the location of the potentiometers. Note that corner spring-damper units have been removed for clarity in the picture.

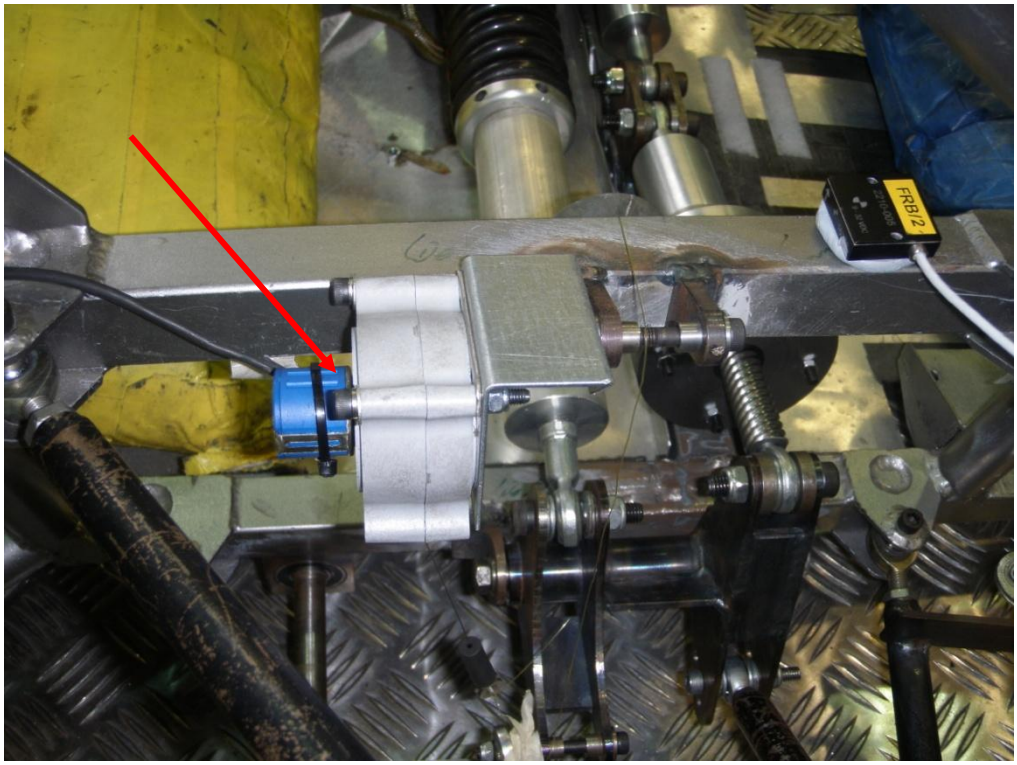

Figure 4-23: Front strut displacement potentiometer position

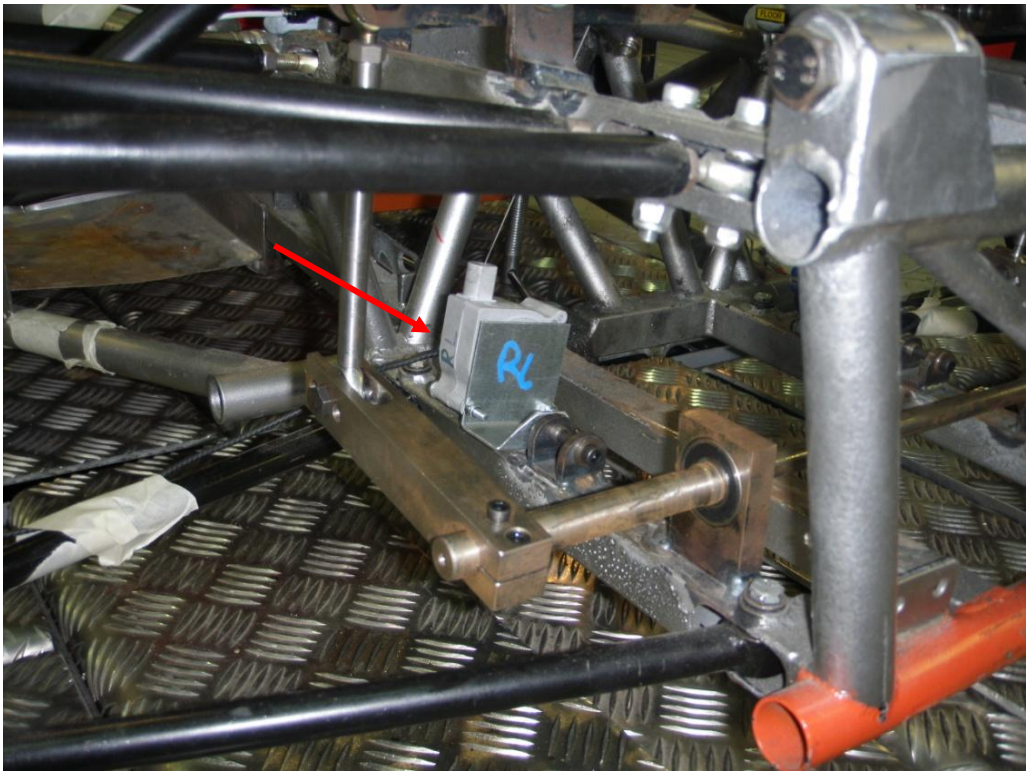

Figure 4-24: Rear strut displacement potentiometer location

4.5.3. Four-Post Rig Operation Procedure

Once the car was instrumented, the tyre pressures had to be properly set to normal race conditions. The tyre pressures modify the vertical tyre characteristics and therefore have an important impact on the dynamic response of the car. Pressures may change slightly during a test session, so they are frequently reset. Tyre pressures can also be changed to study the behaviour of the suspension from the beginning of the race (low pressure) to the end of the race (high pressure).

With tyre pressures properly set, corner weights are measured and reset if necessary. First, corner weights are checked accounting only for the car. After that, fuel is added and the driver enters the cockpit and new measurements are taken. If the weight distribution does not coincide with normal race conditions, modifications to the suspension static settings are made to regain the desired weight distribution. Due to Health & Safety policies at Oxford Brookes University, a physical person is not allowed to be inside a racing test car at any time during rig testing. According to this policy, the driver is substituted by ballast. Sand bags are used to replicate the weight of driver. Colour coded sand bags have been used to simulate the weight of different human body areas:

- Red coloured sand bag (18 kg): Two sand bags have been used to simulate human torso.
- Yellow coloured sand bag (15 kg): Used to simulate the weight of the legs. One or two yellow sand bags would normally be used depending on driver's weight.
- Blue coloured sand bag (10 kg): Used to simulate upper body and head and driver's feet.

In addition to this, if fuel is not available, sand bags could also be used to simulate the weight of fuel load. Sand bags can then be placed into the driver's cockpit until desired overall weight and weight distribution are reached. Figure 4-25 shows an example of weight setting.

Corner Weights	FL	FR	RL	RR	Total	% Front	% Cross	% Left
Car Only	97,7	95,7	168	173	534,4	36,19	50,65	49,72
Car + Driver +15 kg	122	123	179	200	624	39,26	51,60	48,24
Car + Ballast	123	121	176	200	620	39,35	52,10	48,23

Figure 4-25: Four-post rig weight setting procedure

If suspension displacement transducers are not positioned directly above the wheel centreline to a vertical position above it in the chassis, as is the case in most racing cars, an installation ratio (IR) must be measured. In this case, the installation ratio represents the wheel movement relative to the suspension potentiometer movement. In order to obtain the installation ratio, the springs and dampers must be disconnected from the suspension and the car has to be placed onto axle stands. The actuator height is set so that the wheels are in race track ride height conditions. With the wheels free to move relative to the chassis, a nonlinear low frequency sine wave (see Figure 4-26) is then applied. Using the Dynosoft MX software, an 'XY' graph is plotted to obtain the installation ratio. In this graph, the actuator displacement (y-axis) has been plotted against suspension displacement (x-axis) for each corner. The gradient of this plot represents the installation ratio (See Figure 4-27).

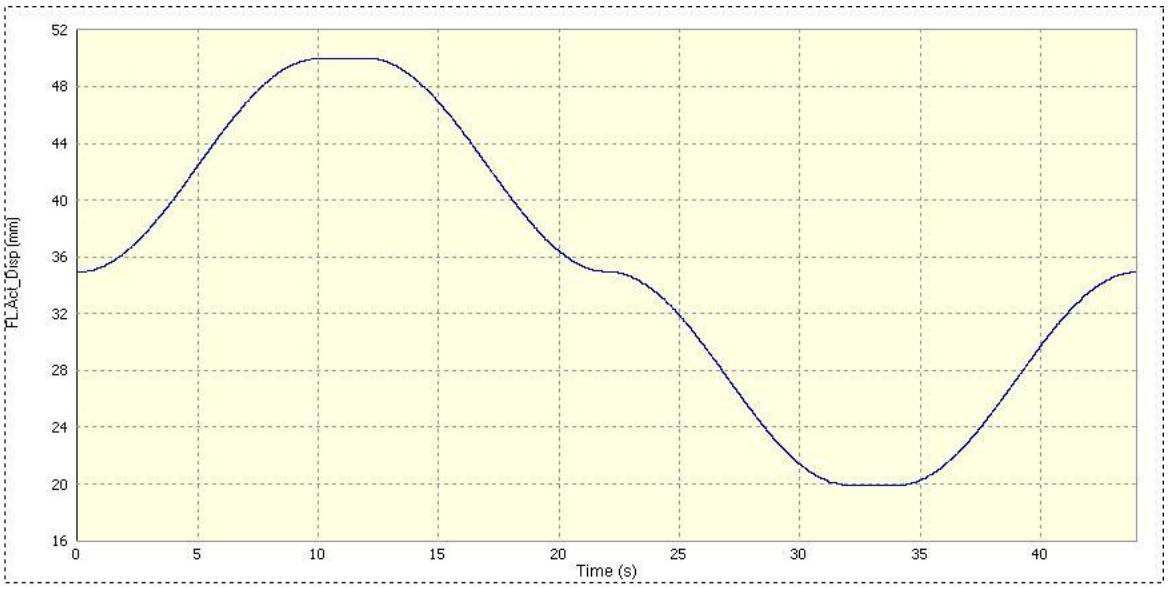

Figure 4-26: Installation ratio test input wave

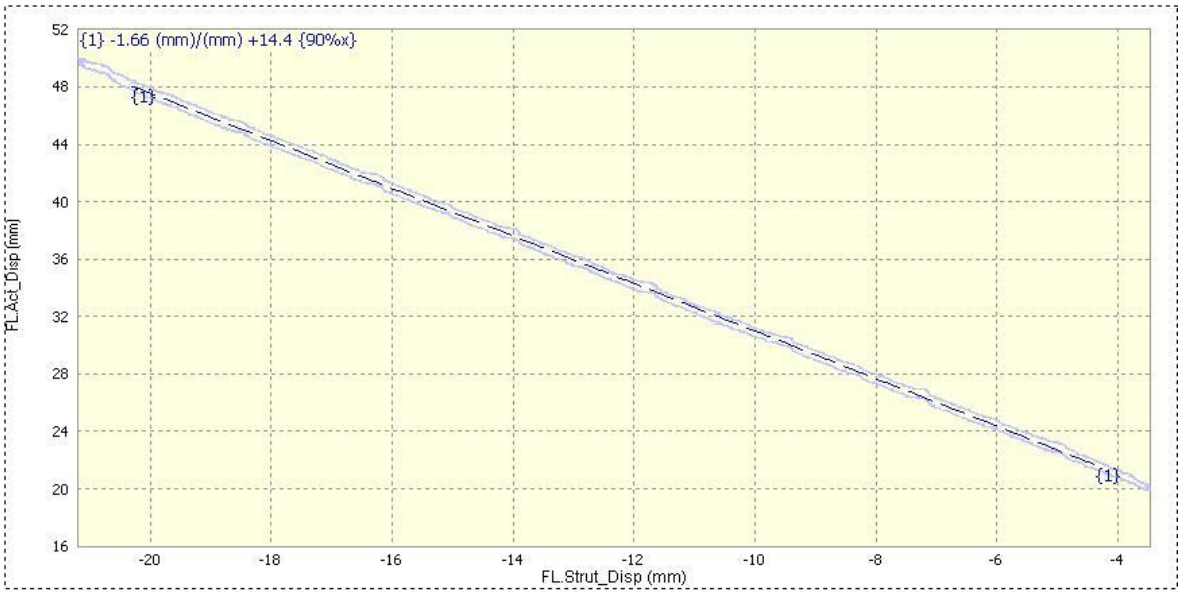

Figure 4-27: Actuator displacement vs Suspension displacement – IR measurement

Before re-connecting spring and dampers to the suspension, unsprung masses are estimated. A constant amplitude sine wave is applied to each wheel. The input frequency of this sine wave has been selected so that a measurable acceleration is induced at the hub without causing excessive tyre deflection. Pad force and hub acceleration are then recorded and a 'XY' graph is plotted. Assuming that the disconnected corner suspension is a SDOF system, the following equation is used to estimate the unsprung mass:

$$CPL = m_u \cdot a_{hub} \qquad (4.7)$$

Where *CPL* represents the measured contact patch force from the actuator load cells, a_{hub} represents the acceleration measured by the hub accelerometer and m_u represents the estimated unsprung mass.

Figure 4-28 depicts a 'XY' plot of *CPL* versus a_{hub}. A linear regression was applied to obtain the gradient of the plot. Note that the loading and unloading cycles in this test follow different paths. This is due to the damping induced by the tyre and suspension friction.

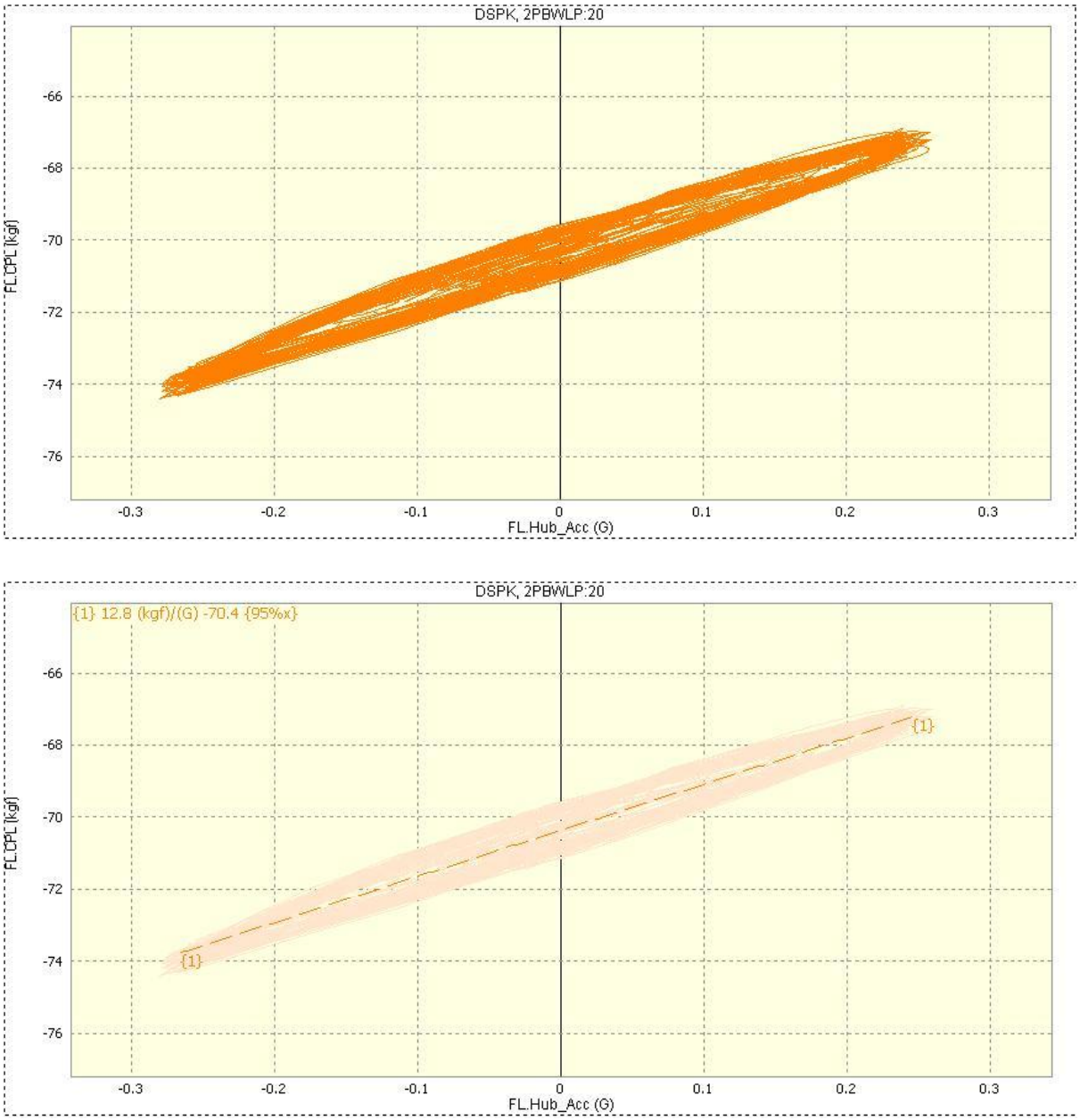

Figure 4-28: Experimental unsprung mass estimation: experimental data (upper) and linear regression (lower)

Once IRs and unsprung masses have been obtained for each corner, the spring – damper units can be re-connected to the suspension and axle stands can be then removed. The vehicle is now ready to begin the dynamic analysis. In order to do so, an appropriate road input must be selected so that experimental data obtained from rig test will be representative of the behaviour of the vehicle. The main characteristic of a road for ride dynamic studies is the road roughness (Gillespie, 1992). Roughness represents the profile elevation of a road along the distance of this road. This road profile can be considered in general terms as a random signal (Davis & Thompson, 2001; Kropác & Múcka, 2008). As with any random signal, the road elevation can be decomposed into a series of sine waves via Fourier transformation.

Useful representation of this transformation is the Power Spectral Density (PSD). Figure 4-29 shows an example of the road elevation signal of a race track and its associated PSD representation against spatial frequency or 'wavennumber'.

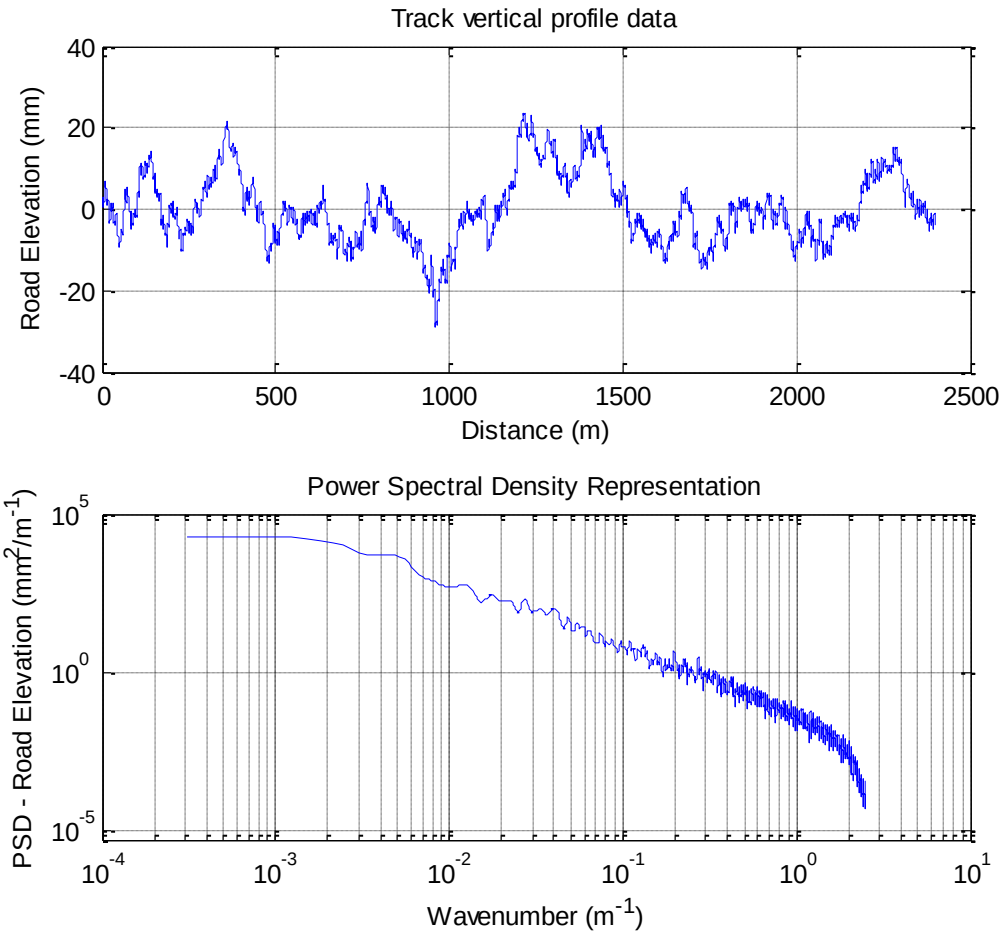

Figure 4-29: Example of race track vertical profile: actual profile (upper) and PSD representation (lower)

Although each race track has its own particular PSD, the PSD characteristic shown in Figure 4-29 is common to all roads (Gillespie, 1992). According to this, this PSD characteristic can be approximated to a simple mathematical expression (Verros, et al., 2005):

$$G_\Omega = G_0 \cdot \Omega^{-n} \qquad (4.8)$$

Where G_Ω represents the amplitude of the PSD of the road elevation profile, G_0 represents the road roughness index, n represents the waviness and Ω is the spatial frequency.

Moreover, inputs used on the test rig must be introduced as functions of time rather than space. According to this, equation (4.8) must be modified to be expressed as a function of linear frequency f rather than spatial frequency Ω. In order to do so, the vehicle is assumed to

travel at constant forward velocity V_x. Therefore, linear and spatial frequencies can be related as follows:

$$f = \Omega \cdot V_x \tag{4.9}$$

And so, equation (4.8) can be re-arranged as follows:

$$G_{\mathrm{f}} = G_{f0} \cdot \mathrm{f}^{-n} \tag{4.10}$$

Where G_f represents the amplitude of the PSD of the road elevation profile with respect to linear frequency f and Gf_0 can be expressed as:

$$G_{f0} = G_{\Omega} \cdot {V_x}^{n-1} \tag{4.11}$$

Equation (4.10) can then be represented as a straight line in a log-log plot and parameters G_{f0} and n can be estimated by linear regression. Equation (4.11) highlights that both road roughness index and vehicle forward speed produce the same impact in the generation of road input excitations, i.e. an increase in PSD amplitudes can represent either a vehicle travelling at the same speed on a rougher road or a vehicle travelling along the same road at higher speed. Figure 4-30 shows an example of experimental PSD and the linear approximation achieved with equation (4.10).

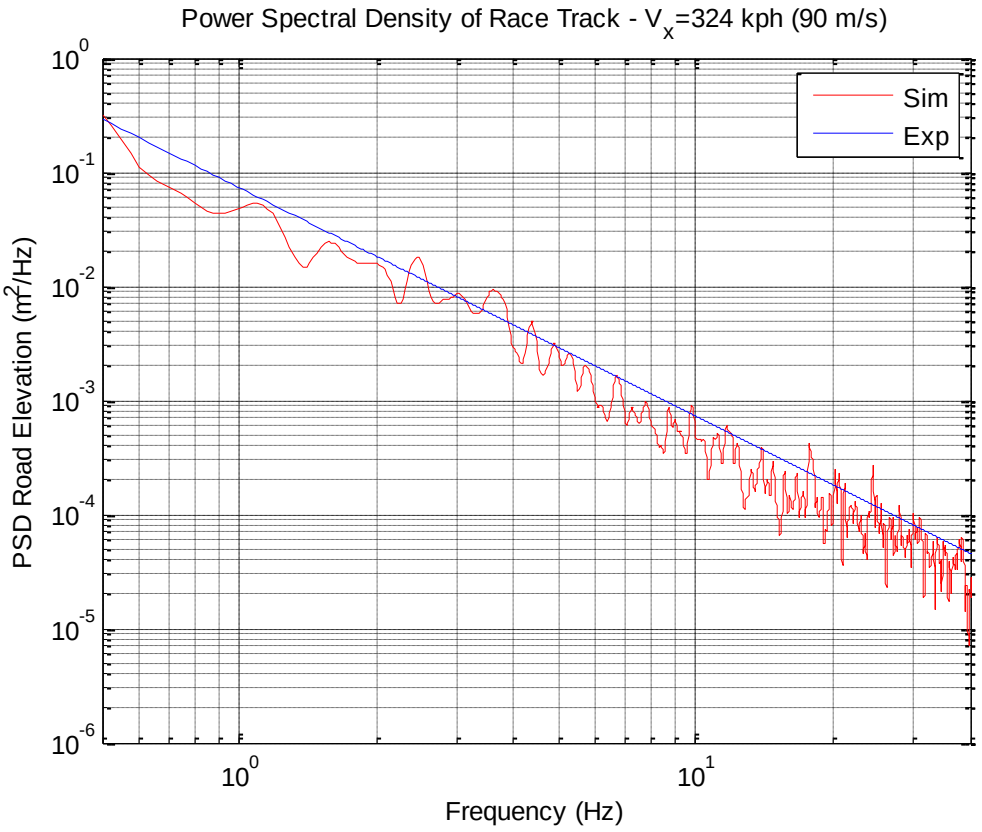

Figure 4-30: PSD of race track elevation profile for a vehicle travelling at 90 m/s

In this research work, the approximation of road profile PSD obtained in equation (4.10) has been used to construct swept sine test inputs (Orlando, et al., 2008). Swept sine waves offer a series of advantages with respect to other test signals:

- Easy control of frequency and amplitude.
- Good signal-to-noise ratio – minimal signal processing for obtaining frequency response functions (FRFs).
- Efficient testing time.

This swept sine input is characterised by the fact that road elevation gradient presents a constant peak velocity amplitude (CPV). Furthermore, in order to reduce the time required to sweep from initial to final frequency, the frequency of the input signal increases exponentially according to equation (4.12).

$$f = f_0 \cdot k^t \qquad (4.12)$$

Where f represents the instantaneous frequency, f_0 represents the initial frequency, t represents time and k is the sweep rate.

An exponentially increasing frequency allows sweeping from 0.5 to 40 Hz in 60 seconds, so testing time can be minimised. An example of the described test input is shown in Figure 4-31.

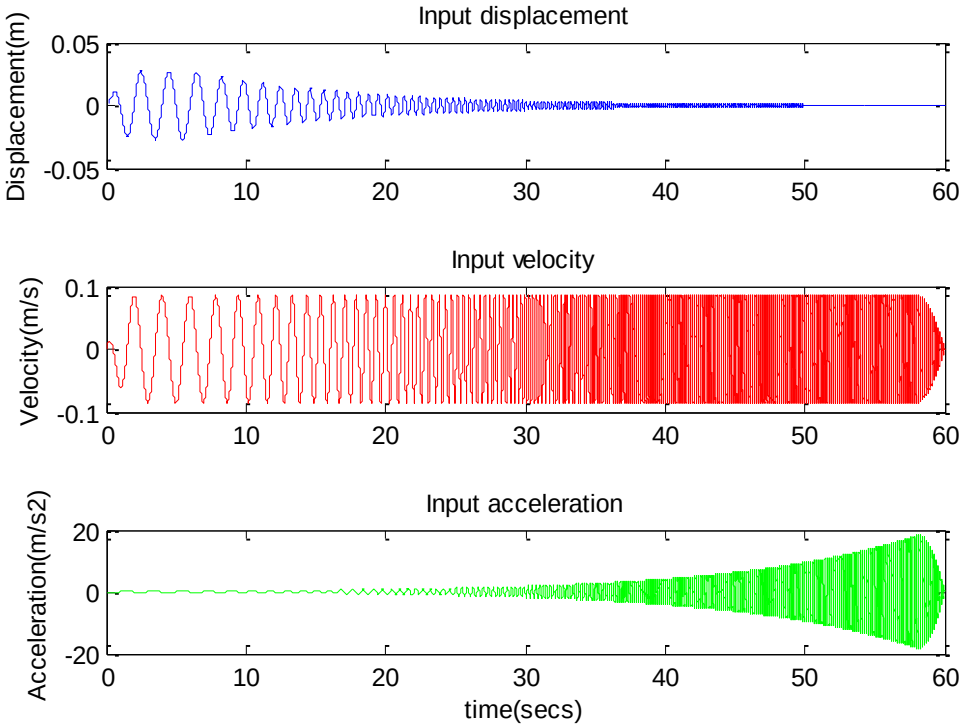

Figure 4-31: Example of rig test swept sine input – displacement (upper), velocity (middle) and acceleration (lower)

Furthermore, vibration modes have been studied separately in order to simplify the analysis and facilitate the parameter estimation process. In addition to this, several input amplitudes have been tested. As concluded from equation (4.11), different input amplitudes represent either the car travelling along the same road (or race track) at different speeds or the car travelling at the same speed along different road. Table 4-7 summarises the set of input displacement amplitudes used in each vibration mode in order to carry out the experimental testing in this research work. Note that the displacement amplitude shown in Table 4-7 refers to the amplitude measured for $f_{0.}$

Mode	Amplitude (mm)
Heave	20
	25
	30
	35
Pitch	20
	25
Roll	30
	20
	25
Warp	4
	8

Table 4-7: Summary of test inputs used in experimental testing

After tests have been carried out, time-domain data from sensors is obtained. Dynosoft MX software presents limited processing and analysis capabilities, so data is exported as '.txt' files to allow for more complex analysis in in-house built software. The following section briefly describes the operating principle of this post-processing tool.

4.5.4. Frequency Analysis and Parameter Estimation Software

Because of the limited analysis capabilities of Dynosoft MX, new software had to be developed in order to estimate vehicle suspension parameters and to conduct frequency-domain analysis of the experimental data. This software was designed and developed by Bennet (2012). Detailed explanation of data filtering processes, complex analysis and parameter estimation algorithm can be found in his work (Bennett, 2012). The main functions of this software are to obtain the frequency response functions (FRFs) of measured dynamic magnitudes; to support advanced suspension and vehicle dynamics analysis; and to estimate the required parameters for accurate vehicle simulation.

The software was written as a Graphical User Interface (GUI) in Matlab. Figure 4-32 depicts the main command window of the program.

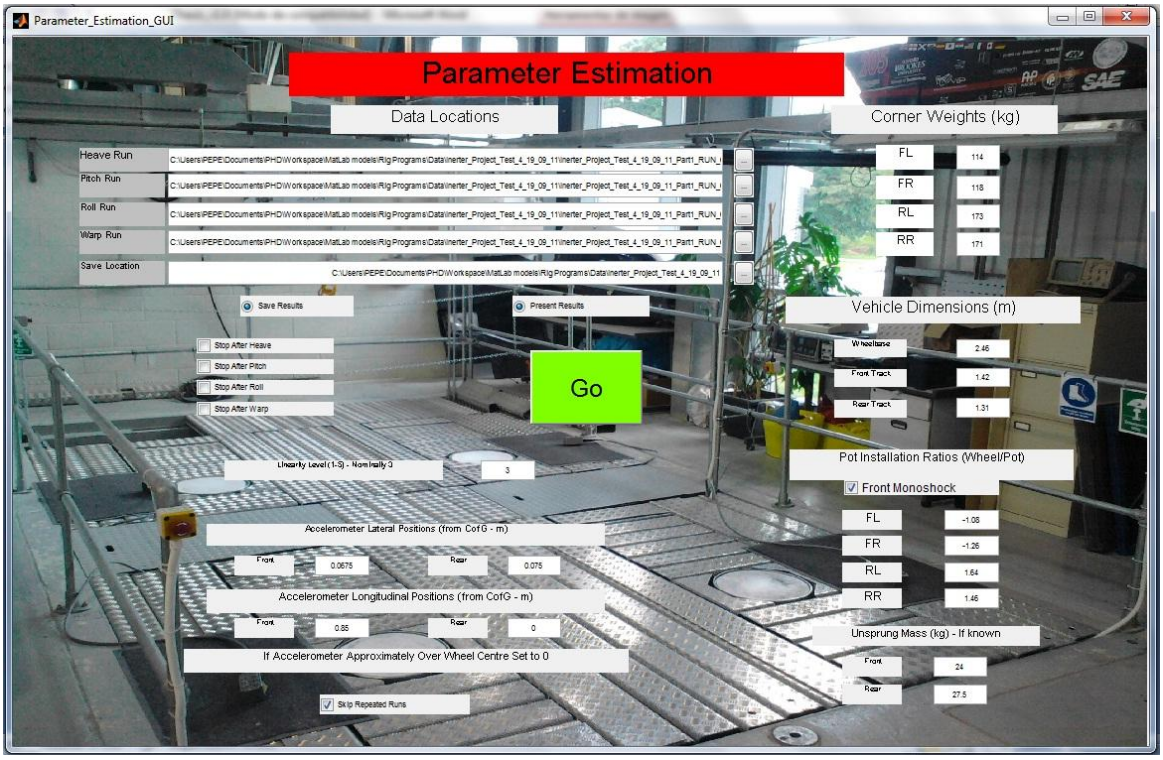

Figure 4-32: Parameter Estimation command window

In order to run the program, two types of input data must be provided: static vehicle parameters and dynamic data from rig tests. Static parameters include corner weights, wheelbase and tracks dimensions, installation ratios, lateral and longitudinal accelerometer position from CoG and front and rear unsprung masses if known. The dynamic data from rig tests include raw time-domain data for each vibration mode, or inputs from different road profiles. The exported data from the rig user PC software is then used as an input in the software.

One of the key features of the parameter estimation program developed by Bennet (2012) is that it can estimate unsprung mass from dynamic test data when this parameter is unknown and cannot be measured as described in the previous section (see Figure 4-28). The accuracy of this process is mostly dependent on the dynamic response of the vehicle around the hub excitation mode. Unsprung mass estimation process works well for lightly damped road cars. However, most race cars present a highly damped hub mode with imperceptible resonant amplitude peak around the hub mode frequency. This makes the estimation task increasingly difficult and usually leads to high estimation errors (over 30% estimation error). In this research work, both front and rear unsprung masses are measured as described in section 4.5.3 in order to minimise parameter estimation errors.

After the program is run, an output '.mat' file is produced for each vibration mode. These '.mat' files contain FRFs for direct measured magnitudes such as body acceleration, hub acceleration, suspension displacement and FRFs for indirect magnitudes such as tyre displacement, suspension velocity, suspension force, suspension dynamic stiffness, tyre dynamic stiffness, dynamic mass, dynamic CoG position, ride height, suspension offset, pitch and roll acceleration. These functions are saved as complex arrays so that amplitude and phase angle can be condensed in one vector. The .mat file also contains all the required parameters for vehicle simulation and nonlinear damper characteristic. These '.mat' files can then be used to compare data from different setups.

This software has been extensively tested and successfully applied to different cars during four-post rig test sessions (Bennett, 2012).

4.5.5. Extensions of current parameter estimation method

Although the analysis software described in the previous section can deal with a wide range of vehicles, it has some limitations. The main limitation is that the estimation process does not account for a suspension incorporating inerters. According to this, in order to continue using this program for the particular needs of this research work, some extensions needed to be made.

In the original program developed by Bennet (2012), the suspension dynamic stiffness FRF is used to work out the linearised parameters of a suspension layout without inerters as shown in Figure 4-33.

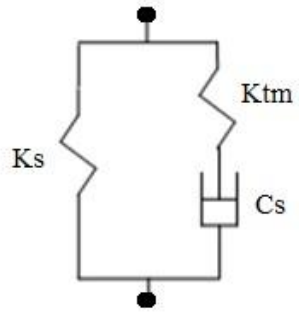

Figure 4-33: Current parameter estimation program suspension model – No inerters (Bennett, 2012)

The general dynamic stiffness of any suspension system K_{dyn} can be defined as:

$$F_{susp} = K_{dyn} \cdot x_{susp} \;\rightarrow\; K_{dyn} = \frac{F_{susp}}{x_{susp}} \qquad (4.13)$$

Where F_{susp} represents the force created by the suspension and x_{susp} represents the suspension relative displacement. The suspension relative displacement x_{susp} can be obtained as a direct measurement from the strut displacement sensors and F_{susp} can be obtained from the equation of motion (EOM) of the unsprung mass as:

$$F_{susp} = m_u \cdot \ddot{x}_u - CPL \qquad (4.14)$$

Where the hub acceleration $\ddot{x}_u$ and the contact patch force *CPL* can be obtained as direct measurements from the hub accelerometer and actuator load cell respectively. Moreover, the unsprung mass m_u has been already obtained as described in section 4.5.3. Therefore, by using equations (4.13) and (4.14), the experimental FRF of dynamic suspension stiffness K_{dyn} can be obtained.

Moreover, by applying equation (4.13) in Laplace transform to the suspension layout shown in Figure 4-33, an analytical expression for K_{dyn} can be obtained in terms of Laplace operator terms as:

$$K_{dyn} = \frac{(k_s + k_{tm}) \cdot c_s \cdot s + k_s \cdot k_{tm}}{s \cdot (c_s \cdot s + k_{tm})} \qquad (4.15)$$

An unconstrained Nelder-Mead simplex nonlinear optimisation algorithm is used to minimise the errors between experimental dynamic suspension stiffness and its analytical expression (equation (4.15)) for a prescribed frequency range. This algorithm is implemented as a built-in function of Matlab called *fminsearch* (The MathWorks Inc., 2012). This process draws estimated spring stiffness k_s, damping coefficient c_s and top mount stiffness k_{tm}.

In this research work, an extended vehicle suspension model incorporating real inerter has been proposed (see Figure 4-34). A detailed discussion of this new suspension model is provided in Chapter 5.

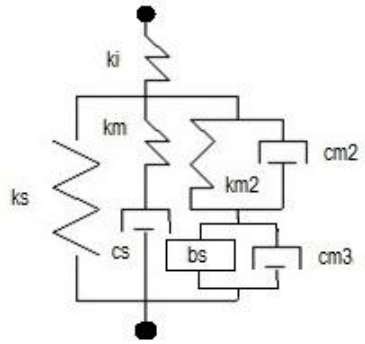

Figure 4-34: Suspension layout with real inerters

Furthermore, the suspension optimisation process has been modified. It was observed that the use of an unconstrained Nelder-Mead simplex algorithm led to erroneous results. These errors where observed to happen especially for stiff suspension settings, due to the inaccuracies in suspension dynamic stiffness introduced at low frequencies[4]. In order to overcome this problem a constrained least squares minimisation problem has been used because of the superior performance over an unconstrained algorithm (The MathWorks Inc., 2012). A constrained algorithm allows the user to set sensible bounds for each of the variables to be identified and the algorithm provides more accurate results.

Moreover, because of the amount of parameters to be estimated in Figure 4-34, an important effect was noticed: because of the large number of suspension parameters to be estimated, different sets of estimated suspension parameters produced similar good approximations between analytical and experimental dynamic stiffness. However, unless the correct set of estimated parameters is used, the simulation model will not be robust enough to predict real changes in the suspension and therefore the model will not be valid for optimisation purposes. In order to overcome this problem, the estimation process has been split into two stages. Firstly, the vehicle was tested without inerters fitted so that k_s, k_{tm}, c_s and k_i parameters could be estimated. Then, the inerters were reconnected to the suspension so that the rest of suspension parameters b_s, k_{tm2}, c_{tm2} and c_{tm3} can be estimated. This multi-level estimation process produces more accurate results.

Another limitation of the current software lies in the estimation of the tyre elastic properties. As described in Chapter 2, many vehicle models used for ride dynamic analysis incorporate a linear vertical tyre model due to its simplicity. However, an experimental study has been

[4] Note that, for stiff suspensions at low frequencies, displacement measurements are very small and the acceleration signal is very noisy.

carried out in this research work to assess the validity of this assumption. In this study, tyre stiffness and damping characteristics was been obtained from experimental data using a similar procedure as the one used for estimating suspension parameters. According to this, the general dynamic stiffness K_{tyre_dyn} of any tyre can be calculated as follows:

$$F_{CP} = K_{tyre\_dyn} \cdot x_{tyre} \rightarrow K_{tyre\_dyn} = \frac{CPL}{x_{tyre}} \tag{4.16}$$

Where *CPL* represents the measured dynamic tyre load and x_{tyre} represents tyre deflection. This tyre deflection x_{tyre} can be experimentally obtained as follows:

$$x_{tyre} = x_u - x_{input} \tag{4.17}$$

Where x_{input} is the measured input displacement recorded from actuator displacement sensor and x_u represents the unsprung mass displacement and can be obtained from measured hub acceleration $\ddot{x}_u$.

When working in the frequency domain, the dynamic tyre stiffness K_{tyre_dyn} can be expressed as a complex number $z=a+b\omega j$. For general vibrations theory, the real part of this complex number represents the elastic term of the system and the imaginary part represents the damping term. Therefore, tyre stiffness kt and tyre damping ct can be obtained as follows:

$$k_t = real\left(K_{tyre\ dyn}\right) \tag{4.18}$$

$$c_t = {imag\left(K_{tyre\ dyn}\right)}/{\omega} \tag{4.19}$$

Figure 4-35 shows an example of the estimated tyre stiffness k_t versus tyre deflection x_t obtained from the process explained above for a vehicle with and without inerters. A similar behaviour can be obtained when tyre damping c_t is plotted against the rate of tyre deflection $v_t = \dot{x}_t$. A number of conclusions can be drawn from this study: firstly, tyre characteristics do not exhibit a linear behaviour. Results suggest that some interaction exists between the tyre characteristic and the tyre deflection regardless of the type of suspension used. Causes for this behaviour could reside in the complex construction of a tyre, nonlinear elastic behaviour of the rubber that composes the tyre's tread and/or variations in the local pressure at the contact patch due to dynamic vibration. Secondly, it can be observed that tyres are subjected to much higher deflections when suspensions incorporate inerters. This is due to the fact that, as concluded in Chapter 3, inerters cause an increase of vibration transmissibility

from input to the body at high frequencies. This, in turn, causes a less controlled hub mode which leads to higher vibration amplitudes around the hub mode and therefore, larger tyre deflection. Lastly, even though both suspension cases exhibit a nonlinear tyre behaviour, the variation in tyre stiffness experienced with a conventional suspension suggests that, if no experimental data is available, a linear tyre model could be a reasonable approximation due to the fact that the maximum variation of k_t is relatively low (< 15%). However, this linear approximation is not valid when the suspension incorporates inerters due to the much larger tyre deflection.

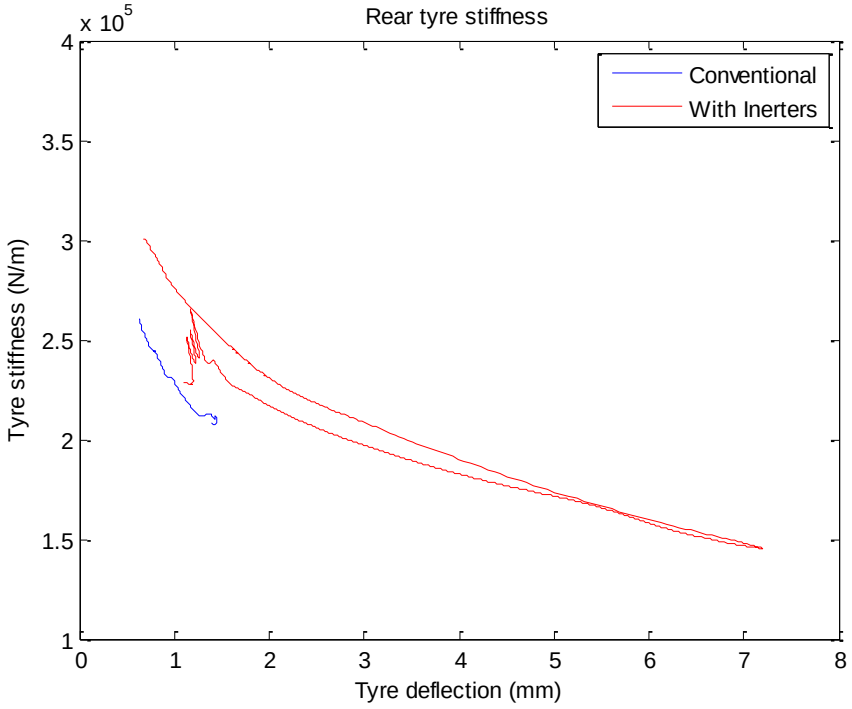

Figure 4-35: Estimated tyre stiffness versus tyre deflection from a suspension with and without inerters

This study highlights therefore the need to develop a new nonlinear tyre model that can provide accurate results when suspensions incorporate inerters. Hence, an exponential nonlinear vertical tyre model has been developed in order to overcome this problem. The analytical expression of this model is shown in the following equations:

$$k_t = a \cdot e^{-bx_t} + k_{t0} \tag{4.20}$$

$$c_t = d \cdot e^{-nv_t} + c_{t0} \tag{4.21}$$

A detailed description of this tyre model will be provided in Chapter 5. Parameters a_0, b, k_{t0}, d_0, n and c_{t0} are used to define the model. A constrained least-squares algorithm (The

MathWorks Inc., 2012) has been used to fit the tyre model presented in equations (4.20) and (4.21) and therefore to obtain an estimation of these parameters.

Finally, further extensions to the original parameter estimation software (Bennett, 2012) comprise the inclusion of new FRFs for dynamic front and rear ride heights and dynamic longitudinal weight distribution variation. According to this, an expression for front and rear dynamic ride heights *RH* has been obtained as follows:

$$RH_i = x_{si} - x_{inputi} \quad for\ i = F, R \tag{4.22}$$

Where x_{si} represents the displacement of the sprung mass at the axle i and can be obtained from measured body acceleration $\ddot{x}_s$ by either double-integrating the time domain signal or by dividing by ω^2 the frequency domain signal. x_{inputi} represents the measured actuator displacement at the axle i and.

Moreover, the dynamic longitudinal weight distribution variation *WDist_Dyn* can be expressed as follows:

$$WDist\_Dyn(\%) = \frac{CPL_F}{CPL_F + CPL_R} \cdot 100 \tag{4.23}$$

Where CPL_F, CPL_R represent front and rear dynamic loads at the tyre contact patch respectively.

These FRFs will be used in later chapters of this research work to create performance based objective functions for suspension optimisation.

4.6. Summary

The design and description of the practical inerters incorporated as part of the test vehicle and the experimental apparatus used in this research work has been presented and discussed in this chapter. In order to study the behaviour of a suspension fitted inerters experimentally, an old Formula Student chassis has been used as a test car. This test car required some re-design in order to accommodate all the new suspension components. Moreover, real inerters needed to be designed and manufactured. The design process from the identification of a need to the delivery of the final product, i.e. a test vehicle incorporating real inerters, has been described.

Furthermore, the Multimatic four-post rig is the test facility presented to test the new suspension featuring inerters in this thesis. The main components of this facility including the hydraulic, instrumentation and control systems have been described and the operating principle of the rig has been discussed.

Finally, the current suspension analysis and parameter estimation software was developed by Bennett (2012). The key features of the software were described and extensions were proposed to account for real inerters and nonlinear tyres. This extended parameter estimation software is used extensively in the work described in Chapter 5 in order to estimate vehicle, suspension and tyre experimental parameters from the test car incorporating real inerters designed in this chapter and to validate the new virtual vehicle model against experimental data from four-post rig testing.

5. Vehicle Suspension Modelling and Validation

5.1. Introduction

Vehicle models are theoretical representations based on mathematical expression of the physical working principles of an actual vehicle. Simulation models are powerful tools for virtual analysis and optimisation. These models allow vehicle engineers to study and investigate new improved solutions long before the car is manufactured. Furthermore, since there is no need of track data for simulation, they do not require a complete full-scale physical prototype to be built. Hence, vehicle simulation and modelling is cost and time effective.

Depending on the level of analysis required and the stage of the process design, vehicle models can range from very simple theoretical approximations to highly complex vehicle dynamics representations. When determining the model complexity, a compromised solution must be selected based on usefulness, accuracy and computational effort. In this research work, a vehicle model has been developed in order to fulfil two main objectives: the first objective is to analyse the ride dynamics of a race car suspension featuring inerters; and the second is to develop an algorithm for suspension optimisation. In order to analyse and optimise vehicle suspensions with some degree of reliability, the simulation model must be capable of replicating the dynamic behaviour of the physical system.

In this chapter, an investigation into the simulation capabilities of different commercial modelling software packages has been carried out in order to determine the software framework in which vehicle models will be developed. Before proceeding with the development of the suspension layout, different levels of model complexity have been considered with regard to usefulness, accuracy and computational requirements. Finally, a vehicle model that accounts for real inerters and nonlinear tyres has been developed and validated with experimental data obtained from four-post rig testing. Discussions with regard to model accuracy and possible sources of error have been carried out.

5.2. Selection of the most suitable Modelling Software

Several commercial software packages are available for the design and development of vehicle models for simulation. A study with a simple linear 4-DOF half-car model (see Figure 5-1) has been carried out in order to determine the most suitable commercial software to be used in the present thesis.

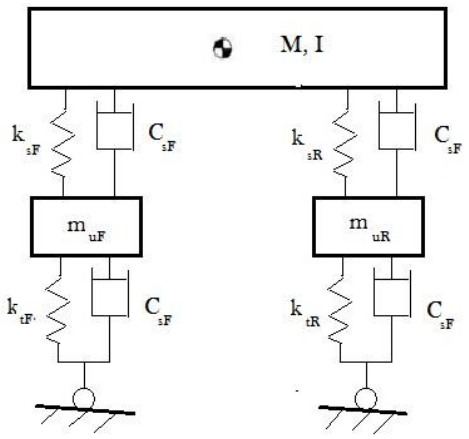

Figure 5-1: 4-DOF Half Car model

Three different commercial software packages were analysed:

- MSC.Adams
- Simulink
- SimMechanics

MSC.Adams is a software package dedicated to the analysis and simulation of mechanical systems. MSC.Adams allows the creation of mechanical multi-body dynamic (MBD) systems by the definition of objects, joints and motion within a three dimensional environment. (MscSoftware, 2012).

Simulink is an environment for multi-domain simulation and Model-Based Design for dynamic and embedded systems. It provides an interactive graphical environment and a customizable set of block libraries that let you design, simulate, implement, and test a variety of time-varying systems. Simulink operates under the platform of MatLab. Full interaction between MatLab and Simulink is possible (MathWorks, 2012).

SimMechanics is a block diagram modeling environment for engineering design and simulation of rigid body mechanics and their motion, using standard Newtonian dynamics of forces and torques. Instead of deriving and programming equations, one can use this multibody simulation tool to build a model composed of bodies, joints, constraints, and force elements that reflects the structure of the system. SimMechanics also operates inside Matlab. Models built in SimMechanics can be coupled with Simulink models (MathWorks, 2012).

The model shown in Figure 5-1 has been built and analysed using all three commercial software options. Table 5-1 shows a summary of the input parameters used to model the dynamic system.

Sprung Mass (M)	250 kg
Pitch Moment of Inertia (I)	200 N/m^2
% of Front Weight Distribution (%fwt)	50 %
Front Unsprung Mass (m_{uF})	20 kg
Rear Unsprung Mass (m_{uR})	25 kg
Front Suspension Stiffness (k_{sF})	125000 N/m
Front Suspension Damping (c_{sF})	1500 Nm/s
Rear Suspension Stiffness (k_{sR})	100000 N/m
Rear Suspension Damping (c_{sR})	1000 Nm/s
Front Tyre Stiffness (k_{tF})	200000 N/m
Front Tyre Damping (c_{tF})	140 Nm/s
Rear Tyre Stiffness (k_{tR})	200000 N/m
Rear Tyre Damping (c_{tR})	140 Nm/s

Table 5-1: Input parameters for Half-car 4-DOF model study

The suitability of each software package has been assessed considering the following decision factors:

- Simulation time: refers to the time taken to obtain a solution to the simulation problem. This is a key factor in the selection of the most suitable modelling package, particularly if optimisation is involved
- Construction time: refers to the time taken to build the model in the virtual environment.
- Graphical interface: refers to visual aids provided by the software during simulation.

- Domain knowledge: refers to the level of understanding of the physical principles of the system required by the user in order to be able to build the model.
- Accuracy: refers to the deviation of the numerical solution provided by the software with respect to the analytical solution of the problem.
- Post-processing: refers to the data managing, processing, filtering and plotting capabilities of the program.

Thus, the half-car model has been built in all three packages and a dynamic simulation was carried out. A 20-mm displacement amplitude CPV swept sine signal has been used as road input for the simulation (see Figure 4-31). The sampling rate used was 1000 Hz. Results drawn for this simulation for each software package have been used to construct a decision matrix according to the criteria discussed:

Criterion	**Weighting factor (%)**	**Commercial software package**					
		MSC.Adams		**Simulink**		**SimMechanics**	
		Raw	Weighted	Raw	Weighted	Raw	Weighted
Simulation time	35	10	3.5	90	31.5	40	14
Construction time	15	80	12	30	4.5	60	9
Graphical interface	5	100	5	10	0.5	50	2.5
Domain knowledge	10	90	9	20	2	60	6
Accuracy	30	90	27	90	27	90	27
Postprocessing	5	60	3	80	4	80	4
TOTAL	**100%**		**59.5%**		**74%**		**62.5%**

Table 5-2: Decision matrix for selection of simulation software

Simulation of the dynamic response of the vehicle model provided the same results for all software packages, denoting good accuracy capabilities. According to Table 5-2, the most suitable modelling software for the present research work is Simulink. MSC.Adams requires low levels of understanding of the dynamics of the systems, i.e. no mathematical equations of motion need to be derived explicitly. Furthermore, the time required to build the model is low. The level of visualization in MSC.Adams is quite high since the dynamic response of the system can be visualised during simulation. However, simulations in MSC.Adams are computationally very expensive (~1200 secs). On the opposite side lies Simulink. The level of understanding required to construct a physical model is high, since the user must derive all the mathematical equations that describe the physical behaviour of the dynamic system.

Hence, the construction time is also high. No physical visualization of the system is provided in Simulink. However, once the model is built, simulations run very fast in Simulink (< 1sec). SimMechanics offers intermediate capabilities between MSC.Adams and Simulink. All commercial packages offer good data post-processing capabilities, although the fact that Simulink and SimMechanics operate in Matlab provides more flexibility when manipulating data. In this thesis, since suspension models are used for optimisation purposes, the most suitable modelling software is then Simulink.

5.3. Selection of the most suitable Model Complexity

Chapter 2 presented a review of different vehicle suspension models found in the literature. Reported vehicle suspension models range from linear SDOF systems to complex non-linear multi-DOF systems. One of the main goals of the present research work is to develop an experimentally validated vehicle suspension model. This vehicle model must be used for suspension parameter estimation and suspension optimisation.

According to this, the model must allow the determination of experimental parameters from four-post rig testing. The vehicle model must account for all the primary motions that can be measured on a four-post rig test facility. This means that the model will require the definition of as many degrees of freedom as motions can be reproduced on laboratory testing. The model must present a level of complexity so that the dynamics of the physical vehicle can be replicated and the parameter identification method can be applied to any vehicle regardless of its particular suspension configuration.

Increasing model complexity can have a number of potential drawbacks. More complex vehicle models require the estimation of more parameters to be estimated from experimental data. As explained in Chapter 4, as the number of modelled parameters increases, the estimation task becomes increasingly complex and inherently prone to estimation error. Moreover, complex models require longer times to compute the numerical integration of the dynamic system. This computational time will have a critical impact on the efficiency of the optimisation algorithm, since the vehicle model must be simulated several times to produce an optimal solution.

In this thesis, a lumped parameter dynamic vehicle model has been developed. This model represents only the general dynamic response of vehicle and is not intended to simulate detailed kinematic movement of each component. In this vehicle representation, chassis, driver, engine, gearbox and other vehicle systems mounted onto the chassis have been assumed to be clustered in one rigid body with homogeneous mass and inertia properties. This simplification is valid as long as the components of the sprung mass are solidly fixed to the chassis and they are not excited within the frequency range of study. Unsprung masses have been modelled as lumped masses and they have been constrained to move only in vertical direction. In real vehicles, the unsprung mass is composed of many elements such as tyre compound, wheel rim, wheel carrier, brake calliper, part of the suspension arms and part of the suspension dynamic devices. Moreover, the movement of the wheel is not constrained to only vertical motion; instead, wheels describe a 3D trajectory in space. Furthermore, structural deflection of sprung and unsprung masses have been neglected. In a lumped parameter vehicle model, masses are modelled as infinitely stiff bodies and deflection is only produced by massless elastic components such as suspensions and tyres.

The following sub-sections discuss the complexity of the vehicle models selected for parameter estimation and optimisation according to the model design premises presented.

5.3.1. Vehicle suspension model complexity for Parameter Estimation

As mentioned in section 4.5.1, the main modes of vibration that can be reproduced on a four-post rig test facility are heave, pitch, roll and warp or articulation. The simplest model that would reproduce these motions would be a system composed by a solid-rigid body attached to the excitation source via 4 elastic links (see Figure 5-2). Such a system has 3 degrees of freedom.

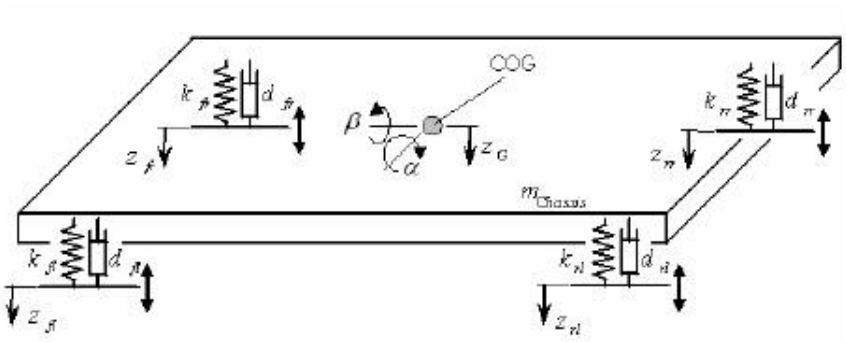

Figure 5-2: 3-DOF Vehicle suspension model (Graf & Kosuch, 2008)

Although this model is allowed to move vertically as well as rotate with respect to the longitudinal (pitch motion) and lateral (roll motion) axes of the body, the model does not account for the motion of unsprung masses nor suspension and elastic tyre effects. In order to include these effects in the analysis, the model can be extended to a 7-DOF system, also known as full-car ride dynamics model (see Figure 5-3).

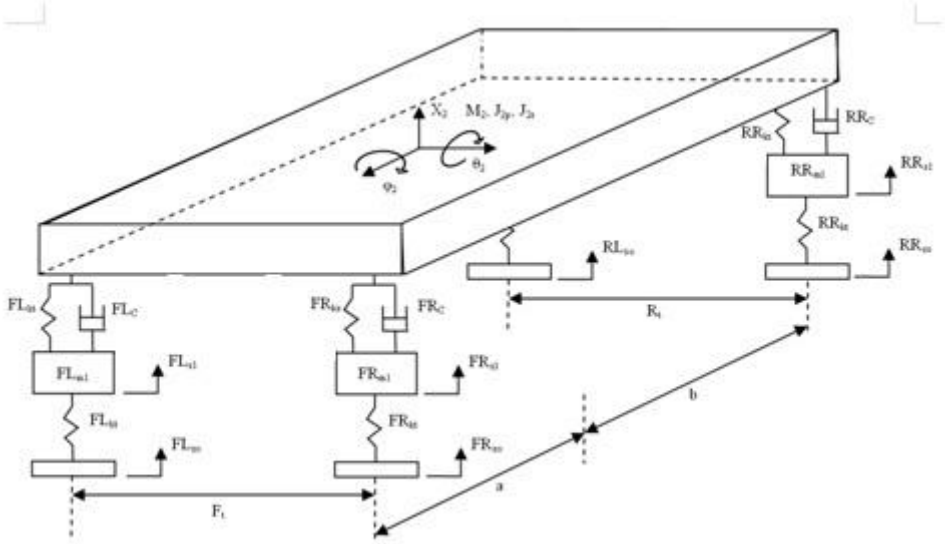

Figure 5-3: 7-DOF Full-car suspension model (Bennett, 2012)

The model shown in Figure 5-3 allows the replication of all the vibration modes experienced on rig testing as well as the estimation of the main suspension and mass properties of the vehicle (see section 4.5.1). However, there are two main limitations to this model. First, in this model, the sprung mass is modelled as a solid-rigid body. In physical race cars, the chassis is designed to be as stiff as possible and other systemss such as engine, powertrain or aerodynamic devices are designed to be solidly attached to the chassis. However some compliance could still occur if the design is poor. Moreover, other masses such as the driver are not rigidly attached to the chassis. This is likely to cause resonant frequencies of these

systems within the frequency range associated with ride and handling dynamics (typically between 0-40 Hz).

In order to illustrate the problem, the dynamic apparent mass m_{dyn} for each axle can be defined as follows:

$$m_{dyn} = \frac{F_{susp}}{\ddot{x}_s} \tag{5.1}$$

Where $\ddot{x}_s$ represents the measured sprung mass acceleration and F_{susp} represents the dynamic force generated by the suspension and can be obtained as follows:

$$F_{susp} = m_u \cdot \ddot{x}_u - CPL \tag{5.2}$$

Where *CPL* is measured contact patch force, $\ddot{x}_u$ is measured hub acceleration and m_u is measured unsprung mass.

Equation (5.1) can be applied to all four corners and axle dynamic masses can be obtained by adding left and right sides of the same axle. Figure 5-4 shows an example of the difference between experimental dynamic mass and simulated with a model such as the one depicted in Figure 5-3. Simulated dynamic mass presents an almost constant value around the static weight for that axle. Small variations are due to the dynamic longitudinal weight transfer due to induced pitch motions in heave. However, noticeable variation occurs in the experimental case especially around 18 and 23 Hz. These resonant peaks demonstrate the fact that the chassis does not behave as a solid-rigid body. Instead of that, the chassis behaves as a multibody dynamic system.

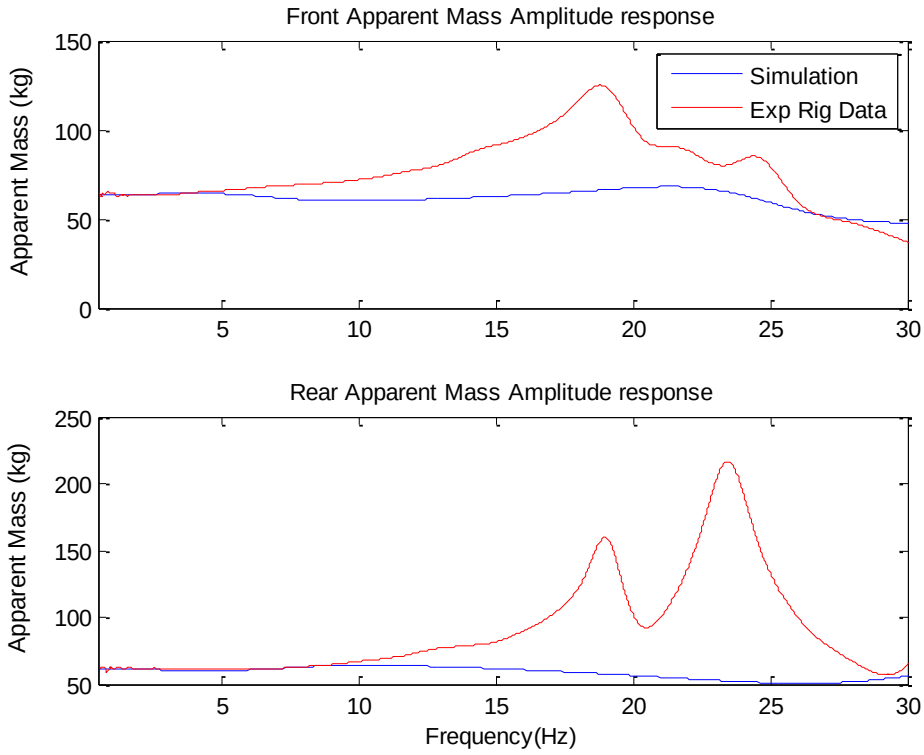

Figure 5-4: Dynamic apparent mass comparison – experimental data and 7-DOF model

Bennett (2012) investigated a chassis composed of several masses. Results suggested that the addition of extra DOFs could lead to a more accurate dynamic representation of the physical vehicle. However, the increased complexity of this model would also increase the simulation time and additional instrumentation would be required to determine properties (mass, location, elastic terms) of the new bodies.

In addition to this, a study has been carried out to analyse the impact of a simplified 1-DOF chassis when validating a vehicle model with experimental data obtained from physical car. A linear 7-DOF full-car model has been used to estimate the parameters of the test car featuring conventional suspensions without inerters. Using the method for parameter identification explained in Chapter 4, a set of vehicle and suspension parameters have been obtained. These estimated parameters have then been used to compare the response of model against experimental data. Validation results are shown in Figure 5-5 and Figure 5-6.

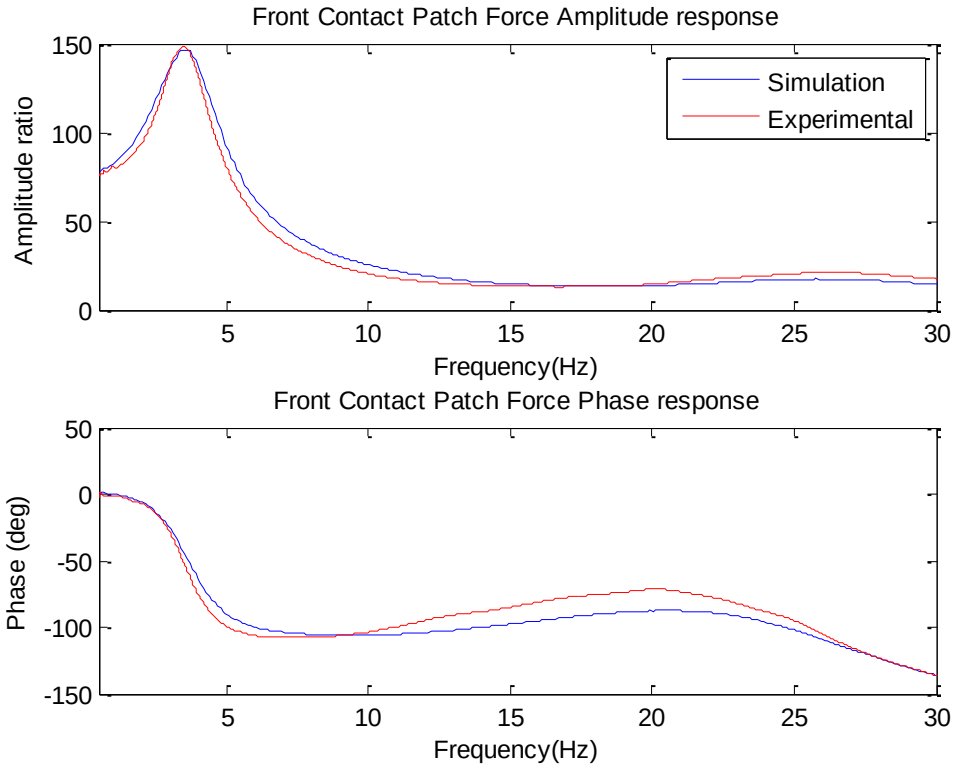

Figure 5-5: Front CPL/Input Acceleration frequency response

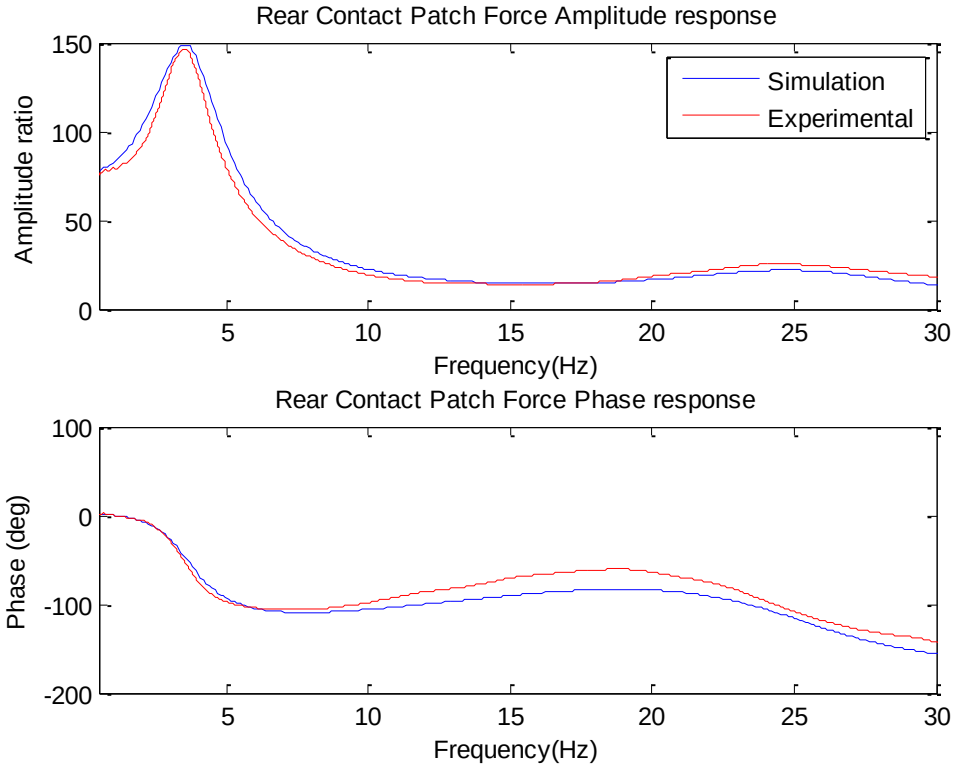

Figure 5-6: Rear CPL/Input Acceleration frequency response

Figure 5-5 and Figure 5-6 show that, even though the apparent mass estimation (see Figure 5-4) is not accurate, a 7-DOF model can still replicate the dynamic behaviour of the system. According to this, it has been decided that the chassis will be modelled as a single solid-rigid body.

The other limitation is the roll response of the system. A 7-DOF model assumes that the body will roll about the CoG of the vehicle. Moreover, this model assumes no lateral friction of the tyres during the roll response. When testing on the rig, Polytetrafluoroethylene (PFTE) pads are fitted on top of the steel pads to reduce the lateral friction between contact patch and pad. However, even with the pads fitted, there is still noticeable friction. In order to accurately represent this motion, the model should account for roll centre and lateral tyre compliance. Moreover, Bennett (2012) demonstrated that the effect of non-rotating wheels has a major impact in the roll response of a vehicle. The study carried out in that research work suggested that the dynamic roll response of the system is velocity dependent. Therefore, correlation between simulation and rig data would not be representative of the real behaviour of the car on a race track. According to this, the roll response in this research work will be used only for parameter identification purposes. Moreover, the roll response of vehicle will not be considered when defining performance based objective functions for suspension optimisation in Chapter 7.

5.3.2. Vehicle suspension model for Optimisation

As discussed in Chapter 2, the suspension optimisation problem requires the minimisation of a cost function J (or a set of cost functions in the case of MOOP) with respect to a set of suspension variables X. The evaluation of this objective function J requires the numerical integration of the set of EOMs that describe the dynamic behaviour of the vehicle system. Hence, the overall computational efficiency of the optimisation solver depends highly on the simulation time of the vehicle model.

As mentioned in Chapter 4, the vehicle has been designed to be symmetric with respect to its longitudinal axis. Furthermore, the roll response of a vehicle on the rig is not representative of the roll behaviour of the physical vehicle on a race track due to the effect of non-rotating wheels. Thus, roll dynamics has been neglected in the study of suspension performance. For these reasons, the vehicle model used in parameter estimation can be simplified to a 4-DOF half-car model when roll motion is neglected.

This simplification presents two main advantages. Firstly, the simplified model has faster simulation time. Since a half-car model has less state variables to be computed during the numerical integration process than a full-car model, increased computational efficiency can be achieved. A performance test was carried out to study the sensitivity of simulation time to the complexity of the model. In this study, a constant peak velocity (CPV) sine swept signal was used as model input. Both, full-car and half-car, models are simulated for 60 seconds with a sampling rate of 200 Hz. Three identical simulations are run for each model and simulation times are averaged. Results of this study are summarised in the following table:

	Simulation Time (secs)	
	Full-car model	Half-car model
Run 1	2.45	0.65
Run 2	2.41	0.66
Run 3	2.47	0.67
Average	**2.44**	**0.66**

Table 5-3: Simulation time comparison – Full-car and Half-car models

Table 5-3 shows that simulation time can be decreased from 2.44 to 0.66 seconds. This means that the optimisation process could converge to an optimal solution almost four times faster. Secondly, the other advantage of the use of a simplified vehicle model in optimisation is related to the definition of the optimisation search space X. A half-car model assumes equal left-to-right suspension parameters. This means that the number of suspension parameters that compose the search space X can be halved with respect to the full vehicle model. Hence, the computational efficiency of the optimisation solver can be increased further.

5.4. Modelling Suspension System Features

The main objective in vehicle suspension modelling is to obtain a reliable model for simulation. A vehicle model is useful only if it can accurately represent the real system and if it can reliably predict changes in the dynamic response according to different suspension settings.

In this section, a comprehensive vehicle suspension model has been developed so that it could be broadly applied to different race car suspension configurations. The model accounts for not only the main linear suspension components but also suspension parasitic effects and nonlinear tyres.

Suspension systems can be modelled as single-input single-output (SISO) systems. A representation of a SISO system is depicted in Figure 5-7. In general terms, a SISO system represents an ordinary differential equation (ODE) which can be expressed in terms of Laplace operator. The relationship between output and input in the Laplace transform can be expressed as a transfer function *G(s)* (Equation (5.3)).

$$G(s) = \frac{Y(s)}{U(s)} \tag{5.3}$$

This transfer function represents the characteristic of the system. In vehicle suspension modelling, relative suspension velocity *v(s)* is considered as the input variable *u* and force at the suspension terminals *F(s)* as the output variable *y* (Smith, 2002).

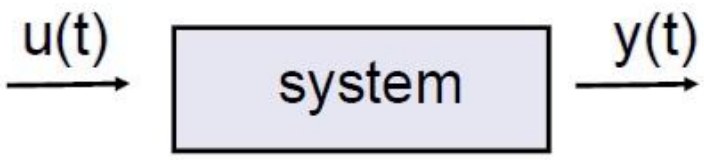

Figure 5-7: SISO system

One of the benefits of expressing a suspension layout as a transfer function in terms of Laplace operator is that this expression can be very easily manipulated to represent the dynamic stiffness in the frequency domain (equation (4.13)). Thus, recalling that Laplace operator $s = \omega j$:

$$G(s) = \frac{F(s)}{v(s)} = \frac{F(s)}{s \cdot x(s)} = \frac{F(\omega)}{\omega j \cdot x(\omega)} = \frac{1}{\omega j} \cdot K_{dyn} \tag{5.4}$$

Furthermore, Simulink has a 'built-in' function that allows the user to directly input any transfer function desired. This method of suspension modelling allows the suspension model to be condensed in one Simulink diagram or block so that the vehicle model can be updated by simply interchanging the suspension block.

The main shortcoming of this suspension modelling method is that the coefficients composing a transfer function in Simulink are time-invariant. Therefore, only linearised suspension systems can be represented with this method. However, the estimation of nonlinear components can be highly complex and errors are likely to be introduced.

Moreover, the addition of suspension nonlinearities will increase model complexity and computational effort required to simulate it. Hence, in this thesis, the transfer function *G(s)* has been used to characterise and model different suspension layouts.

5.4.1. Suspension System Layout featuring Inerters

Chapter 4 introduced and discussed the design of a test suspension incorporating real inerters. In this suspension system, the inerter has been designed so that it works in parallel with a conventional suspension, i.e. in parallel with springs and dampers. According to this design, the simplest suspension model can be composed by the three ideal mechanical elements in parallel. This suspension model has been labelled as suspension type 1. Such a suspension layout has been depicted in Figure 5-8.

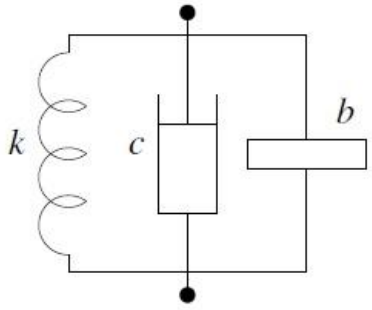

Figure 5-8: Suspension layout featuring with ideal mechanical elements – Type 1

According to Smith and Wang (2004), the characteristic equation of a suspension system can be expressed as the admittance of the mechanical system. Following the force-current analogy, the characteristic transfer function of the suspension layout shown in Figure 5-8 can be expressed as follows:

$$G(s) = \frac{F(s)}{v(s)} = \frac{k}{s} + c + bs = \frac{bs^2 + cs + k}{s} \qquad (5.5)$$

Where *k* is the spring stiffness, *c* is the damping coefficient and *b* is the inertance coefficient of the suspension.

The characteristic transfer function of equation (5.5) can then be used to obtain the simulated dynamic stiffness in the frequency domain following the procedure of equation (5.4). This theoretical response can then be correlated against experimental dynamic stiffness obtained from rig testing. In order to do so, the physical vehicle was tested incorporating real inerters

and the new parameter estimation program developed in Chapter 4 was used to estimate suspension characteristics *k*, *c* and *b*.

Figure 5-9 shows a comparison between the suspension dynamic stiffness obtained from equation (5.5) and the experimental suspension dynamic stiffness. Figure 5-9 shows that theoretical and experimental dynamic stiffness responses follow a similar trend at the beginning of the frequency range. However, as frequency increases, the difference in suspension behaviour also increases. While the theoretical model predicts a quadratic increase in dynamic stiffness, experimental data shows a peak of maximum dynamic stiffness followed by a gradual decrease in magnitude. This suspension model is then likely to cause large errors in the simulated dynamic response of the vehicle. In order to illustrate this deviation between experimental data and simulation, Figure 5-10 and Figure 5-11 show a comparison of the dynamic tyre load variation response of the physical vehicle and virtual simulation.

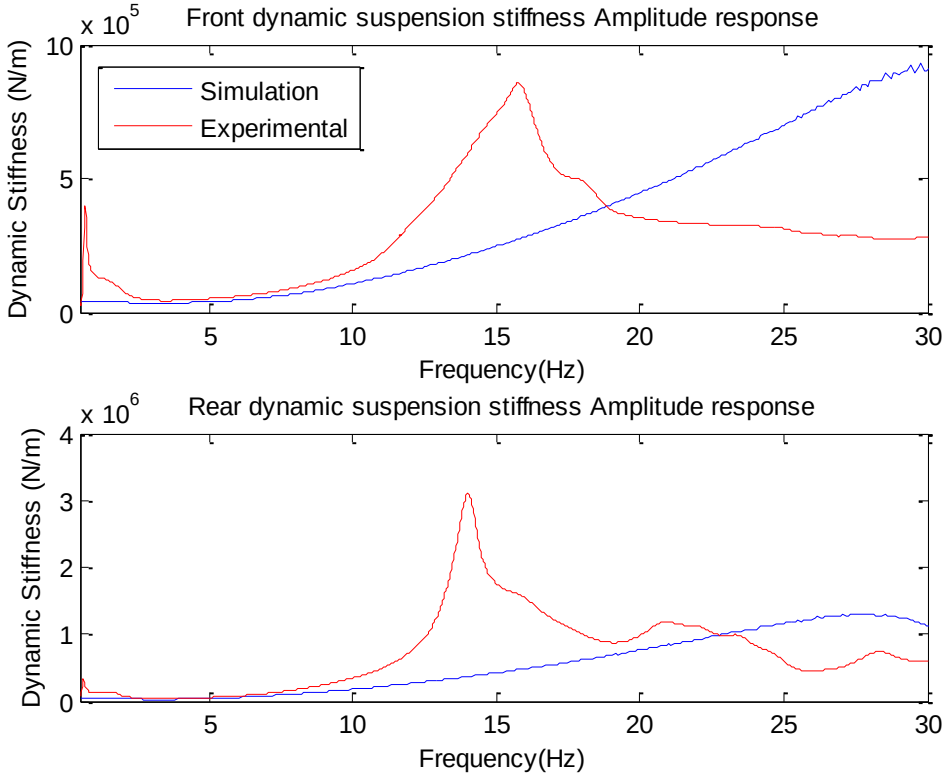

Figure 5-9: Dynamic suspension stiffness comparison: experimental rig data vs. suspension type 1

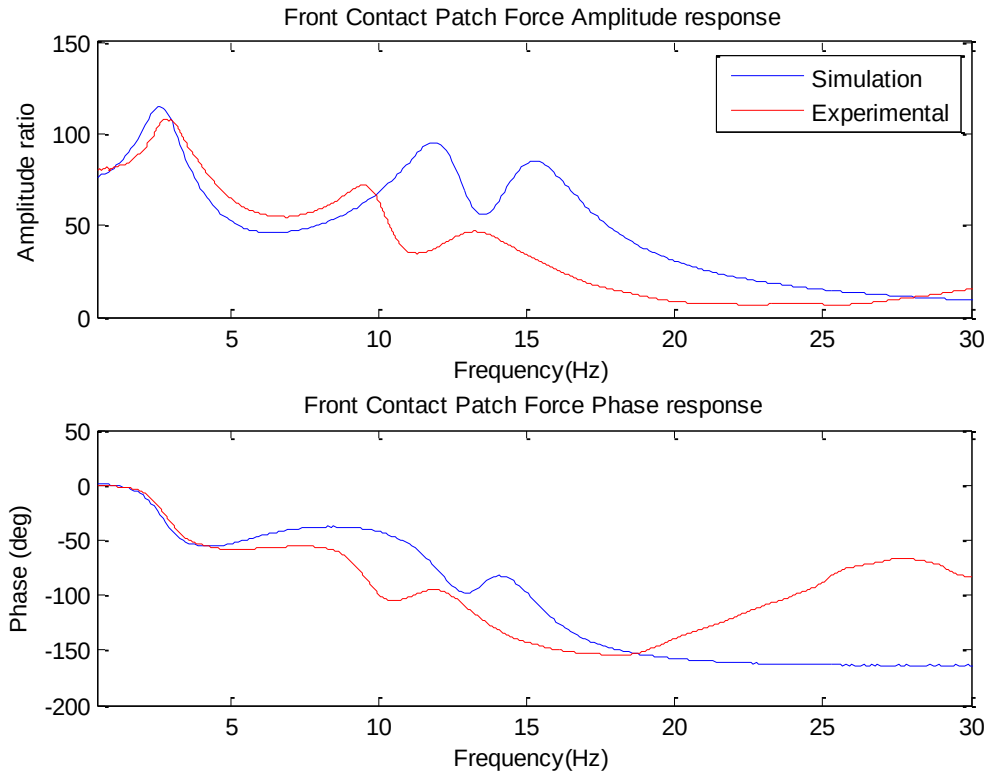

Figure 5-10: Front CPL frequency response: experimental vs. simulation type 1

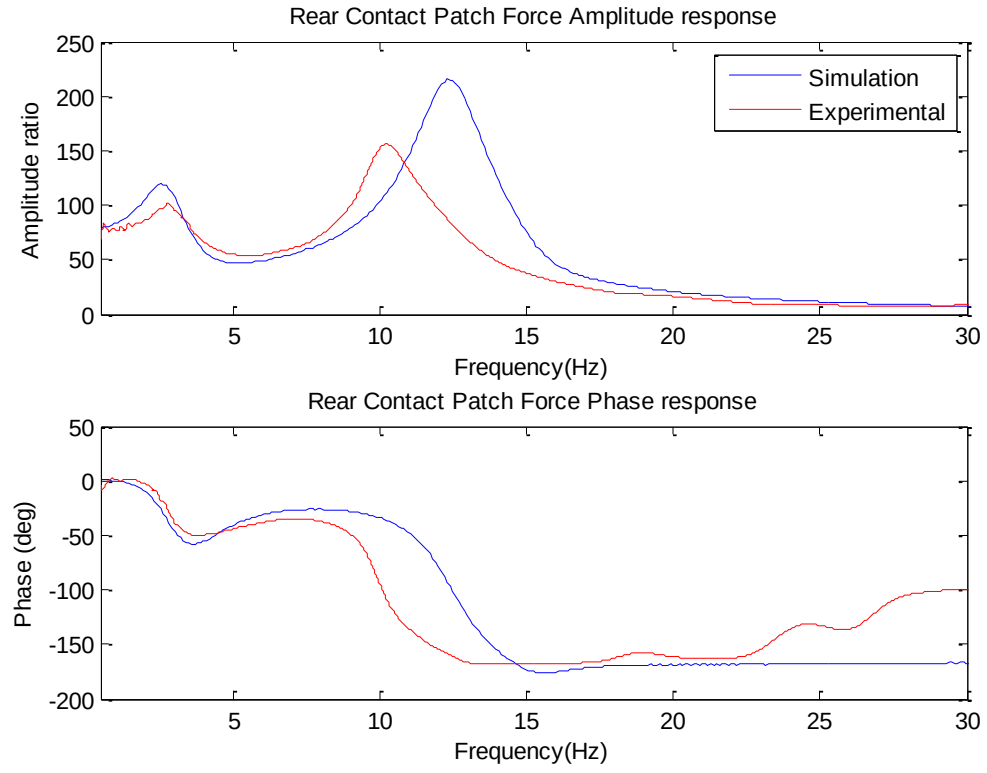

Figure 5-11: Rear CPL frequency response: experimental vs. simulation type 1

From the above figures, it can be observed that suspension model type 1 is not accurate enough to represent the actual dynamic response of a vehicle suspension fitted with inerters. Although the model predicts three resonant peaks in the front axle (Figure 5-10) and two in the rear end (Figure 5-11), the frequency at which they occur and their amplitude do not resemble the experimental dynamic response. Therefore, a more complex suspension model is required in order to obtain accurate dynamic responses of the vehicle in simulation.

An extension of suspension layout type 1 should then include suspension parasitic effects associated with real devices. Dampers usually present a nonlinear characteristic associated to the construction of the device itself. Many different nonlinear damper models have been attempted (Allen, et al., 2006). The simplest damper model is the discrete spring and dashpot model. In this representation, a damper is modelled as a spring in series with a dashpot. Figure 5-12 shows a representation of the discrete spring and dashpot model.

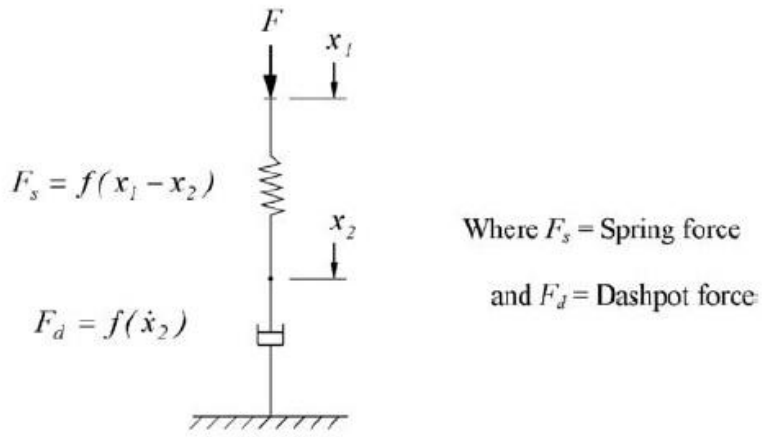

Figure 5-12: Discrete spring and dashpot model (Allen, et al., 2006)

In this model, the dashpot represents the damping force, whereas the spring represents damper parasitic effects mainly associated to damper hysteresis. In the general case, those elements can be modelled as nonlinear functions. In this research work, the parasitic spring k_m has been modelled as a linear spring and the damping characteristic c_s has been linearised.

Furthermore, Wang and Su (2008) developed and validated a model of a real inerter against experimental data. In that work, a ball screw inerter was designed and experimentally tested on a purpose-built rig facility. The experimental inerter model presented in that work accounted for elastic effects, backlash effects and nonlinear friction (see Figure 5-13).

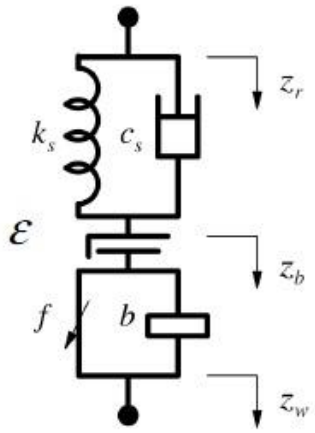

Figure 5-13: Nonlinear experimental inerter model (Wang & Su, 2008)

The model depicted in Figure 5-13 presents several nonlinearities that cannot be represented on a transfer function. In this thesis, a new linearised real inerter model is presented instead. The ball screw model designed and manufactured in this research work has preloaded balls inside the screw race. This preload prevents the mechanism from having backlash effects ($\varepsilon=0$). Moreover, inerter friction has been modelled as a linear viscous damping effect C_f. Finally, compliance effects have been modelled as a linear spring k_b (elastic term) in parallel with a damper C_b (energy dissipation term). These modifications allow the linearization of the experimental inerter model (see Figure 5-14).

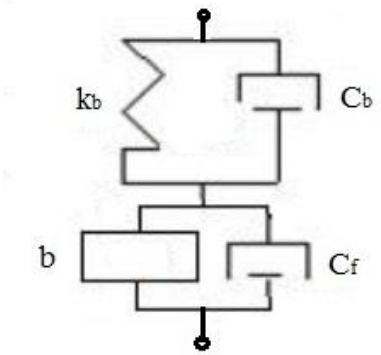

Figure 5-14: Linearised experimental inerter model

Another parasitic effect to take into account is suspension compliance. An important compromise exists in the design of race car suspension components (e.g. wishbones, pull/push-rods or rockers). On one hand, suspension components must be stiff enough so that they are capable of withstanding external forces applied to the chassis through the suspension system. On the other hand, components must be designed to be as light as possible in order to

keep the overall weight of the car low. Even though these components might be designed so that they fulfil all the structural criteria, they may exhibit some dynamic compliance. As the design ride frequency of the suspension increases (i.e. more stiffly sprung cars), the compliance of suspension elements plays a more important role in the dynamic behaviour of the suspension. Therefore, in this thesis, a linear spring has been modelled in series with the main suspension model to account for this suspension compliant effect. This term is called installation stiffness. Ideally installation stiffness must be as high as possible. Low values of installation stiffness causes a loss of suspension effectiveness to control vibrations especially at high frequencies. In order to illustrate this effect, a simple 2-DOF model has been used to show the effect of installation stiffness in the dynamic response of the system. The vehicle data used to simulate this model is summarised in the following table.

Sprung Mass	65 kg
Unsprung Mass	15 kg
Spring Stiffness	38 N/mm
Damping Ratio	0.4
Tyre Stiffness	250 N/mm
Tyre Damping	0.1 N/mm/s

Table 5-4: Vehicle data for installation stiffness study

Three different values of installation stiffness have been evaluated: 100, 200 and 650 N/mm. Results of this study are shown in Figure 5-15 to Figure 5-18:

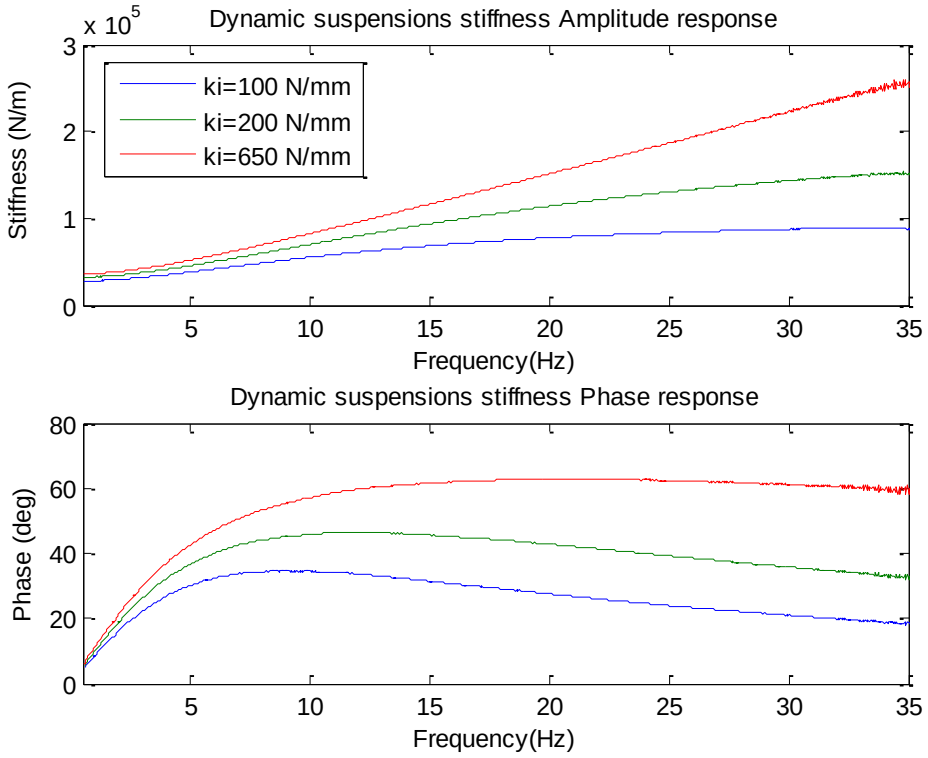

Figure 5-15: Effect of installation stiffness - Dynamic Stiffness frequency response

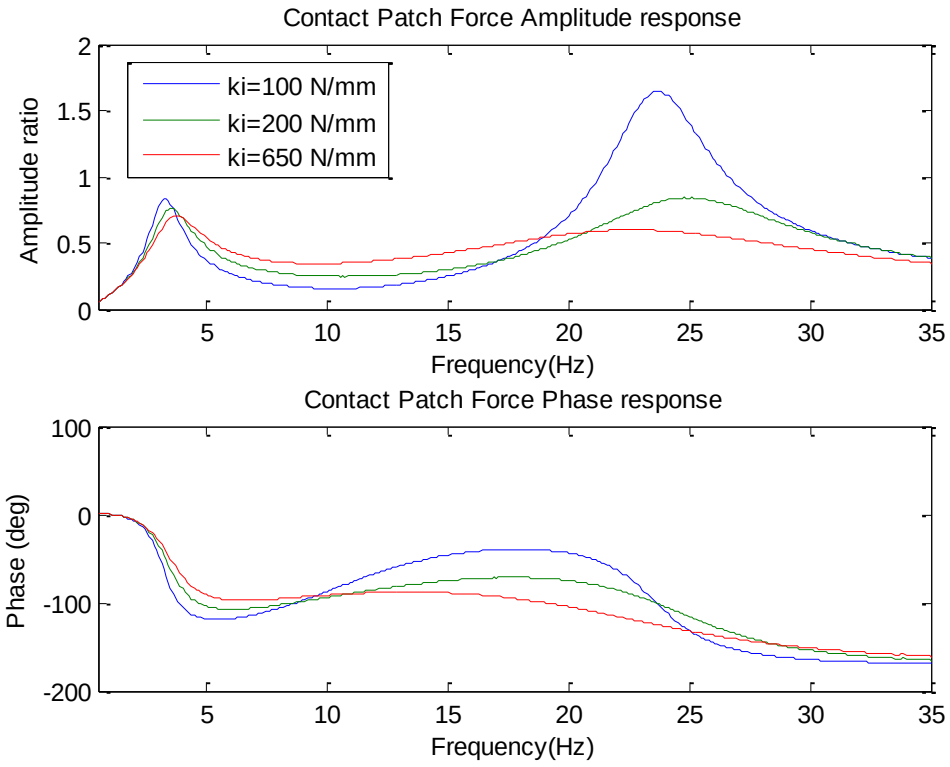

Figure 5-16: Effect of installation stiffness - CPL/Static mass frequency response

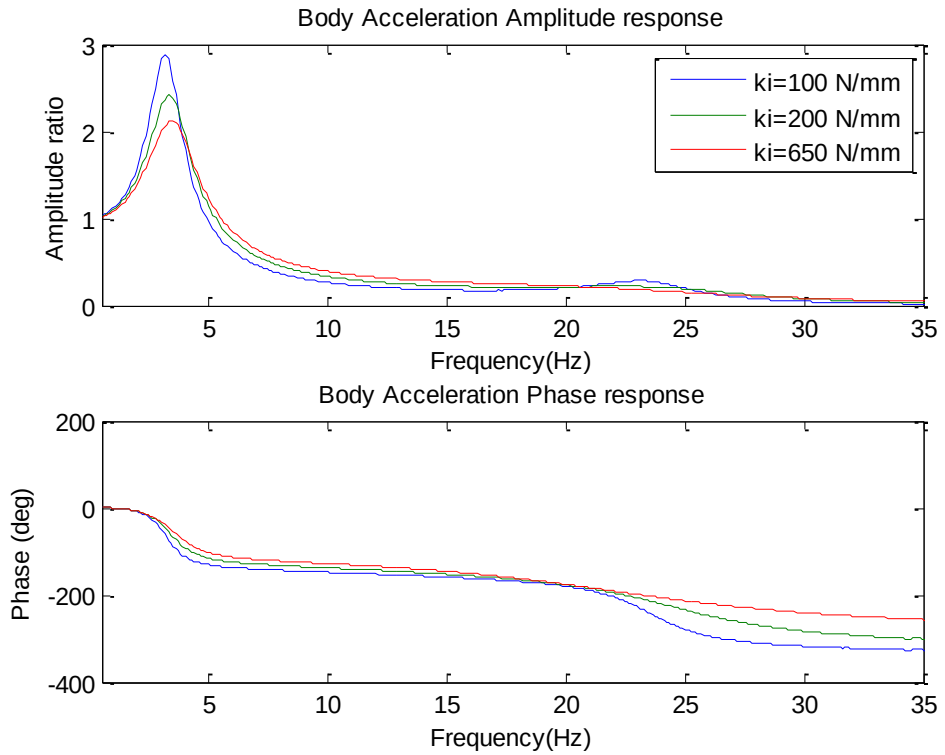

Figure 5-17: Effect of installation stiffness - Body Acceleration/Input Acceleration frequency response

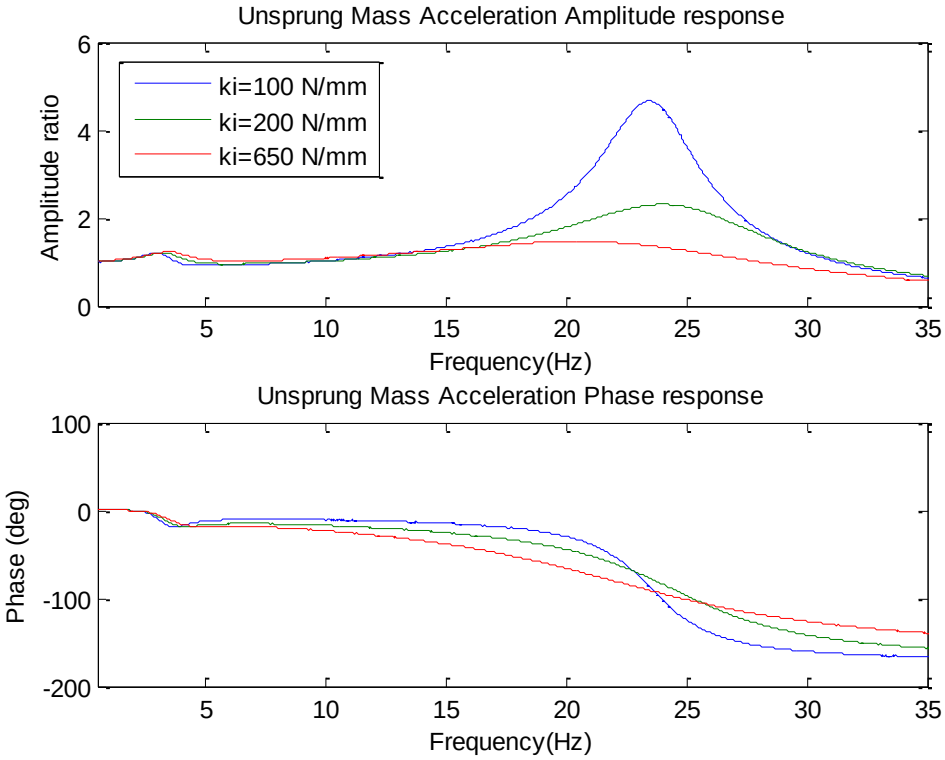

Figure 5-18: Effect of installation stiffness - Unsprung Acceleration/Input Acceleration frequency response

Figure 5-15 depicts the variation of dynamic stiffness with installation stiffness. Since installation and spring stiffness are working in series, a reduction of the installation stiffness causes a decrease of the overall ride frequency of the system. However, the main impact of installation stiffness occurs at higher frequencies (from 5 Hz onwards). Lower values of installation stiffness cause a reduction of the dynamic stiffness of the system, which, in turn, causes a decrease of the effective damping provided to the system. As expected, a reduction of effective damping causes uncontrolled body and hub mode (see Figure 5-16 to Figure 5-18). Under normal conditions, this effect could be counteracted by increasing damping of the system to regain control of body and hub modes. However, Figure 5-19 shows that, by increasing the damping ratio of the system from 0.4 to 0.6, the body mode exhibits a reduced resonant peak. However, an increase in damping has caused little effect at the hub mode (see Figure 5-20).

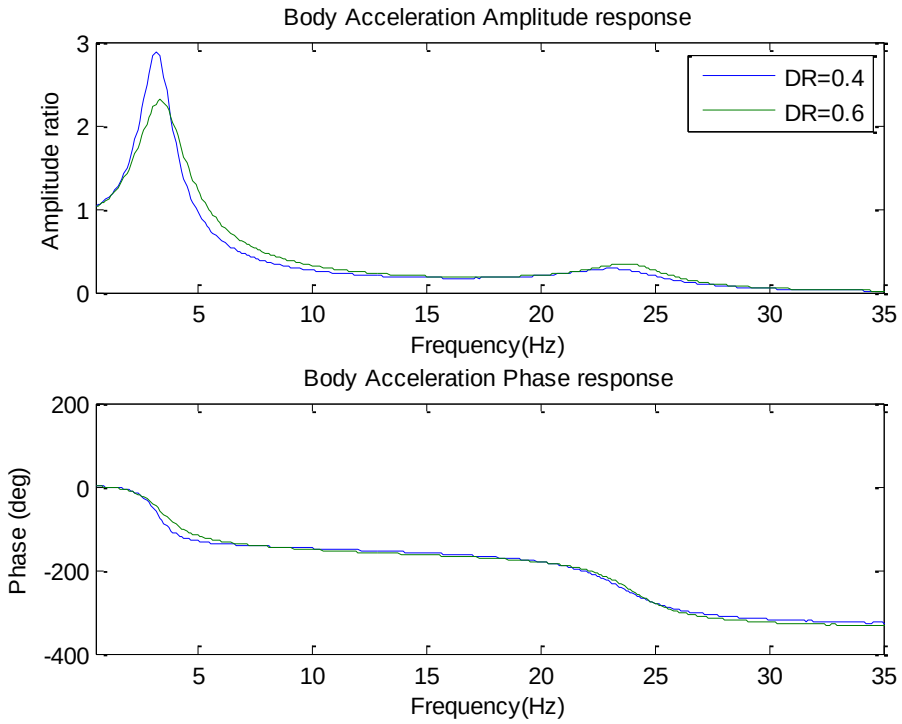

Figure 5-19: Body Acceleration response of 2-DOF system in k_i= 100 N/mm – Damping ratio comparison

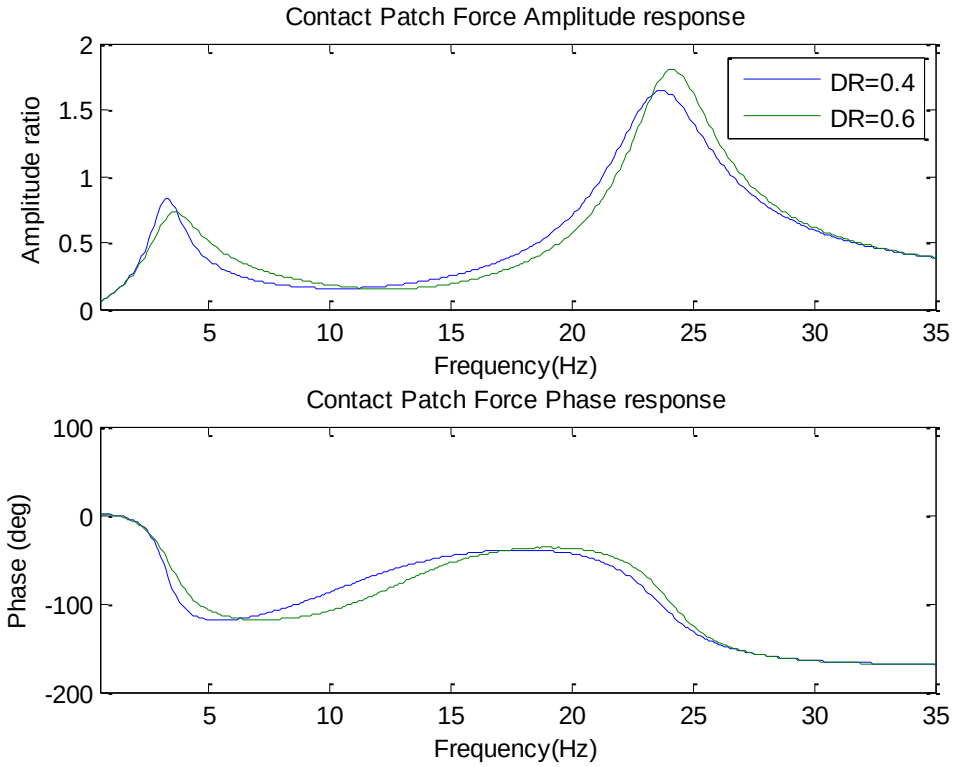

Figure 5-20: CPL response of 2-DOF system in k_i= 100 N/mm – Damping ratio comparison

Hence, the suspension layout type 1 has been extended so that it accounts for all of these suspension parasitic effects. The new suspension model takes into account hysteretic damper effects, friction and compliance inerter effects and overall suspension compliance effects (installation stiffness). This extended suspension model has been labelled as suspension layout type 2 and has been depicted in Figure 5-21.

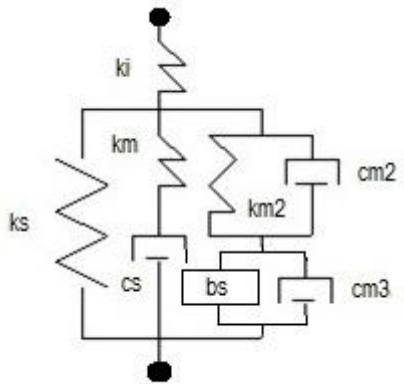

Figure 5-21: Suspension model layout type 2

As with suspension layout type 1, because all the elements composing this extended suspension layout are linear, a suspension transfer function can be obtained. Again the

parameter estimation method discussed in Chapter 4 has been used to identify all the suspension parameters shown in Figure 5-21 from experimental data.

The suspension transfer function can then be used to identify suspension parameters following the process discussed in Chapter 4 and to compare theoretical and experimental dynamic suspension stiffness data. Figure 5-22 shows that the actual suspension dynamic stiffness response can be much more accurately represented with suspension type 2. This suspension model predicts an increase of dynamic suspension stiffness up to maximum and then a gradual decrease at high frequencies. The suspension model has now been used to simulate the dynamic response of the vehicle. Figure 5-23 and Figure 5-24 compare the dynamic response in simulation with experimental data.

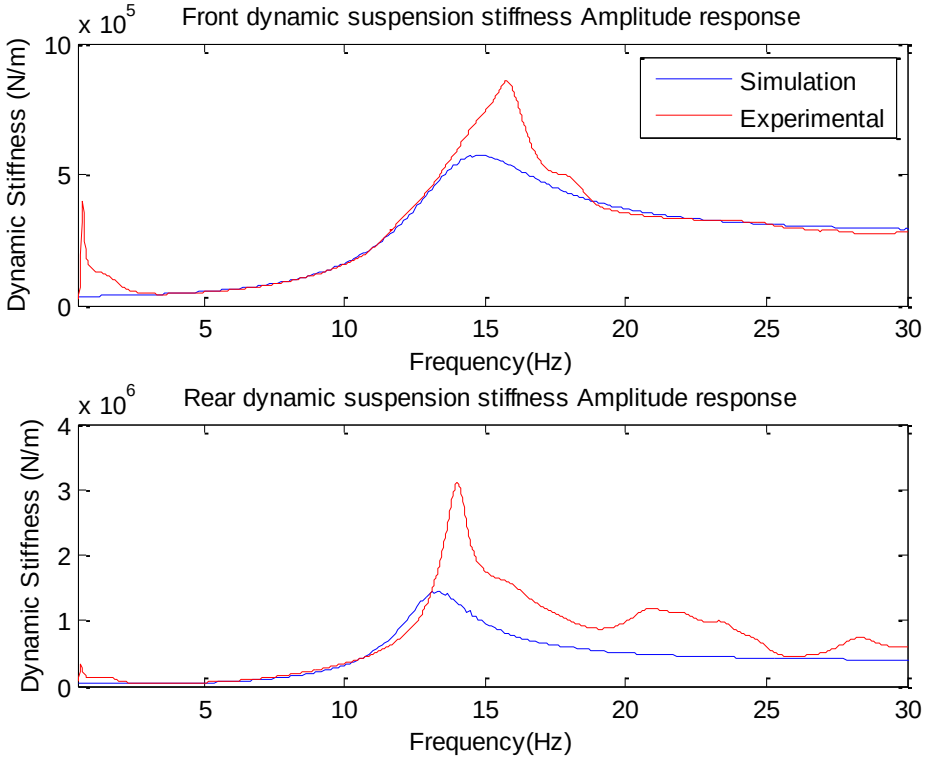

Figure 5-22: Dynamic suspension stiffness comparison: experimental rig data vs. suspension layout type 2

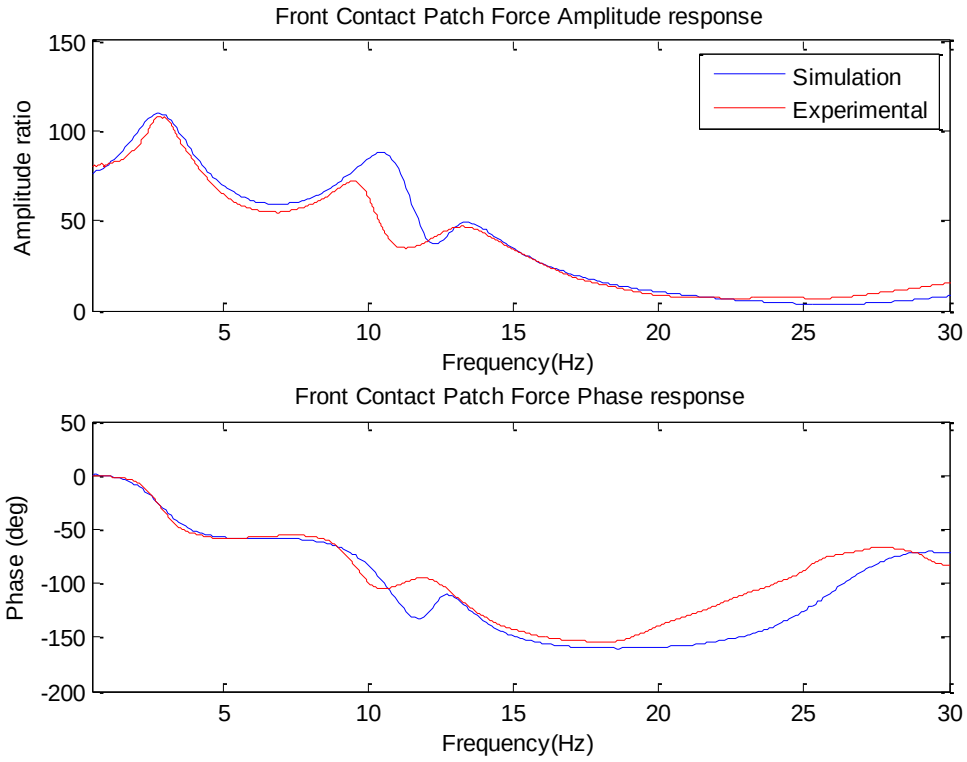

Figure 5-23: Front CPL frequency response: experimental vs. simulation type 2

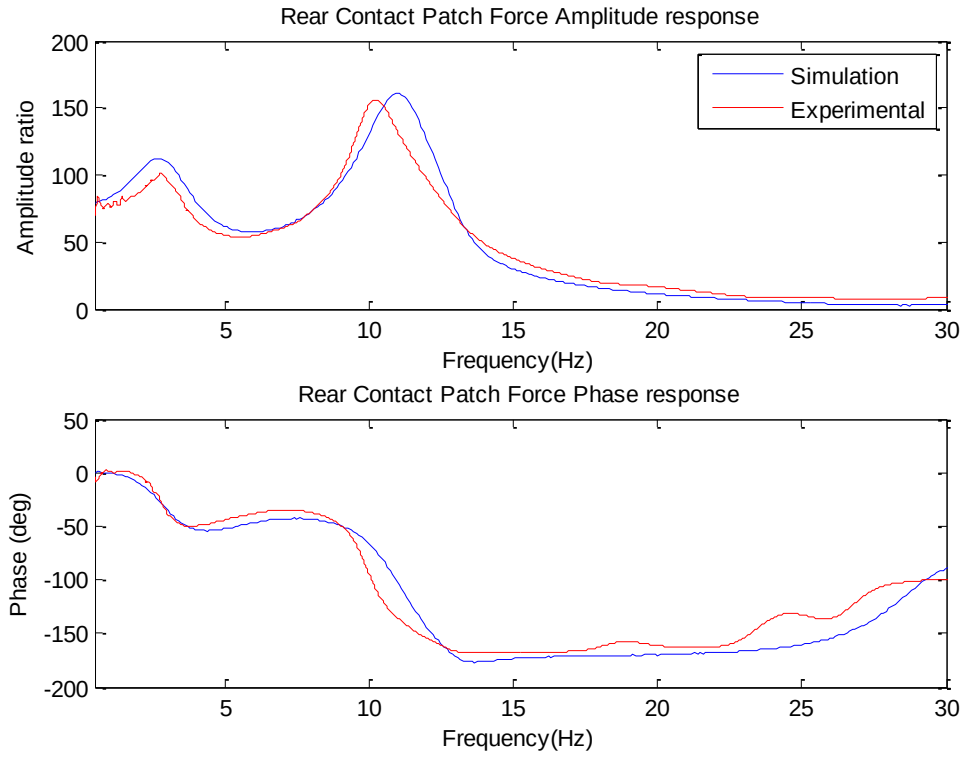

Figure 5-24: Rear CPL frequency response: experimental vs. simulation type 2

Figure 5-23 and Figure 5-24 show better agreement between virtual suspension model and experimental data than with suspension layout type 1 (see Figure 5-10 and Figure 5-11). Resonant peaks in simulation occur closer to the peaks found from experimental testing. However, the simulation model overestimates the amplitude of the hub resonant peak and there is a drift in the frequency at which the hub mode is occurring. At the beginning, it was thought that this extended linearised suspension model was not accurate enough. However, further investigation of the dynamic response of the physical suspension suggested that tyres were not showing a linear behaviour. Next section focuses on the study of the vertical tyre model in the dynamic response of the vehicle.

5.4.2. Non-linear Vertical Tyre Modelling

In Chapter 2, literature related to vehicle suspension modelling was discussed. In some of these vehicle models, tyres were considered as linear springs in order to model the elastic behaviour of the tyre (Todd & Kulakowski, 1990). Other vehicle models also included viscous linear tyre damping in order to account for the energy dissipation (Graf & Kosuch, 2008). Although, this is crude approximation of the general highly nonlinear dynamic tyre behaviour (Pacjeka, 2006), this tyre model has been extensively used in suspension analysis studies due to its simplicity.

A vehicle model incorporating a conventional suspension (no inerter fitted) and a linear tyre model has been used to evaluate the behaviour of actual tyres subjected to rig testing. An experimental test with this suspension configuration was set and tyre characteristics were estimated following procedure presented in equations (4.16) and (4.17). Figure 5-25 and Figure 5-26 show a comparison between experimental tyre stiffness and damping (red trace) and simulation (blue trace) for front and rear axles respectively. Simulated linear tyre stiffness and damping values have been obtained from an estimated as an average value from experimental data across the frequency range. As it can be observed in these plots, tyre elastic properties vary with frequency. Furthermore, experimental data shows that, in the low frequency range (up to 5 Hz), tyres present low stiffness and high damping characteristics. As frequency increases tyre stiffness increases and tyre damping decreases.

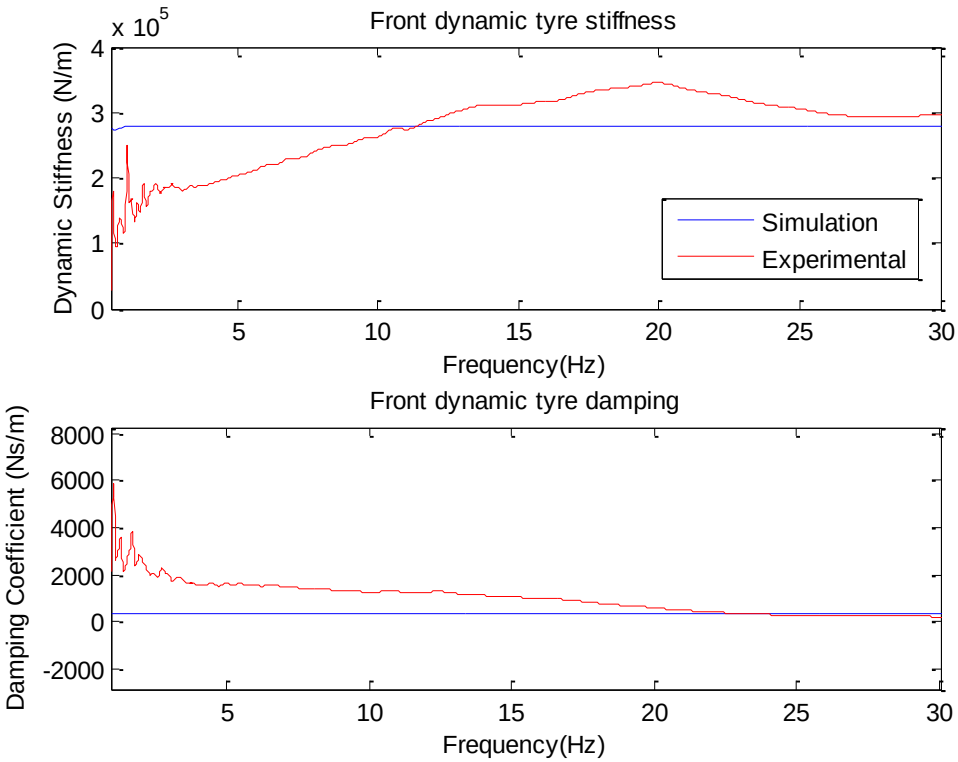

Figure 5-25: Front Tyre Stiffness and Damping comparison – Experimental data vs. linear tyre model

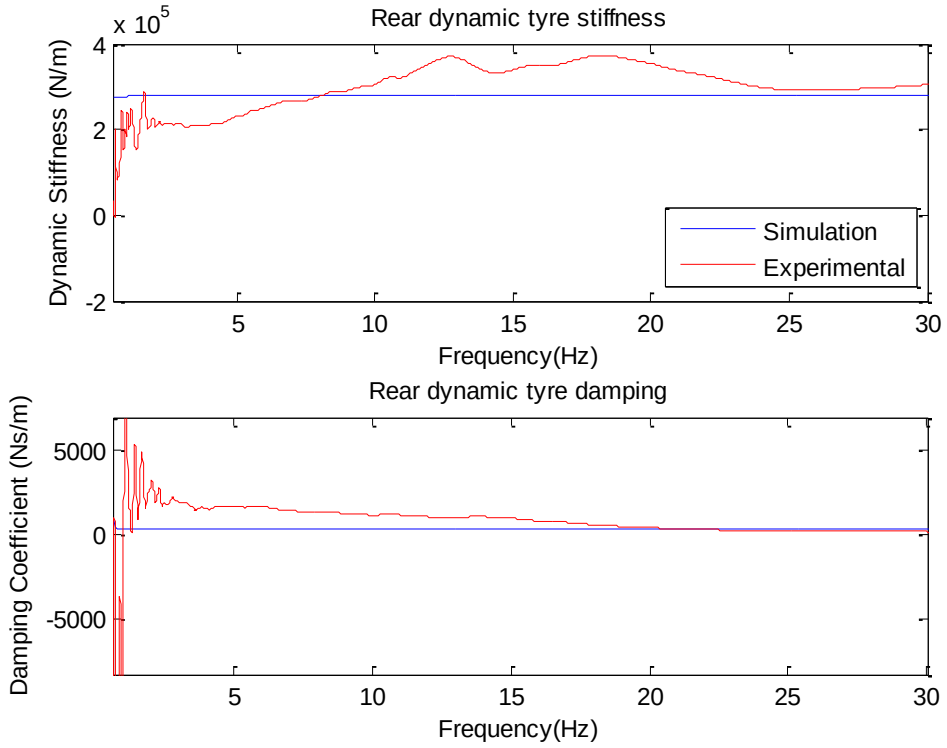

Figure 5-26: Rear Tyre Stiffness and Damping comparison – Experimental data vs. linear tyre model

Furthermore, in order to analyse the impact of varying tyre characteristics in the dynamic response of the vehicle, two sets of tyre characteristics have been defined. Set 1 has low tyre stiffness and high damping representing the tyre behaviour at the beginning of the frequency range. Set 2 represents the tyre behaviour towards the end of the frequency, i.e. high stiffness and low damping. Table 5-5 summarises the tyre properties considered for this study.

	Set 1	**Set 2**
Front Tyre Stiffness	215 N/mm	295 N/mm
Front Tyre Damping	1.25 N/mm/s	0.25 N/mm/s
Rear Tyre Stiffness	220 N/mm	285 N/mm
Rear Tyre Damping	0.8 N/mm/s	0.2 N/mm/s

Table 5-5: Tyre properties for linear tyre model study

Figure 5-27 compares the two sets of tyre characteristic with the experimental tyre characteristic. Figure 5-28 show the front dynamic contact patch load (CPL) response for the two tyre characteristic sets considered in Table 5-5.

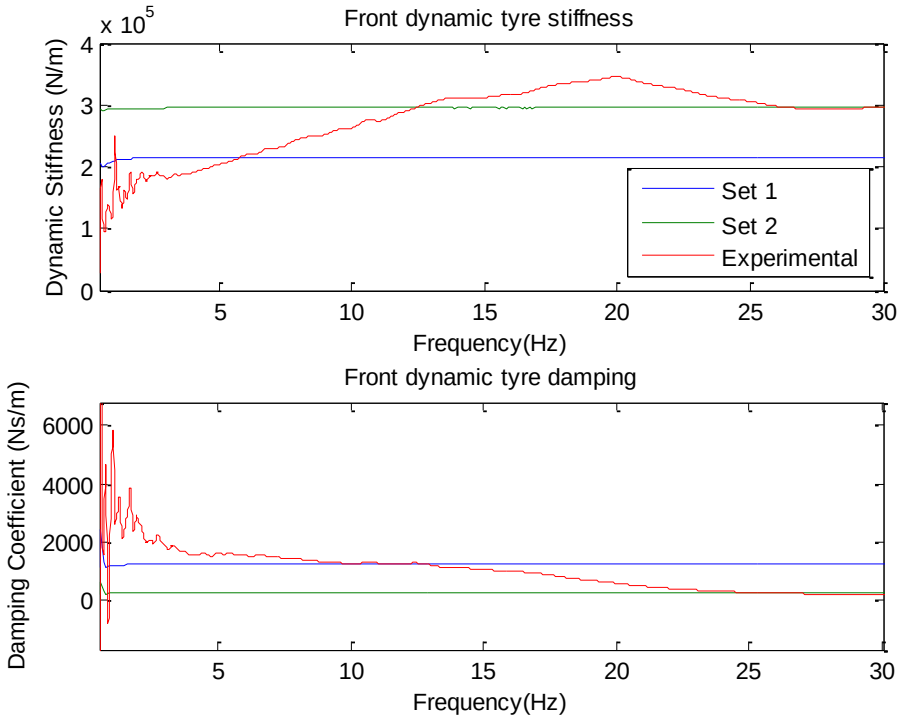

Figure 5-27: Tyre elastic properties – Tyre model comparison

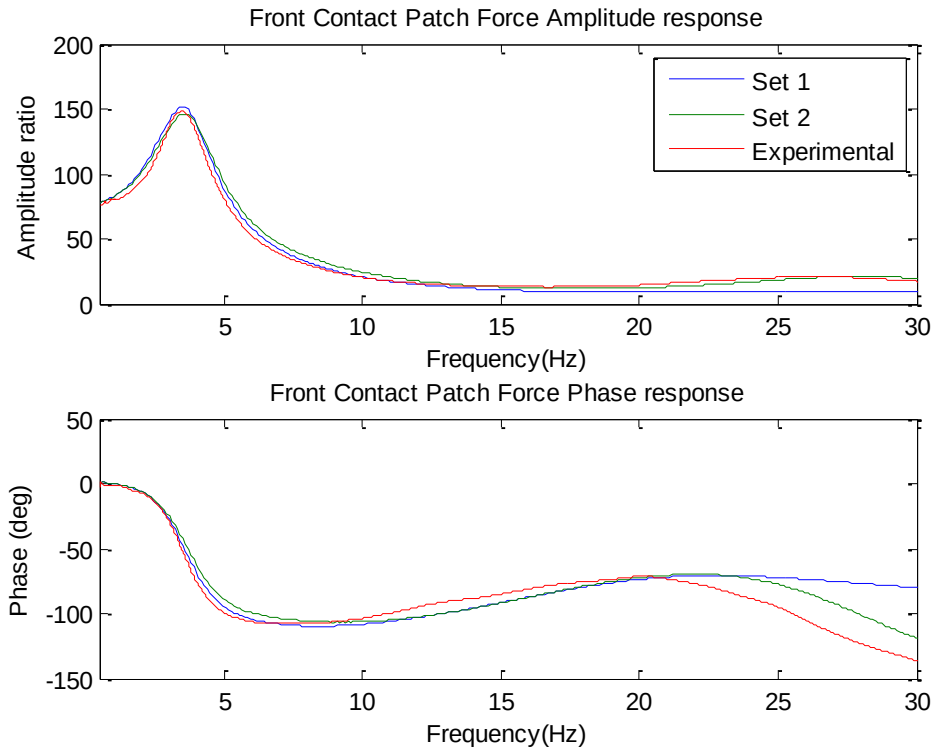

Figure 5-28: Front CPL ratio dynamic response with linear tyre mode

Figure 5-28 shows the difference in the CPL dynamic response of the vehicle related to different tyre models. On one hand, set 1 presents more accuracy in the prediction of the actual damping of the system at low frequencies (blue trace). However, this set fails to model the resonant peak at the hub mode. On the other hand, set 2 predicts a more damped body mode, but it accurately predicts the hub mode (green trace). This means that the vehicle should feature a variable tyre model that accounts for both sets if high predictive accuracy is required across the whole frequency range.

A tyre model that is frequency-dependent could be one solution. However, this model does not contain any information with regard to the phenomena that might cause this apparent nonlinear behaviour. Moreover, this variable model would only be able to generate accurate dynamic responses for local suspension configurations, since the estimation would be based on parameters estimated for a particular suspension system. Further investigation into nonlinear vertical tyre modelling is then required.

An experimental study of the influence of tyre dynamic deflection into tyre elastic properties has been carried out. The vehicle was tested on the four-post rig at two different input displacement amplitudes: 25 and 35 mm. The rest of the suspension parameters remained

unchanged. Experimental tyre deflection and dynamic tyre stiffness responses have been plotted in Figure 5-30 and Figure 5-29 respectively in order to investigate the interaction between both magnitudes. In both figures, the blue trace (Run 3 in the legend) represents the result of the 25-mm input displacement amplitude run and the red trace (Run 7) represents the result of the 35-mm input displacement amplitude run. As expected, a larger road input causes larger deflections on the tyre (see Figure 5-29). Interestingly, Figure 5-30 shows that this increases in tyre deflection cause a reduction of the dynamic tyre stiffness. This suggests that some interaction between both magnitudes exists.

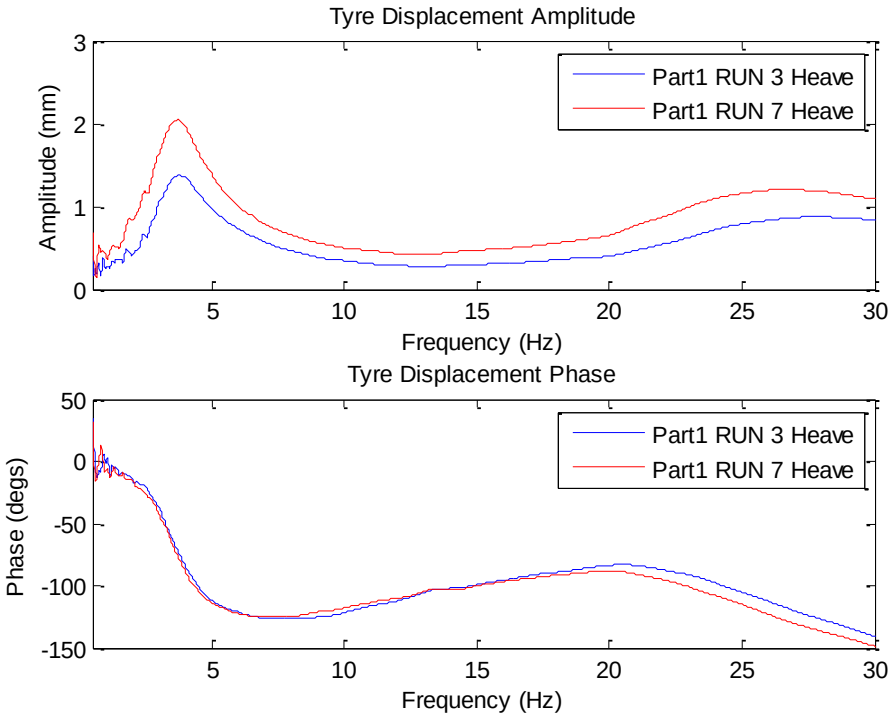

Figure 5-29: Absolute tyre deflection dynamic response at various input amplitudes

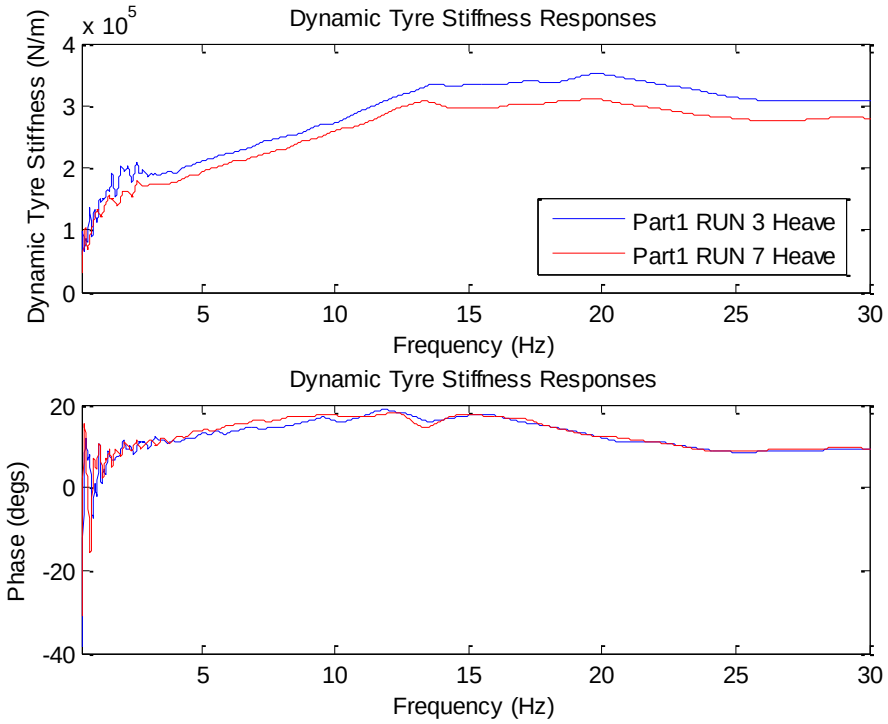

Figure 5-30: Experimental dynamic stiffness response for various input amplitudes

Moreover, a pattern between tyre deflection and dynamic stiffness can be observed from the dynamic responses. At the body mode (3.5 Hz), tyre deflection amplitude reaches its maximum value, which corresponds to minimum tyre dynamic stiffness. After that, the amplitude of the absolute tyre deflection gradually reduces (5-15 Hz) until it eventually reaches a minimum amplitude value. During this frequency range, dynamic stiffness steadily increases until it settles in a maximum value. In the proximity of the hub mode, tyre deflection increases again, which leads to a new reduction of the dynamic stiffness. Therefore, this study demonstrates that tyre elastic properties are tyre deflection dependent rather than frequency dependent.

Hence, having stated that there is a strong relationship between tyre deflection and tyre elastic properties, a nonlinear vertical tyre model must be obtained. Assuming that the tyre is composed by a spring in parallel with a damper, experimental tyre spring and damper characteristics can be derived from the complex expression of dynamic tyre stiffness.

$$K_{tyre}(\omega) = \frac{F_{CP}(\omega)}{x_{tyre}(\omega)} = k_t + c_t \omega j \qquad (5.6)$$

Where $k_t=f(x_t)$ and $c_t=f(x_t)$ represent nonlinear tyre stiffness and damping respectively and x_t represents the tyre deflection. Note that equation (5.6) is expressed as a complex number in which the real part represents tyre stiffness k_t and the imaginary part represents tyre damping c_t multiplied by the angular frequency ω.

The next step is to plot experimental tyre spring and damping with respect to tyre deflection. Note that, when modelling dynamic systems, damping elements are defined as devices capable of generating a force proportional to the relative velocity between component terminals. According to this, tyre damping will be plotted against tyre deflection rate $\dot{x}_t$ in order to keep a consistent definition of the dynamic tyre characteristics with the general dynamic modelling principles.

Figure 5-31 and Figure 5-32 show the nonlinear tyre stiffness and tyre damping characteristics obtained from experimental testing respectively. In order to avoid noisy data due to sensor resolution when measuring small tyre deflections, frequency range has been limited to regions around body (3-12 Hz) and hub modes (15-28 Hz). The first region corresponds to maximum tyre deflection and it has been used to plot tyre deflection, whereas second region corresponds to maximum tyre deflection velocity and it has been used to obtain an accurate tyre damping estimate. Both tyre stiffness and damping present an exponential decay characteristic with respect to tyre deflection and tyre deflection velocity respectively.

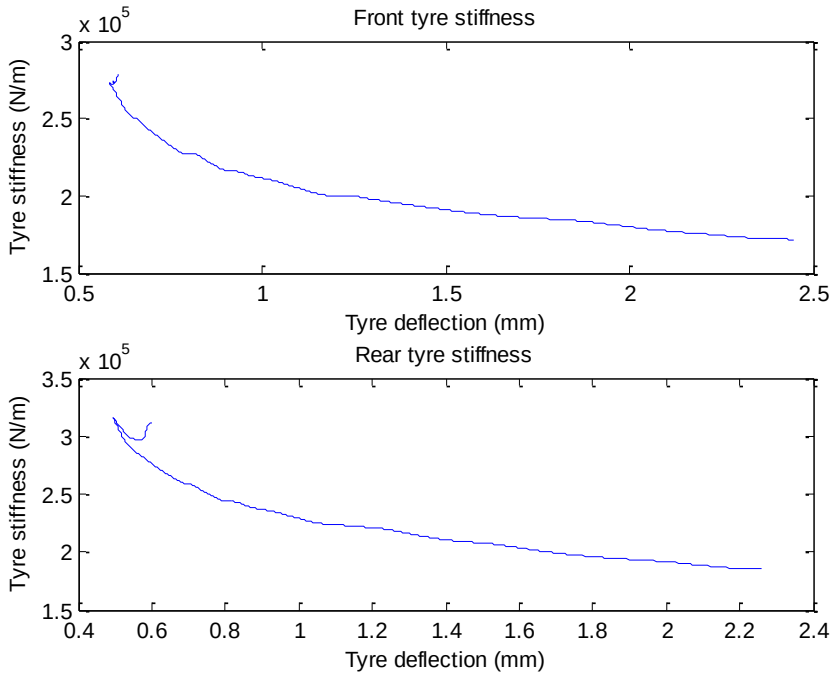

Figure 5-31: Nonlinear experimental tyre stiffness characteristic: Front (upper) and rear (lower)

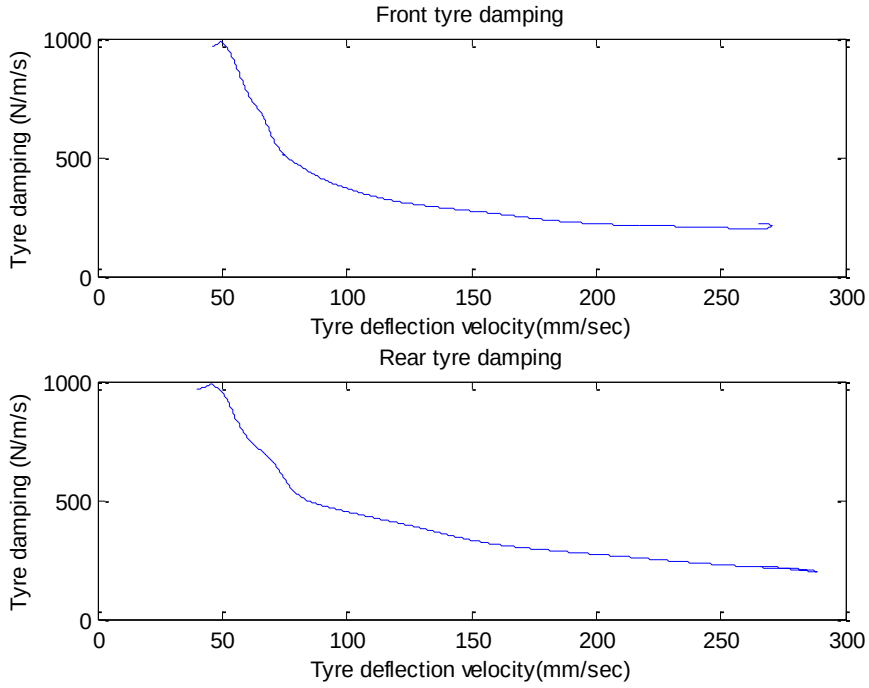

Figure 5-32: Nonlinear experimental tyre damping characteristic: Front (upper) and rear (lower)

According to the results obtained in Figure 5-31 and Figure 5-32, a nonlinear exponential tyre model has been proposed to simulate the actual behaviour of the tyres observed from experimental testing. Hence, the vertical tyre model can be expressed by the following equaations:

$$k_t = a \cdot e^{-bx_{tyre}} + k_{t0} \tag{5.7}$$

$$c_t = d \cdot e^{-n\dot{x}_{tyre}} + c_{t0} \tag{5.8}$$

Equations (5.7) and (5.8) represent a semi-empirical nonlinear vertical tyre model based on experimental data obtained from four-post rig testing. In those equations, parameters *a* and *d* define the initial values of stiffness and damping respectively. Parameters *b* and *n* define the rate of the exponential decay. Parameters k_{t0} and c_{t0} establish an asymptotic bottom limit for tyre stiffness and damping characteristics and provide numerical consistency to the solver.

All these parameters can be estimated following the procedure explained in Chapter 4. An experimental test has been carried out so that model correlation can be analysed. A 30-mm heave run was carried out to the test car fitted with conventional suspension (no inerters fitted). The value of the parameters obtained from the estimation program have been summarised in Table 5-6:

		Front Tyre	Rear Tyre
Tyre Stiffness	**a (N/m)**	171000	178000
	b (mm^{-1})	1250	1400
	k_{t0} (N/m)	195000	185000
Tyre Damping	**d (Ns/m)**	3850	4100
	n (s/mm)	45	50
	c_{t0} (Ns/m)	200	350

Table 5-6: Estimated parameters for tyre model

Figure 5-33 and Figure 5-34 show a good correlation between experimental data and the new nonlinear semi-empirical tyre model developed in this section.

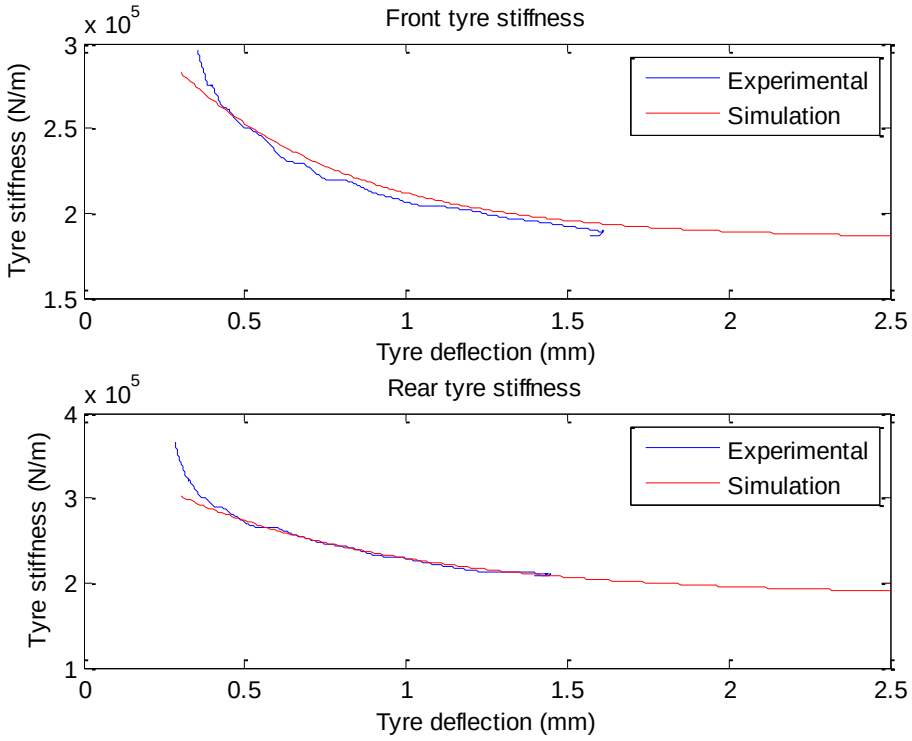

Figure 5-33: Nonlinear tyre stiffness model comparison between experimental vs. exponential model

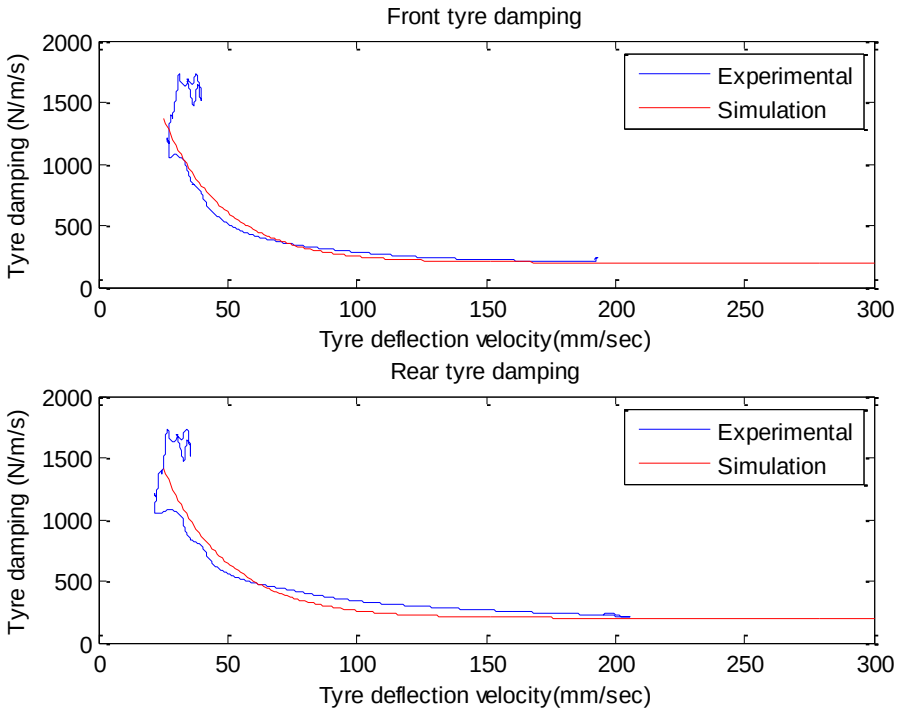

Figure 5-34: Nonlinear tyre damping model comparison between experimental vs. exponential model

Figure 5-35 to Figure 5-38 depict the dynamic response of the vehicle with the new nonlinear tyre model. The model predicts body and hub modes accurately in both axles. Furthermore, a comparison of model accuracy in representing dynamic CPL ratio frequency response between linear tyre model (Figure 5-28) and nonlinear tyre model (Figure 5-35) can be made. The linear tyre model fails to provide accurate results at the body and hub modes at the same time, whereas the nonlinear tyre mode is able to much more accurately represent the actual dynamic response of the vehicle.

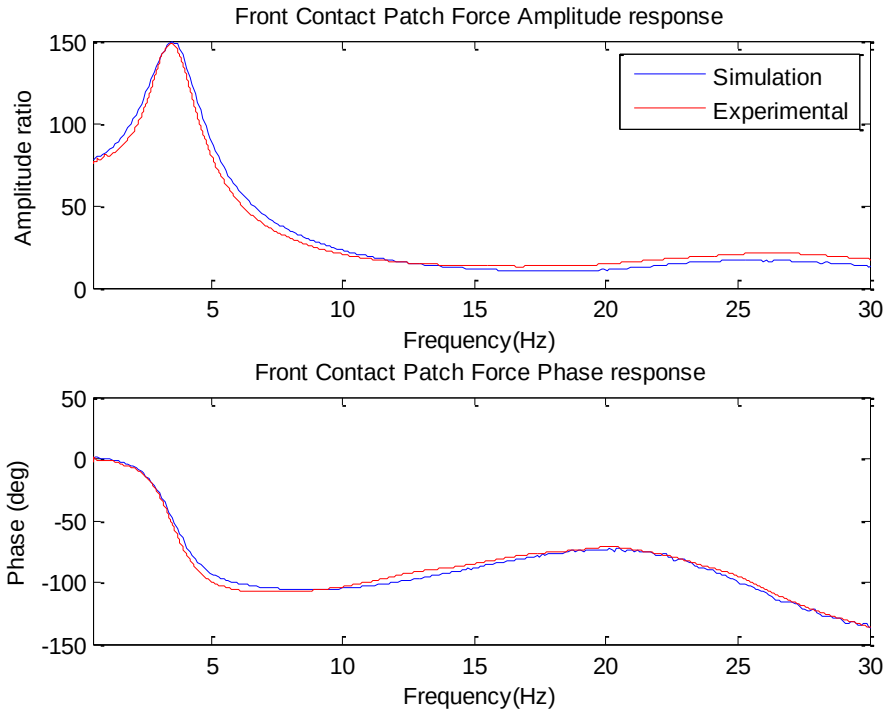

Figure 5-35: Front CPL ratio frequency response with nonlinear tyre model

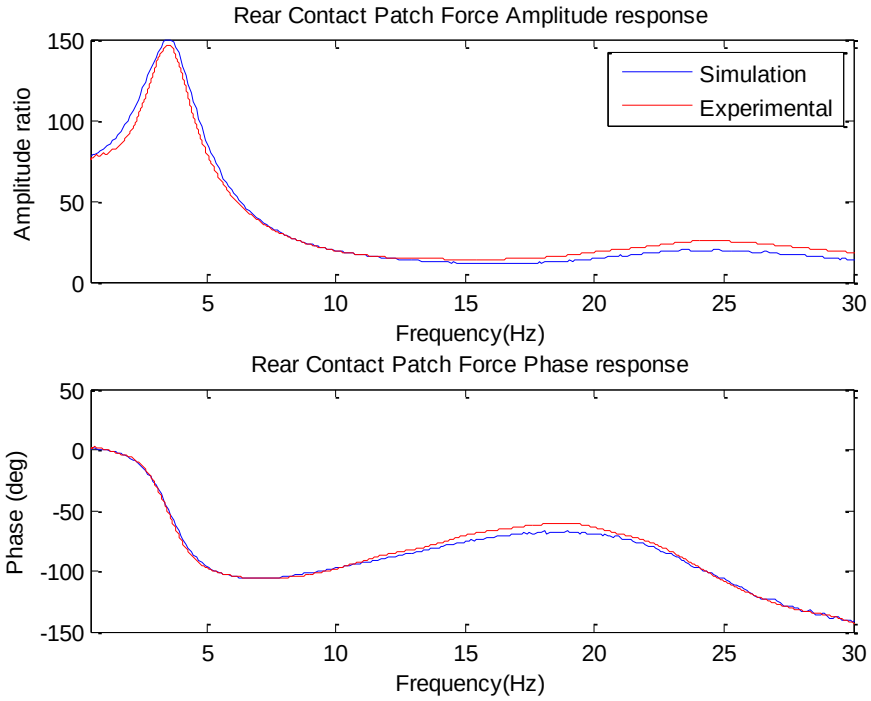

Figure 5-36: Rear CPL frequency ratio response with nonlinear tyre model

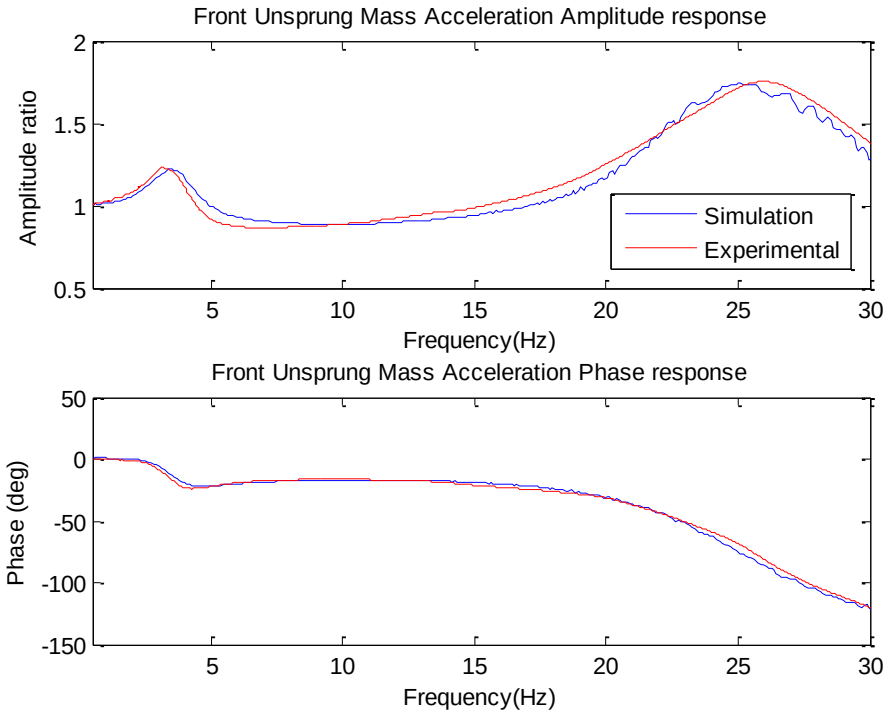

Figure 5-37: Front unsprung mass acceleration ratio frequency response with nonlinear tyre model

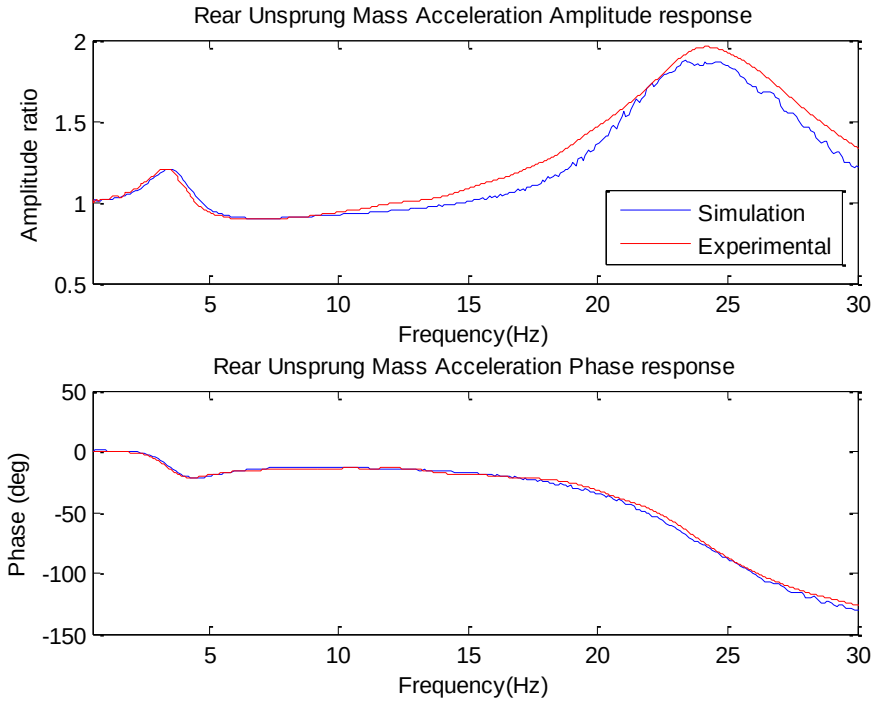

Figure 5-38: Front unsprung mass acceleration ratio frequency response with nonlinear tyre model

Hence, a completed vehicle model can be obtained by integrating this semi-empirical nonlinear tyre model with the suspension model incorporating real inerters developed in section 5.4.1. The following section analyses and discusses thoroughly the validity of vehicle model presented in this section.

5.5. Suspension Validation with 4-Post Rig Test Experimental Results

Simulation models must be validated with experimental data in order to ensure that they are reproducing the dynamics of the actual vehicle to some degree of accuracy and predictability. The vehicle model developed in the previous section has been correlated against experimental data obtained from four-post rig testing. Moreover, the extended parameter estimation program developed in Chapter 4 has been used to identify vehicle parameters and to analyse the correlation between the virtual vehicle model and experimental data.

In order to simplify the estimation and the validation process, only suspension settings have been tuned. The rest of vehicle and tyre properties remained unchanged. Thus, parameters related to vehicle and tyre properties have not been re-estimated for each suspension setting. Table 5-7 and Table 5-8 summarises the set of vehicle and tyre properties obtained from the parameter identification process.

Sprung Mass (m_s)	250 kg
Front Unsprung Mass (m_{uf})	14 kg
Rear Unsprung Mass (m_{ur})	15 kg
Front Weight Distribution (%wt)	50.5 %
Pitch Moment of Inertia (J_p)	30.5 kgm^2
Roll Moment of Inertia (J_r)	28 kgm^2
Wheelbase (l)	1565 mm
Front Track (tf)	1320 mm
Rear Track (tr)	1210 mm

Table 5-7: Vehicle data properties used in validation process

Front a	171000 N/m
Front b	1250 mm^{-1}
Front k_{t0}	195000 N/m
Front d	3850 Ns/m
Front n	45 s/mm
Front c_{t0}	200 Ns/m
Rear a	178000 N/m
Rear b	1200 mm^{-1}
Rear k_{t0}	185000 N/m
Rear d	4100 Ns/m
Rear n	50 s/mm
Rear c_{t0}	350 Ns/m

Table 5-8: Tyre elastic properties used in validation process

The following sections present the validation graphs and discuss the accuracy of the results obtained from comparing experimental rig data with simulation.

5.5.1. Analysis of model accuracy for different inerter settings

In order to evaluate accuracy of the model, several suspension configurations have been set and experimentally tested on the four-post rig. In this way, the model accuracy can be examined under different conditions and model predictability can also be evaluated.

Over the past sections, the vehicle model incorporating a conventional suspension without inerters has been used to carry out several analysis studies. These studies demonstrated that the model was capable of replicating the dynamic behaviour of the physical vehicle. This section focuses on the analysis of this vehicle model incorporating real inerters and on the validation of this model against experimental data. Hence, in order to simplify the validation process, only inerter settings have been modified. According to this, Table 5-9 shows a tuning sheet with all the suspension settings used in this section. Some general considerations must be highlighted with regard to the suspension settings selected: firstly, suspension settings were mirrored from left to right of the test car in order to keep vehicle symmetry with respect to the longitudinal axis. Secondly, springs and pull/pushrod settings were set so that the ride frequency of front and rear axles was around 4 and 3.7 Hz respectively. According to (Milliken & Milliken, 1995), these ride frequencies corresponds to the suspension of race car with mid/high aerodynamic downforce effects. Lastly, damper settings were selected to

provide a damping ratio of about 0.45. According to Milliken and Milliken (1995), this damping ratio offers the optimal road holding performance with a conventional suspension.

Front Springs		500 lbs/in
Rear Springs		500 lbs/in
Front Damper settings	LSB	15
	HSB	10
	LSR	22
	HSR	13
Rear Damper settings	LSB	16
	HSB	10
	LSR	20
	HSR	12
Front Pullrod setting		2
Rear Pushrod setting		2

Table 5-9: General suspension settings

Furthermore, Table 5-10 summarised the different inerter settings tested in order to evaluate the accuracy and predictability of the vehicle model featuring real inerters. These settings cover a wide range of inerter configurations from low to very high inertance.

	Inerter Set-up				
	1	**2**	**3**	**4**	**5**
Front Inerter	2 mm FWM + 1x2 mm disk	6 mm FWM	6 mm FWM + 1x4 mm disk	6 mm FWM + 2x4 mm disk	6 mm FWM + 4x4 mm disk
Rear Inerter	2 mm FWM	6 mm FWM	6 mm FWM + 1x4 mm disk	6 mm FWM + 2x4 mm disk	6 mm FWM + 4x4 mm disk

Table 5-10: Summary of inerter settings tested

In the following sub-sections, suspension parameters are estimated and correlation analysis between experimental data and simulation is carried out for the inerter settings presented in Table 5-10.

Suspension Set-up 1

The parameter estimation technique developed in Chapter 4 has been used to identify all the suspension properties according to the suspension model presented in Figure 5-21. Table

5-11 summarises the values of the suspension parameters estimated. The values of inertance *b* obtained for front and rear axle denote a suspension setting with low inertance.

Front Spring Stiffness (k_{sf})	38000 N/m
Front Damper Rate (c_{sf})	1200 Ns/m
Front Inertance (b_{sf})	8.6 kg
Front Damper Top Mount Stiffness (k_{mf})	225000 N/m
Front Inerter Top Mount Stiffness (k_{m2f})	187000 N/m
Front Inerter Top Mount Damping (c_{m2f})	380 Ns/m
Front Inerter Friction damping (c_{m3f})	300 Ns/m
Front Installation Stiffness (k_{if})	1225 kN/m
Rear Spring Stiffness (k_{sr})	35500 N/m
Rear Damper Rate (c_{sr})	1180 Ns/m
Rear Inertance (b_{sr})	11.5 kg
Rear Damper Top Mount Stiffness (k_{mr})	185000 N/m
Rear Inerter Top Mount Stiffness (k_{m2r})	322000 N/m
Rear Inerter Top Mount Damping (c_{m2r})	520 Ns/m
Rear Inerter Friction damping (c_{m3r})	280 Ns/m
Rear Installation Stiffness (k_{ir})	1950 kN/m

Table 5-11: Estimated suspension parameters – Setup 1

These estimated parameters have then been used to simulate the dynamic suspension stiffness FRF. Figure 5-39 shows a comparison of the experimental and simulated dynamic suspension stiffness responses. As it can be observed, the simulated dynamic suspension stiffness matches the experimental dynamic stiffness response up to about 20 Hz. A detailed discussion of the sources of error that cause this deviation will be provided in section 5.5.3.

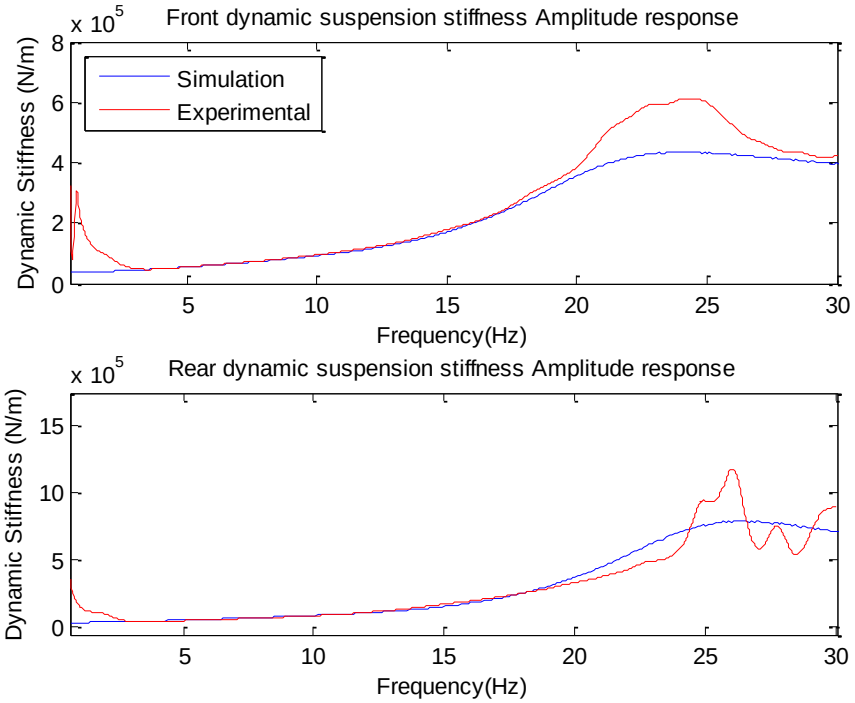

Figure 5-39: Dynamic stiffness frequency response Setup 1: front (upper) and rear (lower)

Furthermore, Figure 5-40 to Figure 5-46 depict the FRF of body acceleration, hub acceleration, CPL variation and pitch acceleration for experimental data on the rig and from simulation. The level of model accuracy is high, since it is able to predict body and hub modes accurately both in amplitude and frequency.

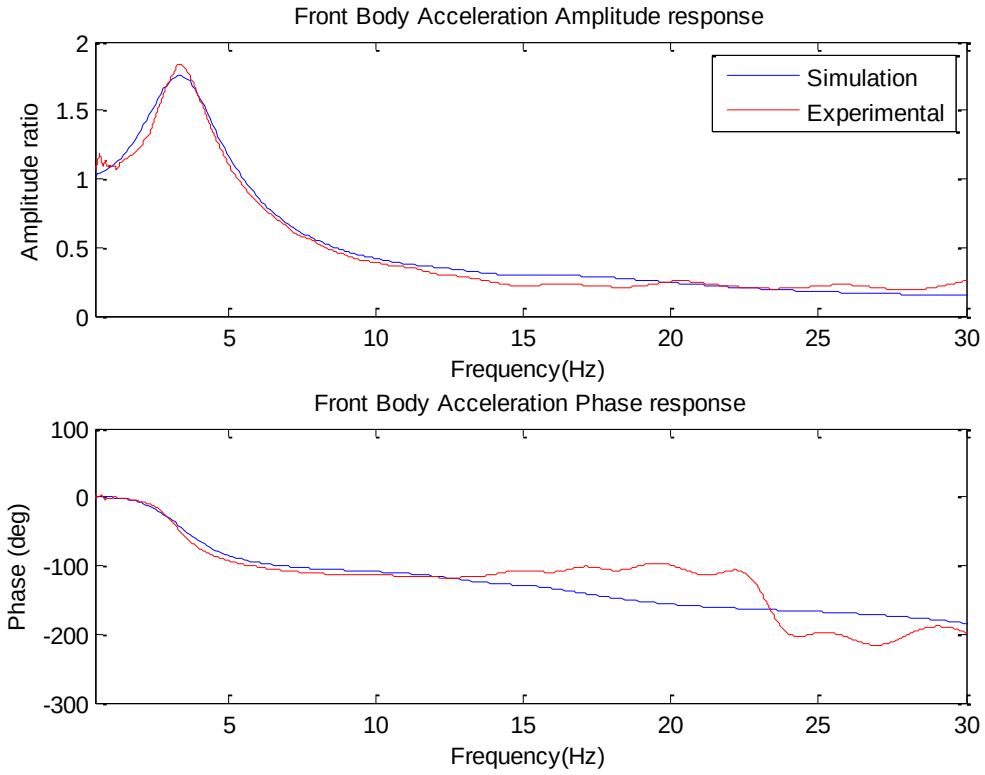

Figure 5-40: Front Body Acceleration Ratio frequency response – Setup 1

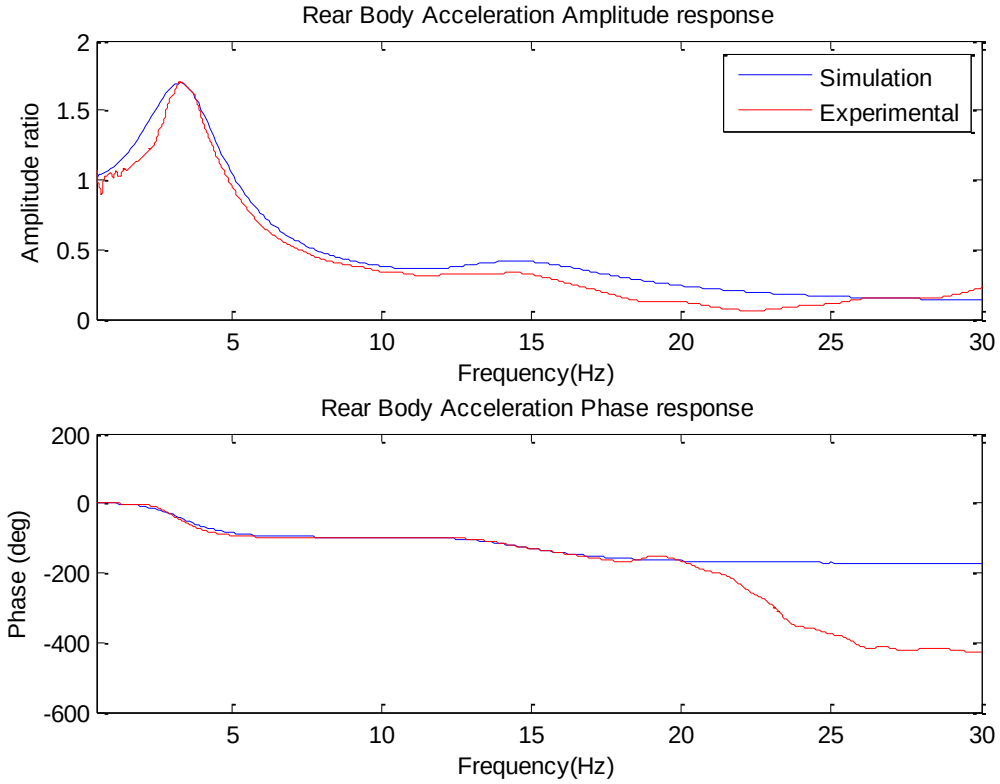

Figure 5-41: Rear Body Acceleration Ratio frequency response – Setup 1

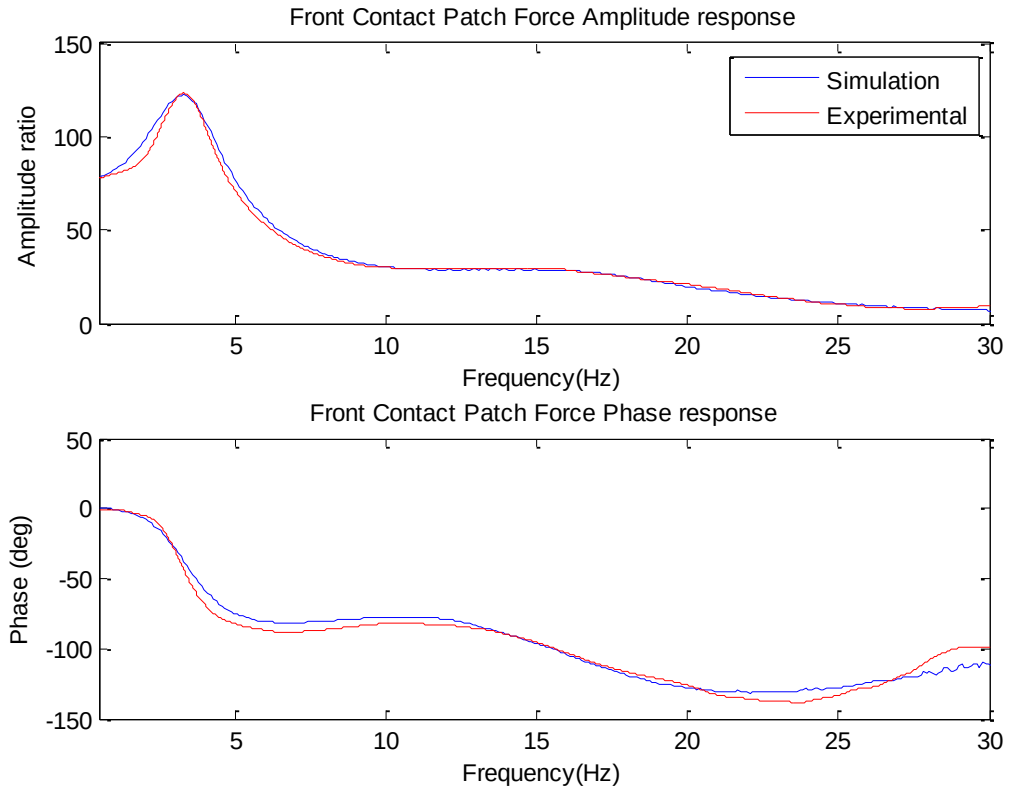

Figure 5-42: Front CPL ratio frequency response – Setup 1

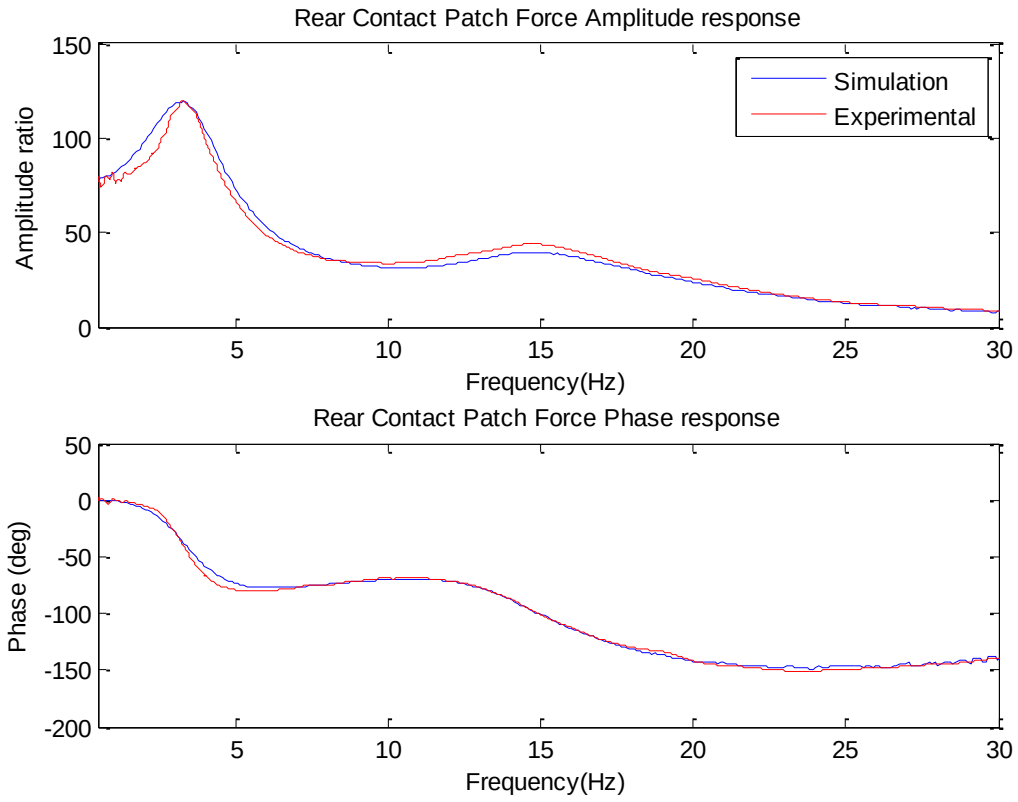

Figure 5-43: Rear CPL ratio frequency response – Setup 1

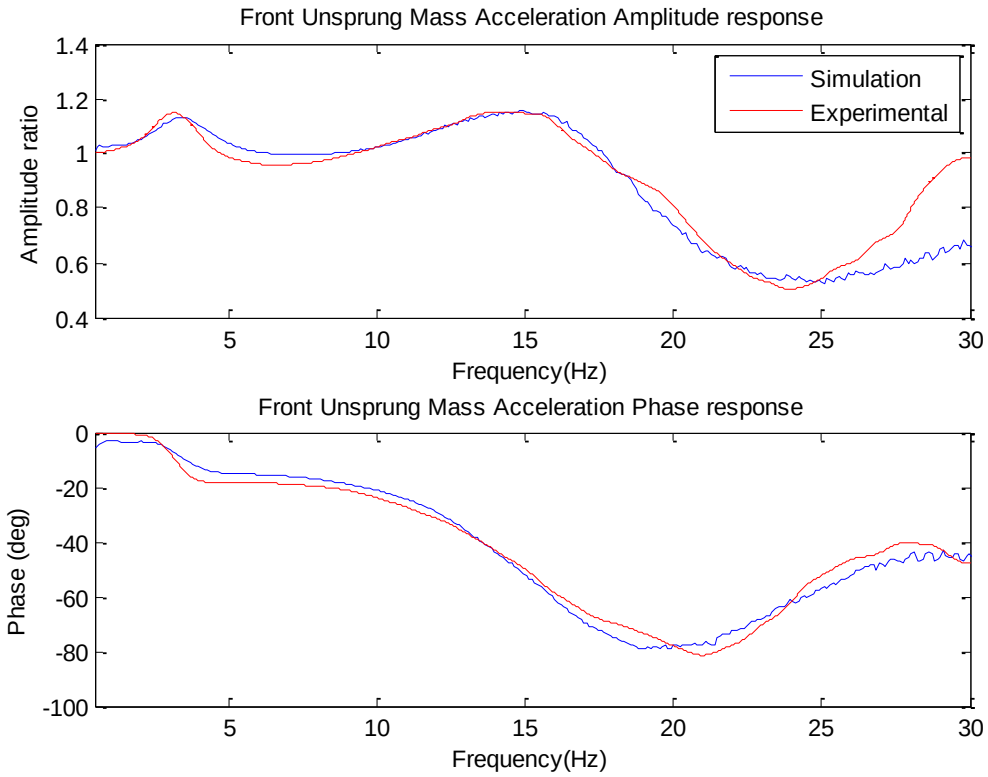

Figure 5-44: Front unsprung mass acceleration ratio frequency response – Setup 1

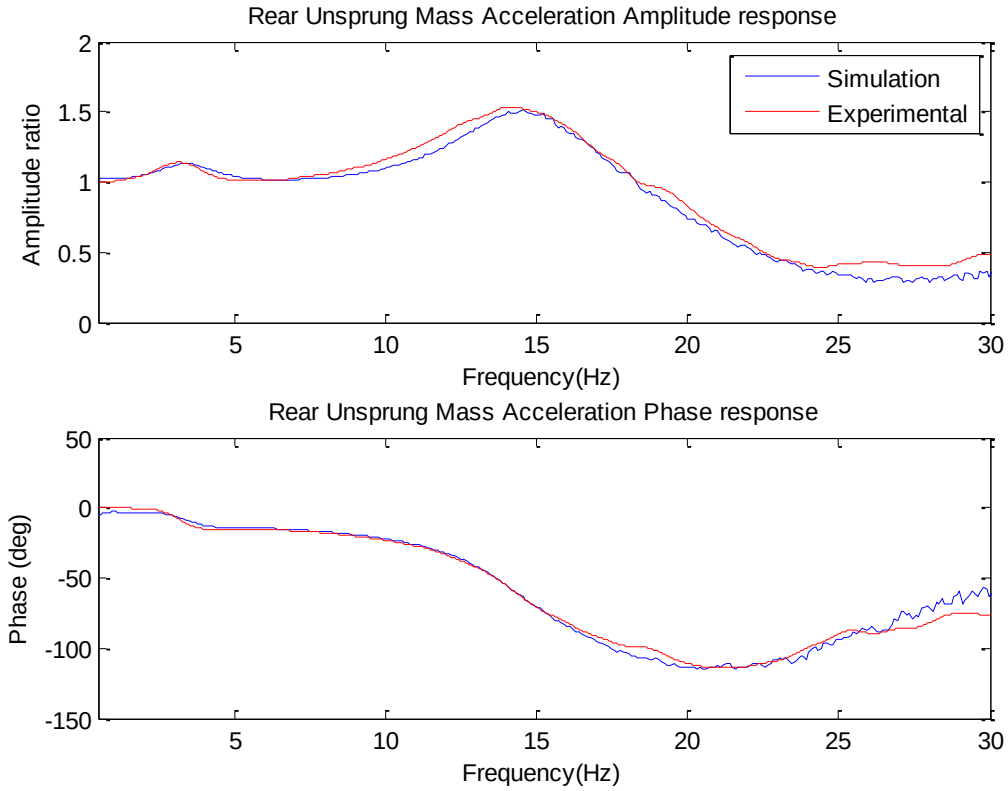

Figure 5-45: Front unsprung mass acceleration ratio frequency response – Setup 1

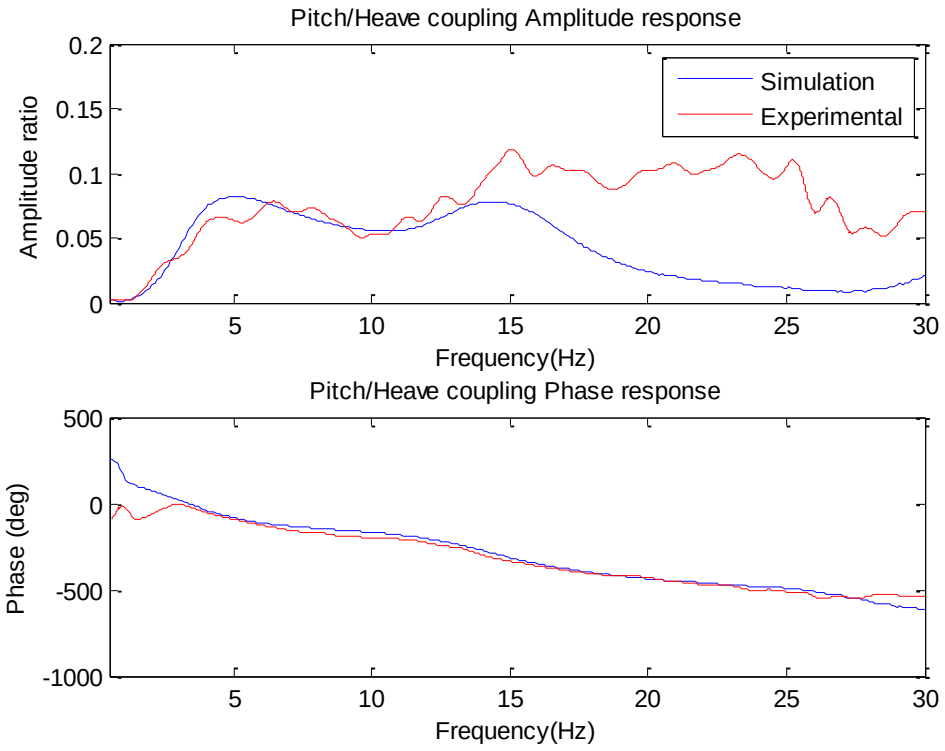

Figure 5-46: Pitch acceleration ratio frequency response – Setup 1

Suspension Set-up 2

A similar parameter estimation procedure has been followed in this case study. However, in this case, because the only suspension parameters that have been modified are front and rear flywheel inertias, only front and rear inertance have been re-estimated. Table 5-12 shows the estimated inertances for both axles. This setting would correspond to a front low and a rear medium inertance configuration.

Front Inertance (b_{sf})	10.5 kg
Rear Inertance (b_{sr})	22.5 kg

Table 5-12: Estimated suspension parameters – Setup 2

FRFs of front and rear dynamic suspension stiffness can be therefore simulated. Figure 5-47 compares the simulated FRFs of dynamic stiffness with the experimental ones. As with the previous case, a good correlation can be achieved up to frequencies about 20 Hz.

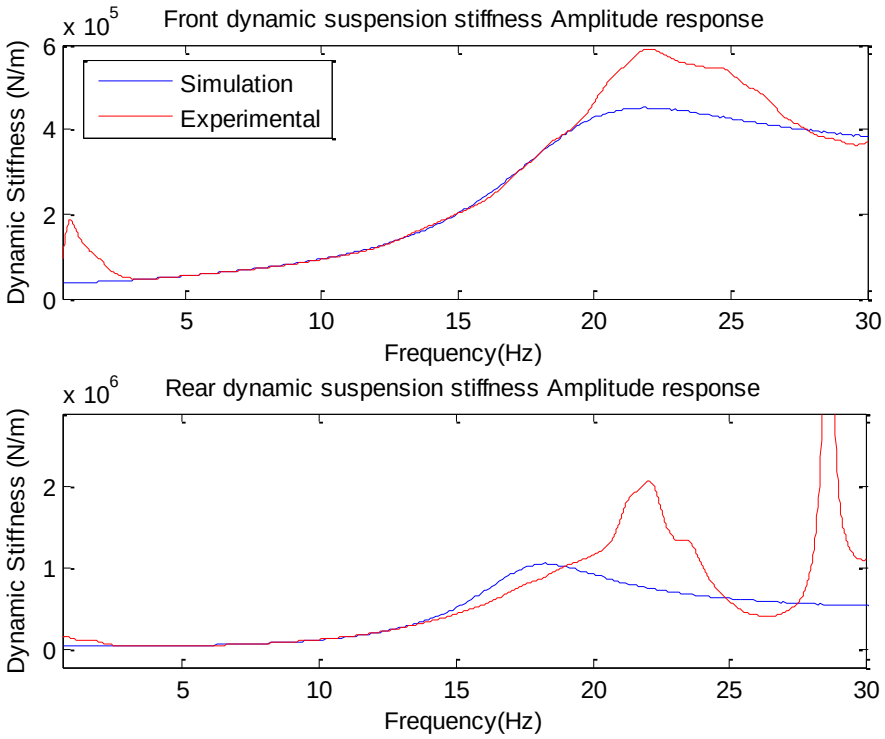

Figure 5-47: Dynamic stiffness frequency response Setup 2: front (upper) and rear (lower)

Figure 5-48 to Figure 5-54 compare simulated dynamic responses with directly measured magnitudes, i.e. body acceleration, hub acceleration and CPL at both ends as well as pitch/heave interaction. Results show a high level of agreement between experimental data and simulation.

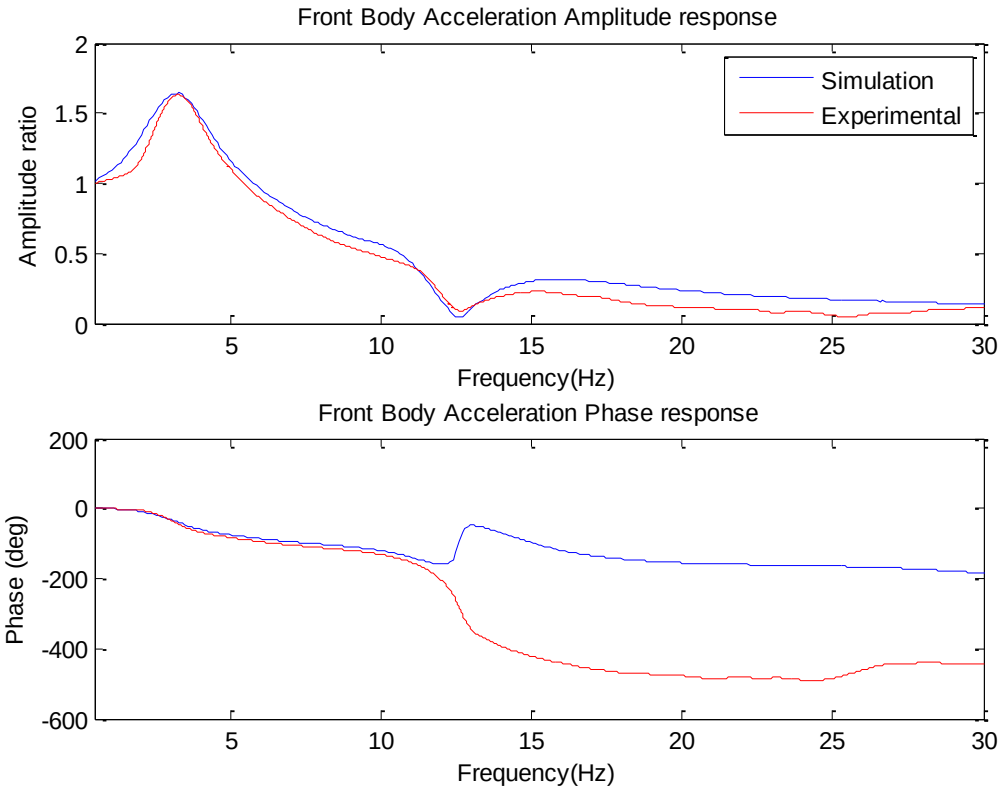

Figure 5-48: Front Body Acceleration Ratio frequency response – Setup 2

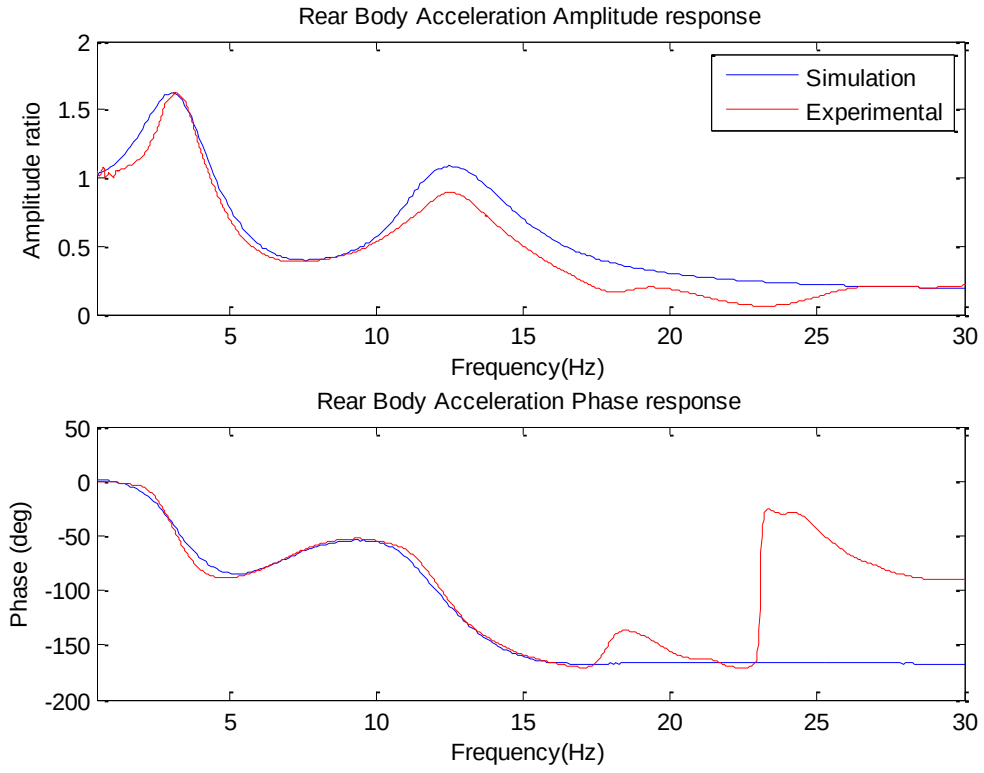

Figure 5-49: Rear Body Acceleration Ratio frequency response – Setup 2

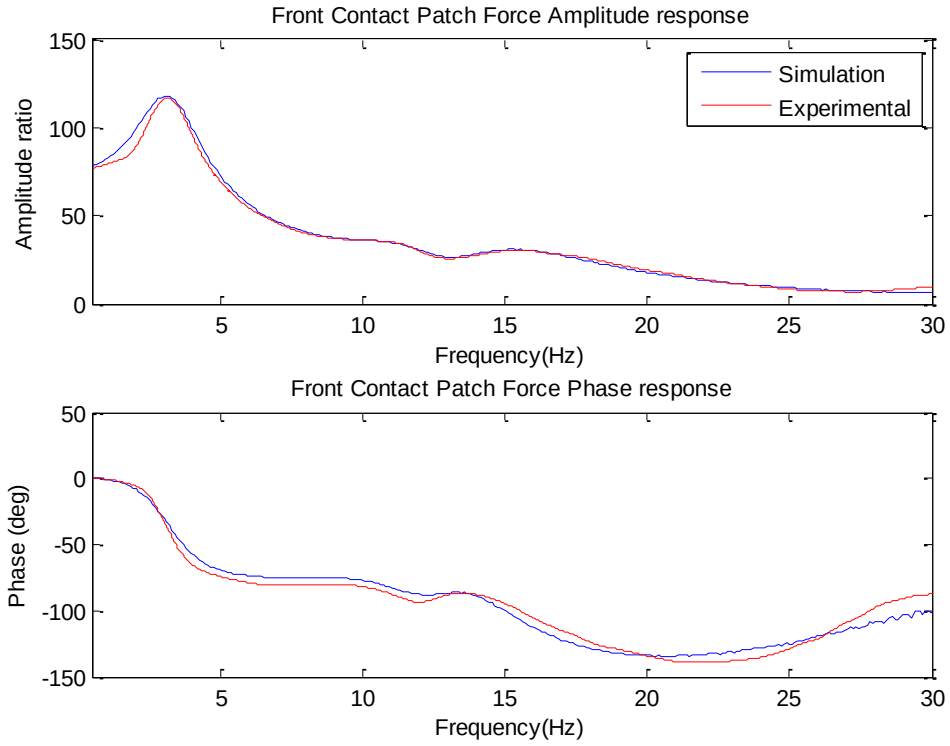

Figure 5-50: Front CPL ratio frequency response – Setup 2

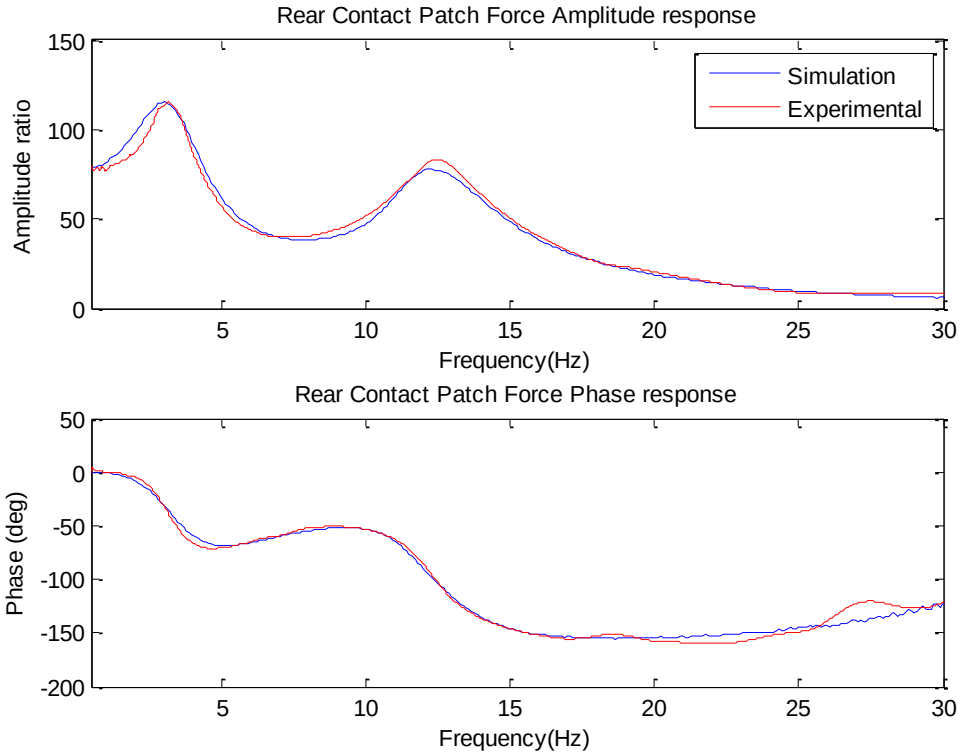

Figure 5-51: Rear CPL ratio frequency response – Setup 2

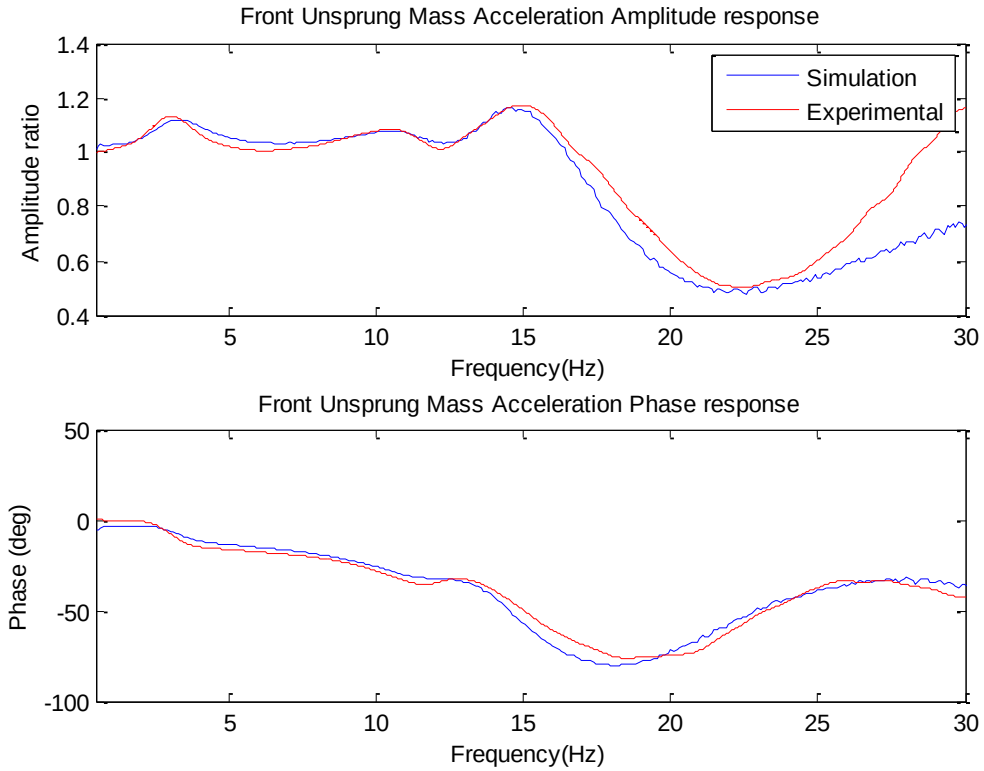

Figure 5-52: Front unsprung mass acceleration ratio frequency response – Setup 2

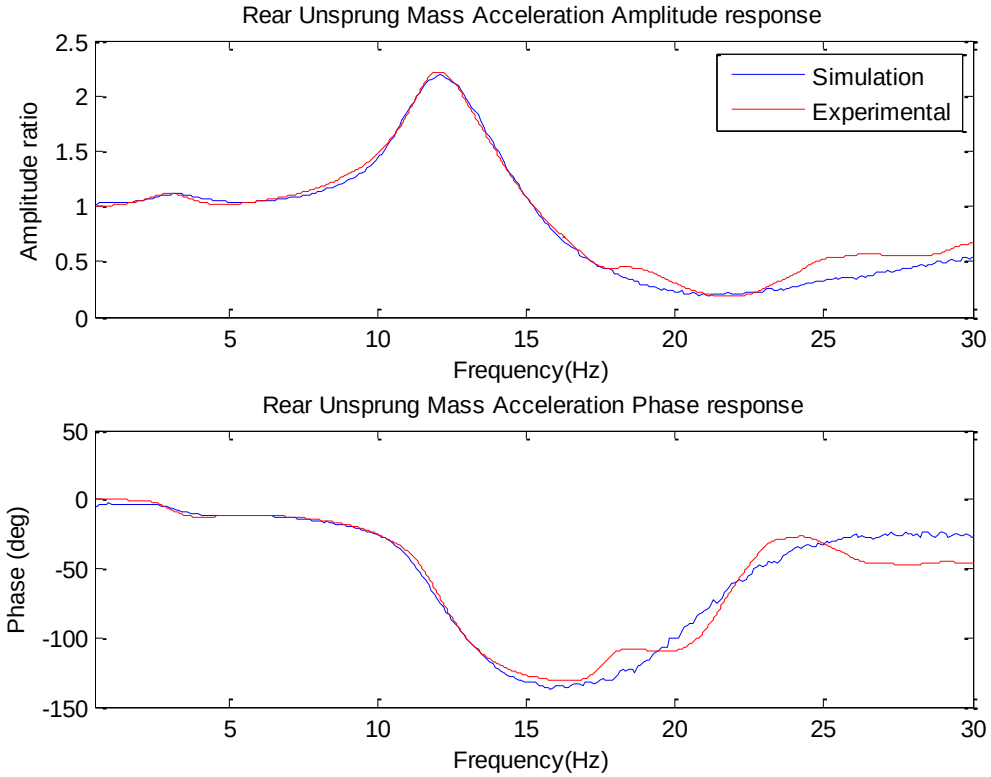

Figure 5-53: Rear unsprung mass acceleration ratio frequency response – Setup 2

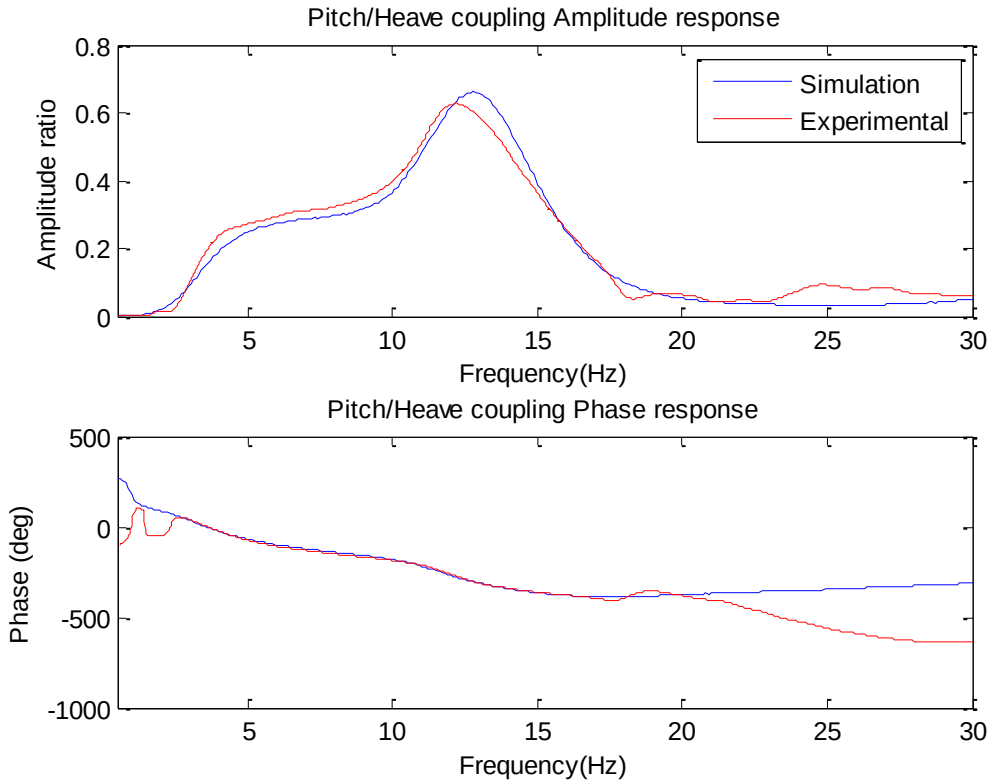

Figure 5-54: Pitch acceleration ratio frequency response – Setup 2

Suspension Set-up 3

Flywheel inertia settings have been increased in this setup to validate the performance of the vehicle model under mid inertance characteristics. In this case, the flywheel of both front and rear inerters has been fitted with a 6-mm FWM plus a 4-mm steel disk. New inertance linear rates have been estimated leaving the rest of suspension parameters unchanged. Inertance values are summarised in Table 5-13.

Front Inertance (b_{sf})	16.5 kg
Rear Inertance (b_{sr})	31.5 kg

Table 5-13: Estimated suspension parameters – Setup 3

Figure 5-55 shows a comparison between experimental and estimated dynamic suspension stiffness responses for front and rear axles.

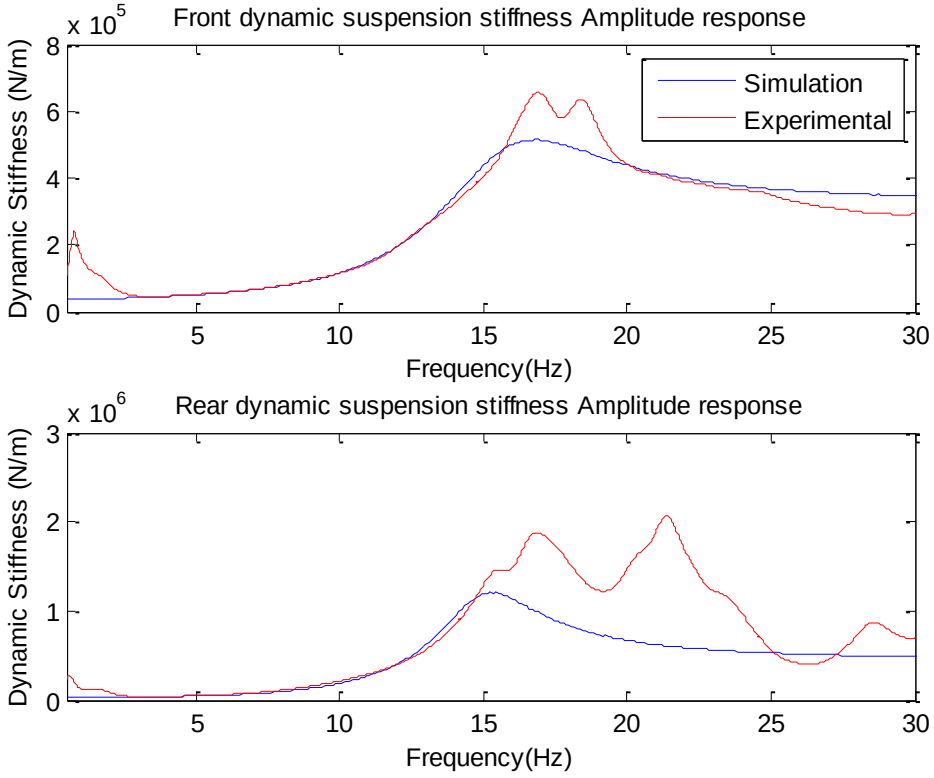

Figure 5-55: Dynamic stiffness frequency response Setup 3: front (upper) and rear (lower)

The model is run again and results are compared against experimental data. Figure 5-56 to Figure 5-62 show the dynamic response of the vehicle measured magnitudes with this new suspension setting in the frequency domain. Although simulated body acceleration amplitude ratio responses at both axles are slightly overestimated, especially in the region around the hub mode, the model can predict the dynamic behaviour of the system with good levels of accuracy.

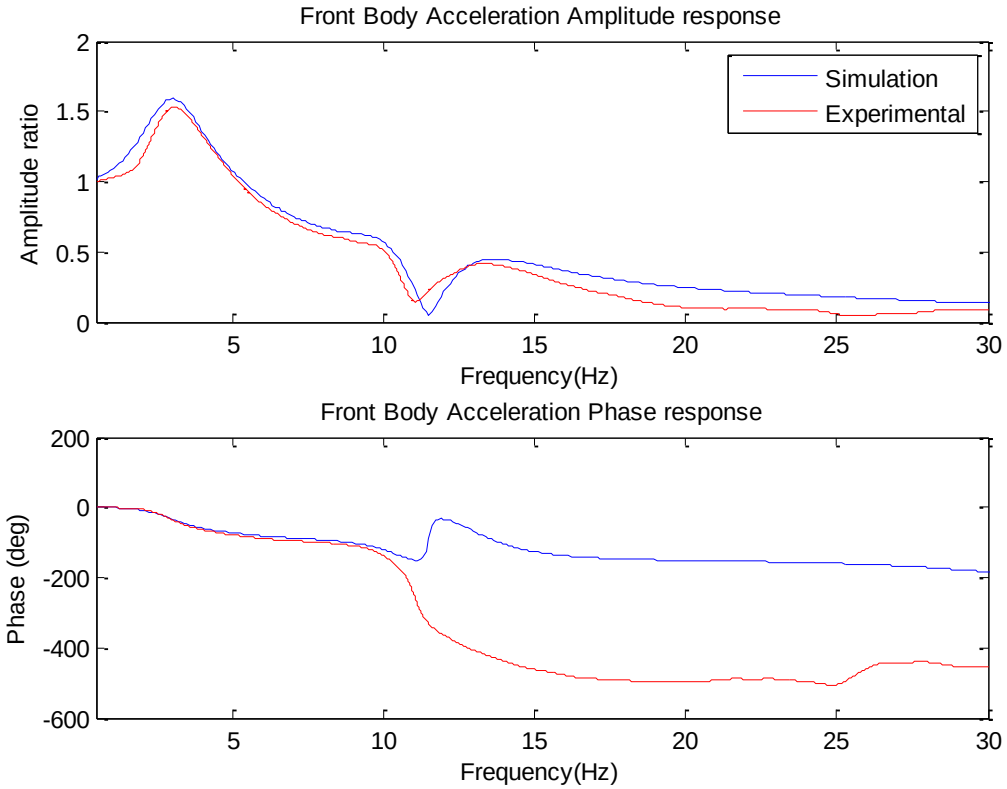

Figure 5-56: Front Body Acceleration Ratio frequency response – Setup 3

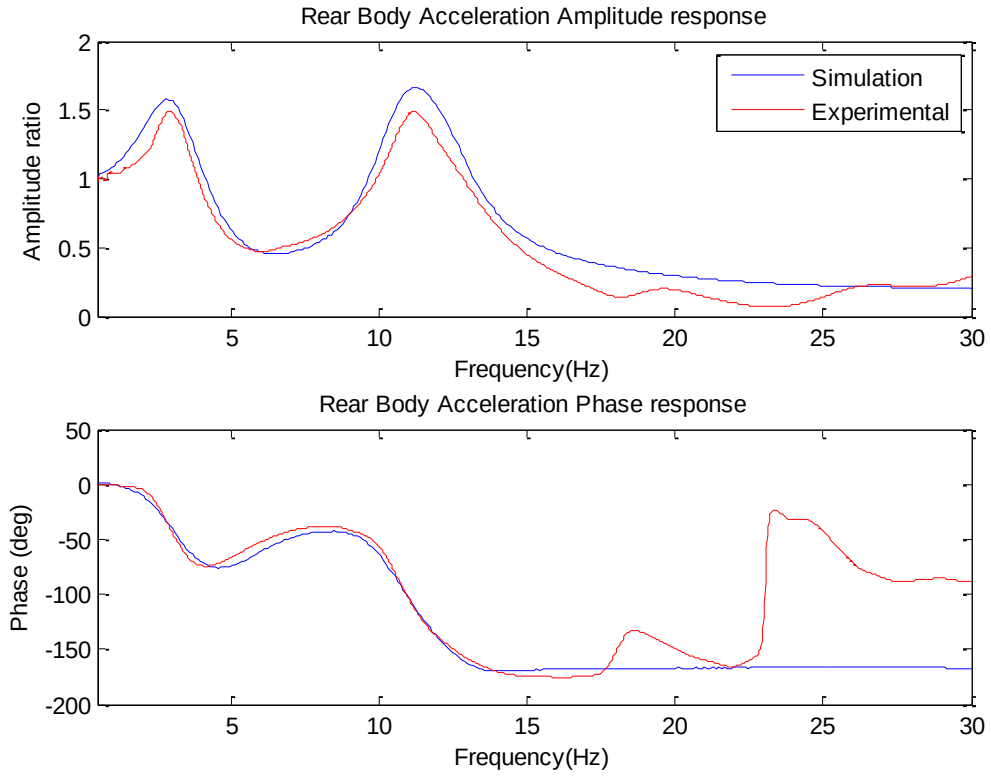

Figure 5-57: Rear Body Acceleration Ratio frequency response – Setup 3

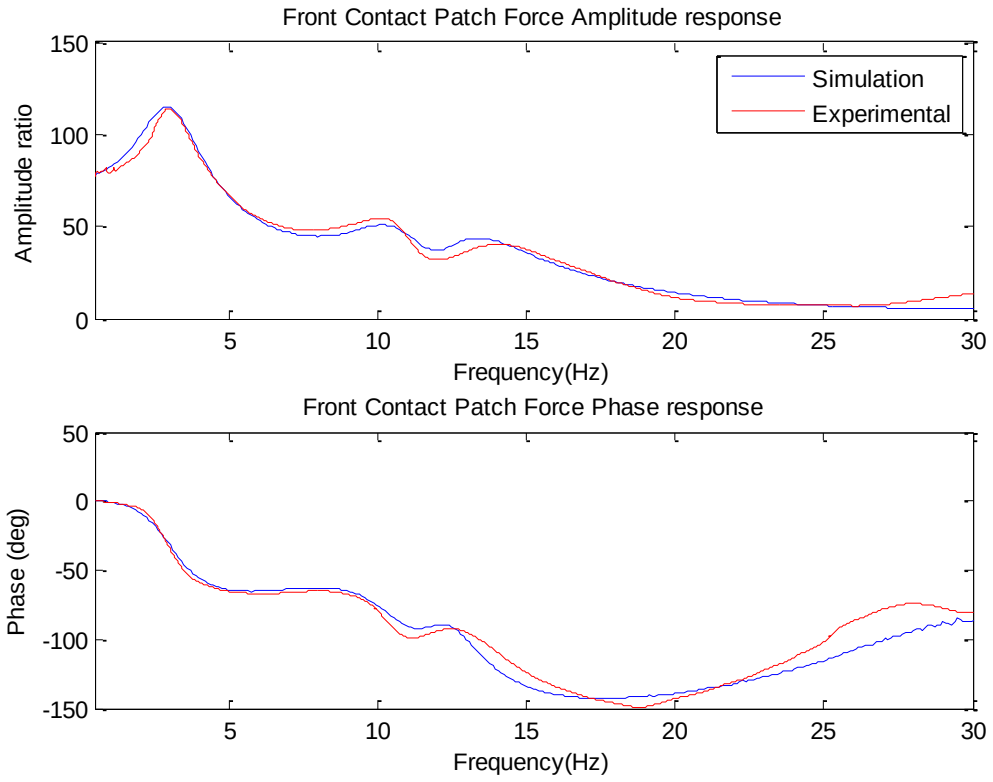

Figure 5-58: Front CPL ratio frequency response – Setup 3

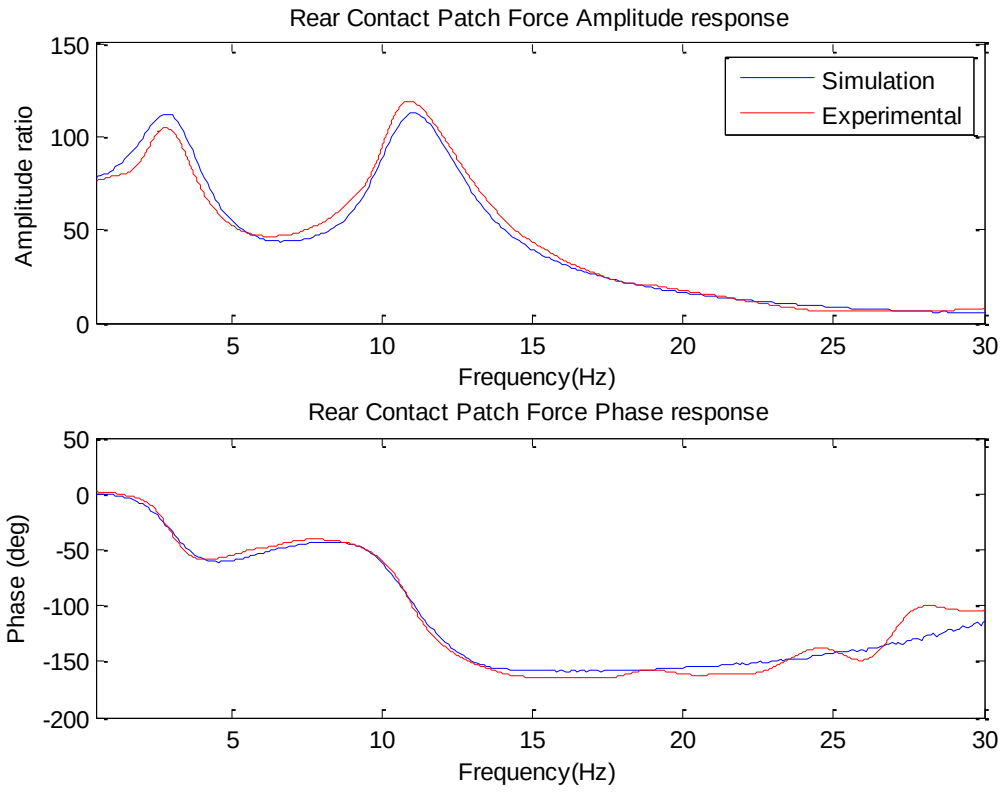

Figure 5-59: Rear CPL ratio frequency response – Setup 3

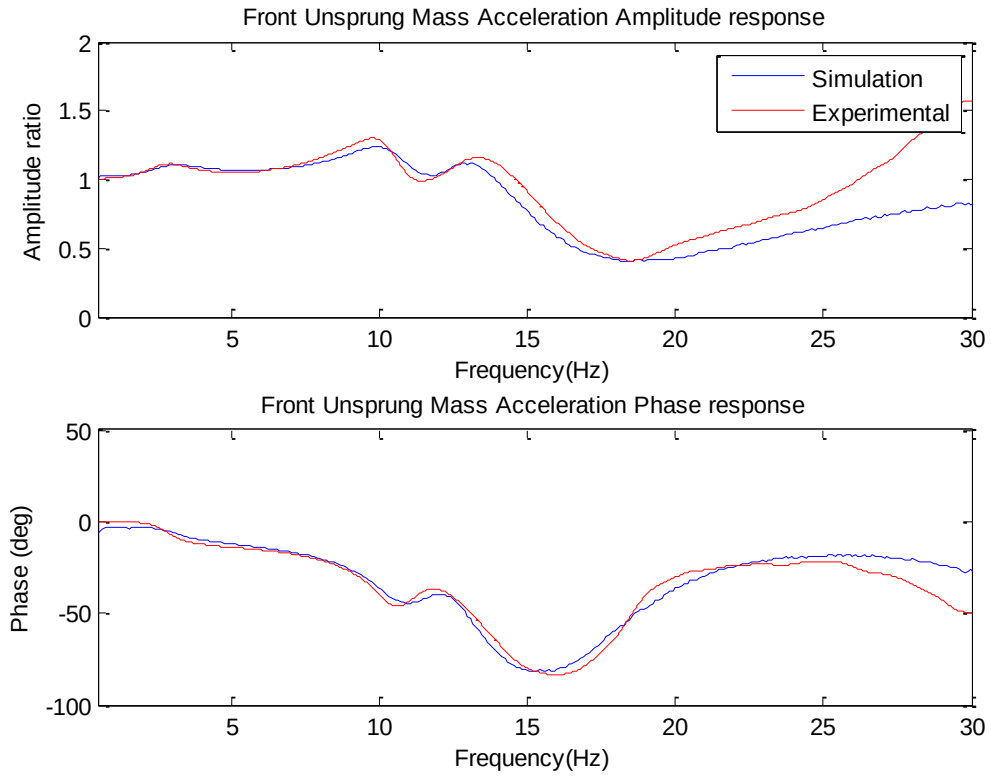

Figure 5-60: Front unsprung mass acceleration ratio frequency response – Setup 3

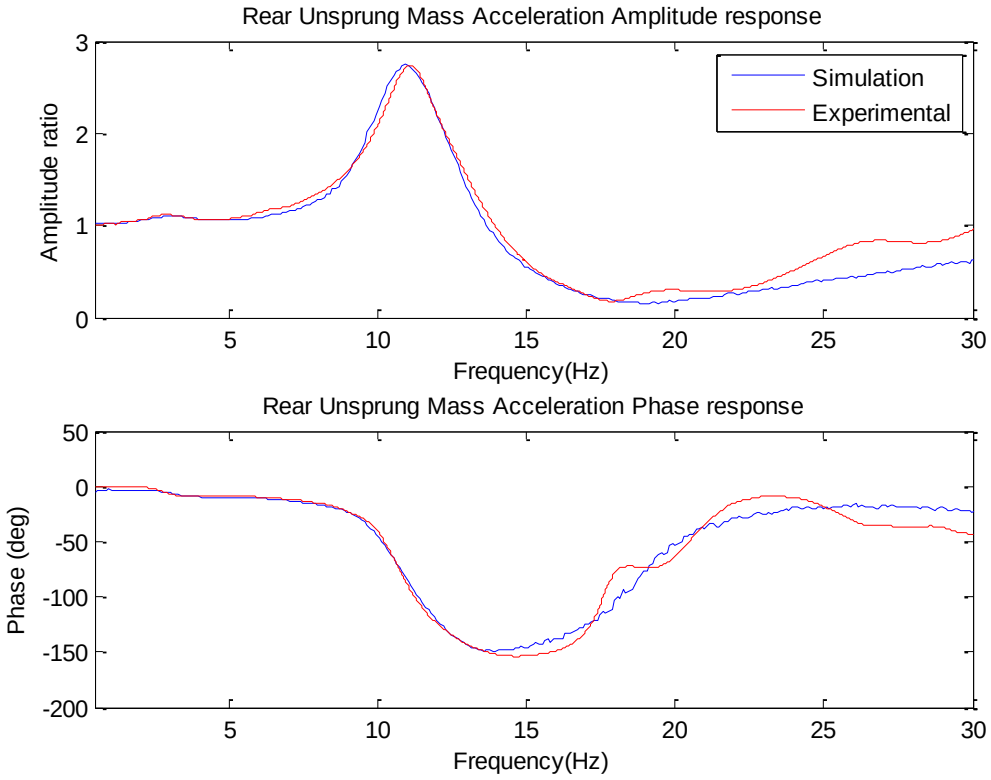

Figure 5-61: Rear unsprung mass acceleration ratio frequency response – Setup 3

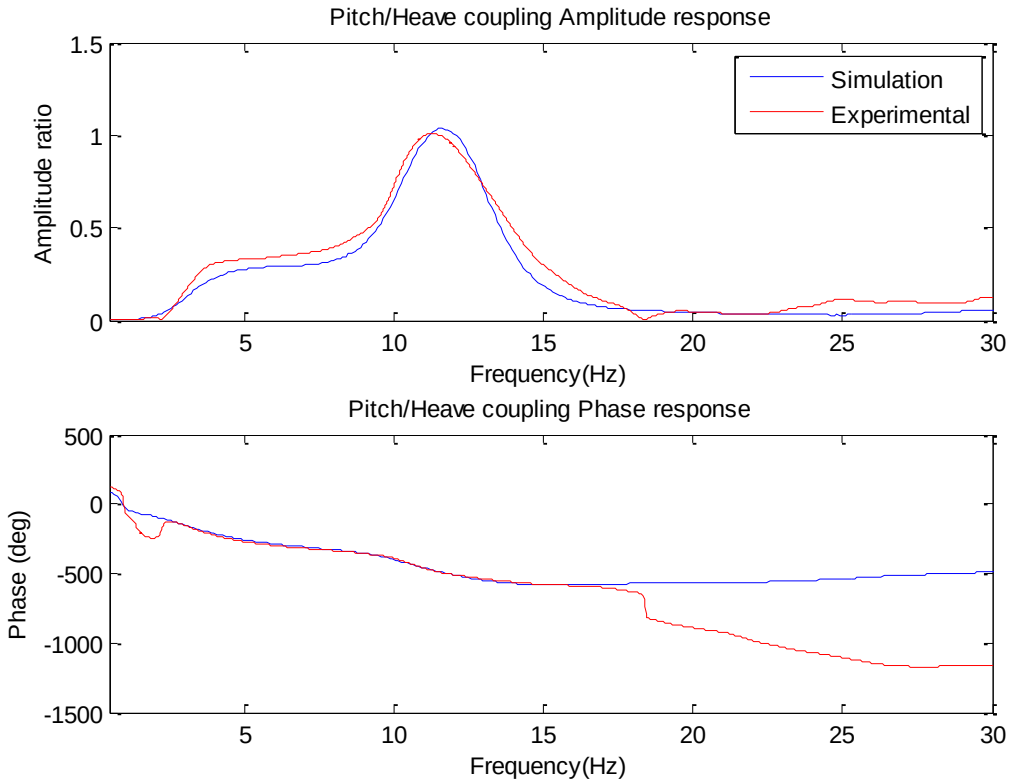

Figure 5-62: Pitch acceleration ratio frequency response – Setup 3

Suspension Set-up 4

Flywheel inertia has been increased further to investigate the model accuracy for high inertance levels. In this case study, both front and rear inerters have been fitted with the same flywheel inertia settings (see Table 5-10). As with previous setups, the parameter estimation program is used to obtain inertance rates. Estimated inertance values are summarised in Table 5-14.

Front Inertance (b_{sf})	20.8 kg
Rear Inertance (b_{sr})	40.5 kg

Table 5-14: Estimated suspension parameters – Setup 4

Comparison between experimental dynamic responses and simulation is again plotted in the following graphs.

Figure 5-64 to Figure 5-70 represent the dynamic response of body acceleration, hub acceleration and contact patch load at both axles. Even though lower levels of agreement between simulation and experimental data can be observed at high frequencies in both body acceleration amplitude response graphs (see Figure 5-64 and Figure 5-65), the model can still

predict the dynamic behaviour of the actual vehicle. Moreover, the accuracy of the model in predicting accurate contact patch load dynamic variation is high.

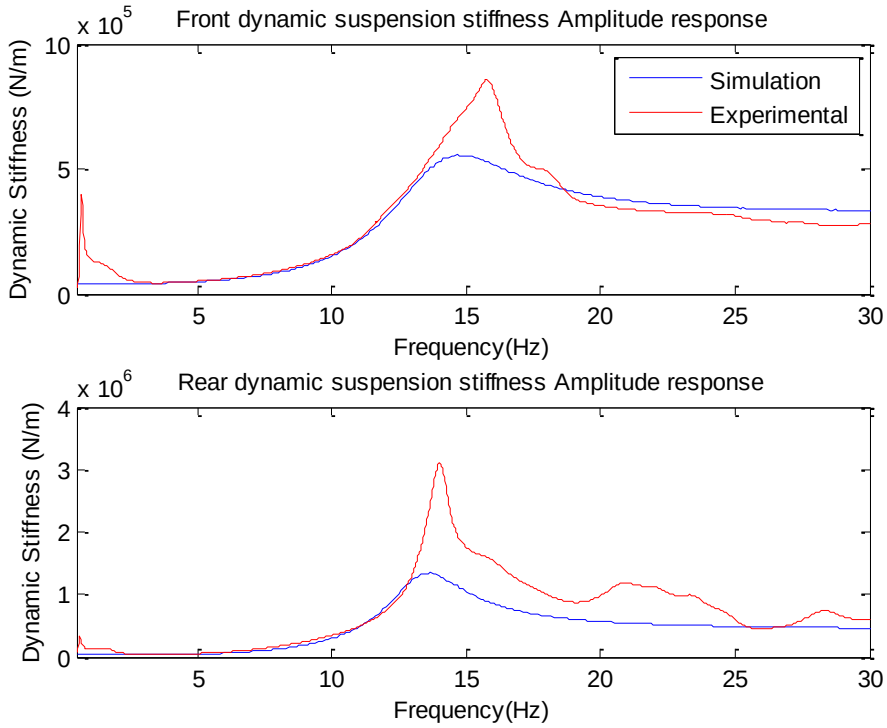

Figure 5-63: Dynamic stiffness frequency response Setup 4: front (upper) and rear (lower)

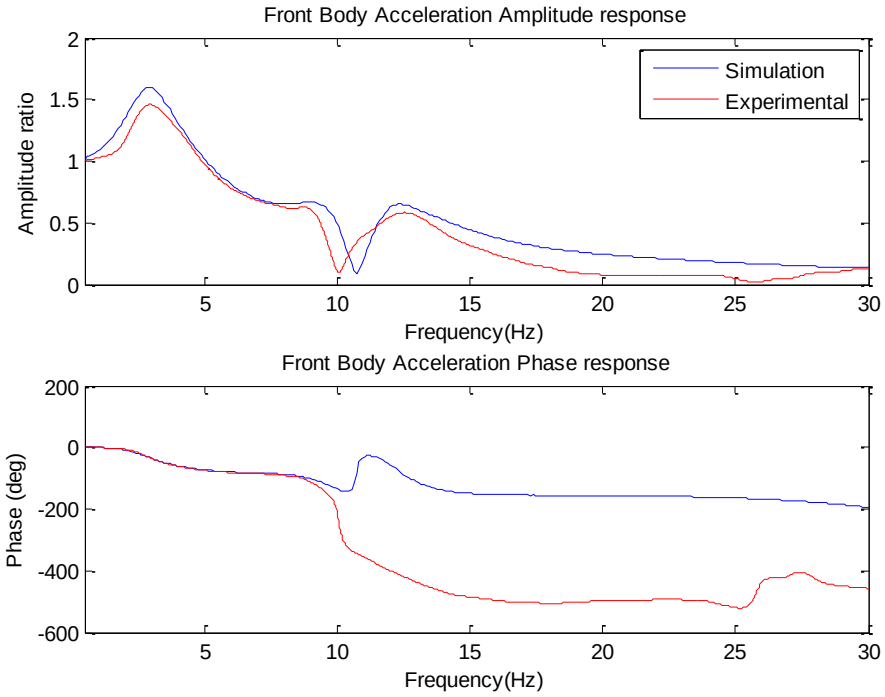

Figure 5-64: Front Body Acceleration Ratio frequency response – Setup 4

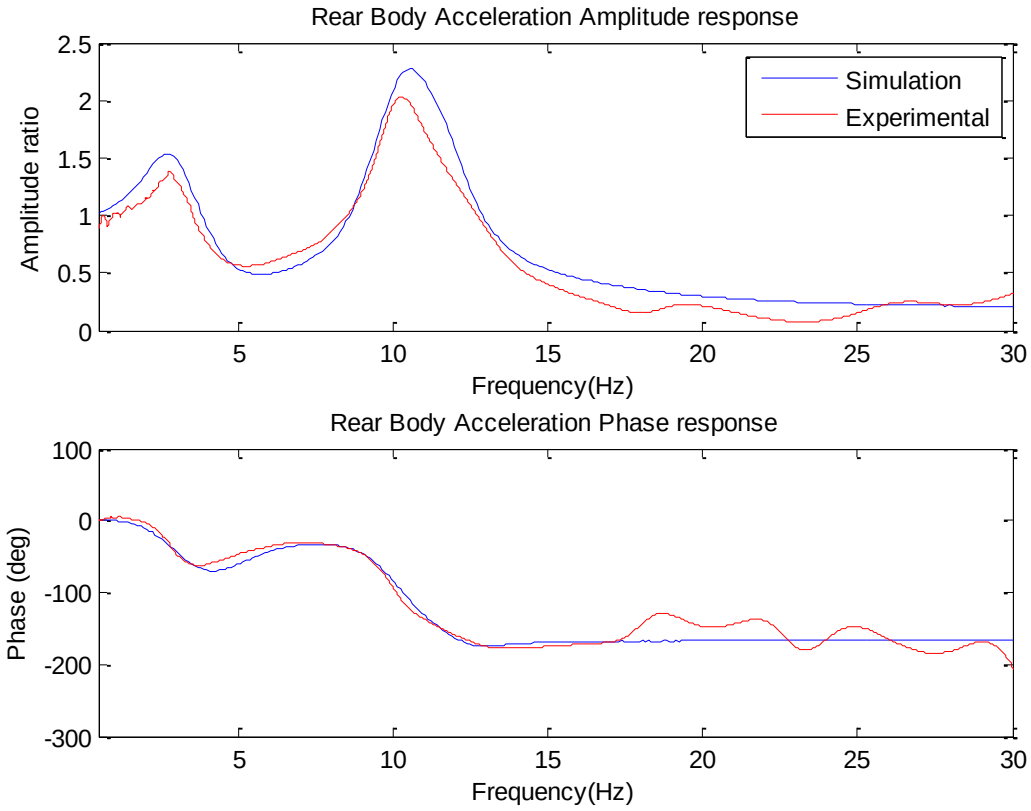

Figure 5-65: Rear Body Acceleration Ratio frequency response – Setup 4

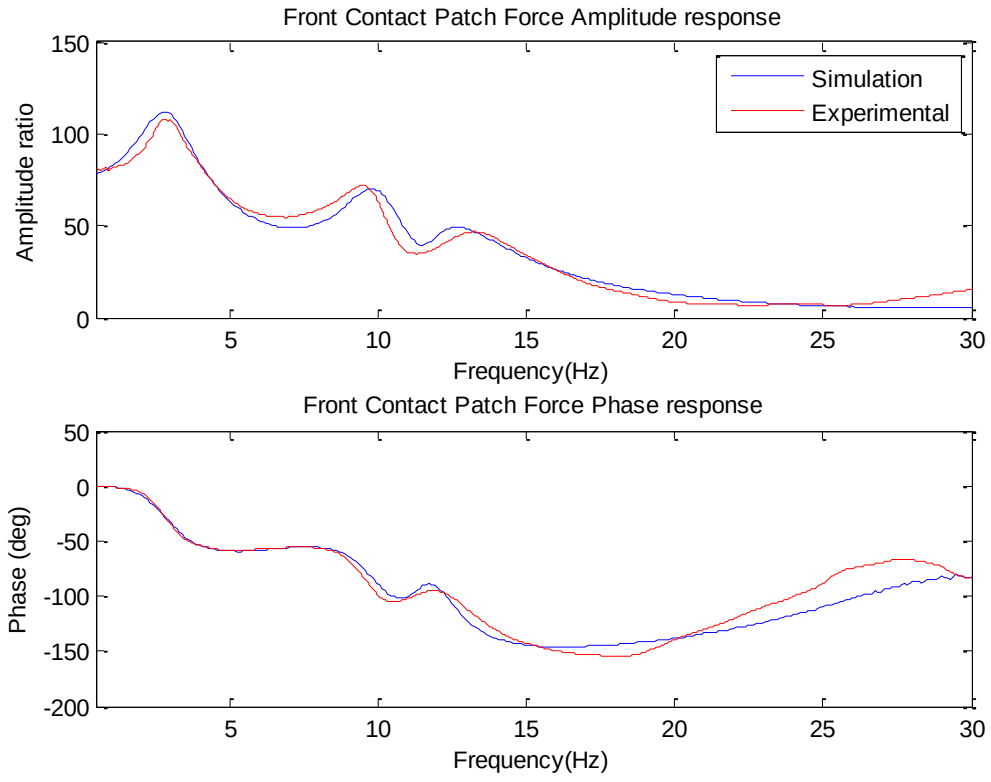

Figure 5-66: Front CPL ratio frequency response – Setup 4

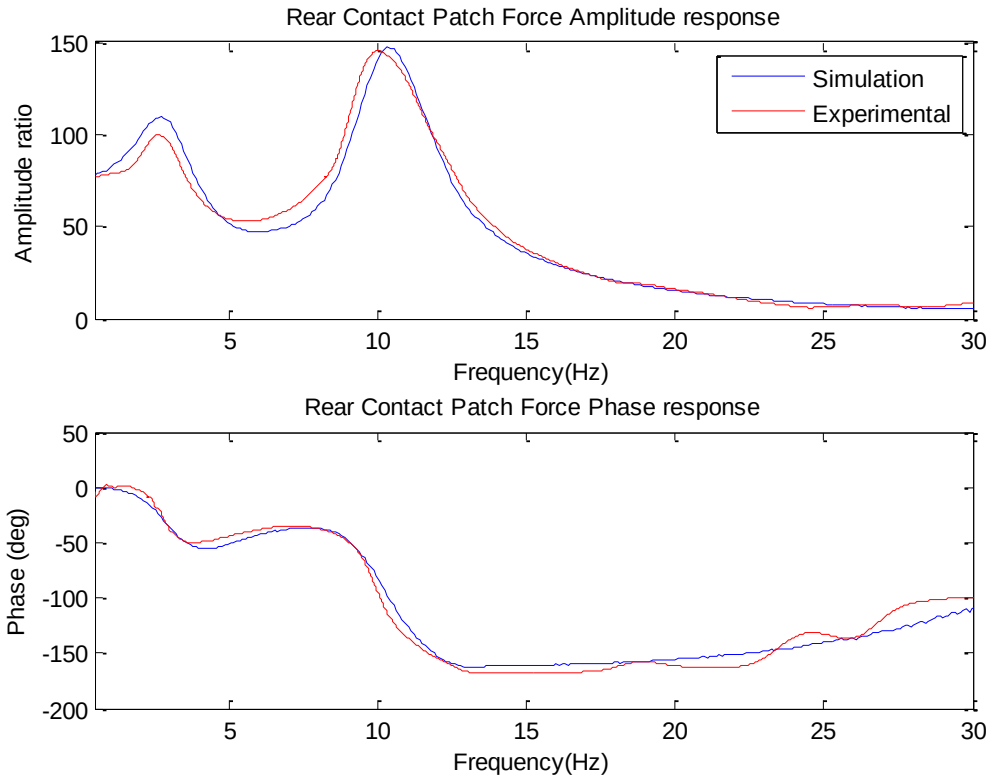

Figure 5-67: Rear CPL ratio frequency response – Setup 4

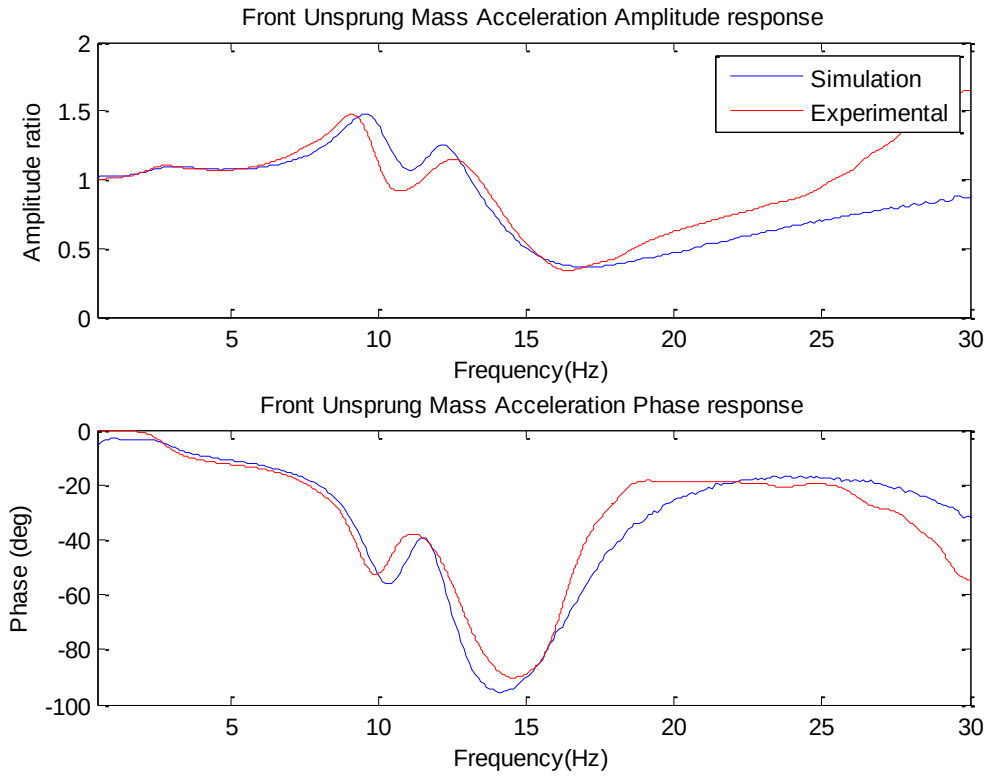

Figure 5-68: Front unsprung mass acceleration ratio frequency response – Setup 4

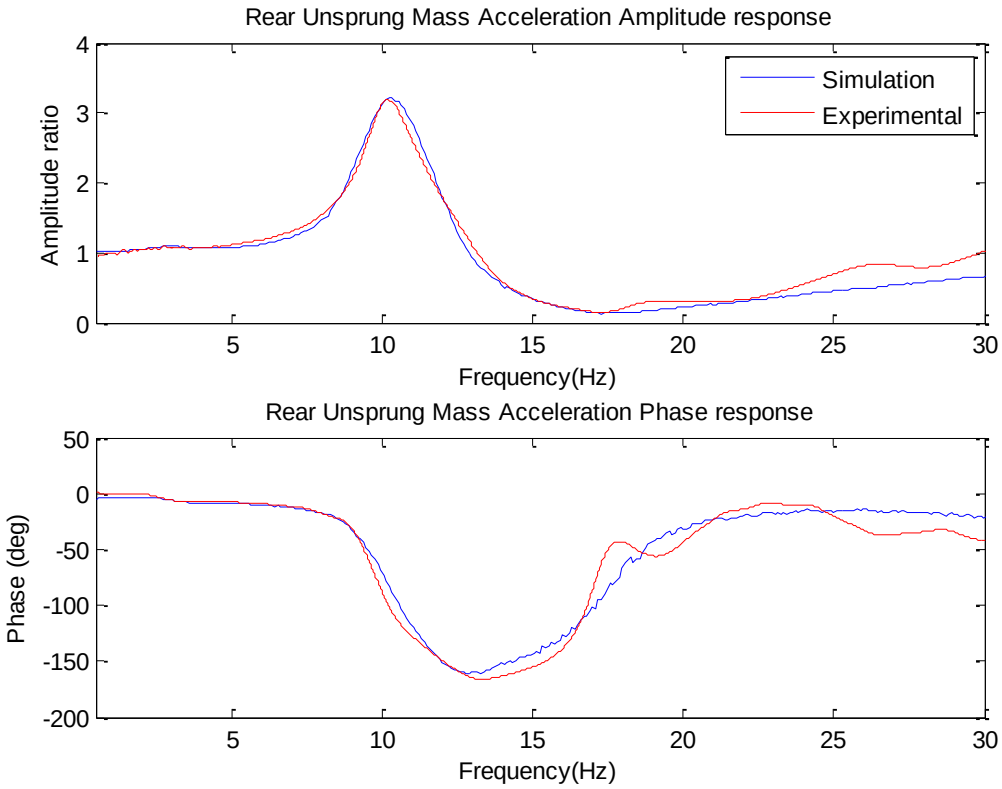

Figure 5-69: Rear unsprung mass acceleration ratio frequency response – Setup 4

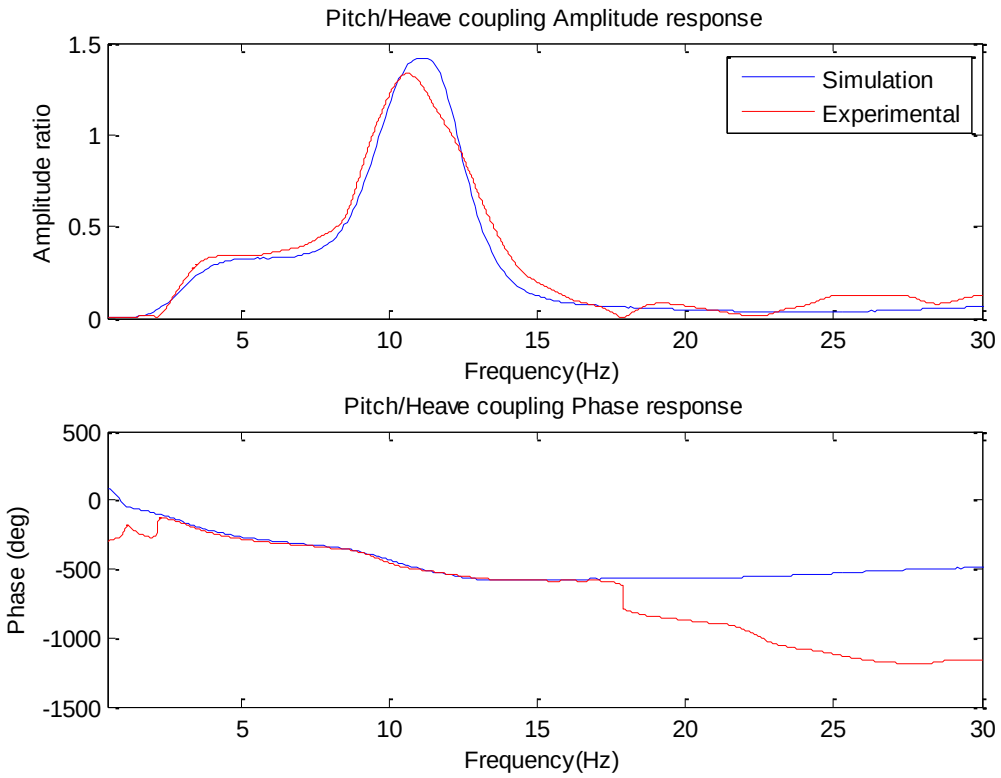

Figure 5-70: Pitch acceleration ratio frequency response – Setup 4

Suspension Set-up 5

The last suspension setting corresponds to very high inertance characteristics. In this case study, flywheel inertia has been further increased at both vehicle ends (see Table 5-10).

Inertance rates have been again estimated considering the rest of suspension values to remain unvaried. Table 5-15 shows the inertance values estimated through the identification process.

Front Inertance (b_{sf})	30 kg
Rear Inertance (b_{sr})	56.5 kg

Table 5-15: Estimated suspension parameters – Setup 5

With the estimated front and rear inertance rates, experimental and simulated dynamic suspension stiffness frequency responses can be compared (see Figure 5-71).

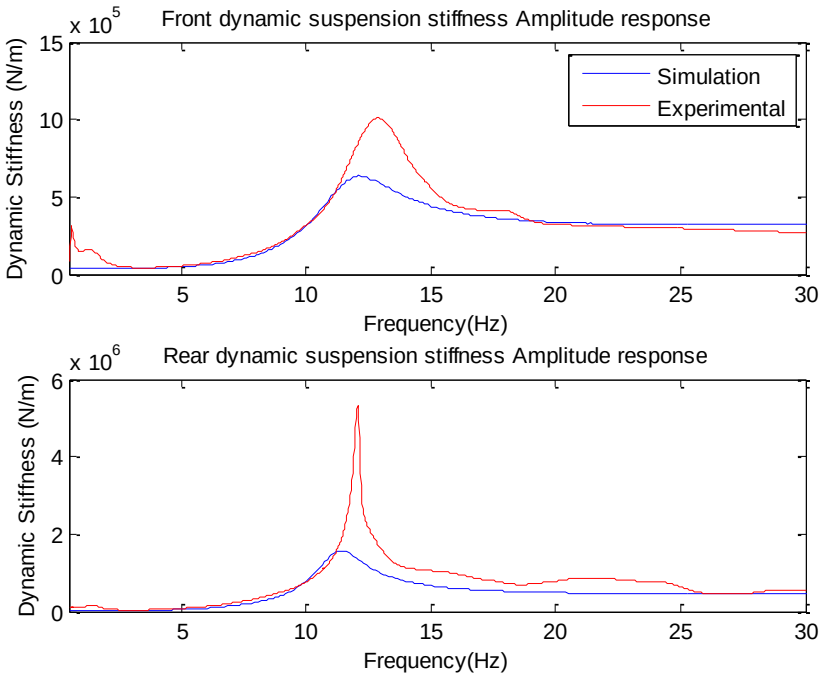

Figure 5-71: Dynamic stiffness frequency response Setup 5: front (upper) and rear (lower)

As in the previous case studies, simulation of the vehicle model has been run and compared against experimental data from the four post rig.

Figure 5-72 to Figure 5-78 show the frequency-domain responses of both the actual vehicle and the model. Although, bigger differences can be appreciated in the setup, especially in body acceleration amplitude ratio responses (see Figure 5-72 and Figure 5-73) with respect to

lower inertance settings, the model can still predict with acceptable levels of accuracy the dynamic responses of the actual vehicle (see Figure 5-74 to Figure 5-77).

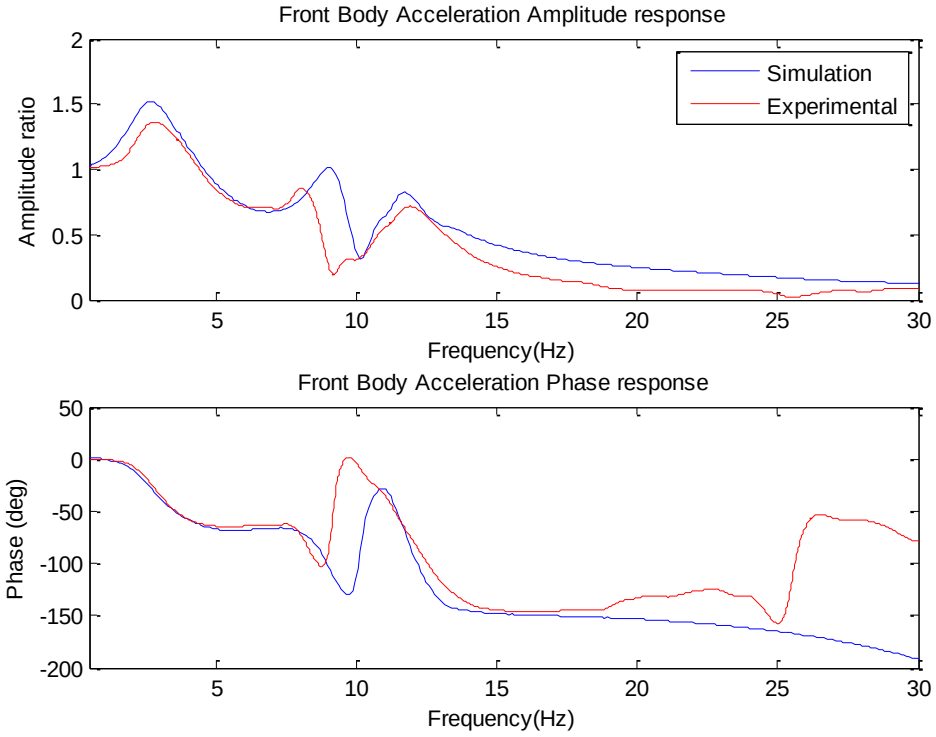

Figure 5-72: Front Body Acceleration Ratio frequency response – Setup 5

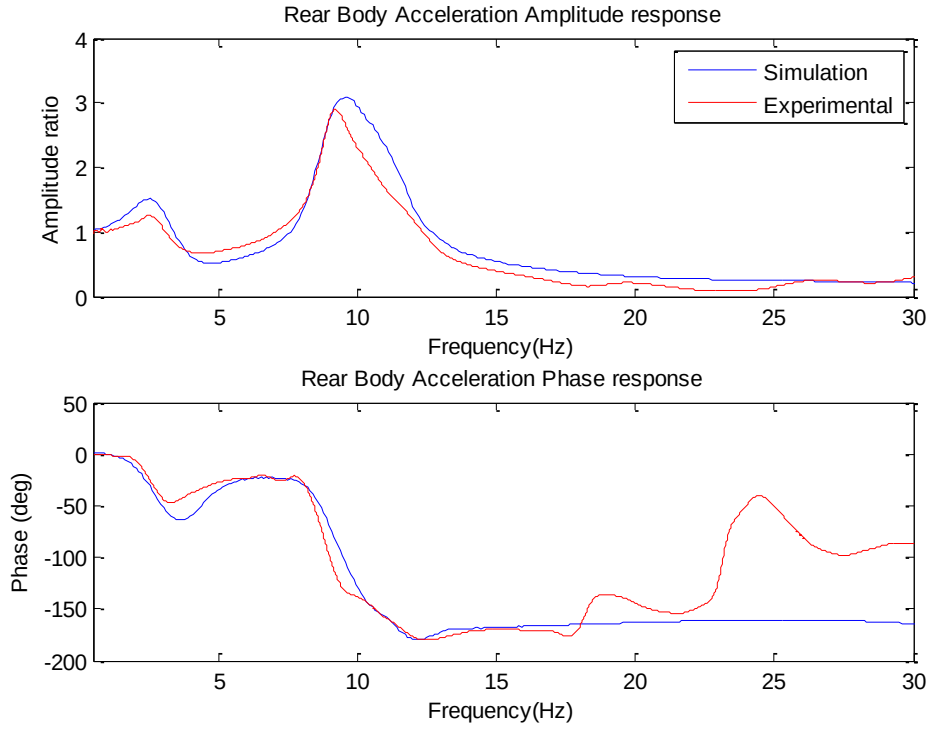

Figure 5-73: Rear Body Acceleration Ratio frequency response – Setup 5

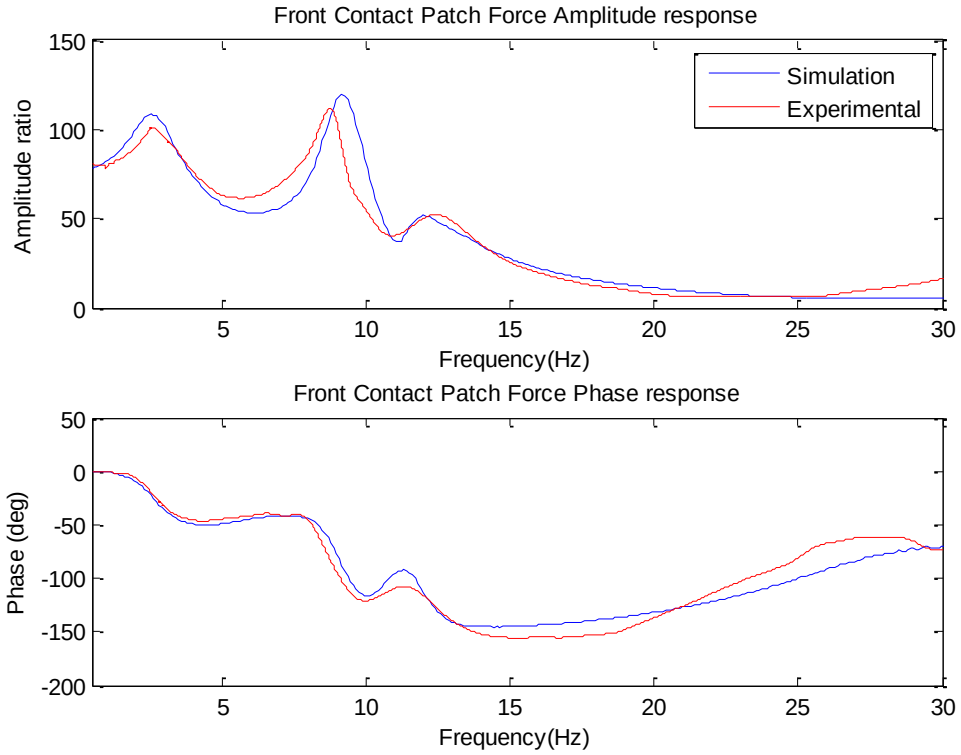

Figure 5-74: Front CPL ratio frequency response – Setup 5

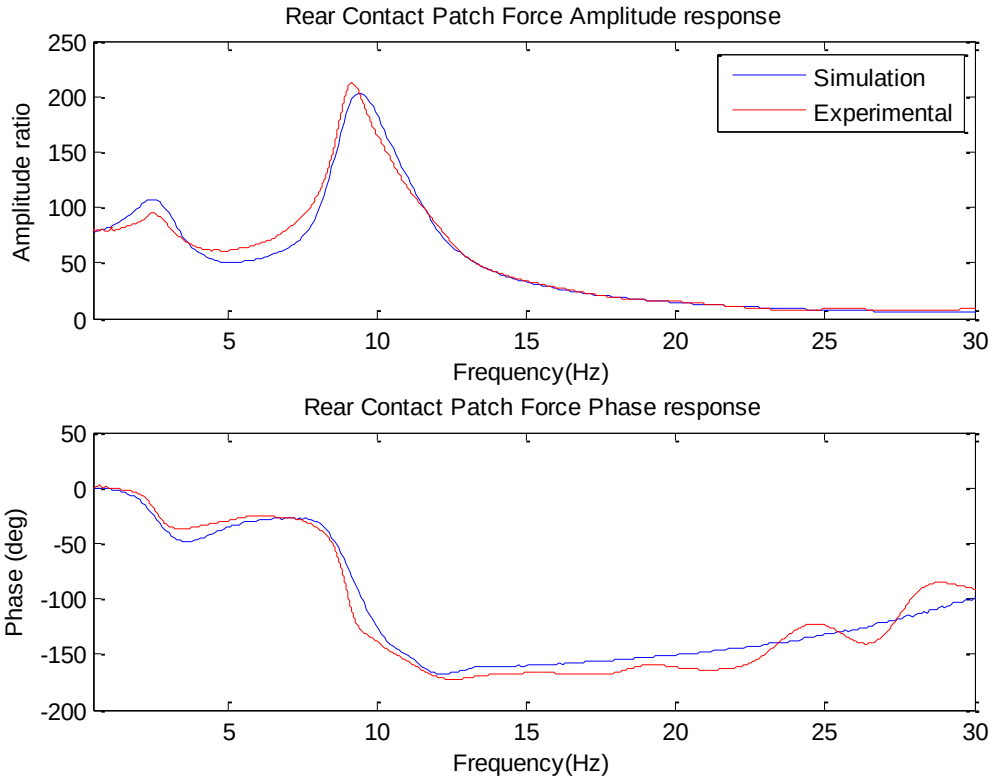

Figure 5-75: Rear CPL ratio frequency response – Setup 5

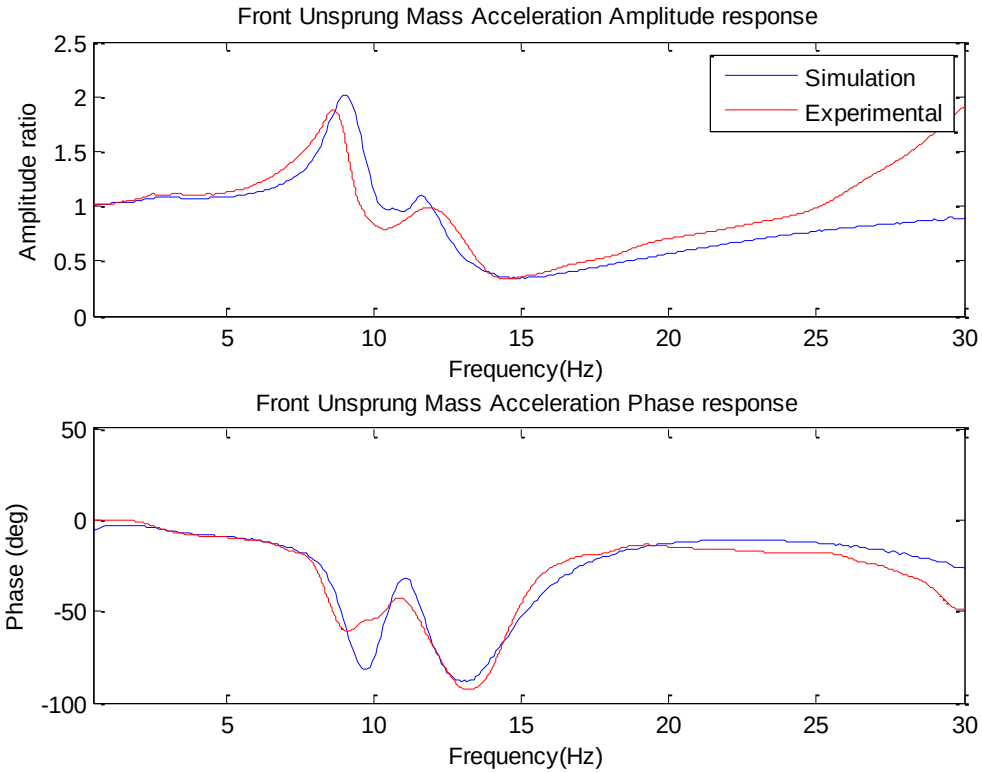

Figure 5-76: Front unsprung mass acceleration ratio frequency response – Setup 5

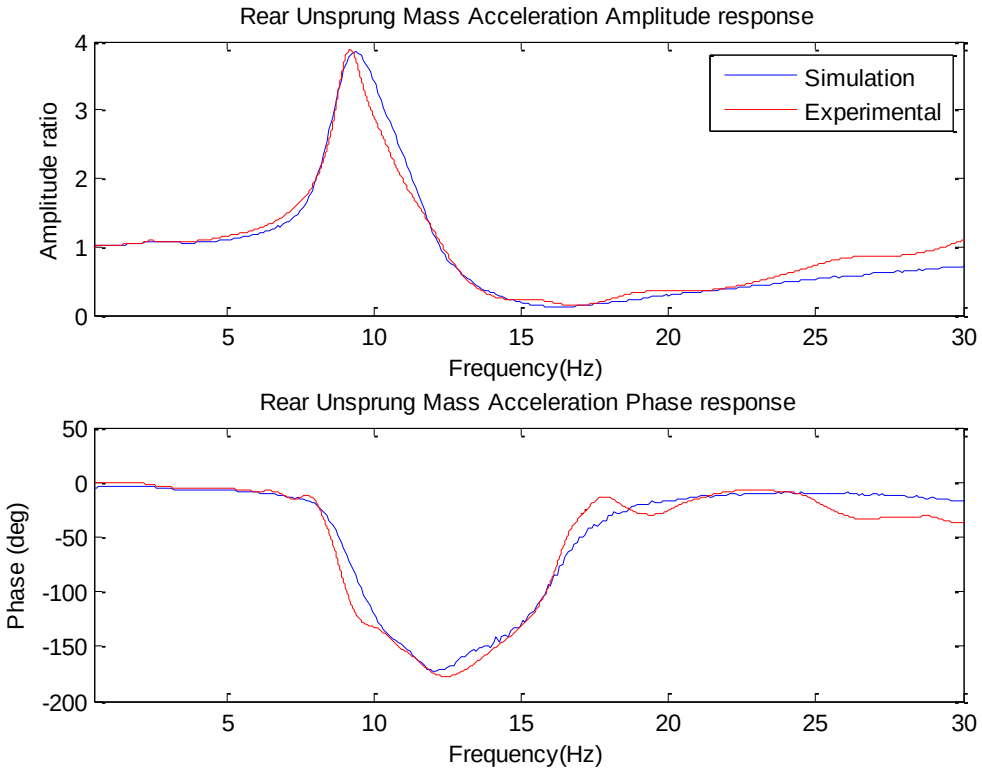

Figure 5-77: Rear unsprung mass acceleration ratio frequency response – Setup 5

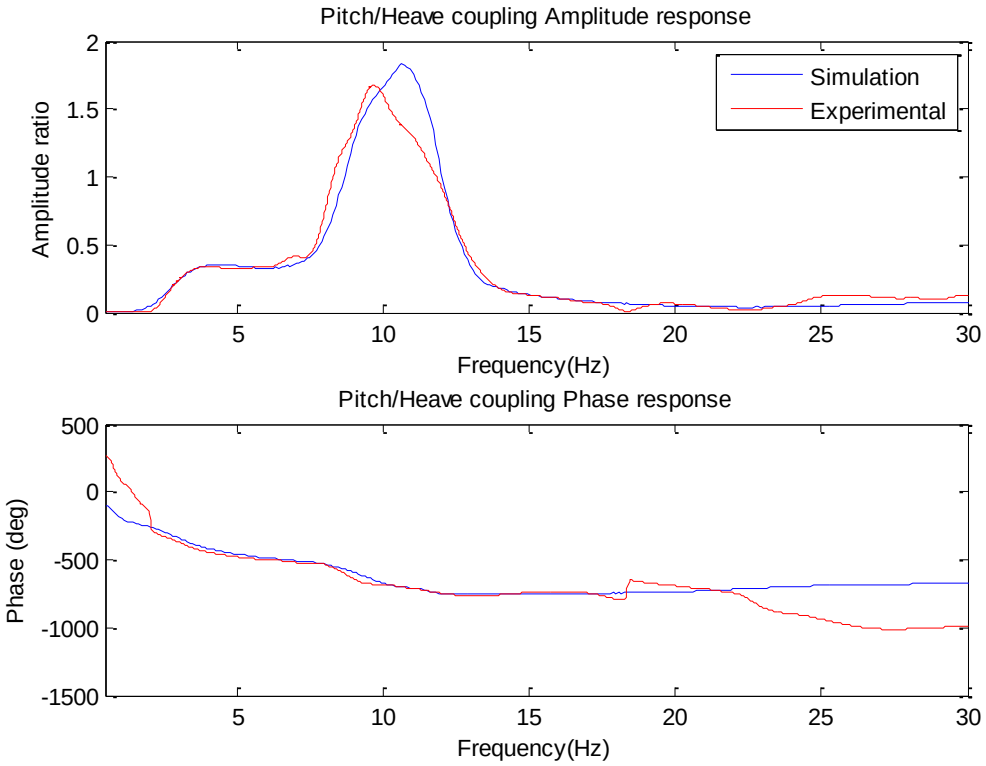

Figure 5-78: Pitch acceleration ratio frequency response – Setup 5

Discussion of results

The analysis of these case studies have shown that the dynamic vehicle model developed in section 5.4 successfully replicates the ride dynamics of a vehicle suspension incorporating real inerters in a virtual environment.

Moreover, the experimental dynamic analysis carried out in this section confirms the conclusions reached in Chapter 3. An increase in inertance *b* induces an increase in dynamic effective sprung mass M_{eff} which leads to the reduction of the amplitude of the FRFs and the resonant frequency at the body mode. However, since the inerter is also connected to the unsprung mass, an increase in b also induces an increase in the dynamic effective unsprung mass m_{ueff}. This causes the natural frequency of the hub mode to decrease dramatically. As discussed in Chapter 4, relatively low frequency hub modes cause larger tyre deflections which affect the elastic properties of the tyre. This, in turn, leads to a less controlled hub mode.

In addition to this, a special remark must be made with regard to the large deviation in phase angle presented in some of the graphs when amplitude ratios tend to zero values. Large differences between experimental and simulated phase responses can be observed in Figure

5-48, Figure 5-56 and Figure 5-62. In those figures, front body acceleration phase response jumps outside the expected phase range $[-\pi,+\pi]$ rad at around 10-12 Hz. Although this sudden phase change has been smoothed out by the post-processing, the actual experimental phase experiences a phase lead similar to the predicted by the model. This is due to the way the post-processing parameter estimation tool constructs the phase response traces from experimental time-domain data (red traces). In the version of the post-processing tool developed by Bennett (2012) used in this thesis, the phase response between output and input signals is calculated from the difference in time at each peak for a given frequency. For low output signal amplitudes (typically less than a 10% of the amplitude of input signal), the noise found in the physical signal could alter peaks identified by the software for a given time period. This causes the miscalculation of phase response for low amplitude ratios in Figure 5-48, Figure 5-56 and Figure 5-62. A confirmation of this behaviour can be noticed in Figure 5-72. In this case, because the amplitude ratio of the front body acceleration is higher than in previous case, the parameter estimation program has succeeded in producing the actual phase response. Similar phase response discontinuities can be observed in pitch acceleration FRFs due to low amplitude ratios.

5.5.2. Analysis of model predictability via suspension optimisation

The main goal of computer simulation is to create virtual models that can be used for analysing the dynamic behaviour of a specific system without the requirement of physical system. Furthermore, if the computer model has been fully validated, then it could be used for virtual optimisation. Although, Chapter 7 covers an extensive discussion on suspension optimisation, a simple single-objective optimisation case study has been analysed in this section. In this way, the predictive capabilities of the model for suspension optimisation can be validated.

In this section, two case studies have been analysed separately:

- Suspension optimisation of a mechanical grip cost function J_1 defined as the algebraic sum of the root-mean-square (RMS) of the amplitude ratio of the FRF of the front dynamic CPL $|F_{CPL\_F}|$ and rear dynamic CPL $|F_{CPL\_R}|$.

$$J_1 = RMS(|F_{CPL\_F}|) + RMS(|F_{CPL\_R}|) \tag{5.9}$$

- Suspension optimisation of an aerodynamic grip cost function J_2: defined as the algebraic sum of the RMS of the amplitude of the FRF of front ride height $\left|RH_F^{Abs}\right|$ and rear ride height $\left|RH_R^{Abs}\right|$.

$$J_2 = RMS\left(\left|RH_F^{Abs}\right|\right) + RMS\left(\left|RH_R^{Abs}\right|\right) \quad (5.10)$$

For each case, a set of suspension parameters that minimises the objective function *J* was obtained using the virtual suspension model without (S1) and with inerters (S2). A detailed discussion of the selection of the suspension parameters that must compose the optimisation search space will be provided in Chapter 7. In this section, front and rear damper and inerter characteristics were used to set the optimisation search space. Table 5-16 shows the limits of the search space selected for these case studies. Note that, for the case of a suspension without inerters, the search space was only composed by front and rear damper characteristics.

	Min. value	**Max. value**
Damper rate (Ns/m)	700	3500
Inerter rate (kg)	0	100

Table 5-16: Design space range – Suspension optimisation validation

According to the material reviewed in Chapter 2, a SQP algorithm was selected to perform the optimisation process due to its strong local-convergence towards a single optimal solution. This optimisation solver has been set making use of the built-in Matlab function for nonlinear constrained optimisation *fmincon* (The MathWorks Inc., 2010).

Once optimised suspension settings were obtained, these results were then used to set the suspension of the physical test vehicle. Experimental tests for each case were run and experimental values for each objective function *J* were calculated from the FRFs of the experimental data according to equations (5.9) and (5.10).

Mechanical grip optimisation

Table 5-17 shows the set of suspension parameters that minimises objective function J_1 in the virtual environment for both suspension configurations.

	Without inerter	**With inerter**
Front Damper Rate	1340 Ns/m	1450 Ns/m
Rear Damper Rate	1160 Ns/m	1240 Ns/m
Front Inerter Rate	-	6.2 kg
Rear Inerter Rate	-	4.8 kg

Table 5-17: Optimised suspension parameters for J_1 - Mechanical grip suspension optimisation validation

These suspension settings can then be used obtain to an experimental value of J_1. Table 5-18 shows the experimental value of J_1 for both suspension settings. A small improvement can be obtained from fitting inerters into the suspension.

	Without inerters	With inerters	Improvement (%)
J_1 exp	85.75	81.37	**5.1**

Table 5-18: Summary of mechanical grip objective function results

Figure 5-79 to Figure 5-82 show the experimental FRFs for each suspension configuration. In these figures, the blue traces represent the optimised FRFs for the suspension setting S1 and the red traces represent the optimised FRFs for the suspension setting S2.

Figure 5-79 and Figure 5-80 show that, on one hand, suspension S2 achieves a more controlled body mode than suspension S1. This means that the use of inerters in S2 allows CPL variations to be reduced around the body mode (low frequency range up to 6-7 Hz). Furthermore, better controlled body mode also induces a decrease in ride height variation on both axles (see Figure 5-81 and Figure 5-82). However, on the other hand, the use of inerters in S2 causes a poorer controlled hub mode (at around 15 Hz), especially at the rear axle. This is due to the fact that the inerter adds a dynamic effective mass to both sprung and unsprung masses, as discussed in Chapter 3.

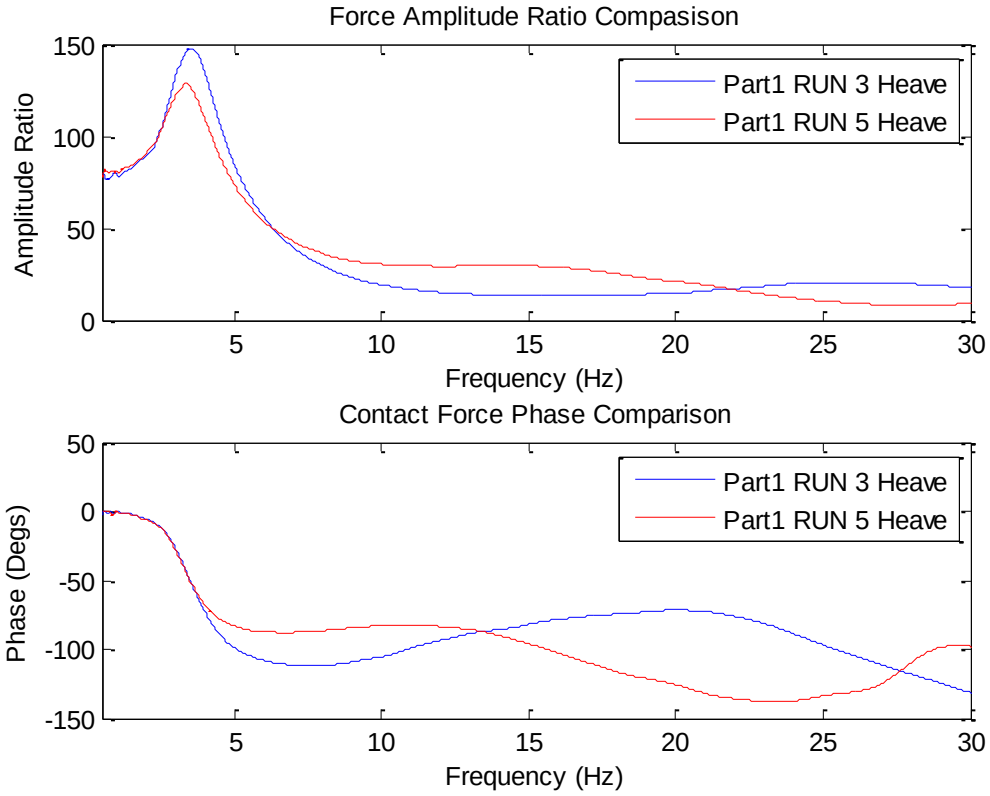

Figure 5-79: Front CPL response – Mechanical grip optimisation

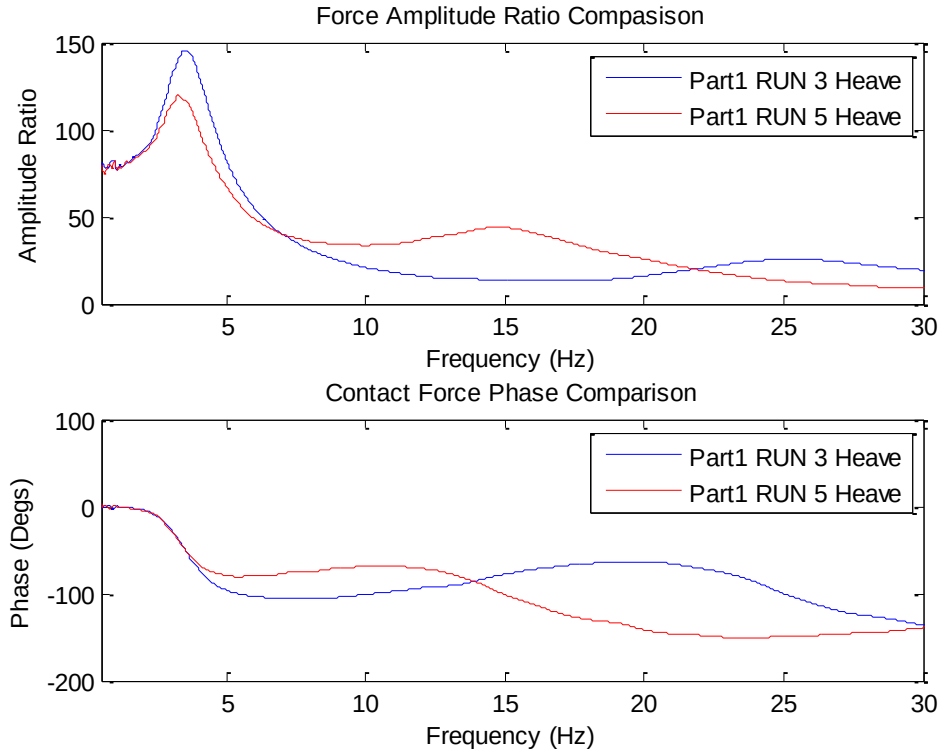

Figure 5-80: Rear CPL response – Mechanical grip optimisation

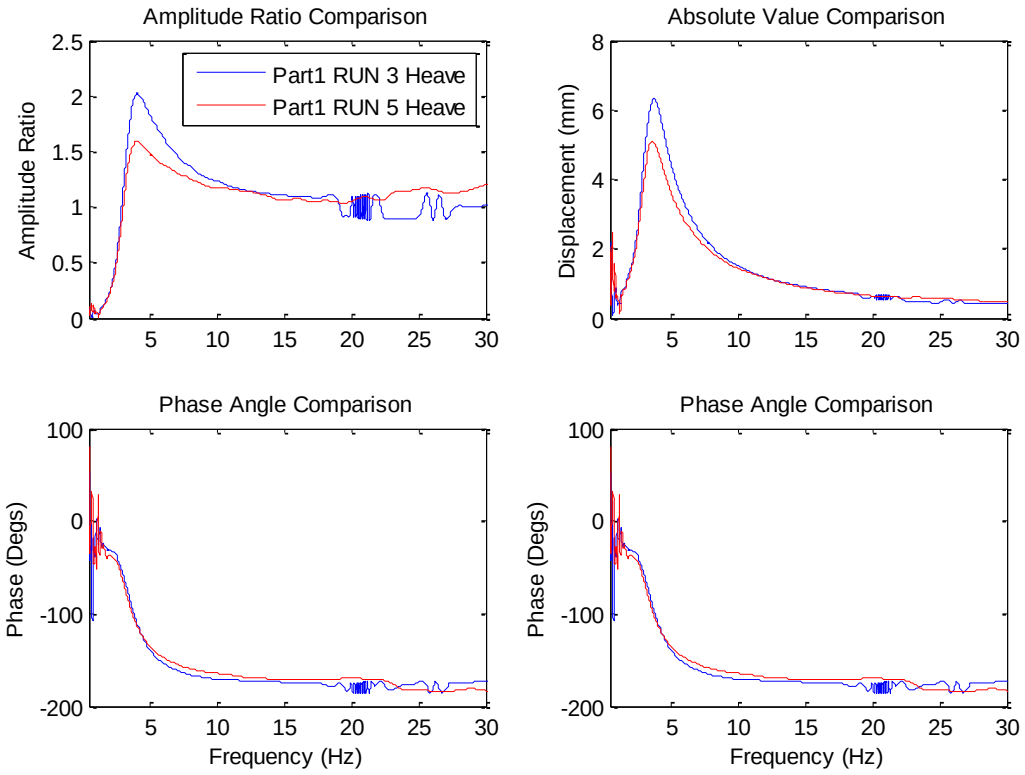

Figure 5-81: Front Ride Height response – Mechanical grip optimisation

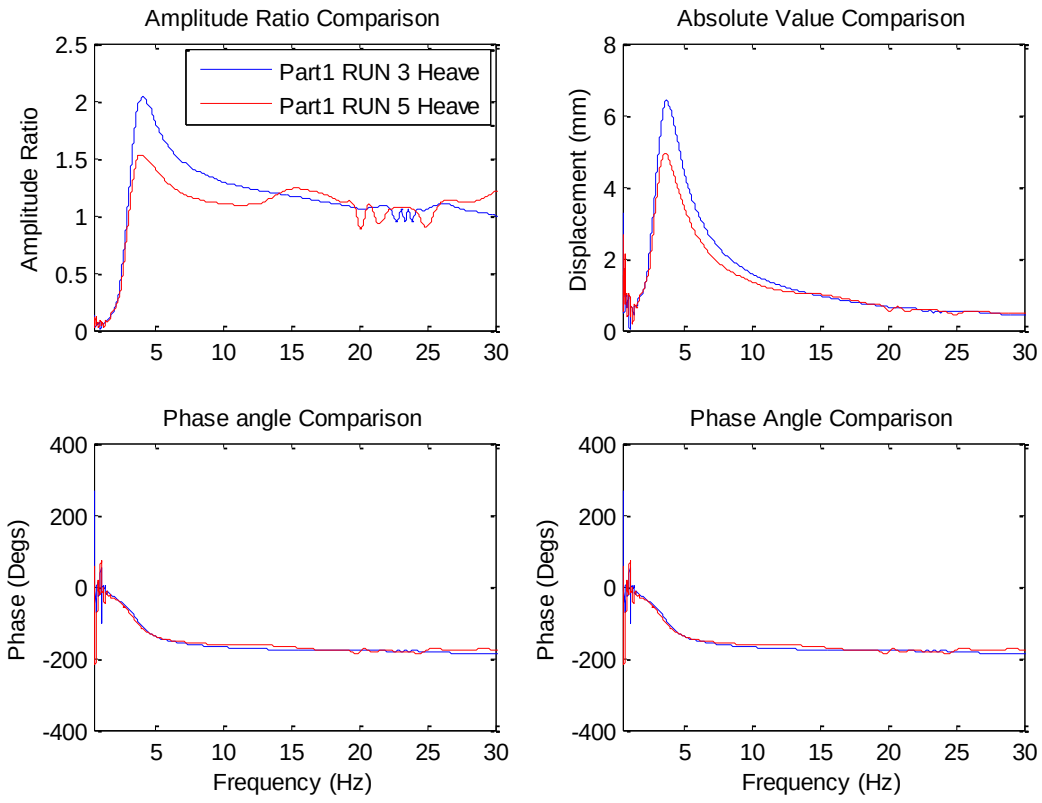

Figure 5-82: Rear Ride Height response – Mechanical grip optimisation

Aerodynamic Grip Optimisation

The same process was carried out for the aerodynamic grip objective function J_2. The simulated optimal suspension parameters are summarised in Table 5-19:

	Without inerters	**With inerters**
Front Damper Rate	2630 Ns/m	3270 Ns/m
Rear Damper Rate	2510 Ns/m	3380 Ns/m
Front Inerter Rate	-	36.8 kg
Rear Inerter Rate	-	43.2 kg

Table 5-19: Optimised suspension parameters – Aero grip suspension optimisation validation

Table 5-20 summarises the improvement in J_2 obtained for a suspension with inerters S2 with respect to a conventional suspension S1.

	Baseline Set-up	Optimised Set-up	Improvement (%)
J_2 exp	2.87	2.27	**20.9**

Table 5-20: Summary of aero grip objective function results

Figure 5-83 to Figure 5-86 show the comparison of experimental FRFs between both suspension configurations. As in the previous case study, blue traces relate to the FRFs for S1 suspension settings and red traces relate to the FRFs for S2 suspension setting.

Figure 5-83 and Figure 5-84 show that, although the dynamic CPL variation has been improved around the body mode, the hub mode is more poorly controlled. This increase of dynamic CPL variation in the range from 7 to 20 Hz will cause a loss in road holding performance and therefore a loss of mechanical grip. However, Figure 5-85 and Figure 5-86 show important improvements in aero grip. A 40% decrease in the peak ride height variation at the body mode has been achieved by the use of inerters. Moreover, due to the effective dynamic mass added to the actual sprung mass, the natural frequency of the body mode has been decreased from 5 to 4 Hz. This means that, because the dynamic variation in ride height would occur at a slower rate, driver could be able to cope more easily with these disturbances.

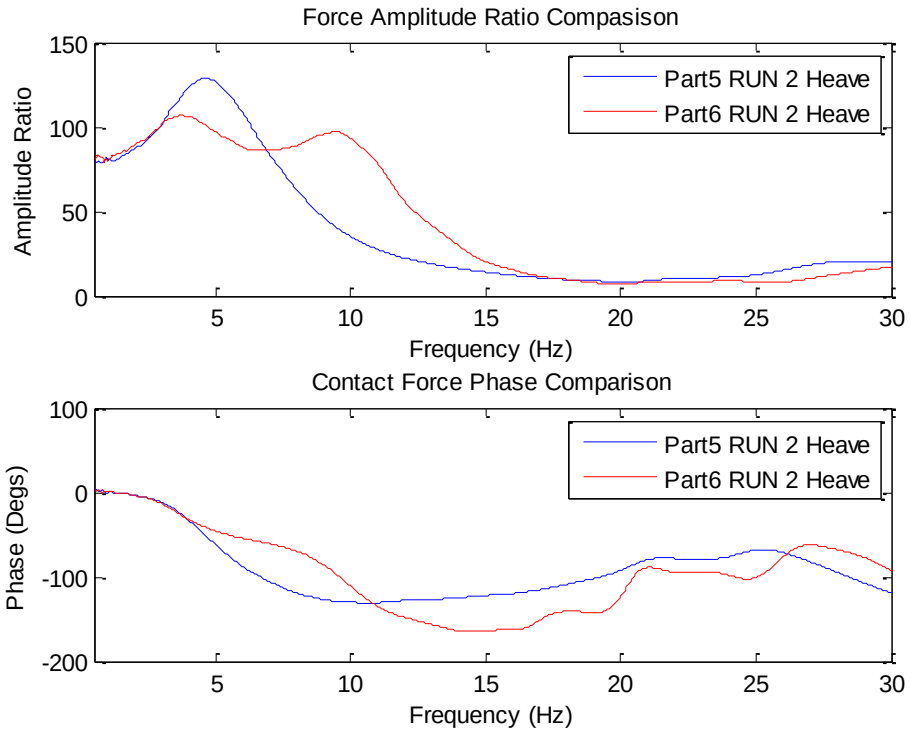

Figure 5-83: Front CPL response – Aero grip optimisation

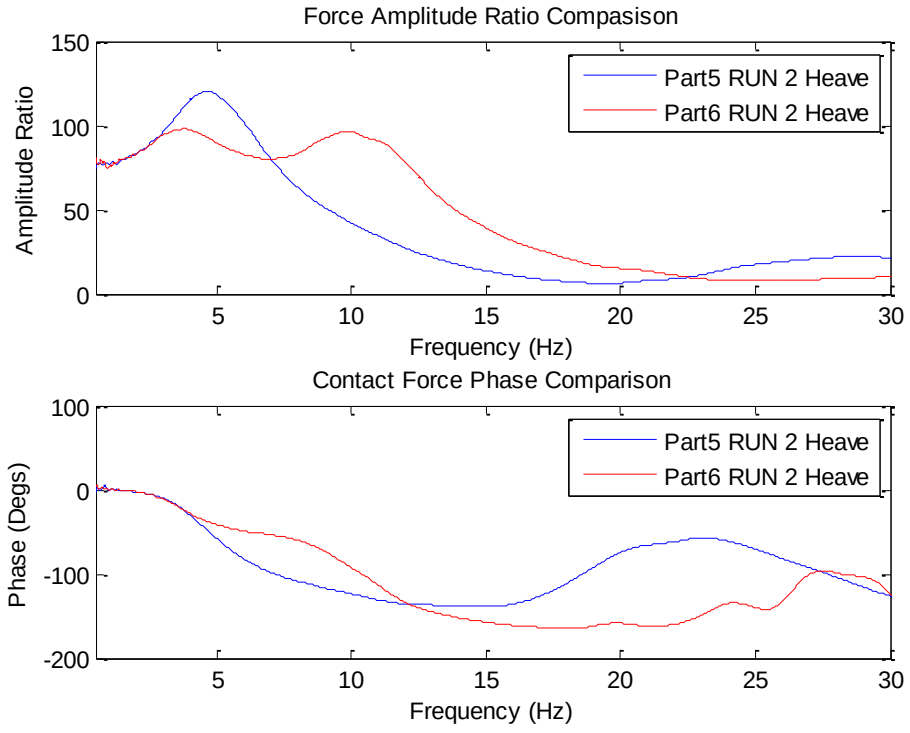

Figure 5-84: Rear CPL response – Aero grip optimisation

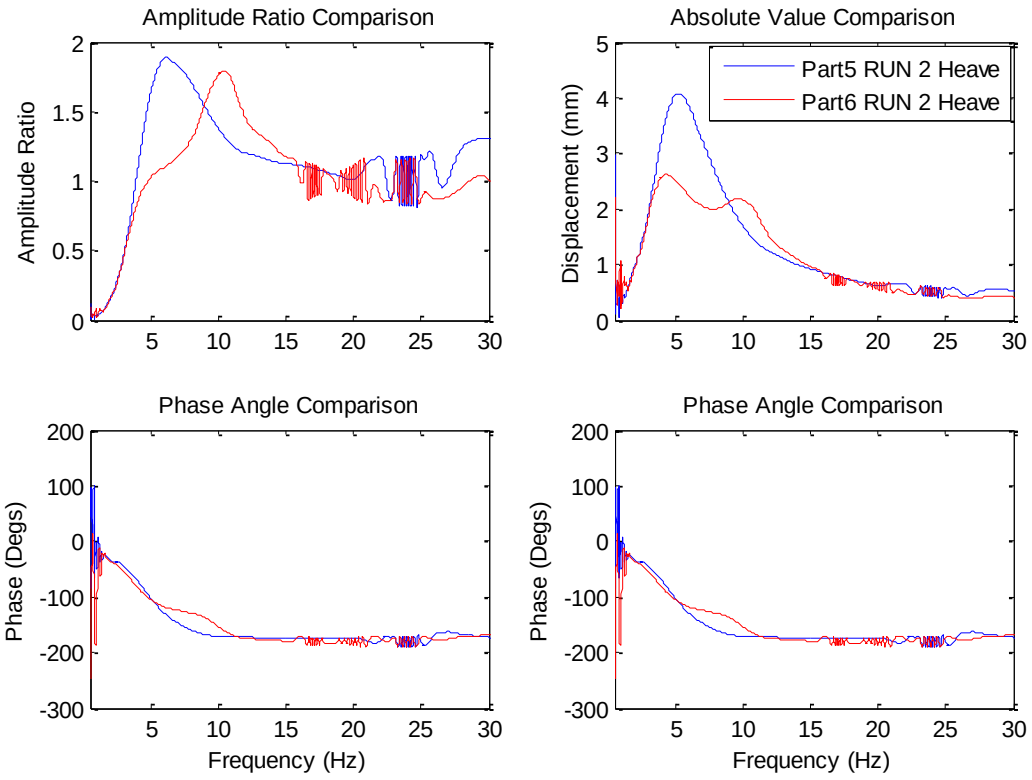

Figure 5-85: Front Ride Height response – Aero grip optimisation

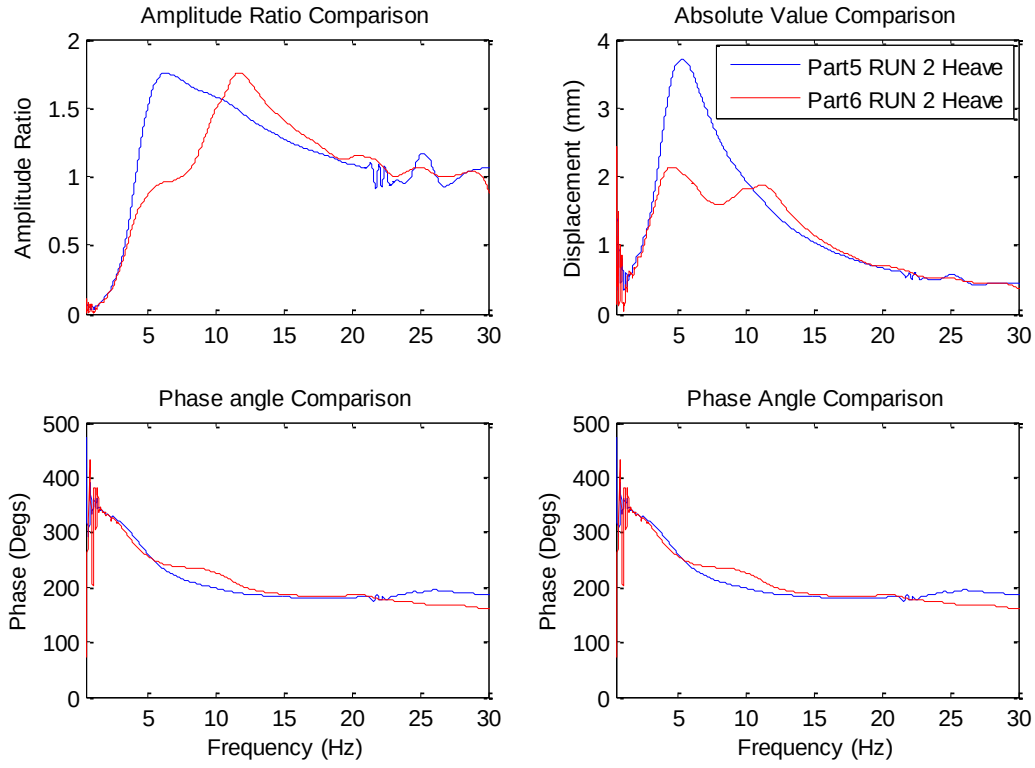

Figure 5-86: Rear Ride Height response – Aero grip optimisation

5.5.3. Analysis of correlation errors

Section 5.5.1 showed that the vehicle model incorporating inerters developed in section 5.4 is capable of replicating the dynamic behaviour of the physical test car for a wide variety of inerter settings. This model could then be used to analyse the ride dynamics of a real car and to investigate interactions between inerters and other suspensions devices without the need of building a prototype car. Moreover, section 5.5.2 demonstrated that the application of an optimisation algorithm to the validated vehicle model with inerters can successfully produce optimised suspension design parameters.

In this section a quantitative analysis of the correlation between experiments and simulation has been carried out. Average errors of the amplitude of the FRF for the magnitudes directly measured by sensors have been obtained. The magnitudes analysed include front and rear CPL variation, front and rear body acceleration and front and rear hub acceleration. In general, average force and acceleration errors have been calculated as follows:

$$a_{error}\ (\%) = \frac{\sum_{j=1}^{N} \frac{\left|a_{Exp}^{j} - a_{Sim}^{j}\right|}{a_{input}^{j}}}{N} \cdot 100 \qquad (5.11)$$

$$F_{error}\ (\%) = \frac{\sum_{j=1}^{N} \frac{\left|F_{Exp}^{j} - F_{Sim}^{j}\right|}{W_0 \cdot g}}{N} \cdot 100 \qquad (5.12)$$

Where a_{Exp}^{j} and F_{Exp}^{j} represents the jth element of the vector containing the measured FRF of acceleration and force respectively.

a_{Sim}^{j} and F_{Sim}^{j} represents the jth element of the vector containing the simulated FRF of acceleration and force respectively.

a_{input}^{j} represents the jth element of the vector containing the FRF of the input (actuator) acceleration.

W_0 represents the static vehicle weight.

g represents the gravitational acceleration.

N represents the total number of elements that compose the FRF vector.

Table 5-21 summarises the average error of all the measured magnitudes for the five suspension settings analysed in section 5.5.1.

	Setup 1	**Setup 2**	**Setup 3**	**Setup 4**	**Setup 5**
Front Body Acc	7.1%	5.3%	5.9%	7.5%	8.5%
Rear Body Acc	7.3%	10.0%	10.8%	12.5%	15.7%
Front CPL	0.7%	1.3%	2.3%	3.3%	3.5%
Rear CPL	1.6%	1.6%	2.4%	2.4%	2.2%
Front Hub Acc	4.7%	6.0%	13.6%	16.4%	18.9%
Rear Hub Acc	4.5%	6.6%	7.5%	9.0%	11.2%

Table 5-21: Summary of validation errors

From the results above, it can be observed that the level of agreement between experimental and simulated is high. Dynamic contact patch load responses are the most accurate measurements with a maximum averaged error of 3.5%. Body acceleration frequency responses present also good levels of accuracy. As it can be observed from body acceleration dynamic response figures (see section 5.5.1), the largest deviation between simulation and experimental data was produced by an overestimation of amplitude at around the hub mode. Since this thesis focuses on performance of a race car rather than comfort, body acceleration FRF has been used to produce the ride height FRFs. According to this, it has been analysed that, even in the worst case scenario (rear body acceleration in setup 5), the difference induced in ride height would be less than 0.3 mm for a 25-mm amplitude road input. Hub acceleration dynamic response presents the highest accuracy errors of all measured magnitudes. From figures shown in section 5.5.1, the largest errors are produced at high frequencies (from 20 Hz onwards). In this high frequency bandwidth, the impact of unsprung mass acceleration in the ride dynamics of the vehicle is quite low since the hub mode occurs at lower frequencies when the suspension incorporates inerters. According to this, a new analysis of the average relative hub acceleration errors has been carried out neglecting the 20-30 Hz frequency band. Results show that the level of accuracy is much higher within the frequency region where hub accelerations have an impact in the overall ride dynamics of the vehicle (see Table 5-22).

	Setup 1	Setup 2	Setup 3	Setup 4	Setup 5
Front Hub Acc	5.3%	2.4%	6.5%	7.8%	8.8%
Rear Hub Acc	4.8%	3.4%	4.1%	6.2%	8.9%

Table 5-22: Hub acceleration average errors – Frequency range 0.5-20 Hz

Furthermore, there is progressive increase of the prediction error as the inertance characteristic increases. This is due to a number of reasons: firstly, the inerter has been modelled as a linear inertance characteristic that include linear parasitic effects such as inerter compliance and friction. These parasitic effects are, however, rarely linear. For low inertance settings, these parasitic effects have a marginal effect on the dynamic response of the suspension, thus the model could be approximated to a linear ideal inerter. As inertance values increase, inerter parasitic effects take over and their impact in the performance of the suspension is much more noticeable (see Figure 5-22). Under these conditions, deviations from linear behaviour will cause a source of error. Nonlinear models, however, do not allow the construction of suspension model via a SISO transfer function. Furthermore, the use of nonlinear models would increase parameter estimation complexity and simulation time.

Secondly, tyre model plays an important role in model accuracy. Section 5.4.2 demonstrated that the use of linear tyre elastic properties would be insufficient if high accuracy is required. Alternatively, a nonlinear exponential model has been proposed to account for the interaction between tyre elastic characteristics (i.e. tyre stiffness and damping) and tyre dynamic deflection. Even though this model is a better representation of the behaviour of the physical tyre, it was observed that the front tyres present a hysteretic behaviour, especially as inertance settings increased. Figure 5-87 shows the differences in front and rear tyre behaviour between a low and high inertance setting. Rear tyres present a mainly exponential-like elastic characteristic for both inertance settings. However, the difference in tyre stiffness characteristic at the front axle is much larger. Although an exponential characteristic can still be appreciated, hysteresis is quite large with a heavy inerter setting. Tyres are very complex and highly nonlinear systems and a detailed study and analysis of nonlinear tyre behaviour is out of the scope of the present research work. Causes of this hysteretic behaviour could come from complex interactions between tyre rubber, tyre carcass, tyre sidewall construction and compressed air at high tyre deflections. It must be noted that, for very low tyre deflections, the estimation of tyre stiffness is not accurate, due to the high noise-to-signal ratio (close to 1). This explains the non-uniqueness of tyre stiffness estimation for a given tyre deflection.

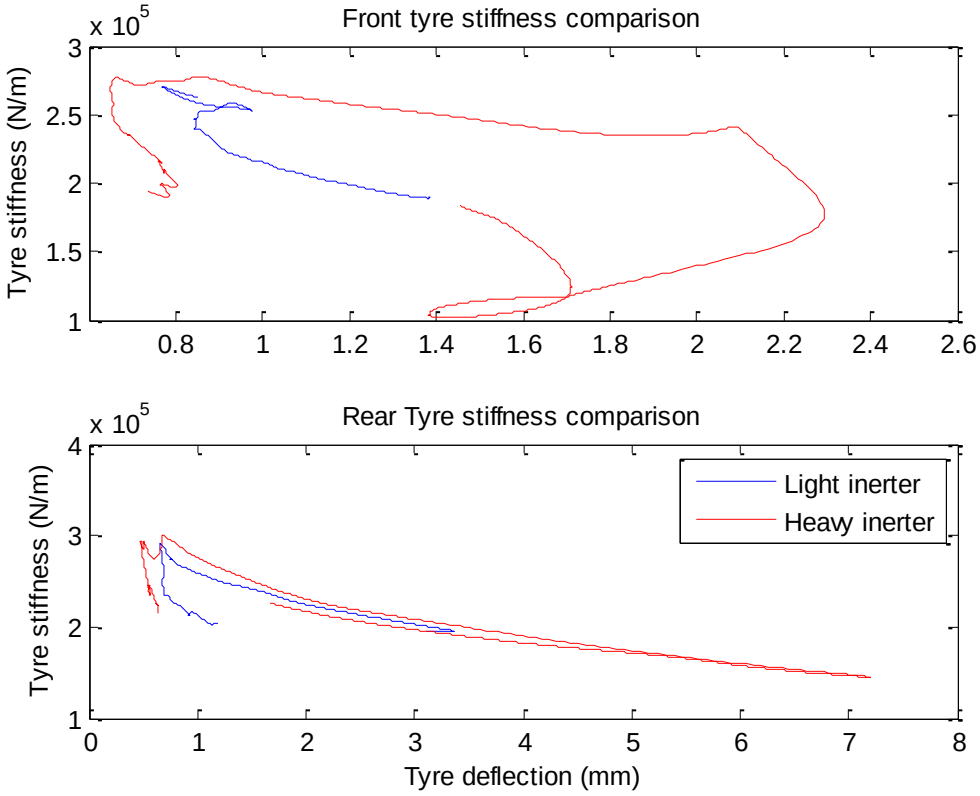

Figure 5-87: Tyre stiffness characteristic comparison – Front (upper) and rear (lower)

Lastly, the mass of the unsprung suspension components has been assumed to be constant for all the inerter settings tested. However, increasing the inerter flywheel causes an increase in unsprung mass as well. The weight of the real inerters designed ranges from about 850 gr. (no flywheel) to 2.25 kg (full flywheel capacity). This variation in actual unsprung weight affects the dynamic response of the system. Figure 5-88 shows the dynamic CPL response for suspension setup 5 with two different (front and rear) unsprung mass estimations. The increase of unsprung mass reduces the difference in amplitude and frequency drift at the hub mode (around 9 Hz) between experimental data and simulation. This means that a correlation relationship between inerter flywheel settings and total unsprung weight should be included into the model in order to improve its accuracy. However, this increase of model complexity would lead to higher model simulation times. Since the model is intended to be used for optimisation purposes and unsprung mass changes would have a relative impact only with very heavy inerter settings, such an extension of the vehicle model has not been applied.

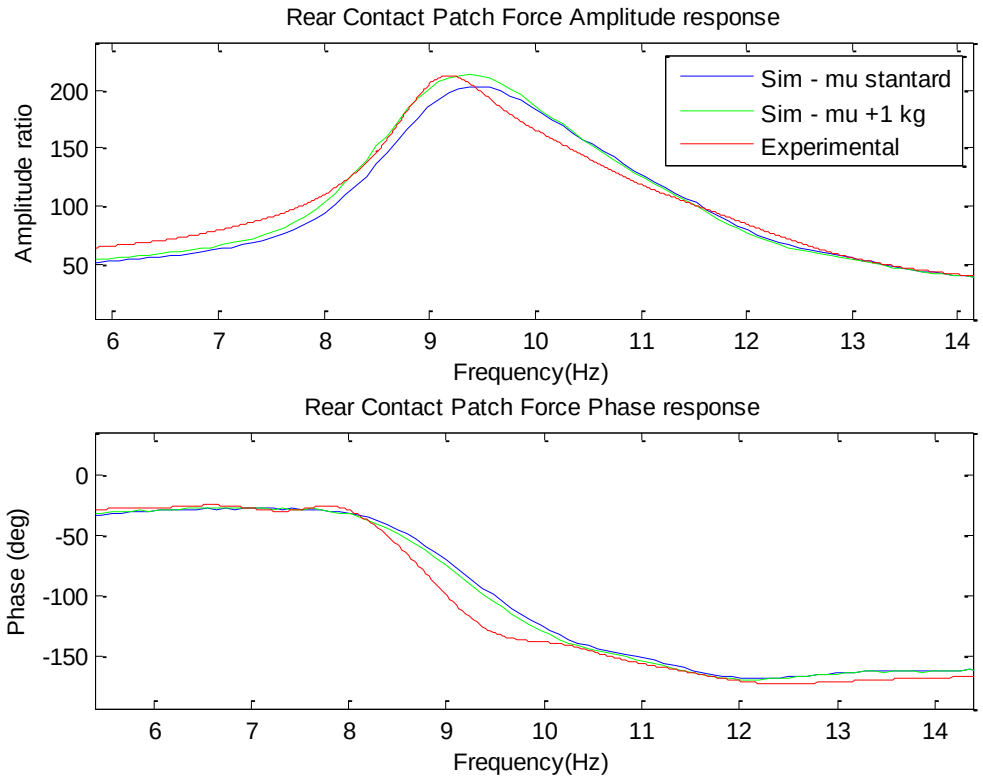

Figure 5-88: Effect of unsprung mass variation in dynamic CPL response

In addition to this, it has been observed that the model tends to overestimate the amplitude of the body acceleration response at high. This is due to a number of reasons: firstly, the model uses a linear damping rate to represent the damper characteristic. Even though the damper settings have been tuned to provide a quasi-linear damping characteristic, physical damper present a digressive characteristic. An increase of high-speed damping rate could cause an increase in body acceleration FRF at high frequencies. Including a nonlinear damper model would increase model accuracy at the expense of a increased model complexity. Secondly, the sprung mass has been modelled as a single solid-rigid body. As suggested by Bennett (2012), a multi-DOF model of the sprung mass could help to characterise the dynamic behaviour of different components of the sprung mass and their impact in the performance of the suspension. However, as discussed in section 5.3, a multi-DOF sprung mass model would require additional instrumentation to measure accelerations of the different body components and the development of a more complex parameter estimation method. Moreover, the additional DOFs would increase the complexity of the model and, in turn, this would reduce its computational efficiency.

In spite of these sources of errors, the model developed in this chapter is capable of replicating a physical suspension incorporating inerters with a degree of accuracy so that the main dynamic features of the system (i.e. natural frequencies and amplitude ratios) can be successfully identified by this model.

5.6. Summary

In this chapter a novel vehicle model featuring inerters for the analysis and optimisation of high performance car suspensions has been developed. Experimental data obtained from four-post rig testing has been used to estimate all the vehicle and suspension parameters. These parameters have then been used to simulate the vehicle model and results have been compared against experimental FRF of the physical vehicle. Several suspension settings have been tested in order to demonstrate the accuracy of the vehicle model over a vast range of inerter configurations. The model has been deemed to successfully represent the dynamic behaviour of a vehicle suspension fitted with physical inerters.

Moreover, the model developed in this chapter has been used as part of an optimisation process. The main purpose of this study has been to evaluate the predictive capabilities of the vehicle model applied to suspension design and optimisation. The model successfully produced optimised suspension settings for two different performance objective functions.

The experimental analysis of the suspension incorporating inerters carried out in this chapter showed that although increasing the inertance characteristic was beneficial for a better controlled body mode at low frequencies, this increase in inertance would cause a deterioration of the dynamic response at higher frequencies due to a less controlled hub model.

A critical discussion of model accuracy has been carried out. Different sources of error between experimental data and simulation have been identified and their impact in the dynamic response of the vehicle has been assessed. Results show that, although potential improvements in model accuracy could be obtained by introducing all these effects, model usefulness would not increase significantly and the parameter estimation process using experimental data from four-post rig testing would be more complex. In addition to this, the computational effort required to simulate the model would increase as well.

This novel vehicle model featuring real inerters will be used in the following chapters to analyse the impact of suspension dynamics into the overall performance of a race car (Chapter 6) and to construct an efficient and reliable suspension optimisation method (Chapter 7).

6. Lap-Time Simulation

6.1. Introduction

Lap-time simulators are powerful virtual tools that allow the analysis of the impact of variations of different components/parameters of a race car on the overall performance of the vehicle, around a specified race track. Provided that the vehicle model represents the behaviour of the actual race car with a useful degree of accuracy and fidelity, a lap-time simulator could offer a series of benefits with respect to on-track testing:

- Reduction of physical on-track testing.
- Increased range of experiments: the impact on vehicle performance of changes in key design parameters such as mass, moments of inertia, weight distribution and/or suspension layout can be analysed and evaluated at the design stage in order to determine the performance sensitivity of the race car to changes in magnitudes that cannot be easily modified on a race track.
- Repeatability: due to the inherent controlled testing environment that virtual tools offer, lap-time simulators offer stable and predictable conditions to run tests.

In the present research work, a fully dynamic lap-time simulation tool has been developed in order to analyse the impact of changes to the racing suspension on the overall performance of a race car.

This chapter is divided into two main development areas: development of the vehicle model, and development of solution algorithm. The first part deals with the description of the vehicle model used in the simulation. Equations of motion describing the dynamics of the vehicle are provided. The second part of the chapter is devoted to the development of the most efficient algorithm for lap time simulation. The algorithm used in this thesis relies on classical numerical methods for solving Optimal Control (OC) problems.

The last part of Chapter 6 presents a practical case study to evaluate the performance of the lap-time simulation tool. A racing car has been simulated around the Bahrain GP Circuit. An analysis of the optimal trajectory and the optimal control inputs has been carried out.

6.2. Full-vehicle Dynamic Equations of Motion

Robust mathematical representation of the behaviour of a real vehicle is paramount in the design and development of a virtual lap-time simulation tool. The vehicle system must be able to replicate with the required degree of accuracy and fidelity the actual dynamics of a real racing car.

In this research work, the vehicle model has been broken down into independent input/output (I/O) modular subsystems that can be interconnected to compose the final vehicle model. This modular modelling approach allows the user to easily interchange, reuse or update different components without affecting the rest of the model. The main subsystems considered in this thesis are:

- Vehicle and wheel dynamics
- Powertrain/Brake model
- Aerodynamic model
- Suspension model
- Tyre model
- Track model
- Driver model

Figure 6-1 depicts a schematic diagram of the relationship between the different modules that compose the overall vehicle model. The diagram highlights that each module could be substituted by a more complex representation without the need to modify the rest of the modules, or restructuring the overall vehicle system.

In this modular modelling architecture, two building modules can be distinguished: force-system and dynamic modules. Force-system modules contain the expressions required to build the forces and moments that will be applied to the dynamic system. The main inputs of force-system models are control inputs and dynamic motions. Dynamic modules contain the set of ordinary differential equations (ODEs) that describe the dynamic behaviour of a body. The outputs of a dynamic module would typically be displacements, velocities and rotations (see Figure 6-2).

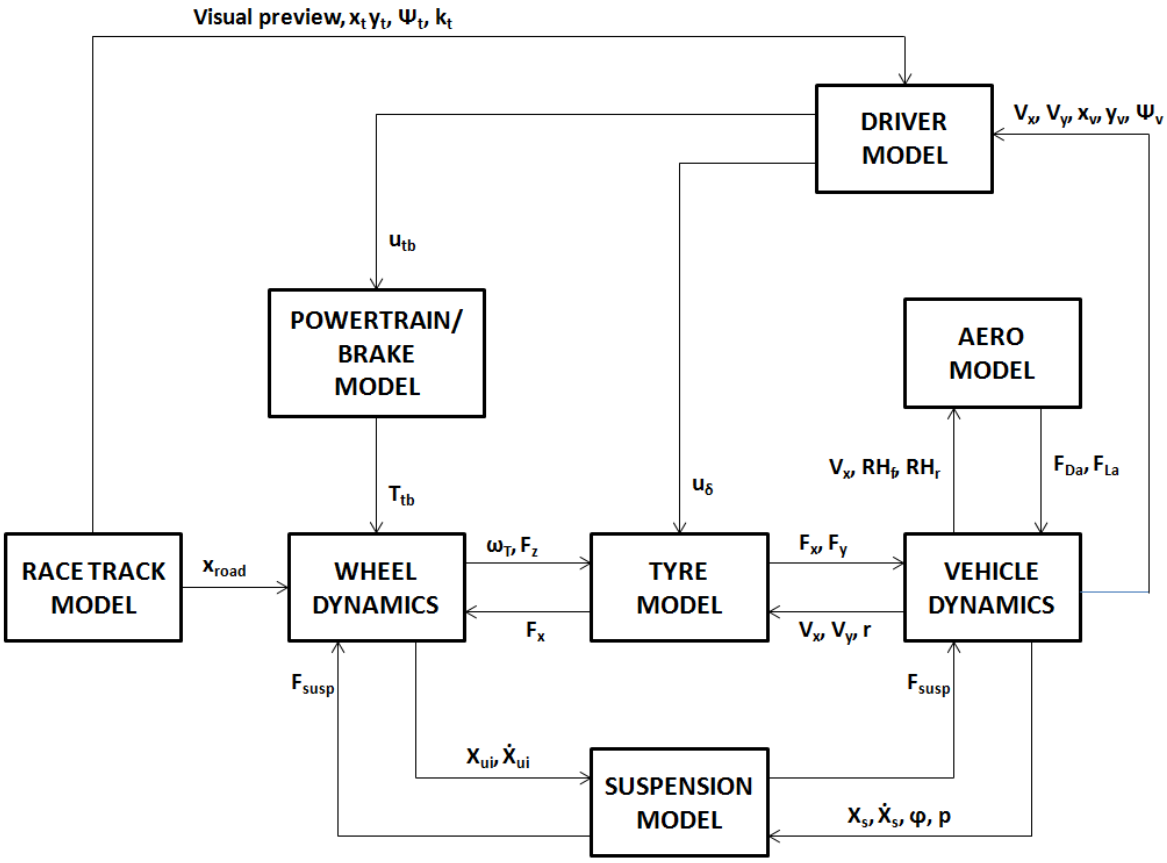

Figure 6-1: Overall Vehicle Model – Modular Modelling

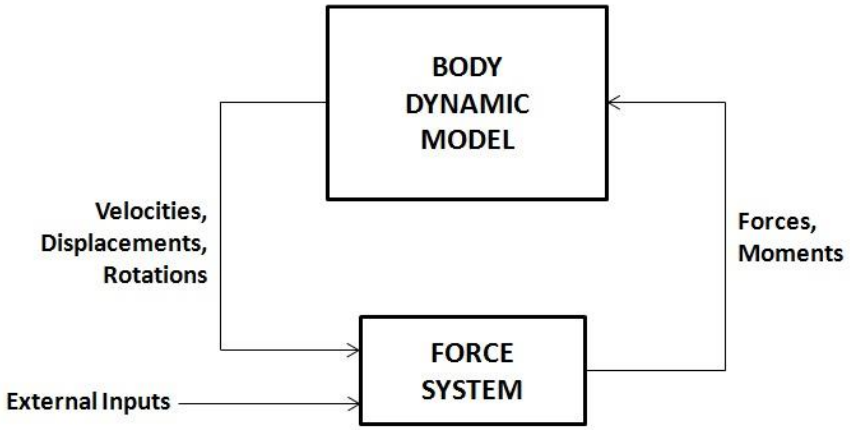

Figure 6-2: Modular Modelling operational approach

In this thesis, Simulink has been used as modelling software, since this package offers an ideal framework for modular modelling. Furthermore, Simulink models can be very easily linked to MATLAB® scripts to produce advanced analyses and optimisations. The following subsections provide a detailed description of each model systems depicted in Figure 6-1.

6.2.1. Vehicle and Wheel Dynamics Model

The basic requirement of the vehicle model is simplicity. As discussed in Chapter 5, model complexity can increase substantially the computational time of simulation. The main goal of this research work is to analyse the influence of suspension dynamics in the overall performance of a race car. According to this premise, a lumped parameter single-track vehicle model has been developed (see Figure 6-3). The model consists of three bodies: one solid-rigid body that represents sprung mass m_s and two more bodies that represent front and rear wheels m_{uf} and m_{ur} respectively. The model depicted in Figure 6-3 has 9 DOFs. The model allows translational motion of the vehicle in all three dimensions in space (longitudinal, lateral and vertical motions) and rotations around two axes (yaw and pitch motion). Front and rear unsprung wheels are connected to the main body via a suspension system. Unsprung masses are assumed to have motion only in vertical direction. Moreover, wheels are allowed to rotate only about the spin axis.

The model depicted in Figure 6-3 neglects rolling motions. As discussed in Chapter 5, the results obtained from the ride analysis of the vehicle suspensions under rolling conditions were not representative of the actual dynamic behaviour in roll of the physical car, so the author decided that by neglecting this motion from the vehicle, improvements in computational efficiency could be achieved without the loss of valuable information.

For such a model, the equations of motion (EOMs) can be expressed as a set of ODEs describing the dynamics of the system. These equations of motion can be written in state-space representation as follows:

$$\dot{\boldsymbol{x}} = f(\boldsymbol{x}(t), \boldsymbol{u}(t), t) \qquad x(t=0) = x_0 \qquad (6.1)$$

With $\boldsymbol{x}(t) \in \mathbb{R}^n$: n-dimensional state vector

$\boldsymbol{u}(t) \in \mathbb{R}^m$: m-dimensional input vector

$t \in [0, t_f]$: independent variable time

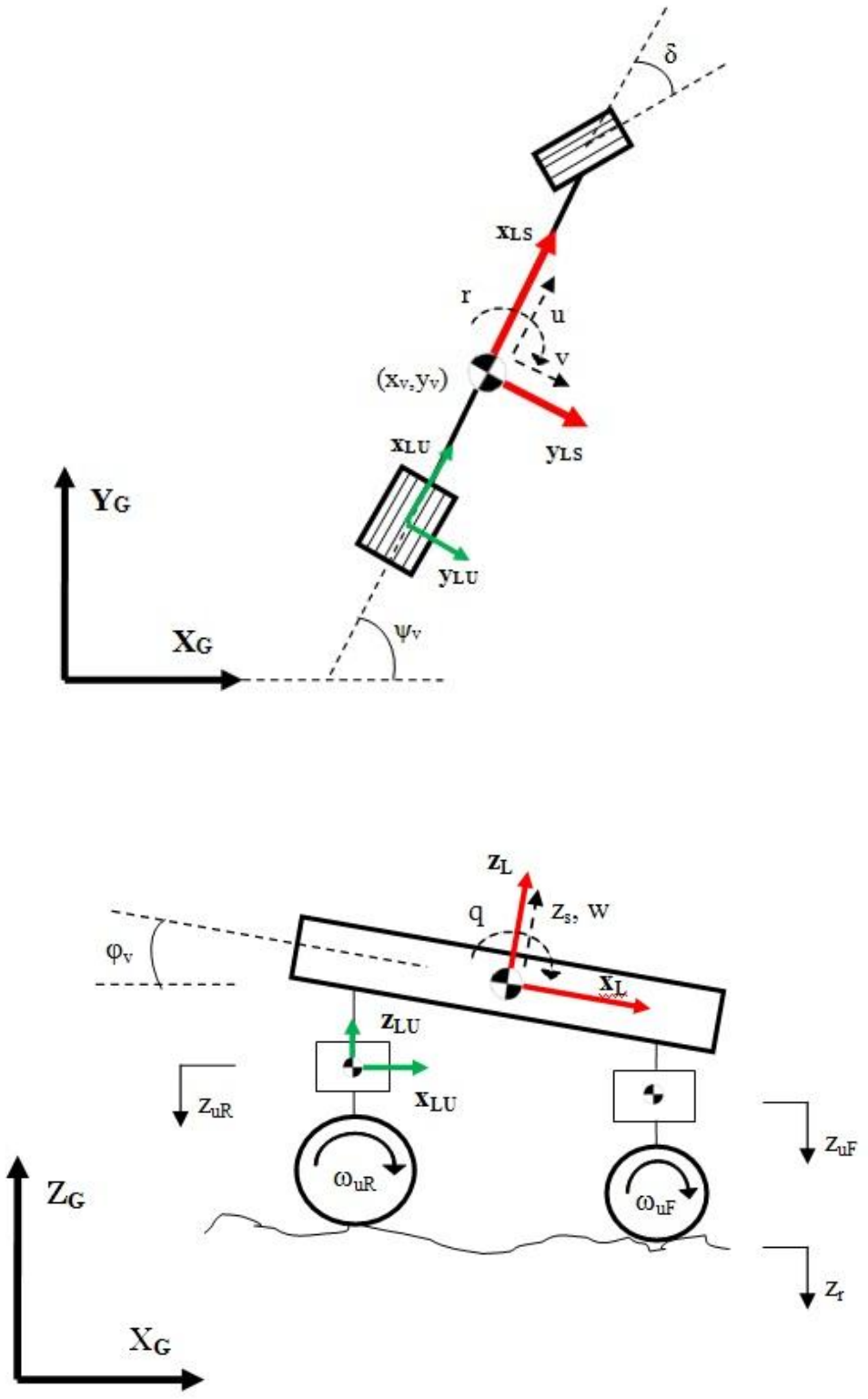

Figure 6-3: Sprung Single Track Vehicle Model: Plan view (upper) and lateral view (lower)

The state vector that defines the dynamic characteristic of the model depicted in Figure 6-3 is composed of the following state variables:

$$\boldsymbol{x}(t) = [\Psi_v \ r \ u \ v \ x_v \ y_v \ \varphi_v \ p \ z_s \ \dot{z}_s \ \omega_F \ \omega_R \ z_{uF} \ \dot{z}_{uF} \ z_{uR} \ \dot{z}_{uR}]^T$$

Where Ψ_v: vehicle heading angle

r: yaw rate

u: longitudinal velocity referenced to body local non-inertial frame

v: lateral velocity referenced to body local non-inertial frame

x_v: X-position in global inertial frame

y_v: Y-position in global inertial frame

φ_v: pitch angle

p: pitch rate

z_s: chassis vertical position

$\dot{z}_s$: chassis vertical velocity

ω_F: front wheel spin velocity

ω_R: rear wheel spin velocity

z_{uF}: front unsprung mass vertical position

$\dot{z}_{uF}$: front unsprung mass vertical velocity

z_{uR}: rear unsprung mass vertical position

$\dot{z}_{uR}$: rear unsprung mass vertical velocity

Two input controls have been considered in this vehicle model: longitudinal throttle/brake control u_{tb} and steering control u_δ. Further discussions with regard to the input control vector are covered in the Driver Model section.

Formal derivation of the equations of motion describing the dynamics of chassis and wheels has been derived from the Lagrange Energy method for quasi-velocities (Genta & Morello, 2009). Detailed derivation of the equations of motion of the vehicle model can be found in Appendix B.

6.2.2. Powertrain/Brake System Model

The powertrain model is composed of engine, gearbox and differential. Figure 6-4 illustrates the layout of the powertrain. In most racing series, regulations rule that power can only be delivered to one axle. In most track-based competitions, the rear axle is configured to produce

the tractive effort on the car. According to this, the powertrain model considered in this research work represents a rear wheel drive (RWD) layout and therefore tractive torque will be only applied to the rear axle.

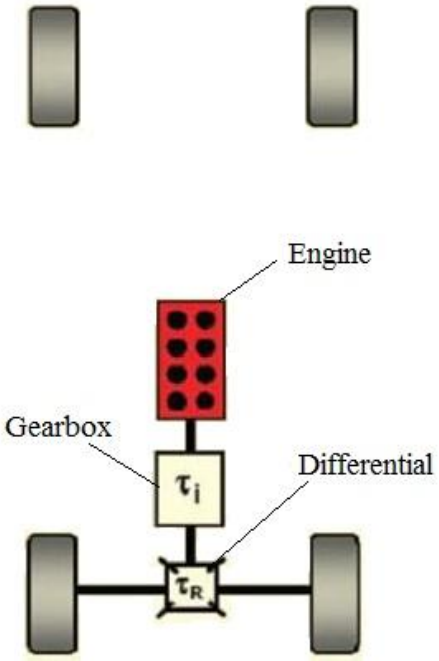

Figure 6-4: Powertrain layout

Engine

The engine is modelled as a 2D lookup table whose entry parameters are throttle opening and current engine speed. The output is the engine torque. Engine speed is obtained from rear wheel rotational speed (ω_{Rear}) and global gear ratio (G_R) as:

$$\omega_E = \omega_{Rear} \cdot G_R \tag{6.2}$$

Figure 6-5 shows an example of a simple engine map.

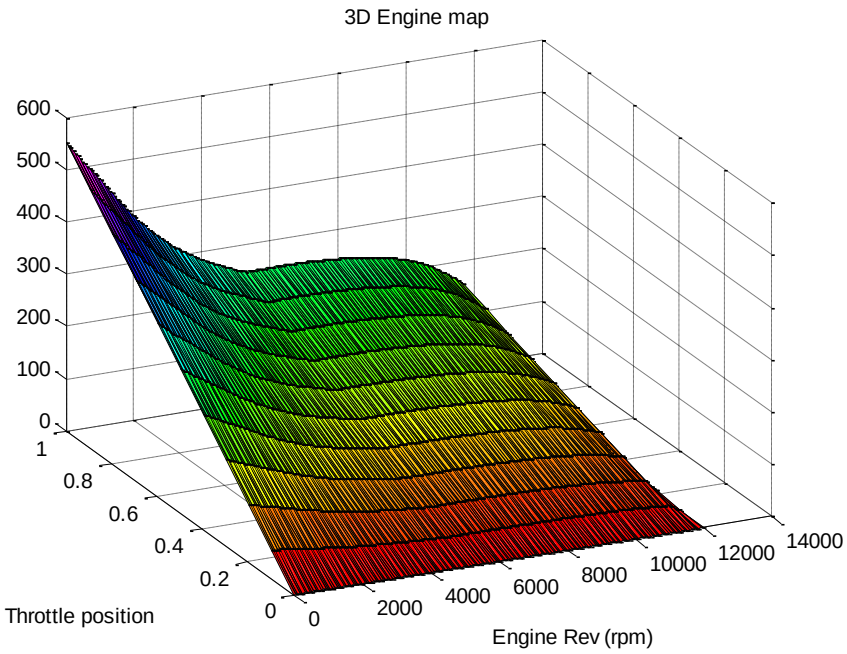

Figure 6-5: Engine map

Exact modelling of complex engine dynamics including mechanical losses, fuel mixture, thermal effects, etc. is outside the scope of the present research work.

Gearbox

A simple 6-speed manual gearbox has been modelled. Each gearbox position is selected as a function of the current vehicle forward speed. A final drive gear (η_F) is multiplied to each gear ratio (η_i) in order to obtain the global gear ratio (G_R).

$$T_\omega = T_E \cdot G_R \tag{6.3}$$

Where T_w: torque to the wheels

T_E: Engine output torque

$G_R = \eta_i \cdot \eta_F$

As with the engine model, complex gearbox dynamics are neglected.

Differential

No differential model is used in the single-track model since rear axle has been modelled as a single wheel.

Braking System

Brake effort is applied to both axles. The braking system has been modelled as the maximum braking torque multiplied by the value of longitudinal control u_{tb}:

$$T_{brake} = T_{bMAX} \cdot u_{tb} \quad , \quad when\, u_{tb} < 0 \tag{6.4}$$

Front/rear brake distribution is modelled as a constant brake bias factor applied to the total braking torque:

$$T_{bf} = T_{brake} \cdot B_f \tag{6.5}$$

$$T_{br} = T_{brake} \cdot (1 - B_f) \tag{6.6}$$

6.2.3. Tyre Model

A semi-empirical Pacjeka tyre model has been used in this research work (Pacjeka, 2006) to describe the planar dynamics of the tyre. Combined longitudinal and lateral forces have been accounted for in the tyre model, although self-aligning moment effects have been neglected in order to keep the model as simple as possible.

The general equation for modelling the steady-state behaviour of the tyre responds to the following equation:

$$y = D\, sin[C\, \text{atan}\{Bx - E(Bx - atan(Bx)\}] \tag{6.7}$$

With $Y(X) = y(x) + S_V$

$x = X + S_H$

Where *Y:* Output force – pure longitudinal force (F_x) or pure lateral force (F_y)

X: Input variable – longitudinal slip ratio (κ) or lateral slip angle (α)

B: Stiffness factor

C: Shape factor

D: Peak value

E: Curvature factor

S_H*:* Horizontal shift

S_V*:* Vertical shift

Equation (6.7) creates a force under pure slip conditions. In order to account for combined slip situations, the tyre model is extended to the following equation:

$$F_i = G_{ij} F_{i0} + S_{Vij} \tag{6.8}$$

Where F_i: Longitudinal or lateral force in combined slip condition

G_{ij}: Weighting factor

F_{i0}: Longitudinal or lateral force in pure slip condition

S_{Vij}: Vertical shift

Figure 6-6 shows an example of the characteristic lateral force created by a tyre as a function of slip angle and slip ratio for a constant vertical load.

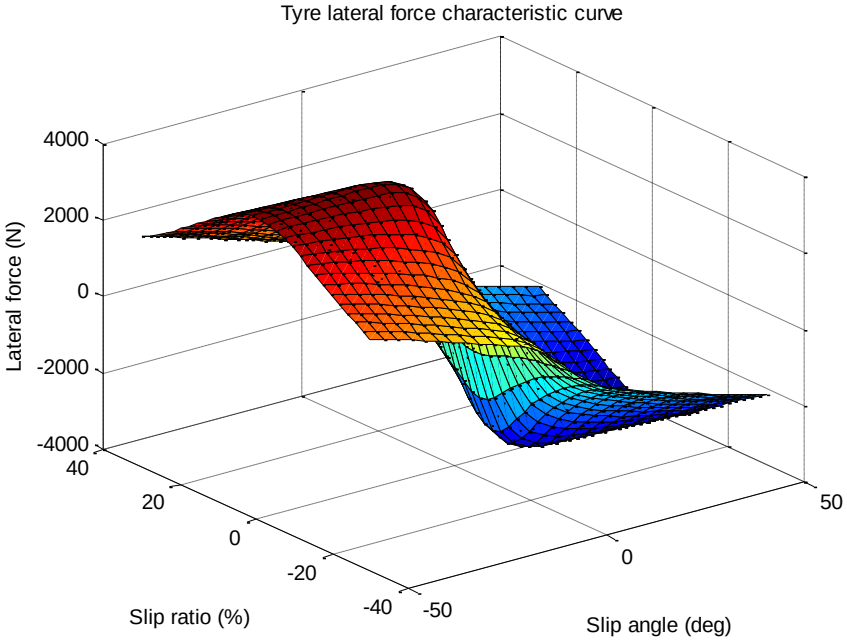

Figure 6-6: Tyre lateral force characteristic curve

The previous tyre model does not account for transient effects when variations in the input variables occur. An extension of this model is to include the concept of relaxation length (Pacjeka, 2006). In this research work, a semi nonlinear single contact point tyre model has been usd to describe the transient behaviour of the tyre in both in-plane and out-of-plane motions. Transient slip characteristics are approximated to a first-order differential equation (see Equation (6.9)). The transient slip is then fed into the steady-state Magic Formula.

$$\frac{1}{\sigma_i}\frac{dx'}{dt} + |V_x|x' = V_{si} \tag{6.9}$$

Where x': transient slip quantity

σ_i: relaxation length

V_x: vehicle forward speed

V_{si}: local wheel speed

Detailed formulation of relaxation length for in-plane and out-of-plane motions can be found in (Pacjeka, 2006). Relaxation length is dependent upon load changes. According to this equation, changes in load with induce transients in the production of lateral and longitudinal forces.

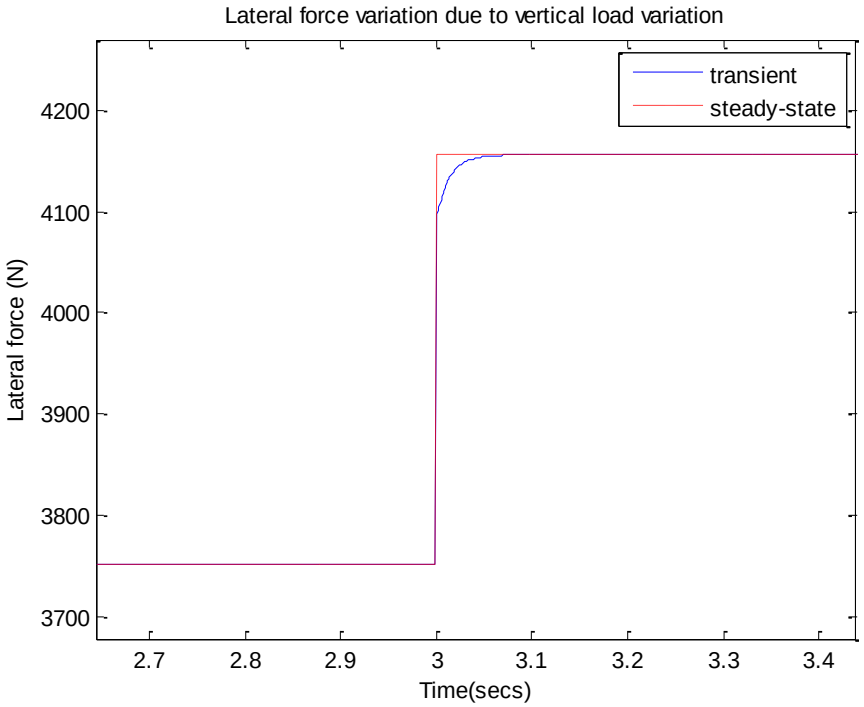

Figure 6-7: Lateral force variation due to vertical load variation: transient vs. steady-state

Figure 6-7 compares the variation of lateral force due to a step change in vertical load for the transient and the steady-state model.

Furthermore, the nonlinear vertical tyre model developed in section 5.4.2 has been incorporated to the vehicle model to account for vertical tyre dynamic effects.

6.2.4. Aerodynamic model

Aerodynamics has a major impact in the performance of modern racing cars. The two major aerodynamic actions considered in this model are the aerodynamic drag and downforce. Lateral wind gust effects, as well as aerodynamic moments exerted on the body have been neglected.

The total force exerted by the air flow into the chassis can be obtained as the integration of the local pressure *p* over the whole vehicle surface area *A*:

$$F_A = \int p\, dA \tag{6.10}$$

Obtaining the exact pressure distribution around a surface such as race car bodywork is not feasible due to the high amount of sensors that such task would require. In classical vehicle dynamics literature, a semi-empirical approximate model has been used to describe aerodynamic forces (Gillespie, 1992):

$$F_{Da} = \frac{1}{2} C_D A \rho V^2 \tag{6.11}$$

$$F_{La} = \frac{1}{2} C_L A \rho V^2 \tag{6.12}$$

Where F_{Da}: Aerodynamic drag force
F_{La}: Aerodynamic down-force
V: vehicle forward speed
A: vehicle frontal area
ρ: air density
C_D, C_L: drag and lift (or downforce) coefficients

Drag and lift coefficients must be experimentally obtained from the car through wind tunnel or track testing or can be estimated through CFD simulation. These two empirical coefficients depend on several factors such as body orientation and location with respect to ground levels, aero-elasticity, throttle position, engine mapping, etc. In addition to this, the downforce distribution between front and rear axles is a critical parameter in vehicle performance and stability, especially at high speeds.

The simplest aerodynamic model is to assume that drag and lift coefficients and aerodynamic distribution are constant regardless of any changes in the influencing factors. A more complex model considers that changes in body location and attitude with respect to ground level have an impact in the value of drag and lift coefficients and aero distribution. Thus, these magnitudes are dependent upon body ride height at the CoG and body attitude. Assuming that the chassis is a solid mass, body ride height at the CoG and body attitude can be transformed into front and rear ride heights and therefore, construct the so-called 'aero maps' with respect to these variables.

Figure 6-8 shows an example of aerodynamic drag and lift coefficients and aero distribution maps with respect to front and rear ride heights.

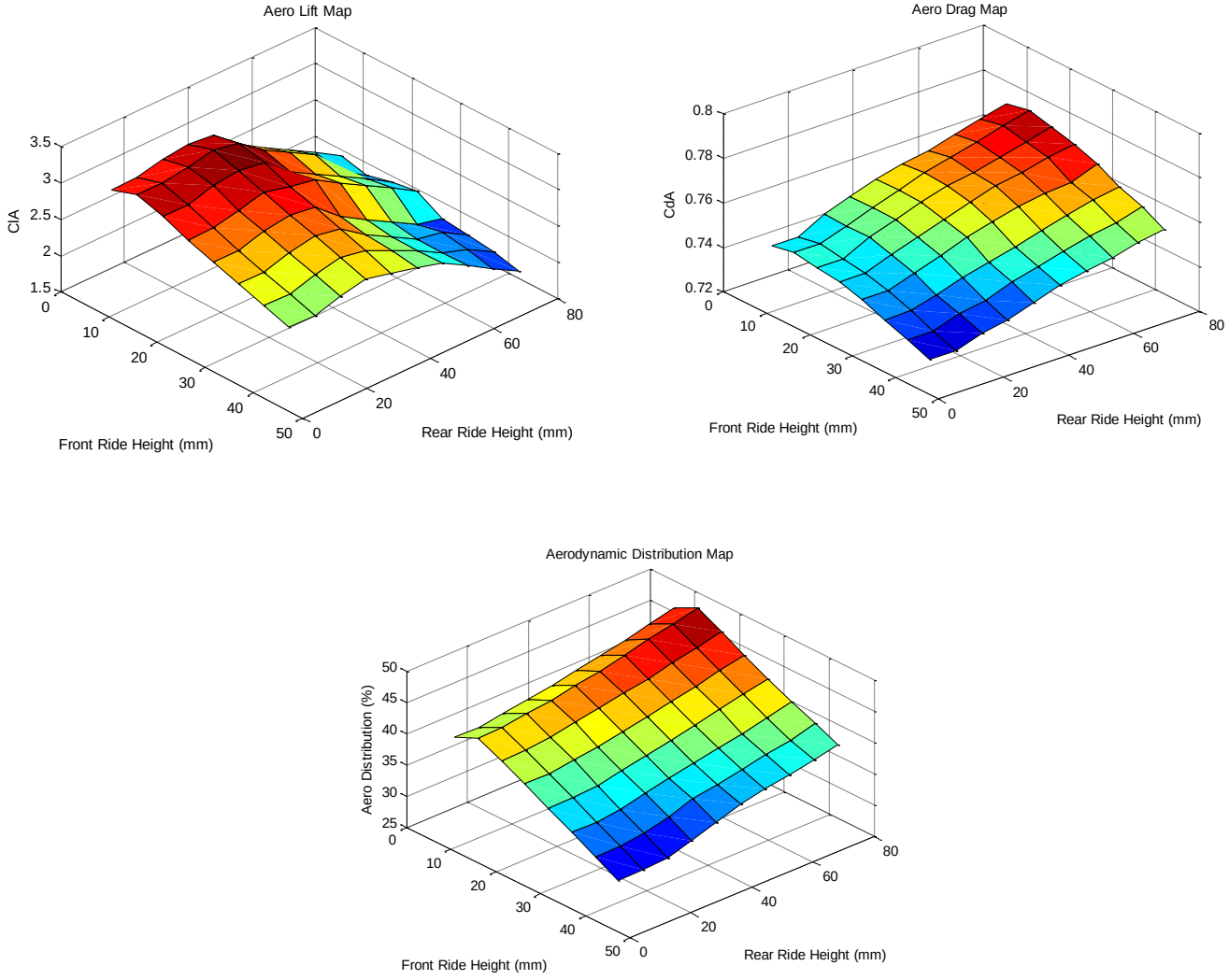

Figure 6-8: Aerodynamic maps

No transient aerodynamic effects have been accounted for in this model.

6.2.5. Suspension Model

The main aim of the lap time simulation tool is to study the effects that suspension dynamics induces in planar dynamics and to analyse the impact of inerters in the overall performance of a race car. According to this, the experimentally validated suspension model developed in Chapter 5 (see Figure 5-21) has been used in this vehicle model.

6.2.6. Track Model

Track maps are included into the vehicle model as lookup tables. Track maps contain information related to x- global coordinate x_t, y- global coordinate y_t, heading angle Ψ_t and track curvature k_t (or radius of curvature r_t) expressed as a function of the independent variable path distance s (see Figure 6-9).

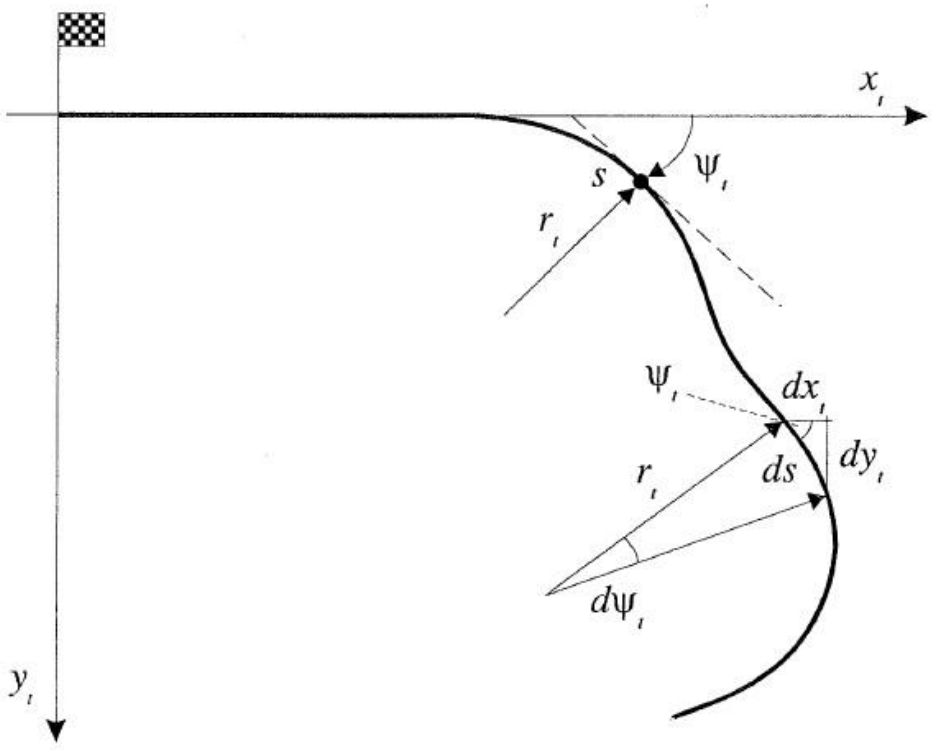

Figure 6-9: Track map definition (Casanova, 2000)

Furthermore, vertical road profiles could be added to each tyre in order to account for vertical excitation due to road unevenness. As with parameters that define the track path, the vertical road profile can be represented with respect to the travelled distance s and input as a lookup table into the overall model.

6.2.7. Driver Model

Race car drivers act as complex controllers always trying to stabilise the vehicle (plant) whilst exploring the limits of grip to obtain the fastest lap time. It is out of the scope of the present research work to investigate and produce a highly accurate driver model.

In this thesis, however, the driver is assumed to have control over throttle and brake controls as well as steering inputs. Figure 6-10 shows a diagram of driver model operation.

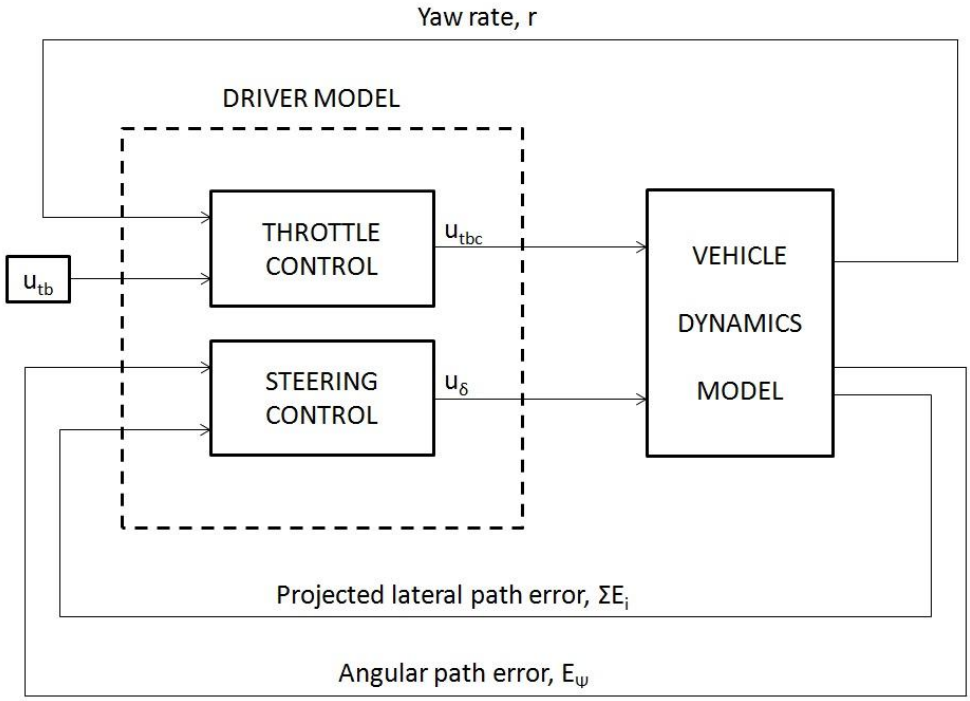

Figure 6-10: Lap-time simulator driver model

Throttle/Brake control

Although real drivers are provided with different throttle and brake controls (different pedals), the use of both controls simultaneously is rare in track-based racing series. According to this, the present model assumes that the driver can actuate either the throttle or the brake.

$$u_{tb} = \begin{cases} u_{throttle}, & 0 < u_{tb} \leq 1 \\ u_{brake}, & -1 \leq u_{tb} \leq 0 \end{cases} \tag{6.13}$$

An additional yaw rate closed-loop proportional controller has been added to throttle/brake input control. The driver then uses the actual yaw rate measurement to modulate the

throttle/brake input inputs (see Figure 6-10). The control law can be summarised in the following equation:

$$u_{tbc} = u_{tb} + K_r \cdot r \tag{6.14}$$

With $K_r = \begin{cases} K_r, & u_{tb} < 0 \\ -K_r, & u_{tb} \geq 0 \end{cases}$

r: Yaw rate

u_{tbc}: closed-loop throttle/brake control

Steering control

A nonlinear steering controller based on path preview has been used in this research work. The main scheme of the controller proceeds from the path following steer model proposed in (Casanova, 2000).

According to Casanova's work, for a particular location along the trajectory of the vehicle, an optical lever L_p can be defined as the product of a preview time T_p and vehicle forward speed V_x. (see Figure 6-11).

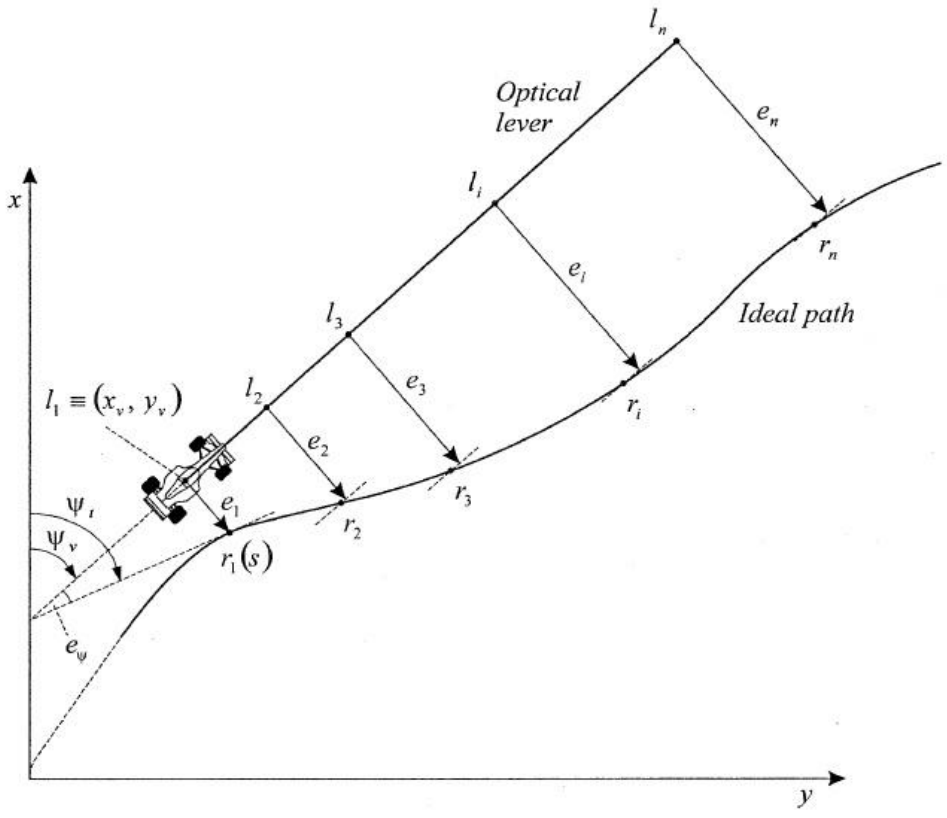

Figure 6-11: Steering driver model (Casanova, 2000)

A number of *n* preview control points l_1, l_2, ...l_n are selected along the optical lever. The first control point is located in the current location of the CoG of the vehicle. For a specified *s* location, the CoG of the vehicle will have $x_v(s)$ and $y_v(s)$ spatial coordinates and $\Psi_v(s)$ orientation.

A vector of preview distances s_P is constructed. This vector of preview distances is then used to obtain the coordinates of preview control points x_L and y_L:

$$\begin{cases} x_L = x_v(s) + s_P \cdot \cos(\Psi_v(s)) \\ y_L = y_v(s) + s_P \cdot \sin(\Psi_v(s)) \end{cases} \tag{6.15}$$

For $L = l_1, l_2, \ldots l_n$.

For each of the previous preview points, trajectory points on the ideal path r_1, r_2, ...r_n can be obtained from track map data and lateral offset errors can be calculated and fed into the steering controller. Vehicle angular orientation of the current state can be also compared against ideal path orientation and used as additional input to the controller (see Figure 6-12).

$$\begin{cases} e_i = (y_{Ri} - y_{Li}) \cdot \cos(\Psi_v) - (x_{Ri} - x_{Li}) \cdot \sin(\Psi_v) \\ e_\Psi = \Psi_v - \Psi_t \end{cases} \tag{6.16}$$

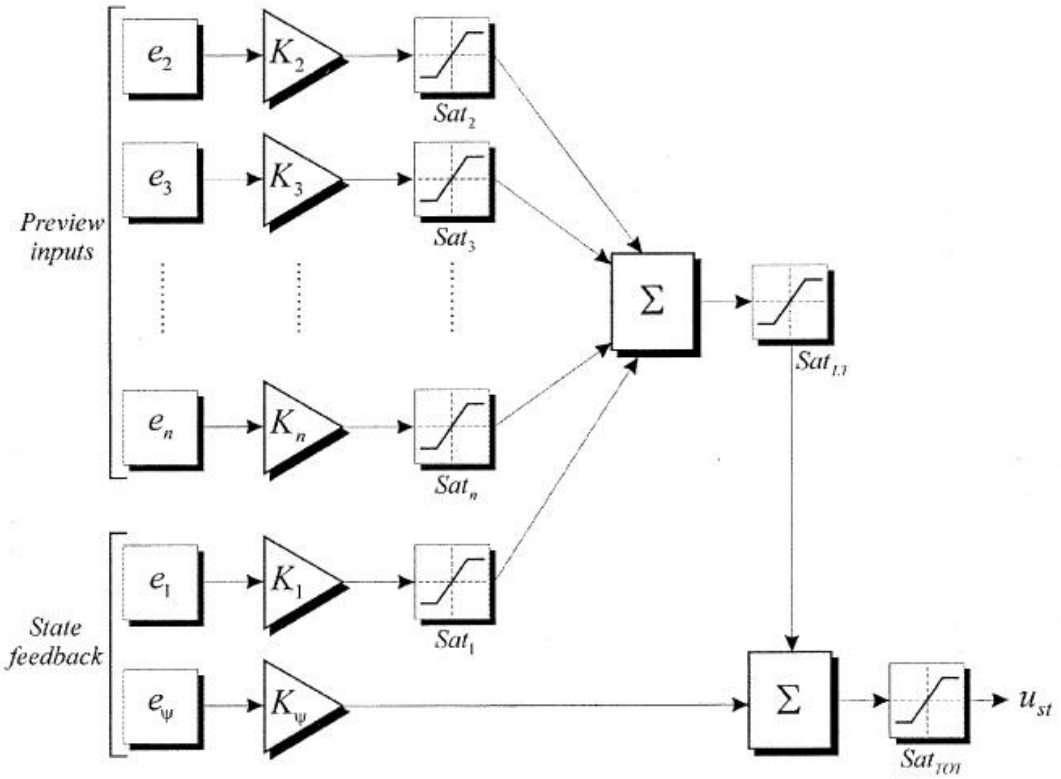

Figure 6-12: Nonlinear path preview steering control scheme (Casanova, 2000)

Finally, a set of control gains K_ψ, K_1, ..., K_n can be defined in order to construct steering controller:

$$u_\delta = K_1 \cdot e_1 + K_\Psi \cdot e_\Psi + \sum_{i=2}^{n} K_i \cdot e_i \tag{6.17}$$

In addition to this, saturation limits are set to the individual controllers to prevent the tyres from exceeding the limits of saturation and inducing under/oversteering moments.

6.3. Minimum Time Manoeuvre - Problem Statement

The problem of finding the minimum time manoeuvring (MTM) can be expressed as one of Optimal Control (OC) theory (Casanova, 2000). In general OC theory, the OC problem can be defined as determining a control u^* that minimises a performance index J (Kirk, 2004) subjected to a set of dynamic and boundary (equalities or/and inequalities) constraints. Mathematically this can be expressed as:

$$\begin{aligned}
&\min_{u} && J = h\big(x(t_f), t_f\big) + \int_{t_0}^{t_f} g(x(t), u(t), t)dt \\
&subject\ to && \dot{x}(t) = f(x(t), u(t), t) \quad with \quad x(t_o) = x_0 \\
& && C_{in}(x(t), u(t), t) \leq 0 \\
& && C_{eq}(x(t), u(t), t) = 0 \\
& && u_{min} \leq u(t) \leq u_{max}
\end{aligned} \tag{6.18}$$

$for\ all\ t \in [t_0, t_f]$

In the case of transient lap-time simulation virtual tools, the OC problem can be stated as finding a set of longitudinal and steering controls that minimises the time taken for a race car to complete a lap around a race track. In this problem, the EOMs describing the behaviour of the vehicle represent the set of dynamic constraints and the limits of the race track are considered as boundary constraints.

In the following subsections, a detailed solution approach to the problem stated in equation (6.18) will be presented.

6.3.1. Independent variable transformation

Equation (6.1) presented the general mathematical form of a dynamic system with respect to independent variable time *t*. However, in lap-time optimisation problem t_f is not constant. For this reason, it is convenient to consider the travelled space *s* on the centreline of the race track as the independent variable and therefore express the dynamic system in terms of space instead of time. A conversion factor $F_{t\text{-}s}$ is then required to transfom the system from time domain into space domain:

$$F_{t-s} = \frac{dt}{ds} \tag{6.19}$$

Applying the rule of chain into the left-hand side of equation (6.1) and introducing expression (6.19),

$$\dot{\boldsymbol{x}}(t) = \frac{d\boldsymbol{x}}{dt} = \frac{d\boldsymbol{x}}{ds} \cdot \frac{ds}{dt} = \frac{d\boldsymbol{x}}{ds} \cdot \frac{1}{F_{t-s}} \tag{6.20}$$

The transformation from time to space domain can be obtained by equating (6.20) to the right-hand side of the dynamic system expressed in (6.1):

$$\frac{d\boldsymbol{x}}{ds} = F_{t-s} \cdot f(\boldsymbol{x}(s), \boldsymbol{u}(s), s) \quad , \quad \boldsymbol{x}(s=0) = \boldsymbol{x_0} \tag{6.21}$$

The expression for the conversion factor of a vehicle constrained to travel along the centreline can be obtained as:

$$F_{t-s} = \frac{1}{\sqrt{{V_x}^2 + {V_y}^2}} \tag{6.22}$$

However, since the vehicle is allowed to take different trajectories within the limits of the race track, the conversion factor must also take into account the relative position and orientation of the vehicle with respect to the centreline. Detailed derivation of this expression can be followed in (Casanova, 2000). The final expression of conversion factor is as follows:

$$F_{t-s} = \frac{1 - d \cdot k_t}{V_x \cdot \cos(\Psi_v - \Psi_t) - V_y \cdot \sin(\Psi_v - \Psi_t)} \tag{6.23}$$

Where *d*: distance from vehicle CoG to track centreline expressed as:

$$d = (y_v - y_t) \cdot \cos \Psi_t - (x_v - x_t) \cdot \sin \Psi_t \qquad (6.24)$$

6.3.2. Definition of the minimum lap-time cost function

As stated in previous sections, the overall aim of a lap-time simulation tool is to find a set of control inputs so that the time taken for the race car to complete a lap around a circuit is minimal. According to this goal, a mathematical cost function *J* that expresses time taken to a car to complete a lap around a circuit must be obtained. From equation (6.19), time differential *dt* can be calculated from independent space differential *ds*:

$$dt = F_{t-s} \cdot ds \qquad (6.25)$$

In computational methods, differential equations are equivalent to incremental expressions, and therefore equation (6.25) can be re-written as:

$$\Delta t = F_{t-s} \cdot \Delta s \quad , for\ s = [s_1, \dots, s_i, \dots\ s_n] \qquad (6.26)$$

A time vector can be obtained for the cumulative sum of time increments Δt as:

$$t = \sum_{i=1}^{n} \Delta t \qquad (6.27)$$

Finally, the cost function *J* can be expressed as the last value of time vector obtained from equation (6.27):

$$J_t = t_n \qquad (6.28)$$

6.4. Multilevel optimisation algorithm - Solution Method

A method must be developed in order to solve the MTM problem characterised in section 6.3. Several approaches have been reviewed in Chapter 2. In previous work, driver longitudinal and steering input controls have been assumed to be independent between each other and the problem of obtaining the optimal racing line came implicitly solved when attempting to minimise lap time (Casanova, 2000; Kelly, 2008). According to these approaches, the general OC problem formulated in section 6.3 is transformed into a constrained non-linear programming (NLP) problem in which the search space is composed by a set of discretised

longitudinal and steering input controls subjected to the dynamics of the vehicle model and constrained by the limits of the race track.

A number of issues must be addressed when developing a solution approach to the OTM problem, the first of these being that the solution method must be robust. On the limit of adhesion, the use of completely decoupled control inputs causes vehicle instabilities (vehicle going off the line or vehicle spinning off). Real drivers use a combination of throttle/brake and steering controls in order to simultaneously maintain vehicle stability and negotiate the race track as fast as possible. In order to overcome robustness issues, Casanova (2000) proposed a multiple shooting algorithm in which the race track is split into sections short enough in order to prevent the vehicle from becoming unstable. This method introduces additional continuity constraints to the problem. Kelly (2008) defined stability constraints and used a Model Predictive Control (MPC) algorithm to provide the driver model with a preview horizon. Secondly, computational efficiency issues must also be addressed. When transcribing the OC problem to a Nonlinear Programming (NLP) problem, NLP solvers augment the performance index or cost function with search space variables and constraints, therefore increasing the complexity and number of DOFs of the augmented cost function. Both previous solution approaches required the use of independent longitudinal and steering control inputs as search space variables. Furthermore, in order to increase the robustness of the algorithm, both methods required the introduction of additional constraints in order to limit the development of dynamic instabilities.

Following the research work carried out in the field, a direct method has been used to transcribe the OC problem into a NLP problem. Once the problem has been transcribed into a NLP problem, a nonlinear constrained optimisation solver is then used to obtain the solution of the NLP problem. In this thesis, a Sequential Quadratic Programming (SQP) algorithm built in MATLAB® function *fmincon* has been used as NLP solver (The MathWorks Inc., 2010).

In the present work, a novel multilevel optimisation algorithm (MLOA) has been proposed with the aim to increase the robustness and efficiency of the solution method. MLOA proposes an alternative transcription method from OC problem to NLP program. MLOA uses a closed-loop driver steering control model to tackle the racing line optimisation problem and a coupled longitudinal control model to minimise the lap-time.

MLOA can be split into two solution levels:

- Trajectory Planning
- Lap Time Minimisation

The following sections detail the transcription procedure from the initial OC problem to the NLP problem.

6.4.1. MLOA level 1: Trajectory Planning

The time taken to complete a lap depends on the distance travelled and the speed carried by the race car. According to this principle, the driver will be able to reduce lap time whenever it reduces the travelled distance within the confines of the race track and/or it increases its forward speed. Under this premise, the optimal racing line is considered to lie within the shortest possible path (SP) and a line that produces the highest possible speed, i.e. the minimum curvature path (MCP). Hence, although the actual optimal racing line depends on the complex dynamic behaviour of the race car, the problem of trajectory planning will be bounded optimisation problem between SP and MCP lines.

Finding the SP and MCP racing lines can be considered as a pure geometric constrained optimisation problem since the solutions must always lie inside the limits of the circuit. In both cases, the optimisation problem is transcribed into a NLP problem. In order to carry out this transcription, the track is discretised into a finite number of segments. Each of the discrete trajectory point can be characterised by the spatial coordinates of the lower and upper bounds of track, as shown in Figure 6-13:

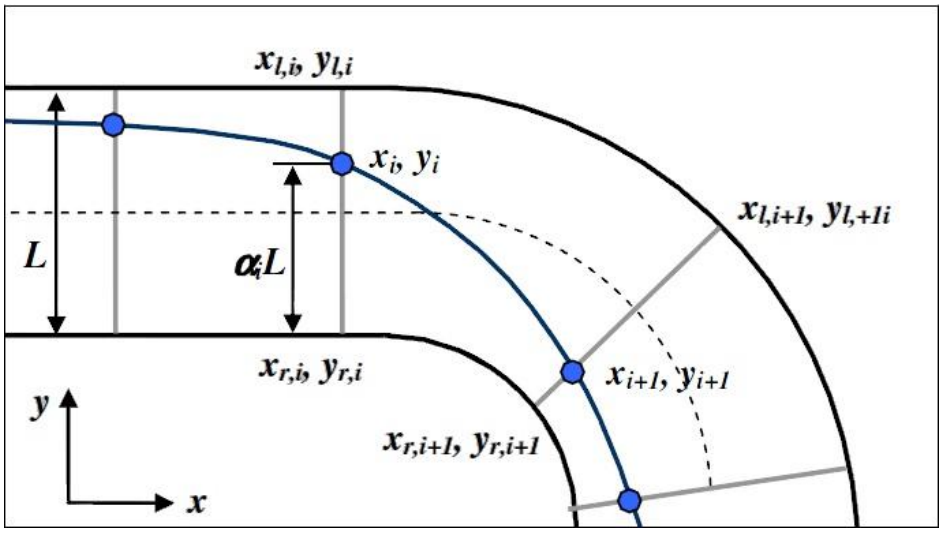

Figure 6-13: Race track discretisation (Braghin, et al., 2008)

Assume P_i represents the position vector of the i point in the trajectory:

$$\boldsymbol{P}_i = x_i\vec{\imath} + y_i\vec{\jmath} = [x_{LBi} + \alpha_i \cdot (x_{UBi} - x_{LBi})]\vec{\imath} + [y_{LBi} + \alpha_i \cdot (y_{UBi} - y_{LBi})]\vec{\jmath} \quad (6.29)$$

Where α_i is a normalised parameter that ranges from [0,1] and determines the position of P_i along the track width. Any trajectory will be described by a vector $\boldsymbol{\alpha} = [\alpha_1, \dots, \alpha_n]$, where n represents the number of discretised points. Thus, the problem of finding a desired trajectory can be translated into a problem of identifying all the parameters contained in the $\boldsymbol{\alpha}$ vector that minimises certain cost function (shortest path or minimum curvature path):

$$\begin{aligned} &\min_{\boldsymbol{\alpha}} && J \\ &subject\ to && 0 \leq \alpha_i \leq 1 \\ &for\ \boldsymbol{\alpha} = [\alpha_1, \dots, \alpha_n] \end{aligned} \quad (6.30)$$

The NLP problem stated in equation (6.30) will be solved by a Sequential Quadratic Programming (SQP) algorithm implement within the MATLAB® function *fmincon.*

Shortest Path (SP) Trajectory Optimisation

In order to obtain the SP trajectory, the cost function must account for total length of the path travelled. The travelled distance can be calculated according to the following expression:

$$d_i = \sqrt{x_i^2 + y_i^2} + d_{i-1} \quad (6.31)$$

$for\ i = [1, n]$

Where d represents the cumulative travelled length.

Hence, SP cost function can be obtained as:

$$J_{SP} = d_n \quad (6.32)$$

When closed tracks are being considered, an additional continuity constraint must be added to the problem:

$$\alpha_1 - \alpha_n = 0 \quad (6.33)$$

The *fmincon* optimisation algorithm can be therefore applied to obtain the Shortest Path racing line. Figure 6-14 shows an example of shortest path trajectory optimisation around a race track.

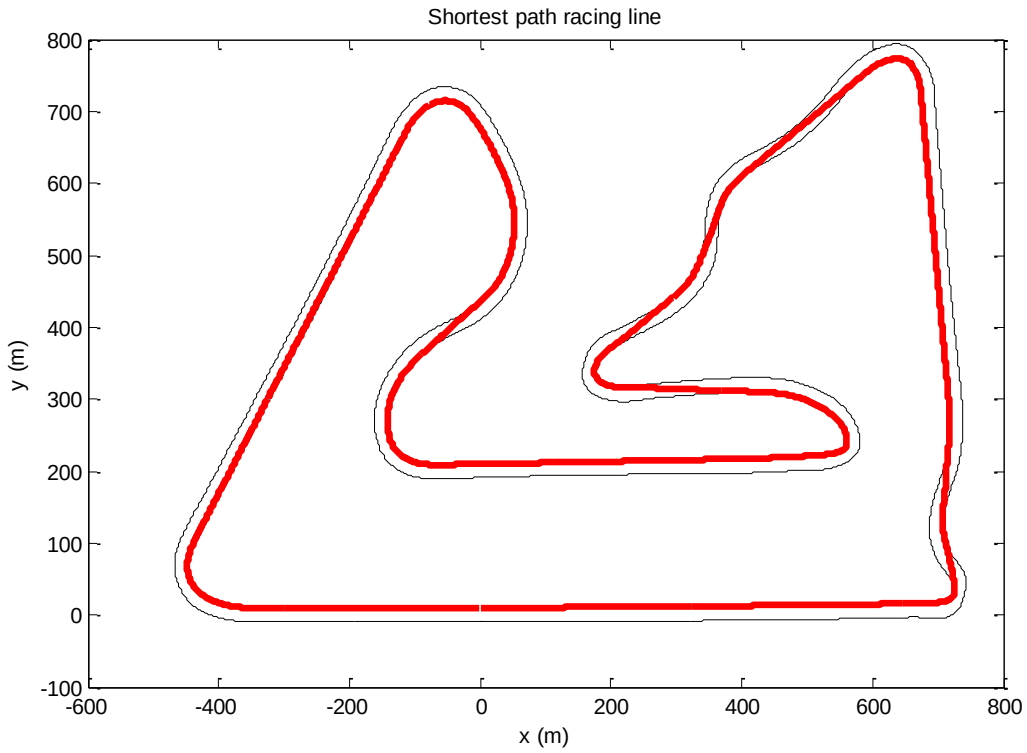

Figure 6-14: Shortest Path racing trajectory

As it can be noticed in the previous figure, the vehicle moves along the inside line in order to minimise the travelled distance. This leads to a racing line where corner radii become small (high path curvature). Thus, in order to be able to stay in this racing line, the vehicle should decrease dramatically its speed.

Minimum Curvature Path (MCP) Trajectory Optimisation

By minimising the curvature of the racing line, the corner radius can be maximised and therefore, for a given maximum lateral acceleration, the corner speed can be optimised. As in the SP trajectory optimisation case, a cost function that expresses the curvature of a trajectory must be developed.

The curvature of a path can be defined as the rate of change in track angle with respect to the rate of change is travelled distance:

$$k_i = \frac{d\Psi}{ds} \approx \frac{\Delta\Psi_i}{\Delta s_i} \tag{6.34}$$

Where: $\Delta s_i = \sqrt{\Delta x_i^2 + \Delta y_i^2}$

$\Delta\Psi_i = \tan^{-1}\frac{\Delta y_i}{\Delta x_i}$

$\Delta x_i = x_i - x_{i-1}$

$\Delta y_i = y_i - y_{i-1}$

Hence, the MCP cost function can be defined as:

$$J_{MCP} = \sqrt{\sum_{i=1}^{n} {k_i}^2} \tag{6.35}$$

MATLAB® *fmincon* optimisation solver is used to obtain the minimum curvature path. Figure 6-15 shows an example of the MCP line. Unlike with SP trajectory, the vehicle uses a larger portion of the available race track to minimise the curvature.

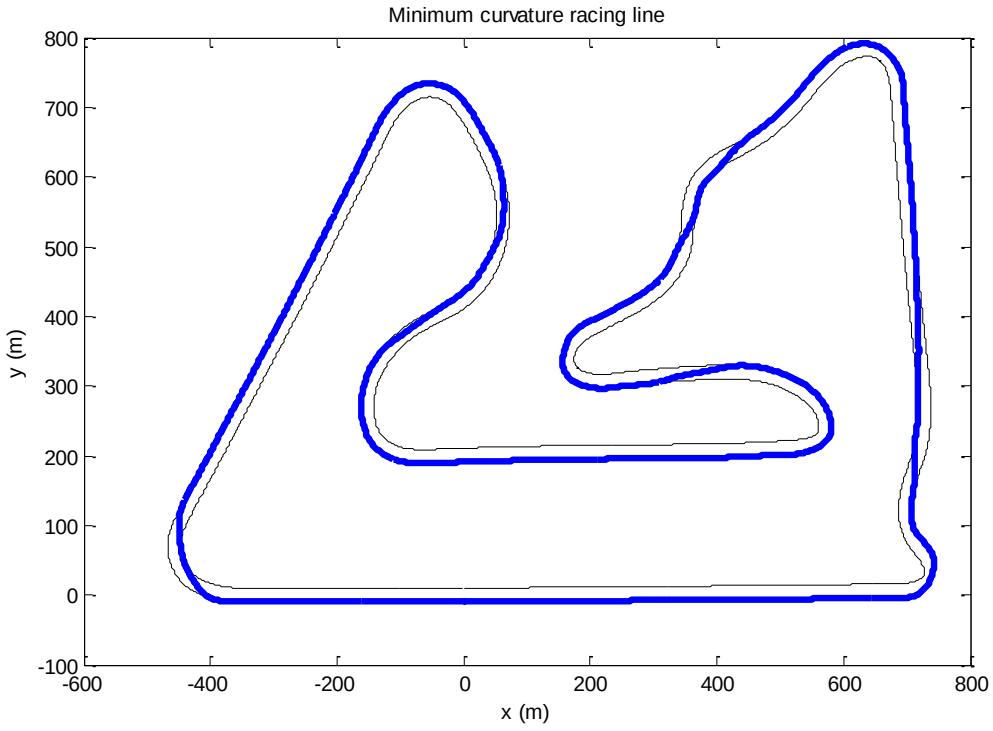

Figure 6-15: Minimum Curvature racing trajectory

6.4.2. MLOA level 2: Lap Time Minimisation

The minimum time manoeuvring problem can be considered as a dynamic problem since the optimal solution is strongly influenced by the dynamic behaviour of the race car. In this second optimisation stage, the optimal racing line can be assumed to be a linear combination between the SP and the MCP trajectories (Braghin, et al., 2008). Mathematically, this can be expressed as follows:

$$OT = \varepsilon \cdot SP + (1 - \varepsilon) \cdot MCP \tag{6.36}$$

Where *OT*: Optimal Trajectory

ε: normalised weighting factor

In a general MTM problem where the longitudinal and steering input controls have been discretised at p and n points respectively, the search space presents $p+n$ degrees of freedom, due to the fact that open-loop driver control inputs has been used. However, if a closed-loop steering control is used, a vehicle should be able to follow a prescribed trajectory with no need to explicitly specify a set of open-loop steering controls.

According to this, the multilevel optimisation algorithm (MLOA) developed in this research work proposes that, with the aid of the steering driver control presented in section 6.2, the n steering control input points can be substituted by the weighting factor ε. Hence, the problem size can be drastically reduced and therefore, the efficiency of the algorithm can be increased. Furthermore, since the vehicle is now constrained to follow a trajectory that is bounded between the shortest path and the minimum curvature trajectories, no boundary constrain are required to define the OC problem. Thus, MLOA transforms the constrained OC problem with $p+n$ DOFs into an unconstrained OC problem with $p+1$ DOFs.

Moreover, since the throttle/brake input control is coupled with a yaw rate controller, the driver can self-modulate the amount of throttle/brake applied under high lateral acceleration conditions, therefore increasing the stability of the vehicle and making the algorithm more robust.

6.4.3. Discretisation Scheme

The transcription of the OC problem into a NLP problem requires the parametrisation of the control variables. The discretisation process involves defining a set of finite number of

control points, which will then be used by the NLP solver as input variables to obtain an optimised solution. According to the MLOA presented in previous sections, only longitudinal control inputs u_{tb} and racing line weighting factor ε are required to define the OC problem, since lateral controls are determined by the closed-loop driver controller.

Throttle/Brake control input u_{tb}

First, the longitudinal control history is discretised into p control points, so that:

$$u_{tb} \quad \rightarrow \quad [u_{tb1}, u_{tb2}, \dots, u_{tbi}, \dots, u_{tbp}] \tag{6.37}$$

The number of discretised control inputs p defines the size of the optimisation problem. Hence, in order to reduce the problem size, a variable discretisation scheme can be selected. According to this, the density of the grid could be increased in areas of the track where the rate of control change is expected to be higher, e. g. braking points or throttle/brake modulation areas. In areas where controls are expected to remain constant, density could be therefore reduced. An example of a variable control input discretisation scheme is shown in Figure 6-16.

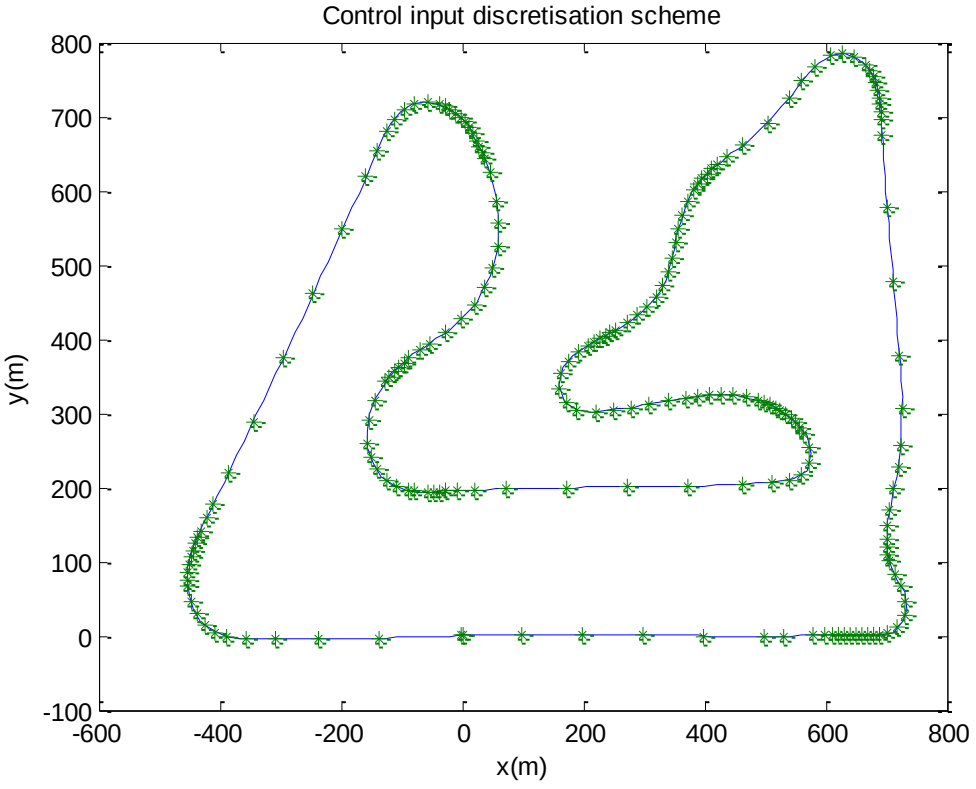

Figure 6-16: Variable control input discretisation scheme

Racing line weighting factor ε

Although the optimal racing line will lie between shortest path and minimum curvature trajectories, actual race tracks are composed by sections of different nature such as long high-speed corners, low-speed hairpins, chicanes, etc. Due to this variable track composition, there may be areas on track where taking the SP line is more beneficial than trying to maximise corner speed and vice versa. In order to allow the algorithm to account for this situation, the optimal trajectory (OT) can be split into sections, so that

$$OT = [OT_1, OT_2, \dots, OT_m]$$

$$\begin{cases} OT_1 = \varepsilon_1 \cdot SP_1 + (1 - \varepsilon_1) \cdot MCP_1 \\ \vdots \\ OT_m = \varepsilon_m \cdot SP_m + (1 - \varepsilon_m) \cdot MCP_m \end{cases} \tag{6.38}$$

$$\boldsymbol{\varepsilon} = [\varepsilon_1, \varepsilon_2, \dots, \varepsilon_m]$$

Where *m* represents the number of sections in which the race track has been split.

By doing so, the problem size will increase from *p+1* to *p+m* dimensions. Note that, a higher degree of flexibility is now introduced to optimisation problem, which would allow the solver to find more optimal trajectories. However, the efficiency decreases with the number of sections *m* in which the race track is split.

An efficient way to split the race circuit into sections is to find *k* crossing points between SP and MCP trajectories (see Figure 6-17). These crossing points represent invariant points by which the vehicle must drive through if optimal time is to be achieved. In between these crossing points, *m=k+1* sections can be created, so that the solver has the freedom to choose the optimal racing line according to the characteristics of the race track for that particular section.

Additional sections could be added as control input in the search space *y* in case particular areas of a race track were required to be studied in more detail. For instance, in a tight chicane where the race car hits the kerbs, the user might be interested in analysing if the car would go faster by running over the kerbs and losing contact with ground or by taking a more twisted racing line and avoiding losing contact. In this case, extra sections will allow local analysis in this particular section.

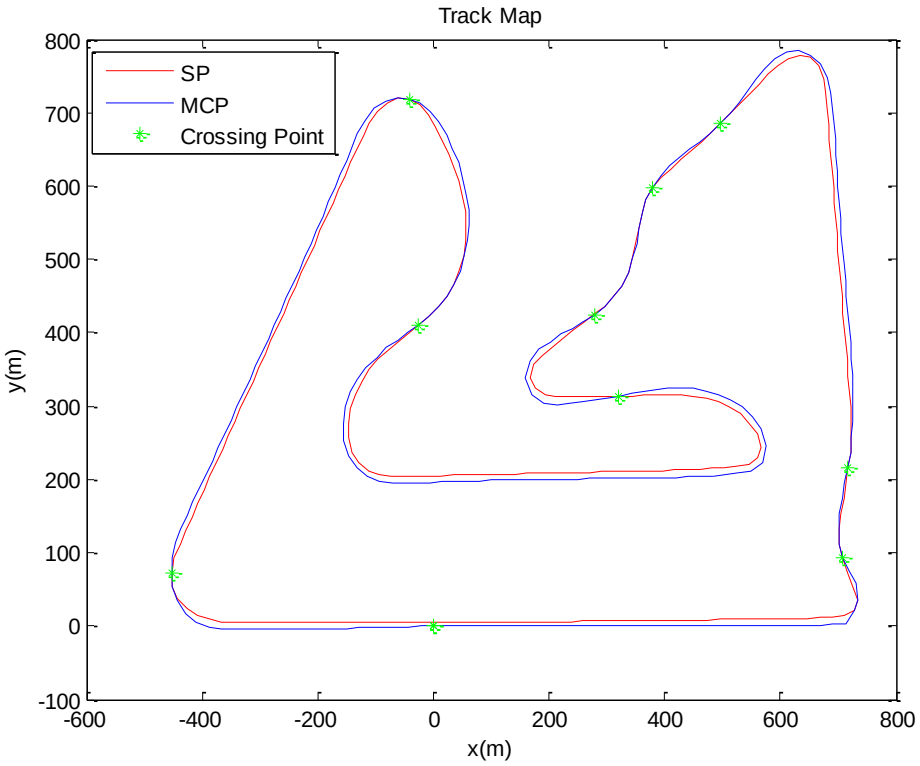

Figure 6-17: Race track - crossing point sections

6.4.4. Initial Guess Algorithm

As stated in previous sections, finding the optimal time represent solving a NLP problem subjected to a highly nonlinear dynamic model. Moreover, a large number of input variables define the search space (in general $p+m$ DOFs). Under these conditions, the cost function is likely to be non-uniform and, instead, present several local minima within the search region. As reviewed in Chapter 2, gradient-based local optimisation solvers (such as the SQP) are very powerful tools in finding local optima from an initial guess. However, these solvers do not ensure that the local optimum will correspond to the actual global optimum, unless the initial guess is located within the basin where the global optimum lies.

An initial guess algorithm is proposed in this research work. The algorithm allows the user to obtain a set of initial control inputs u_{tb0} from track map data. The algorithm works as follows: firstly, the track map is discretised into p points, where p corresponds with the number of throttle inputs. Since track map data is available, the curvature of track k_{ti} can be obtained from equation (6.34) for each point. The inverse of the curvature represent the track corner radii R_{ti}. Assuming constant lateral acceleration a_y, an initial velocity profile for a particular track can be obtained as:

$$V_{xRefi} = \sqrt{a_y \cdot R_{ti}} \quad , \quad for\ i = [1, p] \tag{6.39}$$

Note that, in straight lines, $R_{ti} \to \infty$ and therefore, $V_{xRefi} \to \infty$ as well. In order to prevent this situation a limit forward velocity can be defined so that $V_{xRefi} \leq V_{x0max}$. Figure 6-18 shows an example of the estimated vehicle speed profile for the Bahrain International GP circuit.

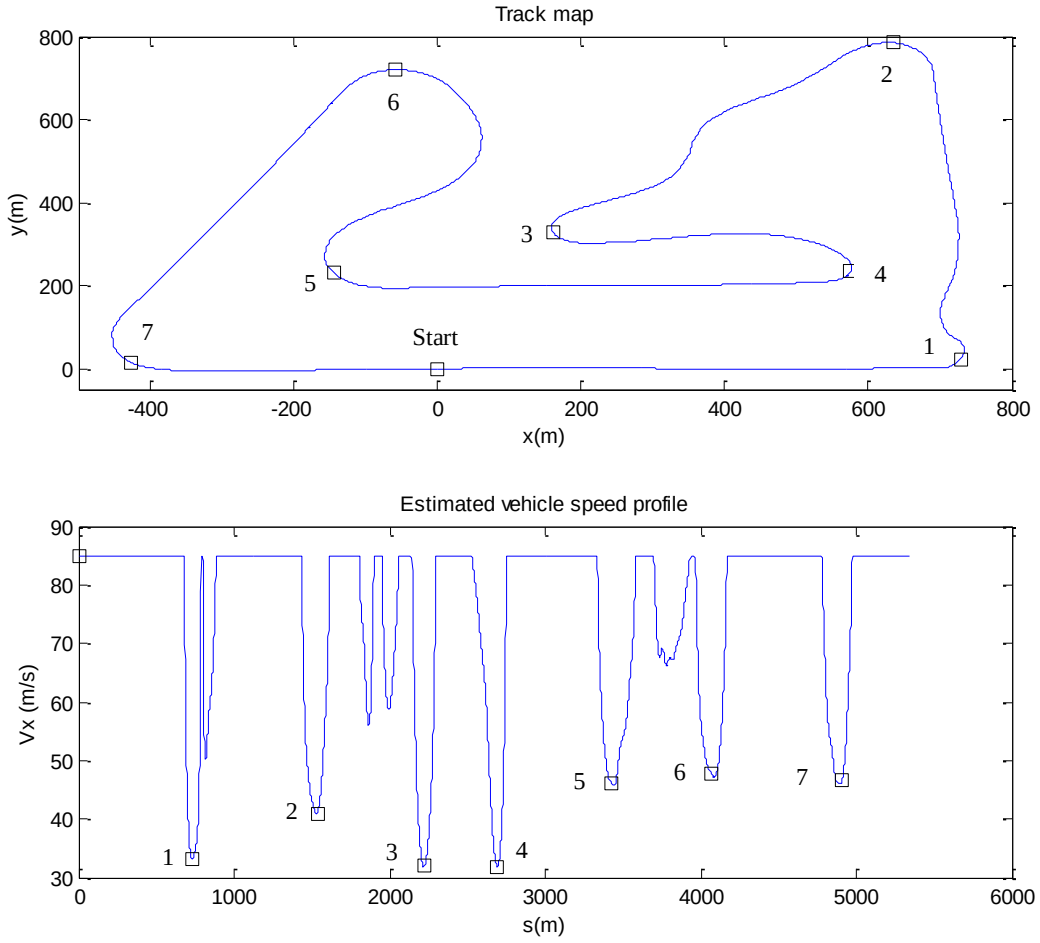

Figure 6-18: Initial vehicle speed profile estimation

A simple closed-loop PID controller has been enabled into the vehicle model so that the estimated vehicle speed profile can be used to obtain the set of initial control inputs u_{tb0} according to the diagram depicted in Figure 6-19. Results of the simulation are shown in Figure 6-20 to Figure 6-22.

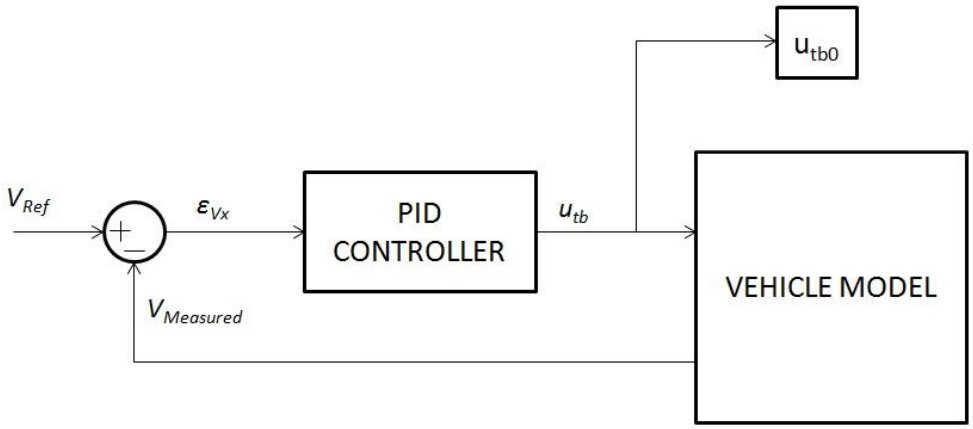

Figure 6-19: Initial control input guess diagram

Figure 6-20 shows a set of initial throttle/brake control inputs u_{tb0}. As it can be observed from this graph, the driver spends most of the time on throttle in an attempt to maximise forward speed. Brake is applied in small portions of time in order to accommodate the speed of the vehicle to handle the corners.

Figure 6-21 shows a comparison between the estimated velocity profile and the real one obtained through simulation. As it can be noticed, although the vehicle is able to match the estimated speed profile at low speeds, due to dynamic limitations of the race car, real forward velocity will never reach maximum estimated speed. A similar situation can be noticed in Figure 6-22. At some points in the circuit, the car is running off the line, particularly in turns 1, 7 and 8. This is due to fact that the estimated forward speed profile has been calculated assuming that, when the car is cornering, all force available from the tyre is used to generate lateral acceleration. However, in the case of the dynamic simulation, the tyre is producing lateral as well as longitudinal forces. This reduces the capability of the tyres to produce enough lateral acceleration so that the vehicle can track the racing line.

This set of control inputs produces a trajectory that violates the limits of the race track. Since the set of control inputs obtained following this algorithm is then used as initial guess of the NLP problem, little attention must be paid to the produced trajectory. However, in order to ensure that the NLP solver does not produce an optimised trajectory that potentially could violate the limits of the race track; the performance cost function of equation (6.28) will incorporate a term that accounts for the deviation of the vehicle from the optimal racing line.

According to this, and considering that the deviation of the vehicle from a prescribed trajectory can be calculated from equation (6.24), a cost function that minimises this deviation across the race track can be defined as:

$$J_{trajectory} = \sqrt{\sum_{i=1}^{n_{Sim}} d_i} \tag{6.40}$$

The final MTM cost function can be therefore formed as a linear combination of the time and spatial deviation performance functions:

$$J = q_1 \cdot J_1 + q_2 \cdot J_2 \tag{6.41}$$

Where J_1: Time cost function (equation (6.28))

J_2: Spatial deviation cost function (equation (6.40))

q_1, q_2: scaling factors used to balance the different nature of the cost functions.

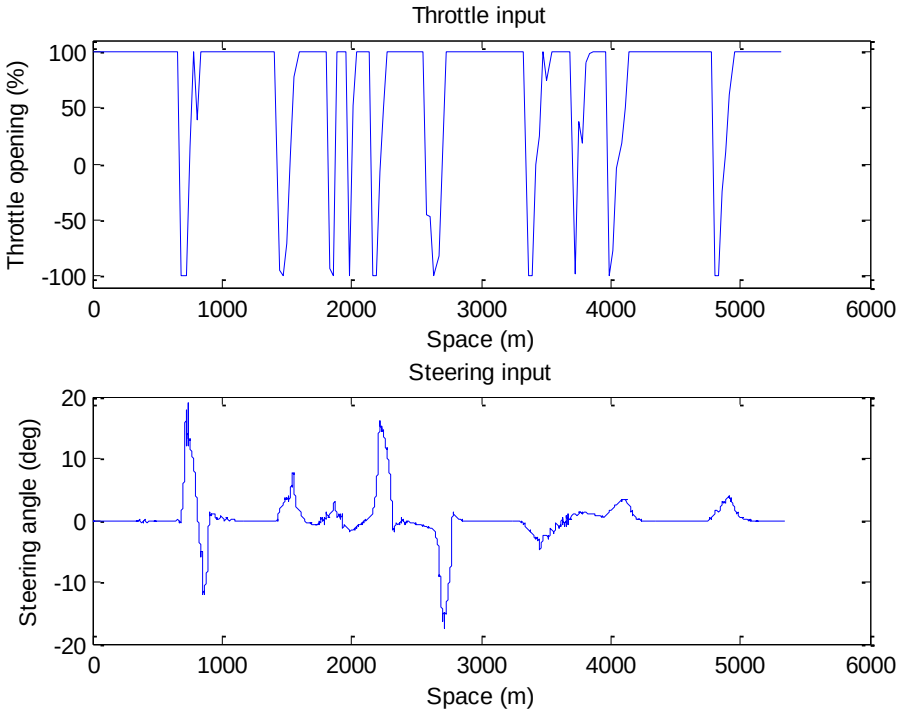

Figure 6-20: Estimated control input initial guess

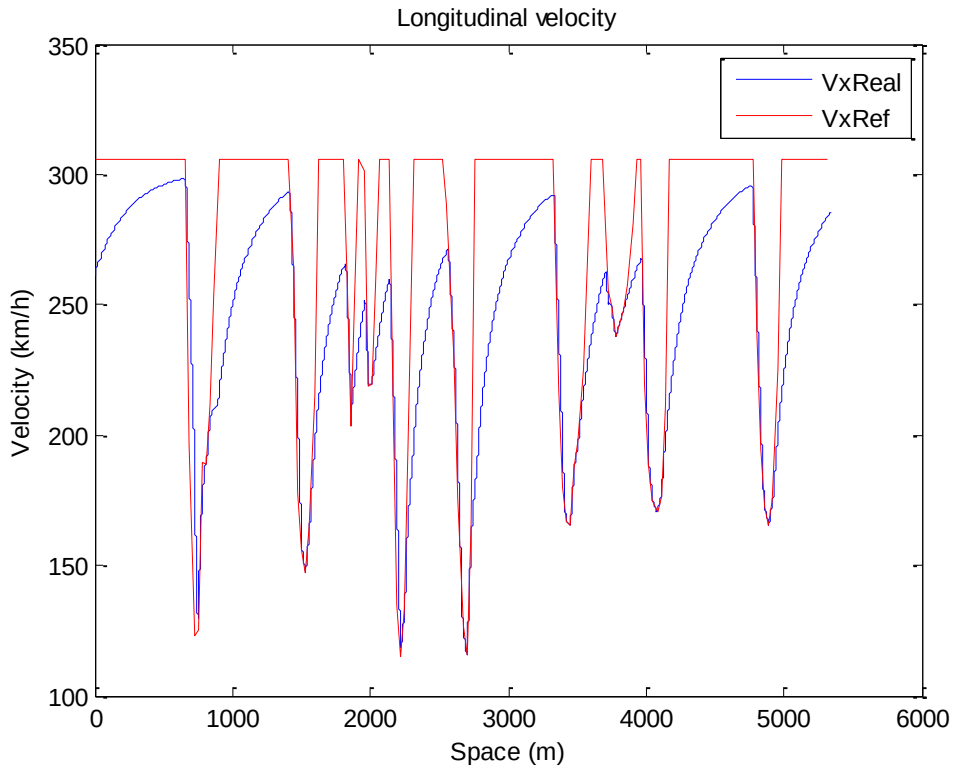

Figure 6-21: Estimated vs. Real vehicle speed profile

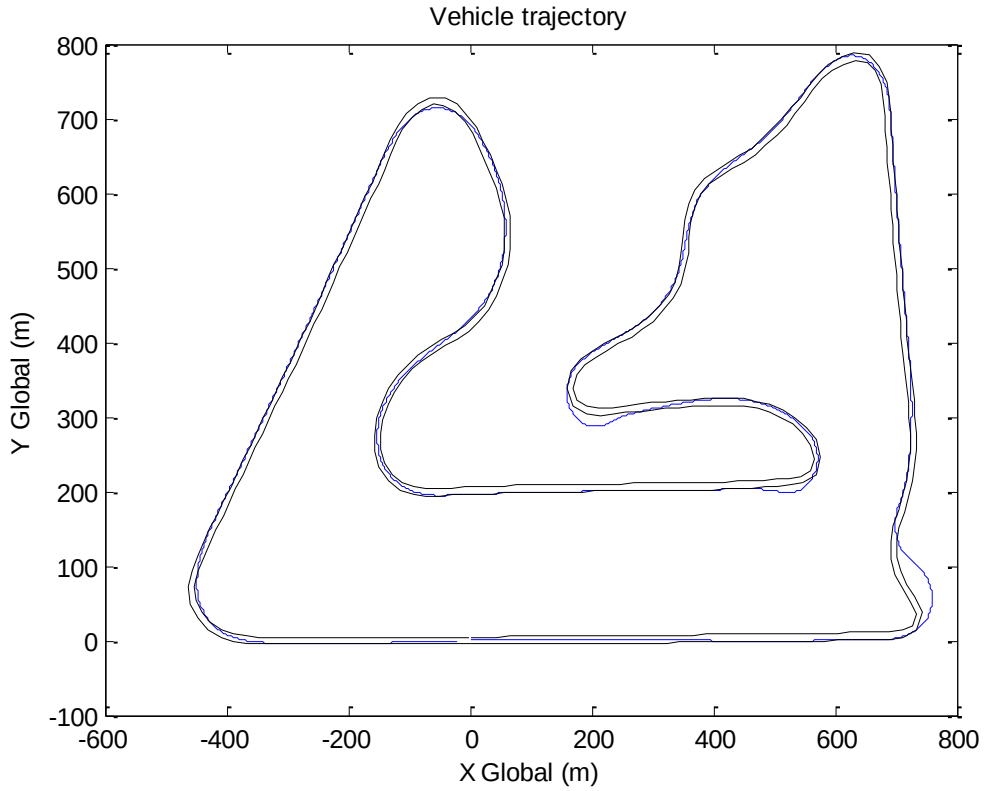

Figure 6-22: Estimated initial guess trajectory

Hence, the MTM problem can be summarised in NLP problem as follows:

$$\begin{aligned} &\min_{\mathbf{y}} && J(\boldsymbol{y}) \\ &subject\ to && \frac{dx}{ds} = \frac{1}{F_{t-s}} \cdot f(x(s), \boldsymbol{y}) \\ &\boldsymbol{y}_{min} \leq \boldsymbol{y} \leq \boldsymbol{y}_{max} \\ &\boldsymbol{y} = [u_{tb1}, \dots, u_{tbp}, \varepsilon_1, \dots, \varepsilon_m] \end{aligned} \tag{6.42}$$

As explained at the beginning of the section, the NLP problem can be solved with a SQP algorithm built in *fmincon* MATLAB® function. The following section presents practical case study of the lap time simulation tool developed.

6.5. Case Study

In this section, the lap time simulation virtual tool developed in previous sections is used in a practical case study. The vehicle model developed in section 6.2 has been driven along a Bahrain GP Circuit as fast as possible. First, the parameters required to set up the optimisation problem are discussed. Secondly, optimal solutions from the optimisation solver are analysed.

6.5.1. Optimal Time Manoeuvring problem set-up

NLP solvers, such as the SQP used in this thesis, require a number of optimisation parameters to be defined. The selection of these parameters will have an important impact in the performance of the algorithm. The optimisation parameters required to the set-up the optimisation are:

- Number of throttle/brake input control discretisation points.
- Number of race track sections.
- Dynamic model integration solver and step size.
- Stopping criteria.

As explained in section 6.4.3, the number of controls inputs defines the size of the optimisation. On one end, a fine control input grid will increase the accuracy of the optimal solution but the efficiency of the solver will decrease, since the number of function evaluations per optimisation iteration increases linearly with the problem size. On the other end, a burden input control grid will increase efficiency of the solver but it could lead to

vehicle stability issues, since input control changes would not react fast enough to the requirements of the model. Variable-spaced input controls are used as a compromised solution between both previous cases. In this example, controls are placed at a relative distance in the range from 8 to 80 m as shown in Figure 6-16. According to this discretisation grid, the total number of control inputs for the Bahrain GP Circuit is 193.

The total dimension of the optimisation problem also is affected by the number of sections in which the race track is divided. According to the crossing point section algorithm introduced in section 6.4.3, the race track has been split into 7 sections leading to 7 racing line weighting factors. Figure 6-23 shows the sections into which the race track has been divided for this particular example. By adding the weighting factors to the control input grid, the total number of independent optimisation variables is therefore 200.

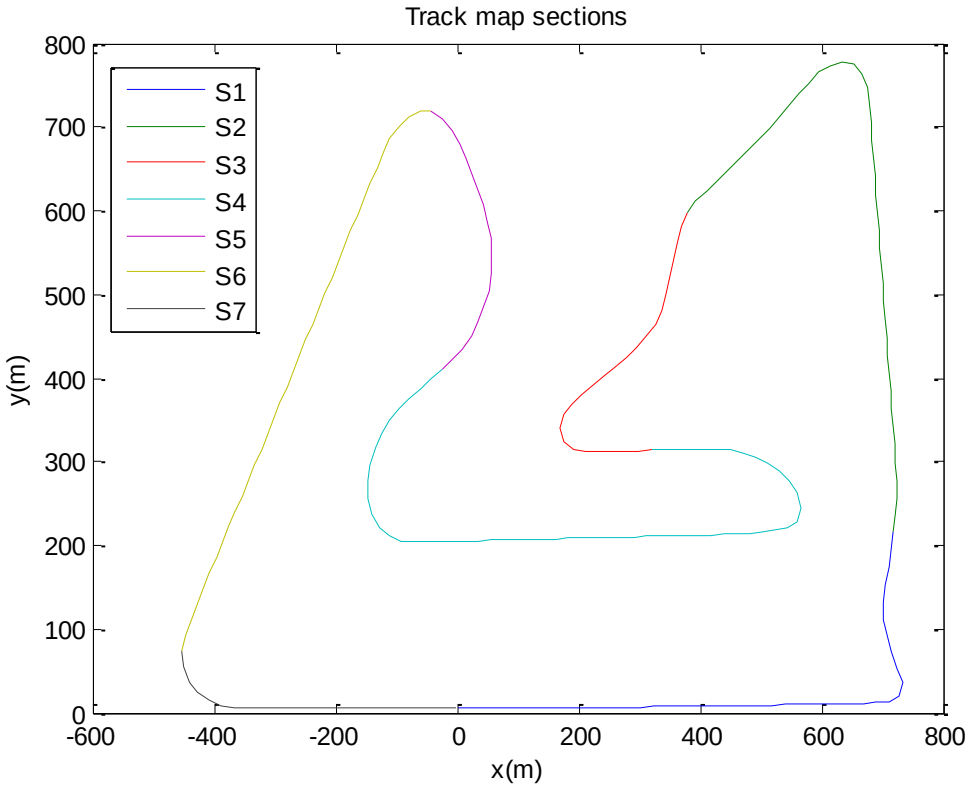

Figure 6-23: Bahrain GP track sections

The selection of the adequate integration method and integration step size will affect the accuracy of the simulation of the dynamic vehicle model (numerical stability) and the computational efficiency of the solver. Simulink allows the configuration of different numerical integration solvers. In this example, a fixed-step 4th-order Runge-Kutta integration solver has been used because it offers a good compromise between numerical stability and

computational efficiency. In addition to this, the step size must be selected so that suspension dynamic effects are not filtered out by the maximum numerical integration sampling frequency. Thus, selecting a step size of 0.1 m and assuming a minimum forward vehicle speed of 15 m/s (54 km/h), the frequency bandwidth would go up to 150 Hz. This bandwidth is suitable enough for suspension and ride dynamics analysis (0.5 – 40 Hz).

The stopping criteria are also an important parameter that determines the computational performance of the optimisation algorithm. Two alternative criteria are considered for stopping the optimisation process:

- Cost function tolerance.
- Maximum number of optimisation iterations.

The value of the function tolerance determines the minimum change in function value below which further optimisation will not produce significant improvements. In this example, the tolerance is set to 1e-6. Alternatively, a maximum number of optimisation iterations can be set to limit the running time in case the rate of convergence is low. In this example the number of iterations is set to 100.

Table 6-1 summarises the selection of optimisation parameters used in setting the optimisation solver:

Number of control input points (p)	193
Control input points spacing	[8, 80] m
Number of track sections (m)	7
Number of optimisation variables	200
Integration solver	Ode4
Integration step size	0.1 m
Function tolerance	1e-6
Number of max. iterations	100

Table 6-1: Summary of optimisation parameters – Bahrain example

The following section discusses the results obtained after the lap-time optimisation has been run.

6.5.2. Bahrain GP Circuit – Results

The lap-time optimisation tool has been run for a high-downforce generic racing car on the Bahrain GP Circuit. The race track presents the following characteristics:

Race Track Length	5412 m
Total number of corners	15
Right-hand corners	9
Left-hand corners	6
Total number of straights	4
Longest straight length	1090 m
Average Width	18 m

Table 6-2: Bahrain GP track main characteristics

For the race track characterised in Table 6-2, a Dell T1500 Precision computer with an Intel i5 processor has been used. The computation was about 4 hours and the optimal solution was produced after 38 optimisation iterations. The optimal lap time is shown in Table 6-3.

Lap Time Optimisation Summary – Bahrain GP Circuit	
Lap Time	**1’25’’340**

Table 6-3: Summary of lap-time optimisation

Figure 6-24 shows the time histories for throttle/brake and steering inputs achieved by the virtual driver model when driving the race car on the limit of performance. Note that, the longitudinal control input time history is noisy, especially when the longitudinal input is in a region close to full throttle. This is due to several reasons: firstly, when the car is exiting a corner, tyres are still producing a certain amount of lateral force, therefore the driver must modulate the throttle input in order to prevent the vehicle from spinning off. Secondly, due to road unevenness, vertical load on the tyres fluctuates constantly (see Figure 6-32), tyre slip ratios are also fluctuating (see Figure 6-28) and therefore there is a variation on the available longitudinal force generated by tyres. Finally, as explained in section 6.2.7, e throttle/brake input is linked to the steering control via a yaw rate proportional control. Thus, variations in yaw rate conditions induce the driver to modulate the throttle/brake input.

Figure 6-25 shows that the optimisation solver manages to produce an optimal trajectory within the limits of the race. Due to the nature of the generic race car configuration used in

this example, the optimal trajectory followed by the vehicle is close to the MCP trajectory, especially in sections with high-speed corners such as turns 11, 12, 14 and 15.

Figure 6-26 and Figure 6-29 represent forward speed, vehicle attitude and vertical position respectively. These graphs show the strong influence of aerodynamics in chassis attitude and vertical position. Figure 6-30 shows how aerodynamic lift coefficient and aero distribution varies with ride height and pitch angle. From these graphs, an inversely proportional relationship between ride height and speed can be observed. In turn, this variation in ride height affects the production of aerodynamic downforce. For instance, a reduction of about 15% of lift coefficient is experienced on low-speed turns (distance travelled 800, 2250 and 2700 m) can be noticed in Figure 6-30. Figure 6-32 represents the history of normal load applied at the tyre contact patch. As it can be observed, normal loads increase drastically with speed, which leads to higher longitudinal and lateral accelerations. A g-g-V diagram has been produced in Figure 6-31. As it can be observed, the maximum available longitudinal and lateral tyre forces increase as speed increases. Hence, this highlights that aerodynamics play important role in the overall performance of the race vehicle.

Finally, Figure 6-29 and Figure 6-32 are characterised by a high frequency content superimposed to the much lower frequency history dictated by the speed trace. This effect is due to the interaction between road inputs and suspension dynamics. Road unevenness induces high frequency vibrations on the chassis which, in turn, excites tyres and modifies the dynamic load at the contact patches. Figure 6-33 depicts the frequency response of front and rear dynamic contact patch loads. In this graph, two resonant modes can be identified for both axles: firstly, a body mode occurring at around 3 Hz, and, secondly, a hub mode at about 15 Hz. Hence, the main goal of a race car suspension is to filter out as much high frequency noise content as possible, so that vibrations induced by uneven road profiles do not cause a significant impact in the dynamics of the vehicle.

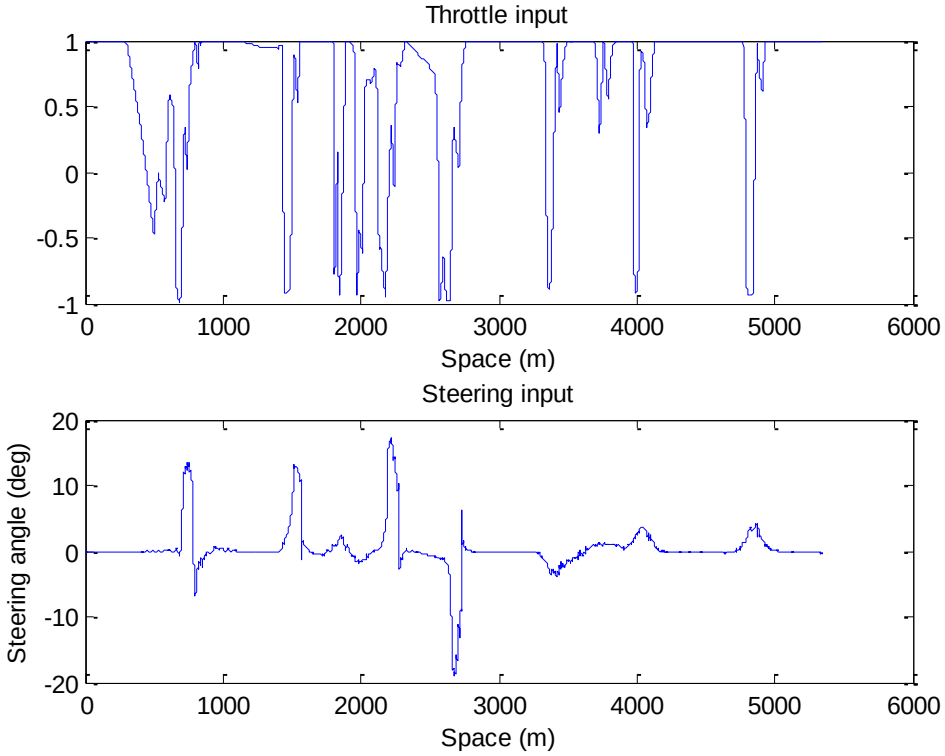

Figure 6-24: Bahrain Example: Control input histories

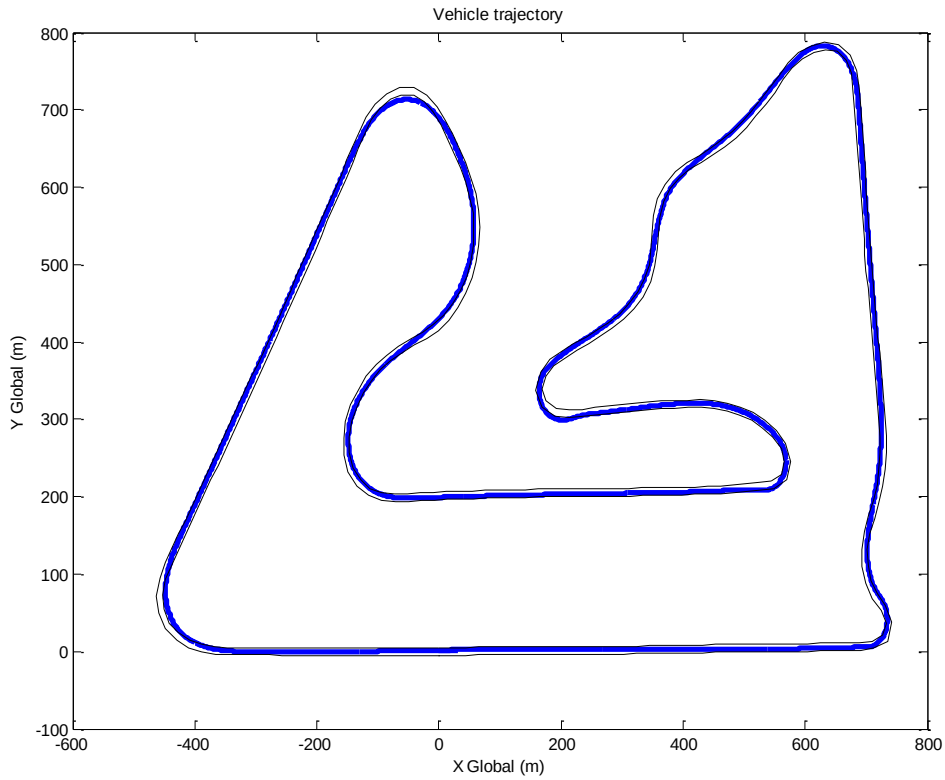

Figure 6-25: Bahrain Example: Optimal trajectory

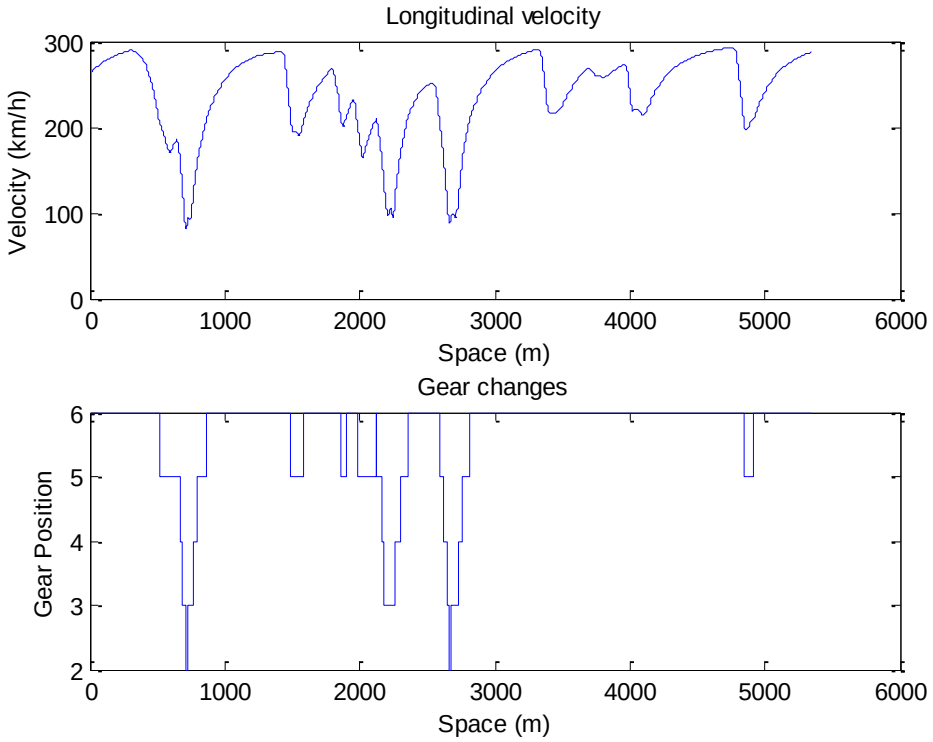

Figure 6-26: Bahrain Example: Forward speed profile and gear change history

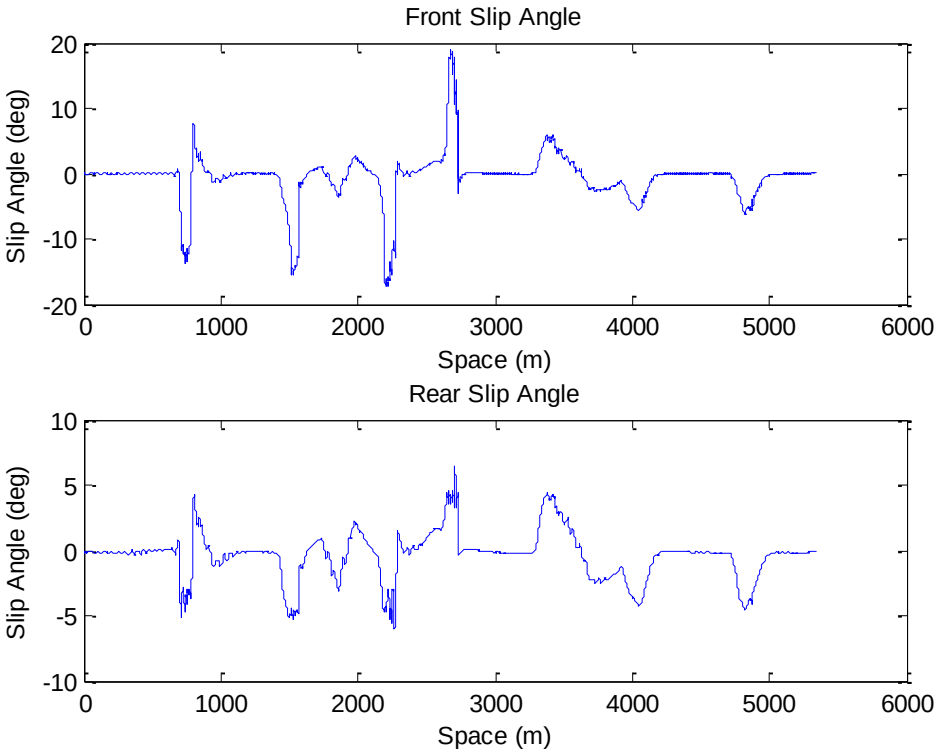

Figure 6-27: Bahrain Example: Front and rear slip angle histories

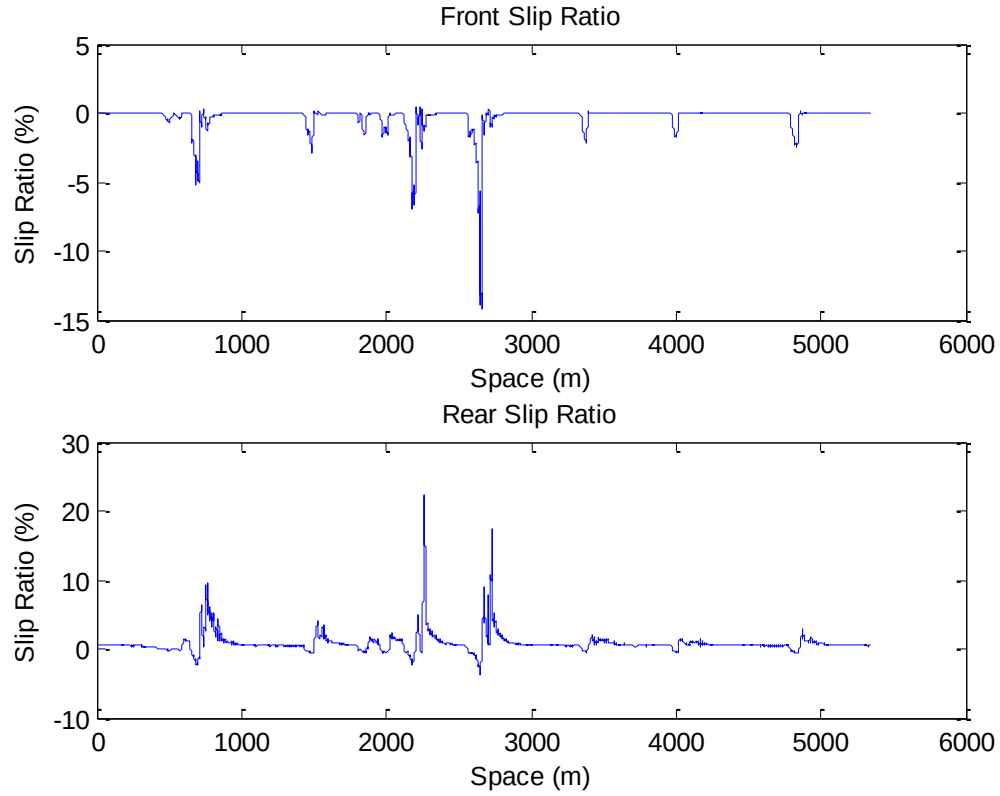

Figure 6-28: Bahrain Example: Front and rear slip ratio histories

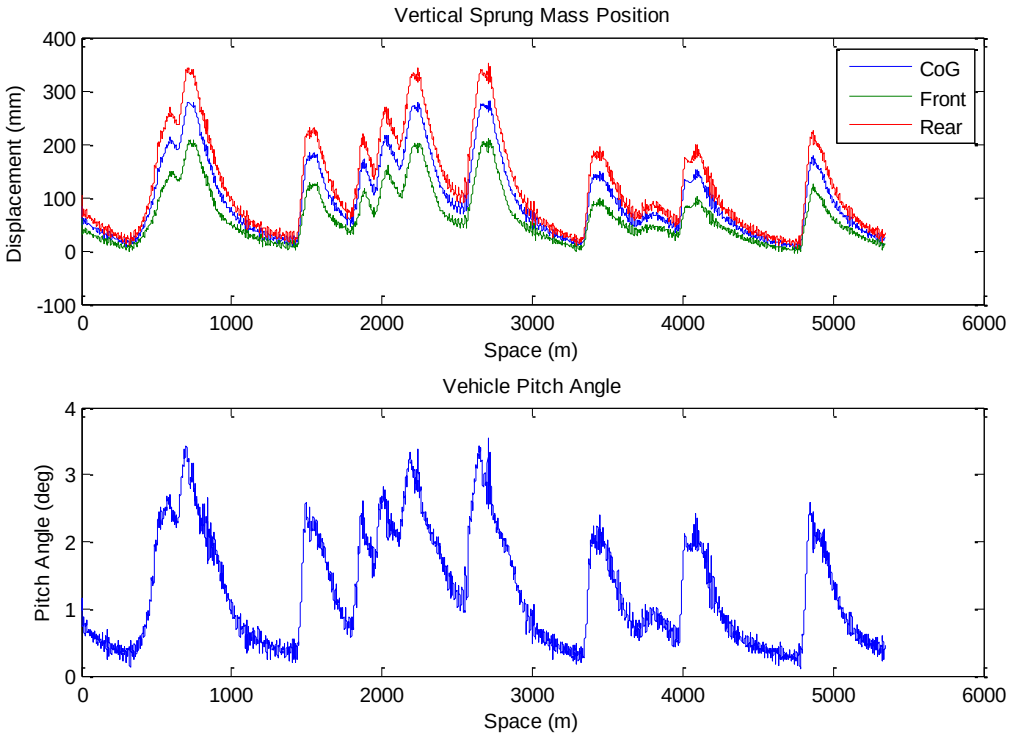

Figure 6-29: Bahrain Example: Ride Height and Pitch attitude histories

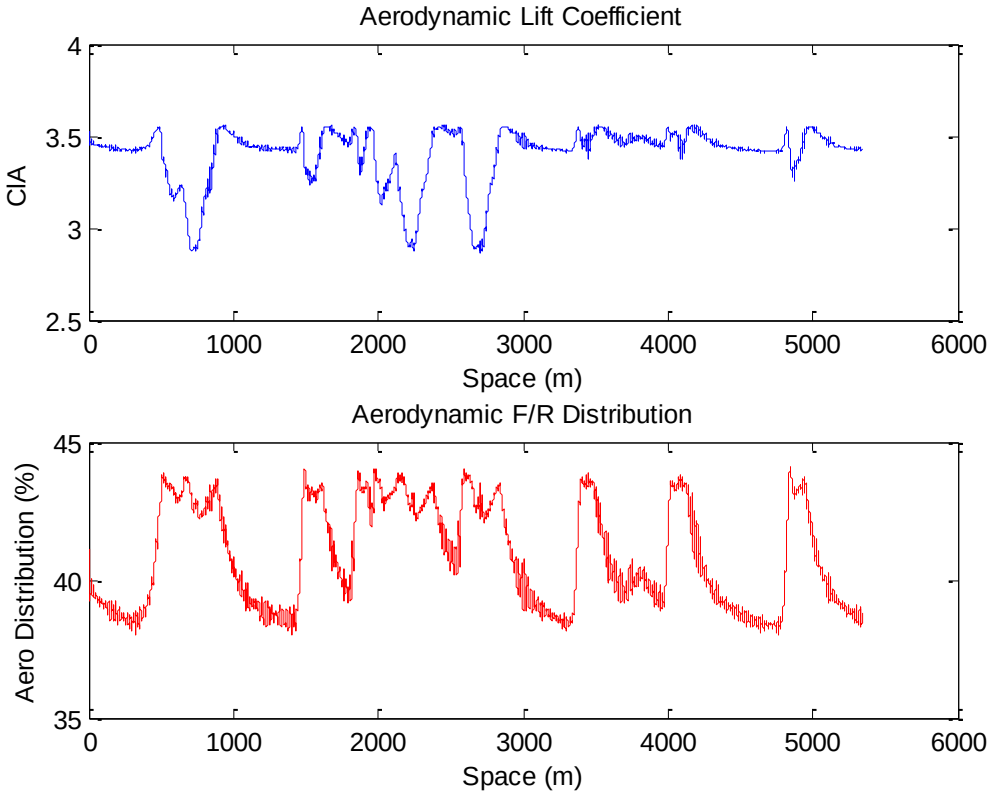

Figure 6-30: Bahrain Example: Aerodynamic Lift and F/R Distribution histories

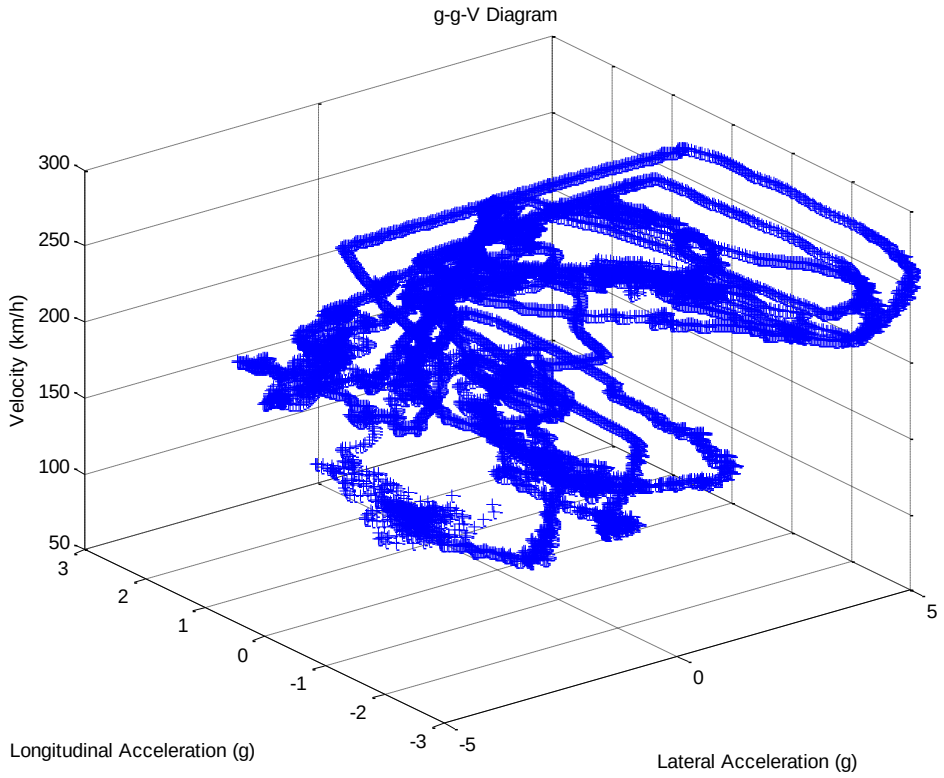

Figure 6-31: Bahrain Example: g-g-V Diagram

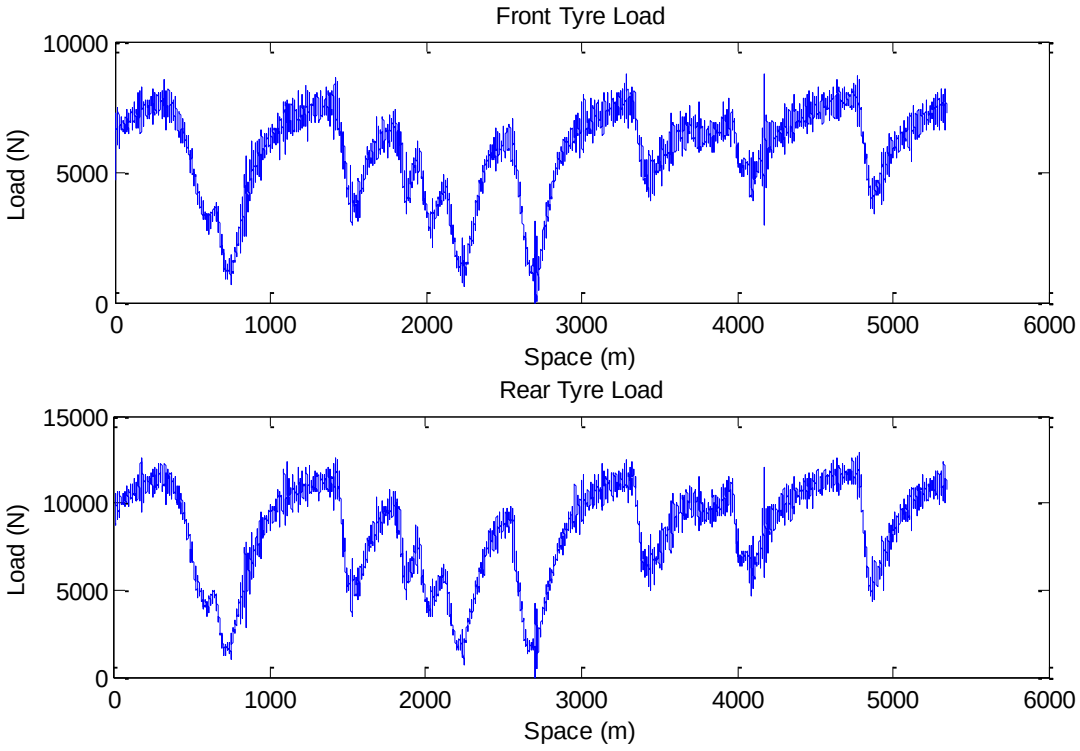

Figure 6-32: Bahrain Example: Front and rear vertical tyre load histories

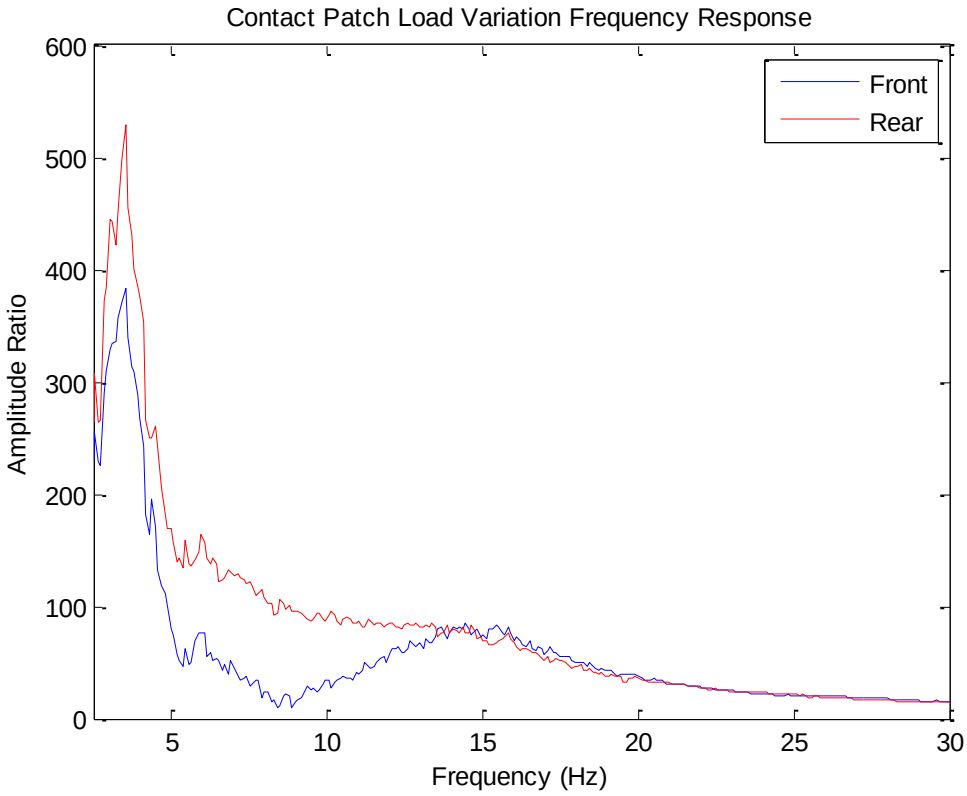

Figure 6-33: Bahrain Example: Contact patch load variation frequency response

6.6. Summary

A novel transient lap-time simulation algorithm has been developed in this chapter. The algorithm uses a multilevel architecture in order to efficiently transcribe the time Optimal Control problem into a Non-Linear Programming problem. A closed-loop path preview steering controller has been used to transform the constrained time Optimal Control problem into an unconstrained one with reduced size. The Non-Linear Programming problem is then solved by a classical gradient-based Sequential Quadratic Programming solver built in MATLAB®.

A vehicle model has been also created using a modular modelling approach. The vehicle is split into subsystems that have been independently modelled. A main vehicle framework has been then set in order to interconnect the building modules and to produce the overall vehicle model. This modular modelling approach allows the user to easily interchange, reuse or update different components without affecting the rest of the model.

The optimisation algorithm has been applied to a case study. A generic racing car with high downforce levels has been driven along a Bahrain GP Circuit. Discussions with regard to algorithm efficiency and robustness have been carried out. It was demonstrated that program framework set-up plays an important role in finding the optimal racing line. Time histories for different dynamic magnitudes can be obtained and used to analyse the performance and sensitivity of different vehicle systems into the overall performance of the race car.

In the following chapter, the lap-time simulation virtual tool will be used as decision maker in a multi-objective suspension optimisation process. The lap-time simulator will be used as key tool in the analysis of the impact of suspension dynamics in the overall performance of a racing car.

7. Suspension Performance Optimization

7.1. Introduction

Suspension systems are a critical part of a racing vehicle. Vehicle suspensions are the only physical linkage between the tyres and chassis. A critical design consideration for a vehicle suspension is that they need to offer proper tyre kinematic attitude so that they can react to the control forces generated at the tyres (acceleration, braking and cornering forces). In addition, from a purely dynamic point of view, the main goals of a vehicle suspension are:

- To keep the tyres in contact with race track.
- To resist chassis motions induced by external forces (inertial and aerodynamic forces).
- To control the weight balance across all four tyres under dynamic situations.

The level of accomplishment of these suspension goals will dictate the performance of the vehicle. Hence, suspension systems must be designed and optimised so that these goals can be achieved and therefore, maximum vehicle performance can be reached. However, in order to meet these goals in an efficient and robust way, an optimisation process must be developed. This chapter presents an objective method capable of optimising a suspension featuring inerters.

Chapter 7 starts with a formal definition of the suspension optimisation problem as a multi-objective optimisation problem. The chapter then follows with the definition of the suspension variables that integrate the optimisation search space and develops a mathematical expression of the evaluation functions that represent the main dynamic suspension goals stated above. Moreover, a novel suspension optimisation method based on metamodeling techniques, multi-objective algorithms and lap-time simulation has been developed. In the last part of the chapter, this optimisation methodology has been applied to optimise a conventional suspension and a suspension incorporating inerters. Discussions on the performance gains obtained from using inerters have been carried out.

7.2. Definition of the Multi-Objective Suspension Optimisation Problem

Analytical suspension optimisation based on the use of mathematical optimisation methods requires firstly an appropriate definition of the optimisation problem. The definition of the optimisation problem also assists in the selection and development of the most well-suited optimisation algorithm. As introduced in Chapter 2, the design and optimisation of race car suspensions must account for several factors. Therefore, a racing suspension system must be optimised for not only one objective but for several objectives, some of which may conflict with each other. Hence, a racing car suspension optimisation problem could be defined as a multi-objective optimisation problem (MOOP). Mathematically, a general MOOP can be defined as follows (Deb, 2001):

$$\begin{aligned} &\min && F(\boldsymbol{x}) = \{f_1(\boldsymbol{x}), f_2(\boldsymbol{x}), \dots, f_m(\boldsymbol{x})\} \\ &subjected\ to && G(\boldsymbol{x}) = \{g_1(\boldsymbol{x}), g_2(\boldsymbol{x}), \dots, g_j(\boldsymbol{x})\} \geq 0 \\ & && H(\boldsymbol{x}) = \{h_1(\boldsymbol{x}), h_2(\boldsymbol{x}), \dots, h_k(\boldsymbol{x})\} = 0 \\ & && x_{iL} \leq x_i \leq x_{iU} \quad , \quad i = 1, \dots, n \end{aligned} \tag{7.1}$$

Where $\boldsymbol{x}=\{x_1, x_2, \dots, x_n\}$ is the vector of n decision variables

$F(x)$ is the vector of m objective functions

$G(x)$ is the vector of j inequality constraints

$H(x)$ is the vector of k equality constraints

x_{iL}, x_{iU} are the limits of the search space for the *i-th* decision variable

This formal definition of a general MOOP will assist in the design and development of an optimisation algorithm that could handle the simultaneous optimisation of several performance objectives, some of which may conflict with each other, and to obtain an optimised suspension solution in a robust and efficient manner.

7.3. Definition of the Design Space

The design space or search space, Z, is defined implicitly by the specification of the design variables $z \in Z$. In a suspension optimisation problem, the design space Z is composed of all

adjustable suspension parameters such as spring stiffness characteristics, damping characteristics and inertance values. According to the half car vehicle model developed in Chapter 5, an initial search space will be composed of the following variables:

Front Suspension Stiffness (N/m)	$\boldsymbol{k_{sF}}$
Rear Suspension Stiffness (N/m)	$\boldsymbol{k_{sR}}$
Front Linearised Damping Coefficient (Ns/m)	$\boldsymbol{C_{sF}}$
Rear Linearised Damping Coefficient (Ns/m)	$\boldsymbol{C_{sF}}$
Front Inertance (kg)	$\boldsymbol{b_{sF}}$
Rear Inertance (kg)	$\boldsymbol{b_{sF}}$

Table 7-1: Definition of Initial Design Space

Anti-roll bar (ARB) stiffness values have been neglected from the design space since the vehicle model does not account for rolling effects.

Furthermore, a preliminary study has been carried out in order to analyse the role of spring stiffness in suspension optimisation when considering only the dynamic response of the vehicle to road irregularities. A simple single-degree-of-freedom (SDOF) system similar to the one represented in Figure 3-4 without an inerter has been used. Due to its simplicity, an analytical expression for the amplitude ratio between output and input displacement can be derived using the same procedure employed in Chapter 3. The final expression of the amplitude ratio is:

$$H(\omega) = \left|\frac{X(\omega)}{Z(\omega)}\right| = \sqrt{\frac{k^2 + (c\omega)^2}{(k + m\omega^2)^2 + (c\omega)^2}} \tag{7.2}$$

Where $H(\omega)$: Output/Input Displacement Amplitude Ratio in frequency domain

$X(\omega)$: Body Displacement in frequency domain

$Z(\omega)$: Base (Road) Excitation Displacement in frequency domain

k: Spring stiffness in N/m

c: Damping Coefficient in Ns/m

m: Body mass in kg

ω: Angular frequency in rad/s

Equation (7.2) represents the characteristic behaviour of a SDOF system in the frequency domain for different spring stiffness values for a constant 0.5 damping ratio (see Figure 7-1). In general terms, softer springs decrease the natural frequency of the system and reduce the vibration transmissibility at higher frequencies.

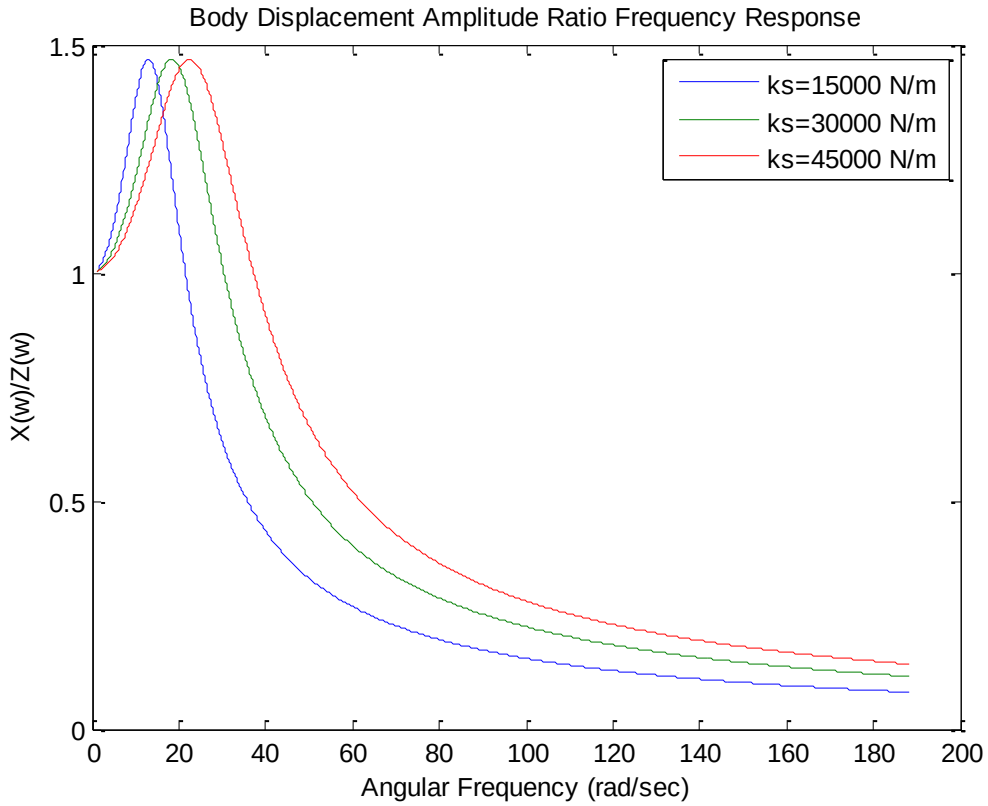

Figure 7-1: SDOF Body Displacement Amplitude Ratio for different k values

However, in order to quantitatively measure the impact of suspension springs in the dynamic response of the system, a measurement of the vibration transmission from input (road irregularities) to output (body) is required. A common tool for quantifying this vibration transmission used in classical vibration dynamics literature is to calculate the root-mean-square (RMS) of the transmissibility function, in this case, body displacement amplitude FRF. The RMS of the body displacement FRF expressed in equation (7.1) RMS_b can be obtained as follows:

$$RMS_b = \sqrt{\frac{1}{n} \cdot \sum_{i=1}^{n} H(\omega)_i^2} \qquad (7.3)$$

Where n: number of samples of the function $H(\omega)$.

Thus, using expression (7.3) and (7.2), an analysis of the variation of stiffness values, *k*, on the RMS of the body displacement can be carried out. Figure 7-2 shows the trend of RMS of the body displacement for different spring values, expressed as ride frequency.

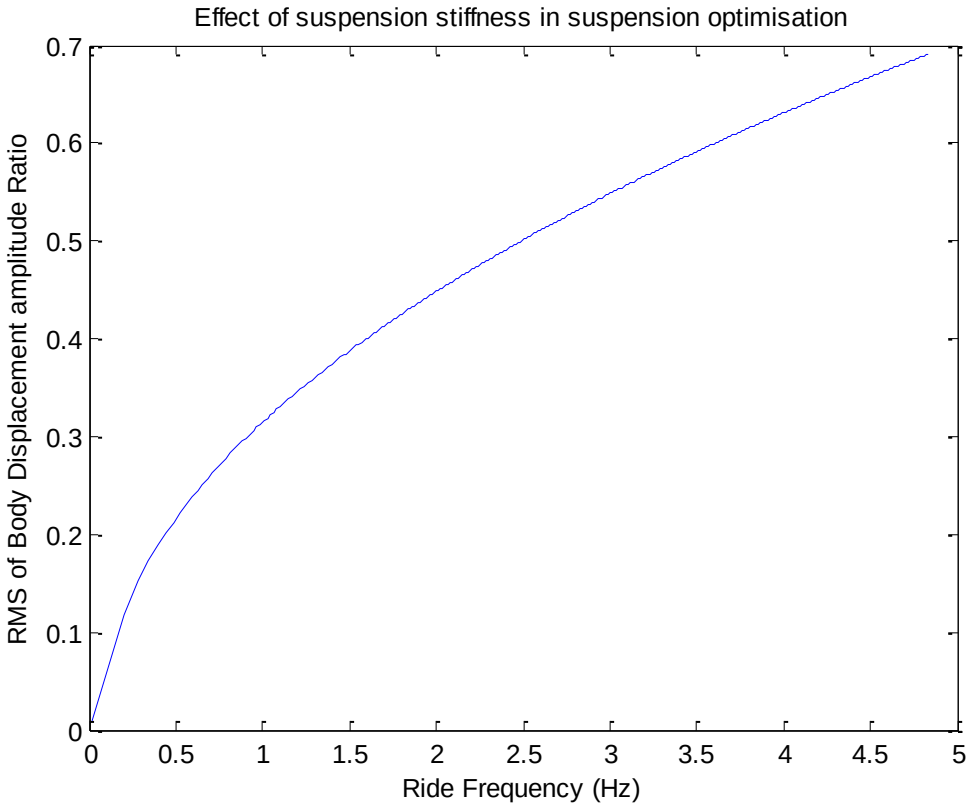

Figure 7-2: Effect of suspension stiffness in the RMS of Body Displacement Amplitude Ratio

It can be observed that body displacement transmissibility decreases monotonically with softer suspension stiffness. On the limit $k \rightarrow 0$, the transmissibility function tends to 0, which leads to the trivial solution that with no springs between road and body, body displacement would be completely independent from road excitations. This means that, when optimising suspension parameters for more complex vehicle models, the optimiser will obtain the softest spring value within the specified spring stiffness search range as optimal solution. According to this, front and rear spring stiffnesses can be therefore discarded from the design space and only damping and inertance values will be considered as input variables to the optimisation process.

Hence, the optimisation process presented in this research work considers that the selection of the optimal spring stiffness is dominated by static and steady-state design constraints such as static deflection, suspension travel, maximum heave, pitch and roll travel under inertial and

aerodynamic forces and steady-state roll distribution, which are outside the scope of the project.

The final search space is therefore composed of front and rear axle damping and inertance coefficients (see Table 7-2).

Front Linearised Damping Coefficient (Ns/m)	C_{sF}
Rear Linearised Damping Coefficient (Ns/m)	C_{sF}
Front Inertance (kg)	b_{sF}
Rear Inertance (kg)	b_{sF}

Table 7-2: Definition of Final Design Space

7.4. Definition of Optimisation Evaluation Criteria

The definition of objective functions *J* is paramount in any optimisation process. In race car suspension design and optimisation, objective functions must accurately express the attributes and goals to be achieved. In Chapter 2, a review of the research literature related to suspension performance cost function definition was discussed.

In this chapter, a series of objective functions have been defined in order to analyse the impact of suspension dynamics with respect to the overall performance of the vehicle in order to produce an optimised race car suspension set-up. As explained in Chapter 5, suspension dynamics studies are carried out in the frequency domain, due to the nature of the road inputs (assumed to be random noise functions with zero mean value and standard deviation σ). Moreover, vehicle vibration modes (Heave, Pitch, Roll and Warp or Articulation) are often decoupled in order to facilitate the analysis of the dynamic behaviour of the suspension.

The aim of this section is to define functions that represent performance features of the race car under the action of dynamic road inputs. The following subsections describe the development of the suspension optimisation performance functions used in this research work.

7.4.1. Mechanical Grip Cost Function

In racing applications, mechanical grip is known as the maximum friction coefficient that can be obtained for a particular racing tyre only through the use of mechanical systems, i.e. excluding aerodynamic effects. There are many factors that affect the generation of

mechanical grip in a race car including overall car weight, weight distribution, CoG height, chassis compliance, suspension kinematics, and suspension dynamics.

It is well-known that the rate of lateral and longitudinal tyre forces with respect to normal load follows a nonlinear convex trend (see Figure 7-3). Under the effect of road unevenness, this nonlinear behaviour implies that random fluctuations of the vertical load around an operating nominal point (i.e. static tyre load) would reduce the average production of lateral (and longitudinal) force for a determined travelled distance *s*, and, therefore, mechanical grip will decrease. Furthermore, (Pacjeka, 2006) demonstrated that increments in lateral and longitudinal forces due to sudden increments of normal load do not occur instantaneously, instead a finite time is required to build up forces (see Figure 6-7).

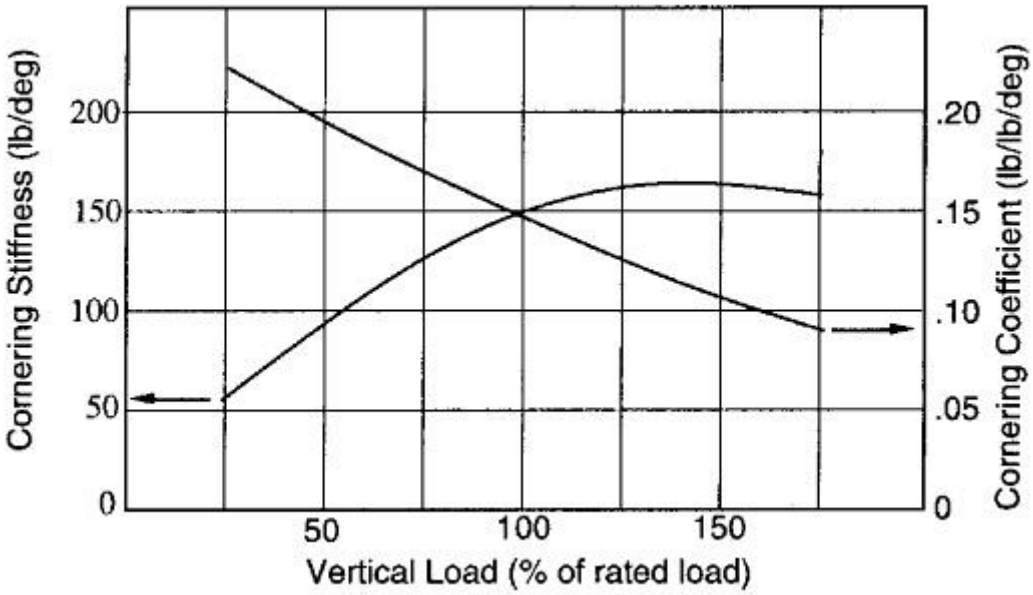

Figure 7-3: Effect of vertical load on cornering performance (Gillespie, 1992)

Hence, from the point of view of suspension dynamics, in order to improve the maximum mechanical grip available on a race car, fluctuations of normal loads on the tyres should be minimised. According to this, a cost function that expresses mechanical grip must include a mathematical expression that quantifies the variation of dynamic tyre load for a specified frequency range. As it was reviewed in Chapter 2, a standard way to define the performance function for mechanical grip can be derived by obtaining the root-mean-square (RMS) of the variation of dynamic tyre load for a range of frequency (or a period of time if signals are in the time-domain). However, most of the literature reviewed focuses on the study of quarter-car vehicle models and therefore, only one wheel of the vehicle is considered in these studies.

In this research work, a half-car vehicle suspension model has been used. Therefore, the cost function for mechanical grip should include the effects of both axles. According to this, the following mathematical model can be derived:

$$J_{MG}^{Mode} = q_f \cdot RMS_{MG}^{front} + q_r \cdot RMS_{MG}^{rear} \quad (7.4)$$

Where J_{MG}^{Mode}: Mechanical grip performance function for an isolated vibration mode

q_{Hf}, q_{Hr}: weighting factors for heave mode between front and rear axles and $\in [0,1]$

The introduction of these weighting factors q_{Hf} and q_{Hr} enables the possibility to bias optimisation towards one of the axles. This implies that if $q_{Hf} > q_{Hr}$, then the optimised suspension configuration will produce better mechanical grip on the front axle. An inverse situation would occur when $q_{Hf} < q_{Hr}$. If $q_{Hf} = q_{Hr}$, the optimisation solver will attempt to obtain a suspension setting that evenly increases the dynamic mechanical grip available in both axles.

Furthermore, in real cars, road excitations are exerted at all four wheels and all the vibration modes are highly coupled. Thus, the overall objective function should include the calculation of dynamic contact patch load for all the vibration modes. However, as discussed in Chapter 5, the analysis of ride dynamics does not produce representative results of the actual behaviour of the physical car for the roll vibration mode and, therefore, it was decided to model the vehicle suspension to consider only heave and pitch vibration modes.. Hence, a cost function should incorporate contact patch load *CPL* variation in heave and pitch modes. According to this, in this research work, a frequency dependent modal weighting function *WF* has been developed. The purpose of this function is to weight the contribution of the different vibration modes to the overall objective function. This weighting function *WF* has been developed from simulated track profile data. This profile data has been created as integrated white noise (IWN) whose PSD profile resembles the one obtained from the swept sine input signals discussed in Chapter 4. This IWN signal is then considered as the input experienced by the front axle. The input excitation at the rear axle has been assumed to be the same as the input at the front axle delayed by the wheelbase in the space domain (see Figure 7-4).

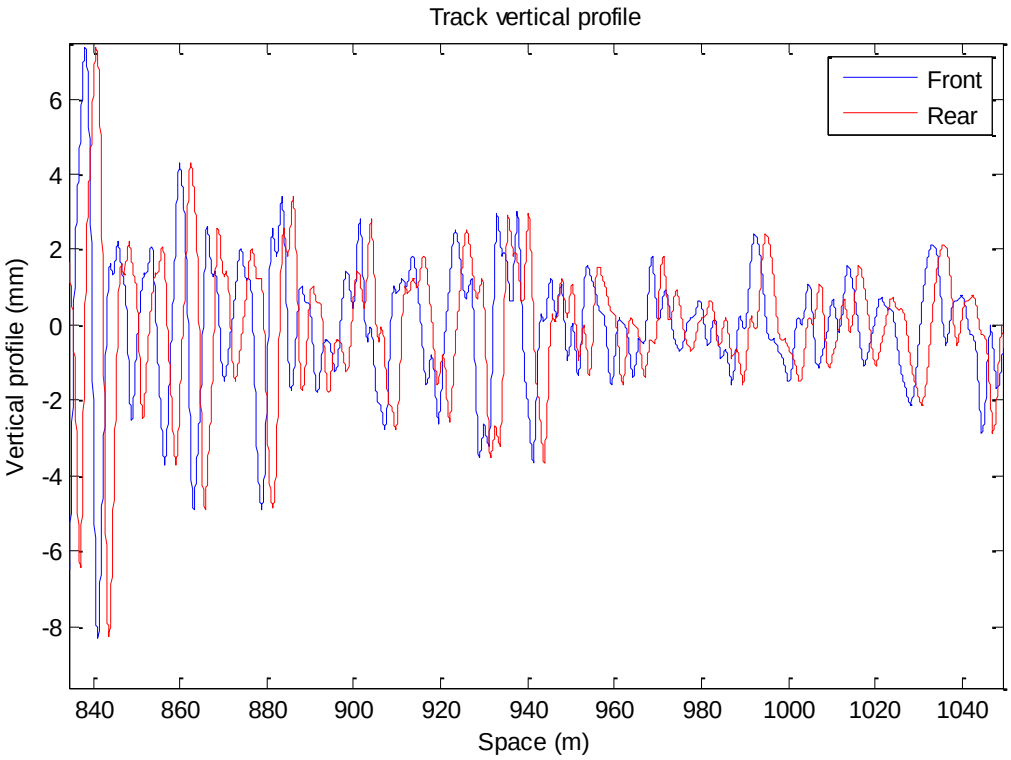

Figure 7-4: Integrated white noise track profile signal

Assuming a solid rigid chassis, the content of pure heave motion z_{Heave} and pitch motion φ_{Pitch} can be obtained as follows:

$$z_{Heave} = \frac{a \cdot z_{rR} + b \cdot z_{rF}}{wb} \tag{7.5}$$

$$\varphi_{Pitch} = \frac{z_{rF} - z_{rR}}{wb} \tag{7.6}$$

Where z_{rF} and z_{rR}: vertical road profile at front and rear axles respectively

wb: wheelbase

a: distance from the front axle to the CoG

b: distance from the rear axle to the CoG

Since cost functions are created from frequency domain data, pure heave and pitch motion are transformed into frequency domain via Fast Fourier Transformation (FFT). Relative amplitude responses for heave and pitch motions are then obtained to produce modal weighting functions *WF* as:

$$WF_{Heave}(\omega) = \frac{|Z_{Heave}(\omega)|}{|Z_{Heave}(\omega)| + |\varphi_{Pitch}(\omega)|} \quad (7.7)$$

$$WF_{Pitch}(\omega) = \frac{|\varphi_{Pitch}(\omega)|}{|Z_{Heave}(\omega)| + |\varphi_{Pitch}(\omega)|} \quad (7.8)$$

Where $Z_{Heave}(\omega)$ and $\varphi_{Pitch}(\omega)$ represent the non-dimensional amplitude ratio of pure heave and pure pitch inputs.

Figure 7-5 shows an example of the modal weighting factors obtained from a IWN input signal at a constant speed of 70 m/s and for the vehicle with a wheelbase wb = 2.565 m.

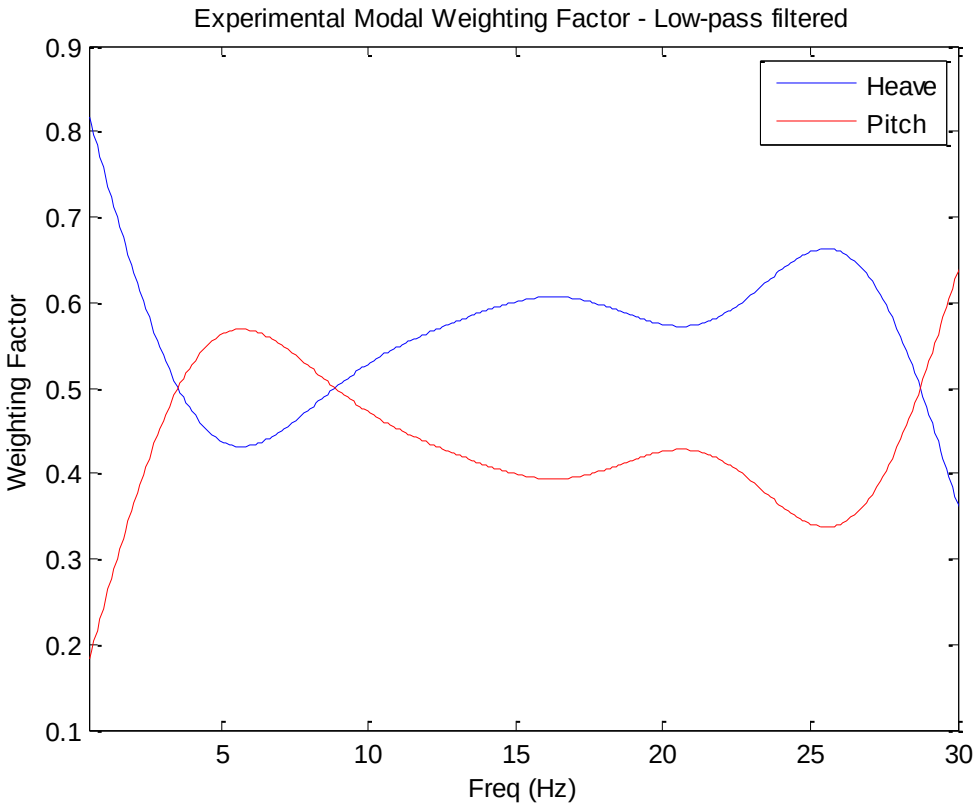

Figure 7-5: Modal Weighting factor

Note that, more accurate modal weighting functions could be obtained from actual track profile data.

These modal weighting functions WF have then be used to weight the contact patch load FRF and, therefore, the RMS of the contact patch load variation as follows:

$$RMS_{MG} = \sqrt{\frac{1}{n} \cdot \sum_{i=1}^{n} [WF(\omega)_i \cdot CPL(\omega)_i]^2} \tag{7.9}$$

Where the RMS_{MG} for front and rear axles in heave and pitch modes can be obtained from equation (7.9)

n: number of samples points of the FRF signal

The overall mechanical grip cost function J_1 can therefore be obtained as a linear combination of objective function for single vibration mode (see equation (7.4)):

$$J_1 = J_{MG}^{Heave} + J_{MG}^{Pitch} \tag{7.10}$$

7.4.2. Aerodynamic Grip Cost Function

In modern motorsports, Aerodynamics is a key performance element in the design of racing cars. When the vehicle is travelling at speed, the air flows around the bodywork of the vehicle and this interaction generates aerodynamic forces that are ultimately transferred to the tyres through the suspension. Equations (6.11) and (6.12) expressed a semi-empirical representation of the forces exerted by the air flow into the chassis.

Aerodynamic grip is hence related to the generation of enhanced tyre lateral and longitudinal forces due to the effect of aerodynamics exclusively. Figure 7-6 shows that, an increase of the aerodynamic lift (or down-force) coefficient C_L[5] leads to a significant increase in the maximum lateral acceleration achievable by the race car for a particular corner radius. The aerodynamic down-force exerts an action to the chassis that it is transferred to the tyre through the suspension system. This aerodynamic action leads to an increase of normal load at the tyre which, in turn, increases the capability of the tyre to generate lateral and longitudinal forces. These larger lateral and longitudinal forces will ultimately induce larger accelerations and, therefore, enhanced performance.

[5] Some authors normalise this coefficient by the front area of the vehicle *A* and, therefore, the aerodynamic lift coefficient is expressed as C_LA.

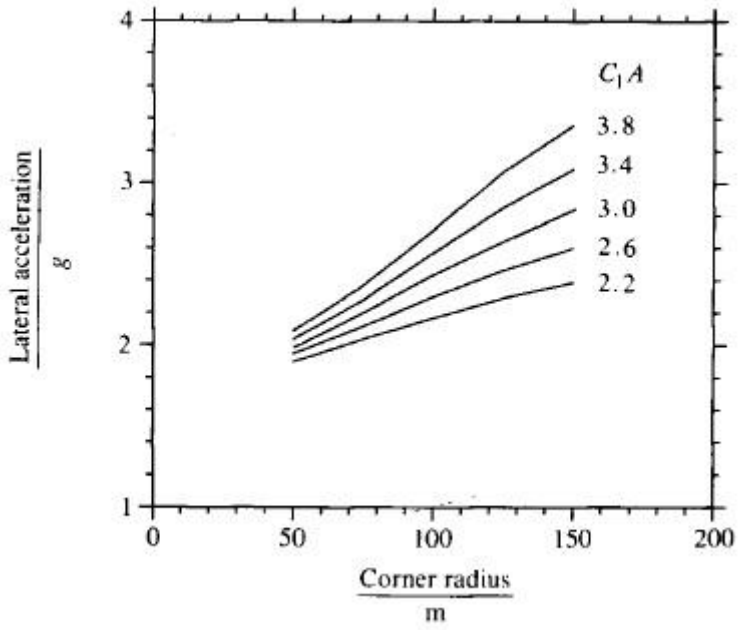

Figure 7-6: Effect of aerodynamics in the cornering performance of a race car (Dominy, 1992)

Although the absolute aerodynamic performance depends mostly in the design of the bodywork, interaction between suspension dynamics and aerodynamics is also an important component in the overall performance of the vehicle. As showed in Chapter 6, the performance of an aero package is highly sensitive to variations in ride height and attitude. It is common practice in the industry that aero-maps are expressed as functions of front and rear ride heights rather than ride height at the CoG and attitude (see Figure 6-8). In Chapter 4, front and rear ride heights *RH* were defined as the difference between the displacement of the sprung mass x_s and the input displacement x_{input} (see equation (4.22)). According to aero-maps showed in Figure 6-8, the main aim of the suspension system in high aerodynamic performance cars is to reduce dynamic variations of ride height so that maximum generation of down-force can be achieved.

Hence, an aerodynamic grip cost function for suspension optimisation must express this interaction between Aerodynamics and suspension dynamic effects. In this research work, the aerodynamic suspension performance is quantified in terms of the dynamic ride height variation. As with the mechanical grip, the root mean square (RMS) function is the most suited mathematical function to quantify dynamic ride height variations. Front and rear axle contributions have been equally accounted for in the design of the objective. The weighting factor developed in the previous section has been also used in this cost function to account for heave and pitch motions. Thus, the cost function can be expressed as follows:

$$J_2 = J_{AG}^{Heave} + J_{AG}^{Pitch} \tag{7.11}$$

Where J_2: Overall aerodynamic grip objective function

J_{AG}^{Heave} *and* J_{AG}^{Pitch}: aerodynamic objective function for a single vibration mode where

$$J_{AG}^{Mode} = q_F \cdot RMS_{RHF} + q_R \cdot RMS_{RHR} \tag{7.12}$$

$$RMS_{RH} = \sqrt{\frac{1}{n} \cdot \sum_{i=1}^{n} (WF(\omega)_i \cdot RH(\omega)_i)^2} \tag{7.13}$$

Equation (7.13) applies for the calculation of RH for front and rear axles in heave and pitch modes

WF: Frequency based modal weighting function

RH(ω): dynamic ride height variation FRF

n: number of samples points of the FRF signal

Furthermore, since the aerodynamic longitudinal force distribution is ride height dependent, the cost function defined in equation (7.11) accounts also for aerodynamic balance effects. Minimisation of dynamic ride height variations will lead to reduction of the variation of the aero distribution and therefore to an improvement of the aerodynamic balance.

7.4.3. Mechanical balance Cost Function

Mechanical balance is another important feature in racing cars. Mechanical balance refers to the amount of grip produced at each axle. A perfectly balanced car would produce lateral axle forces so that the resultant moment around the yaw axis is always zero under steady-state cornering. If the front axle produces less lateral force than the rear axle, the car experiences an understeering situation and is unable to follow the ideal racing line. If the rear axle produces less lateral force than the front axle, then the vehicle experiences an oversteering situation in which the vehicle becomes unstable.

The steady-state mechanical balance of a vehicle depends mostly on weight distribution, tyre cornering stiffnesses and slip angles. However, Mashadi & Crolla (2005) showed that the

understeering characteristic of a vehicle under relatively high lateral accelerations is dramatically affected by the effect of road unevenness.

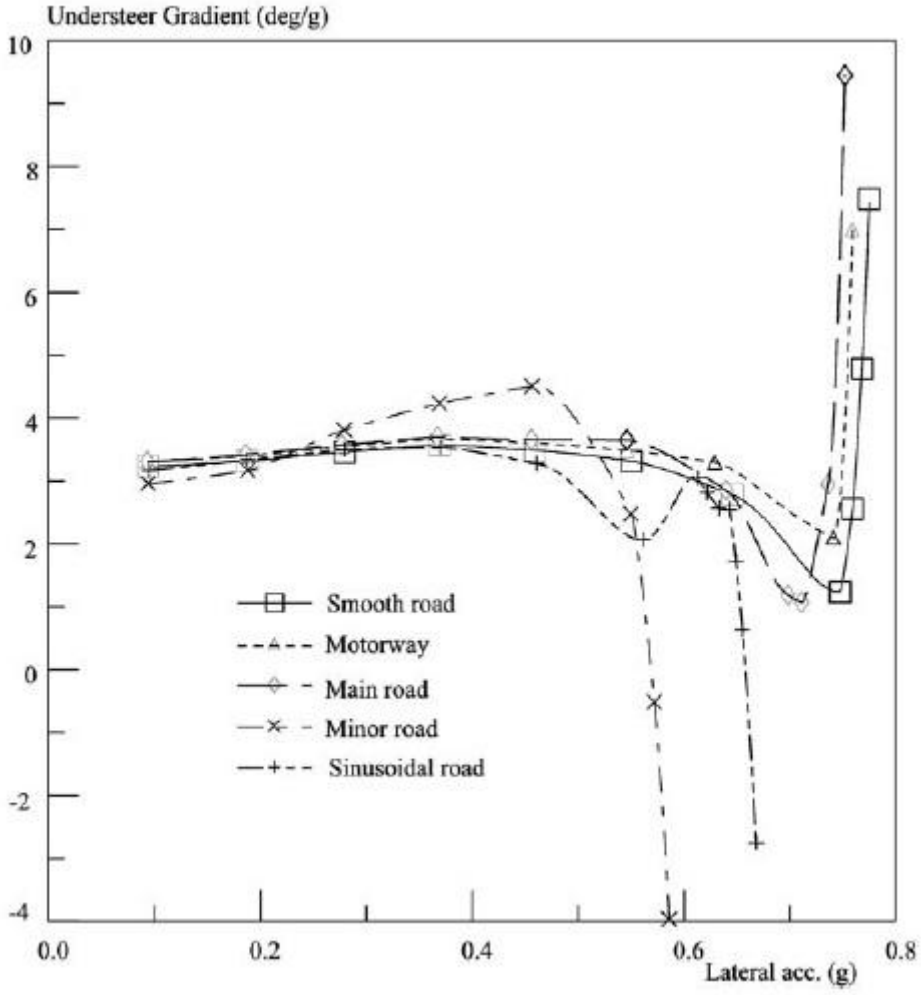

Figure 7-7: Understeering characteristic under different road surfaces (Mashadi & Crolla, 2005)

Hence, in this research work, a cost function that expresses the effect of suspension dynamics on the understeer – oversteer characteristic of a vehicle has been developed.

Assuming a steady-state understeer gradient dictated by the design of the chassis and the selection of the tyres, the dynamic understeer characteristic of a vehicle can be influenced by road excitation through the suspension system. Road irregularities generate dynamic normal load changes at the tyre contact patch. If variations of normal load are different for each axle, the weight distribution under dynamic loads will drift from static weight distribution and therefore this will change the balance of the car. According to this, an expression of the dynamic weight distribution *WDist_Dyn* was defined in Chapter 4 (see equation (4.23)).

From this expression of dynamic weight distribution *WDist_Dyn*, a longitudinal deviation of the position of the dynamic CoG with respect to the static CoG location can be defined as:

$$E_{CoG}(\omega) = \big(1 - WDist\_Dyn(\omega)\big) \cdot wb - a \qquad (7.14)$$

Where $E_{CoG}(\omega)$: FRF of deviation of dynamic CoG from static CoG longitudinal location. As with the previous cost functions, this magnitude can be obtained in both heave and pitch modes

wb: wheelbase

a: distance from static CoG to front axle

As with the rest of the objective functions, the RMS of $E_{CoG}(\omega)$ can be obtained in order to quantify the variation of the position of the dynamic CoG with respect to the static CoG as:

$$RMS_{Balance} = \sqrt{\frac{1}{n} \cdot \sum_{i=1}^{n} [WF(\omega)_i \cdot E_{CoG}(\omega)_i]^2} \qquad (7.15)$$

The mechanical balance objective function J_3 can be obtained by combining the $RMS_{Balance}$ for heave and pitch modes.

$$J_3 = RMS_{Balance}^{Heave} + RMS_{Balance}^{Pitch} \qquad (7.16)$$

7.5. Development of the Optimization Methodology

The main goal of developing a validated vehicle suspension model is that it can then be used to perform analyses in a virtual environment with high levels of confidence. Moreover, results drawn by simulation modelling can be directly applied to the physical car.

In this research work, the validated vehicle model is used, in combination with the performance based objective functions defined in section 7.4, as an input into a suspension optimisation problem in a virtual environment. This process allows an optimal suspension setup to be obtained much more efficiently and robustly than when carrying out experimental testing on a rig facility or a race track.

Figure 7-8 shows the optimisation method proposed in this thesis in order to obtain an optimised suspension setup. The following sections provide a detailed explanation of the different stages of this suspension optimisation.

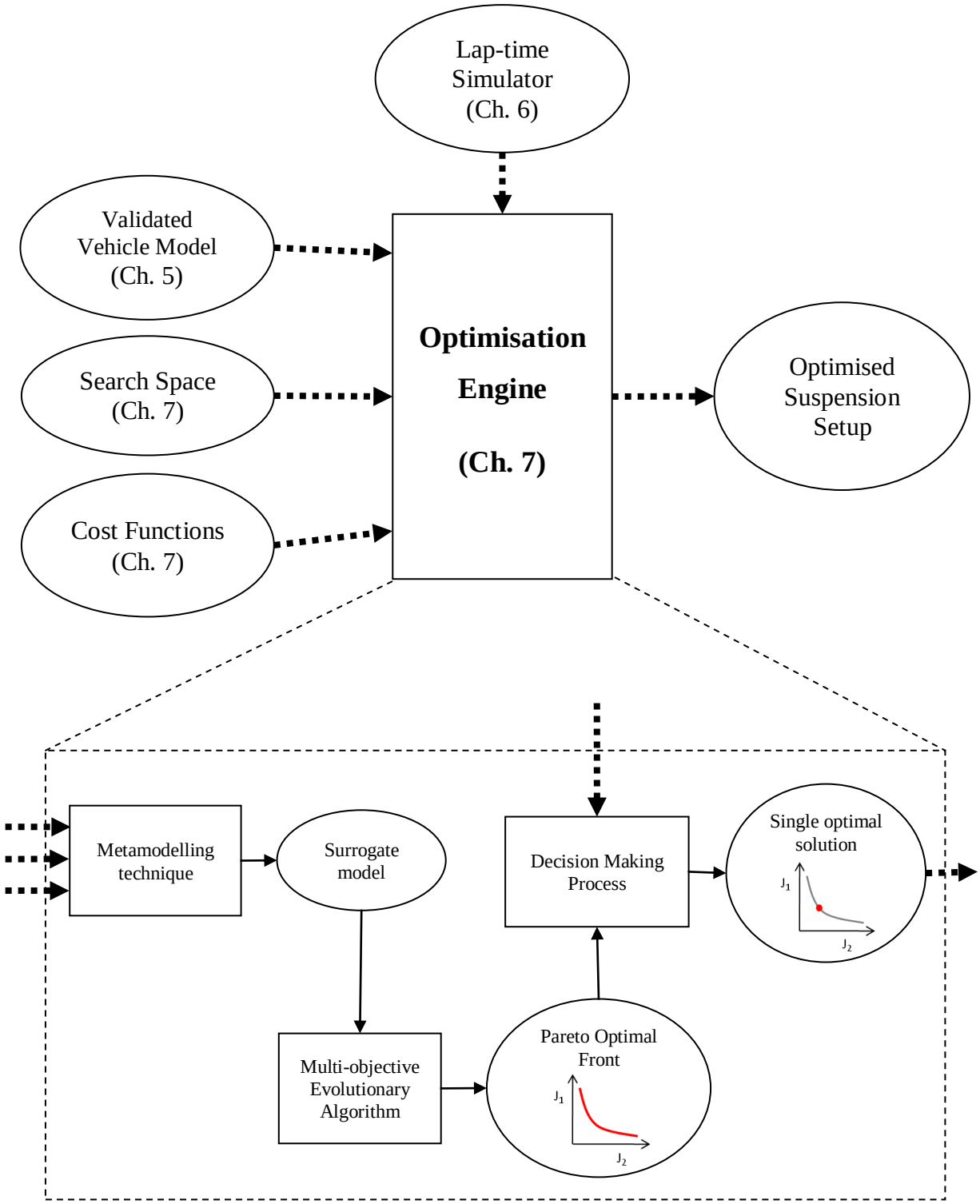

Figure 7-8: Proposed suspension optimisation process layout

7.5.1. Surrogate Modelling using Kriging Method

A vehicle suspension system can be defined as a dynamic model composed of a series of differential equations that describe the motion of system as a function of time *t*. Due to its complexity, the solution of the differential equations that describe a vehicle suspension model can only be obtained by numerical techniques (e.g. Runge-Kutta method). These numerical techniques are often quite computationally expensive.

As defined in the previous section, the definition of the vehicle suspension performance metrics requires the solution of the dynamic system via numerical integration methods. Since the optimisation tool must evaluate these performance cost functions several times (hundreds or even thousands of times) in order to find an optimal solution, the simulation time of the dynamic system will exhibit a great impact in the overall efficiency of the optimisation tool.

In the present thesis, a surrogate modelling technique has been introduced in order to minimise the simulation time of the optimisation tool. Surrogate or metamodelling techniques were first introduced in Chapter 2. These techniques use mathematical and statistical methods to relate model input variables to output variables without the requirement of solving the set of differential equations that describe the behaviour of a particular dynamic system. Metamodels or surrogate models approximate the solution of the cost functions to a mathematical surface dependent only on the input parameters. A surrogate model will therefore substitute the actual dynamic model without any loss of information provided that the surrogate model can replicate with good fidelity the dynamic behaviour of the actual system. Hence, by using surrogate models, numerical integration of the dynamic model is no longer required due to the fact that the variables defined in the search space *Z* are related to the performance cost functions through algebraic equations. Figure 7-9 summarises graphically the advantages of using surrogate modelling for the evaluation of cost functions.

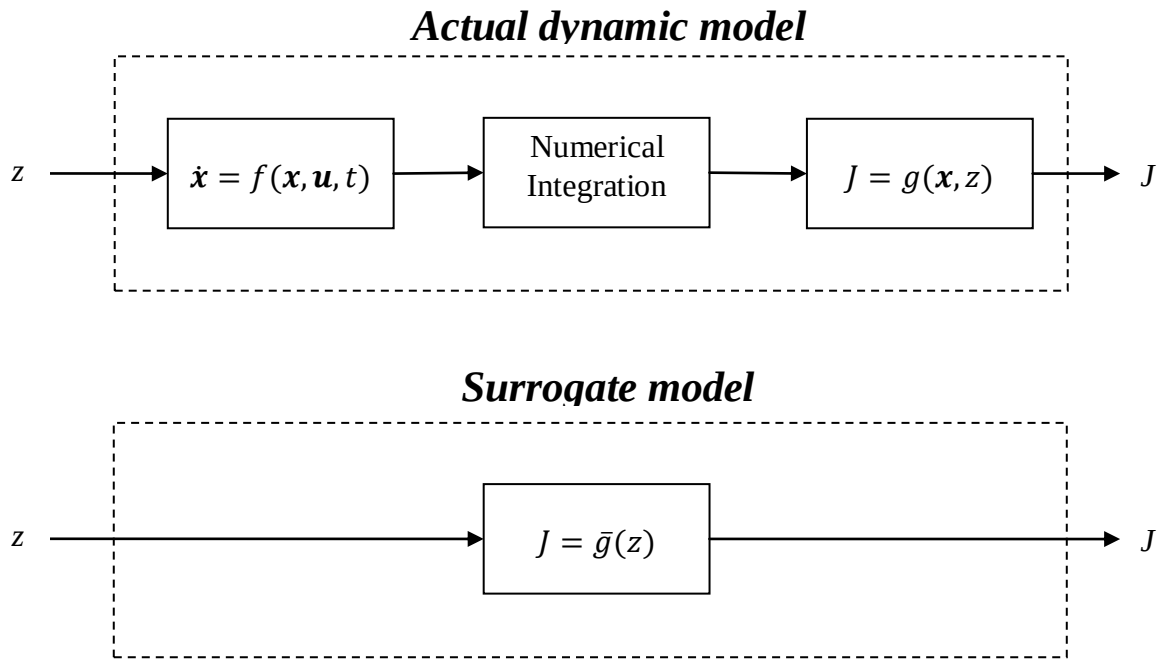

Figure 7-9: Optimisation cost function evaluation through actual dynamic model (upper) and surrogate model (lower)

Regardless of the method utilised to generate approximate models, a finite number of sample points *N* within the search space must be selected. These sample points will be used to create the fitting between the surrogate and original model. In order to efficiently select these points within the search space, a design of experiments (DoE) must be undertaken. Different DoE techniques can be found in literature. In this research work, a Space-filling technique called Latin Hypercube has been used to spread the sample points across the search space.

There are several approaches available in literature for constructing surrogate models (see Chapter 2). In the present thesis, a Kriging metamodelling technique has been used to construct surrogate models for cost functions due to the successful application of this technique in previous studies (Simpson, 1998; Simpson, et al., 2001). Kriging method is a combined model that can be defined as follows:

$$y(\boldsymbol{x}) = f(\boldsymbol{x}) + Z(\boldsymbol{x}) \qquad (7.17)$$

Where ***f(x)*** represents a global approximation of the original function and it is expressed as a polynomial model

$Z(\boldsymbol{x})$ is expressed as a stochastic function that represents localised deviations in between data samples

$\boldsymbol{x}$ represents the input variables

$y(\boldsymbol{x})$ represents the output of the surrogate model

The polynomial function $f(\boldsymbol{x})$ is commonly reduced to a zero-order polynomial function or constant term β (Jin, 2005). The stochastic function $Z(\boldsymbol{x})$ is characterised by zero mean, variance σ^2 and non-zero covariance that can be defined as follows:

$$\mathrm{Cov}\left[Z\left(x^i\right), Z\left(x^j\right)\right] = \sigma^2 \mathbf{R}\left[R(x^i, x^j)\right] \tag{7.18}$$

$i, j = 1, \ldots, N$

Where $\mathbf{R}$ is a NxN symmetric correlation matrix composed of ones along the main diagonal and $R(x^i,x^j)$ is a correlation function between the sample data points i and j. The correlation function can be selected by the user. In this research work a Gaussian correlation function has been used. The Gaussian correlation function can be expressed as:

$$R\left(x^i, x^j\right) = \exp\left[-\sum_{k=1}^{n_s} \theta_k \left|x_k^i - x_k^j\right|^2\right] \tag{7.19}$$

Where θ_k are the unknown correlation parameters used to fit the surrogate model and n_s represents the dimension of the design space x.

In order to test the accuracy of the surrogate model, a simple study has been carried out. A SDOF system has been used to evaluate the performance of a Kriging model. The design space of the analysis is composed by spring stiffness k_s and damping c_s values. Moreover, boundaries to the design space must be set. In this case study, k_s will range from 50 N/mm to 500 N/mm and c_s will range from damping ratio from 800 Ns/m to 15000 Ns/m. Two simple cost functions have been defined: the RMS of the normalised body acceleration and the RMS of the normalised ride height. Both cost functions have been calculated from frequency domain data.

$$J_1 = RMS\left(\frac{\ddot{x}(\omega)}{\ddot{z}(\omega)}\right) \tag{7.20}$$

$$J_2 = RMS\left(\frac{x(\omega) - z(\omega)}{z(\omega)}\right) \tag{7.21}$$

Where $x(\omega)$ and $\ddot{x}(\omega)$ are the body displacement and acceleration in frequency domain

$z(\omega)$ and $\ddot{z}(\omega)$ are the input displacement and acceleration in frequency domain.

A Kriging surrogate model is constructed from the original model using 50 sample points selected through a Latin Hypercube sampling data technique using the built-in MATLAB® function *lhsdesign* (The MathWorks Inc., 2012). Once the metamodel has been built, a set of evaluation points has been selected to evaluate the accuracy of the metamodel with respect to the original model. For brevity at this stage, the evaluation points have been selected such that the damping ratio of the system is always 0.7. Figure 7-10 to Figure 7-12 show the accuracy of the metamodel with respect to the original model. As can be observed, estimation errors are typically below 0.5% across the design space. The estimation error grows to values below 5% at the lower bound of the design space. This suggests that the metamodelling can reproduce the behaviour of the original model with excellent accuracy in regions inside the DoE space and this level of accuracy reduces in regions near the limits of the DoE space.

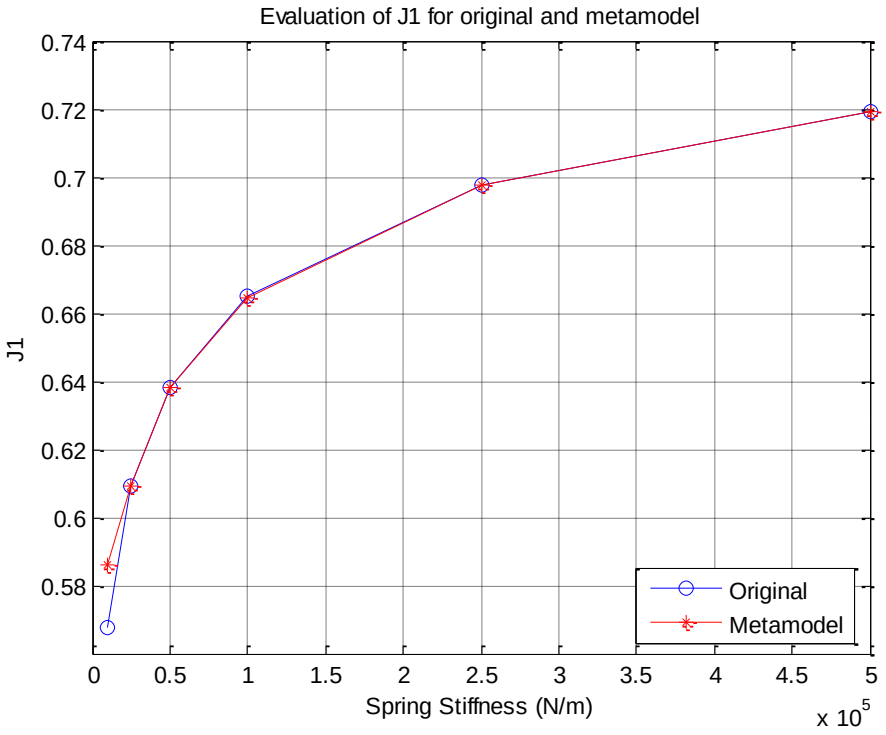

Figure 7-10: Evaluation of the performance of the metamodel in predicting cost function J_1

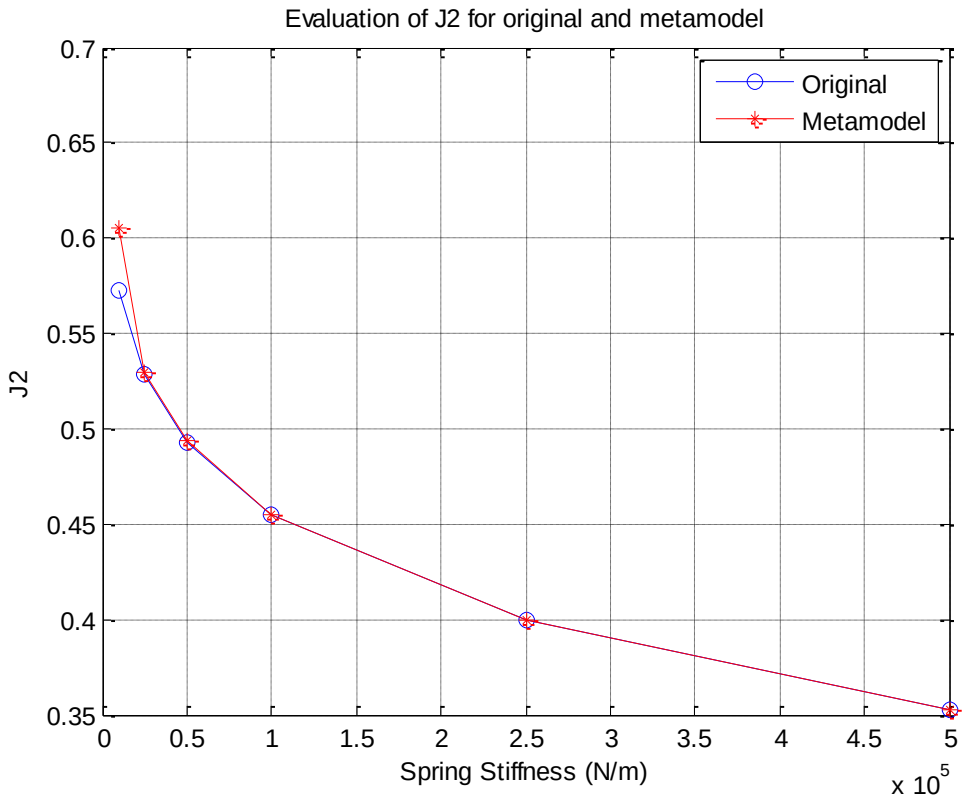

Figure 7-11: Evaluation of the performance of the metamodel in predicting cost function J_2

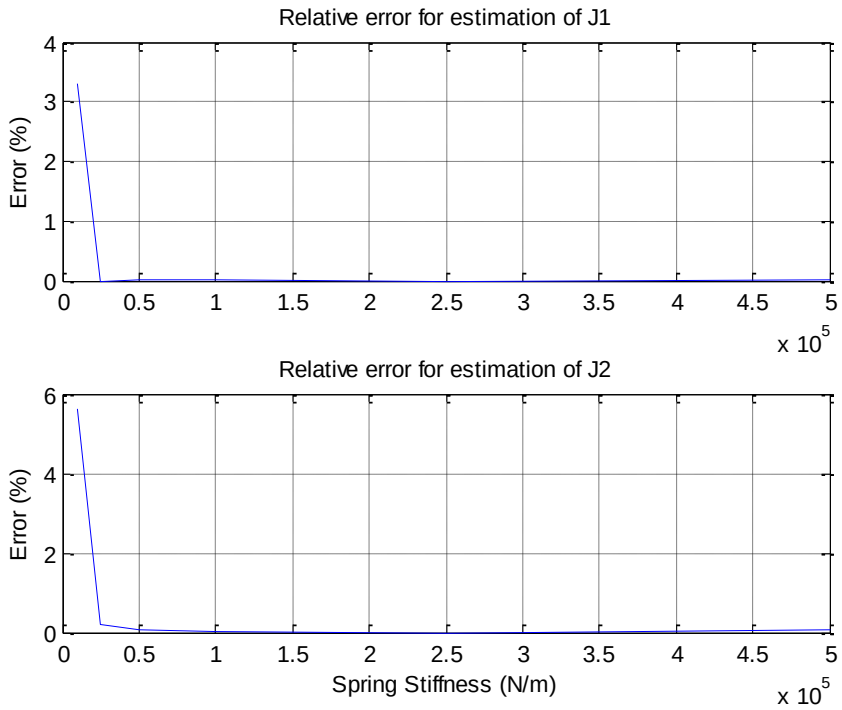

Figure 7-12: Error analysis for estimation of J_1 (upper) and J_2 (lower)

This Kriging technique will now be applied to a more complex case. As explained previously, the evaluation the objective functions developed in section 7.4 requires the numerical integration of the vehicle suspension model developed in Chapter 5. Thus, Kriging metamodelling technique will be used to relate input variables (see section 7.3) to the cost function without the need of the dynamic system.

As explained earlier in this section, a number of sample points must be obtained from the original model in order to construct the surrogate model. The number of sample points used to construct surrogate models affects the accuracy of the metamodel and the construction time. A compromise between accuracy and construction time must be reached. In the present research work, it was found that $n=80$ sample points for objectives J_1 and J_2 and $n=120$ for objective J_3 produced good results in terms of computational time and quality of the metamodel created. 50 analysis points have been randomly selected from the DoE space and objective functions have been evaluated from both the original and the metamodels. Relative errors have been calculated for each point. Table 7-3 summarises the average relative errors and the maximum error obtained for each objective function. As results show, the Kriging metamodelling technique has been able to produce highly accurate surrogate models, with average errors below 0.5 % for objectives J_1 and J_2 and below 2 % for objective J_3. Maximum errors have been also recorded for each objective function: meanwhile maximum errors for J_1 and J_2 are about 1 %, J_3 presents a maximum error of about 5.5 %. As it happened with the simple case study, this error has been obtained for a point lying in a region close to the limits of the DoE space. Thus, in order to avoid errors over 5 %, optimisation search space will contained within the limits of the DoE space.

	Average Error	**Maximum Error**
Objective 1	0.33 %	0.96 %
Objective 2	0.31 %	1.05 %
Objective 3	1.77 %	5.76 %

Table 7-3: Analysis of accuracy of Kriging metamodel for each cost function

Table 7-4 compares construction and simulation times of original and surrogate models for different batches of analysis points $N_{analysis}$. Although simulation time required to evaluate the objectives has been highly reduced with respect to the original model, the additional time required to construct the surrogate models indicates that surrogate models will only be more computationally efficient when large number of objective evaluations are required.

Model	Construction Time	Simulation time		
		$N_{analysis}$=25	$N_{analysis}$=50	$N_{analysis}$=100
Original	-	118 secs	237 secs	466 secs
Kriging surrogate	362 secs	0.005 secs	0.011 secs	0.018 secs

Table 7-4: Summary of computational time of original and metamodel for batch simulation

Furthermore, a multiobjective optimisation process has been carried out for both the original and the surrogate cost functions. Although the optimisation solver used in this case study will be described in the following section, it has been used to demonstrate the efficiency and accuracy of the Kriging method. The main optimisation parameters set for this case study are:

- Initial population: 50 individuals
- Maximum number of generations: 25

Moreover, the hybrid algorithm has been set in sequential mode, i.e. the results of the MOEA are then fed into the local SQP algorithm. Figure 7-13 shows the results of the suspension optimisation. Note that for clarity only mechanical grip (Objective 1) and aerodynamic grip (Objective 2) performance metrics have been plotted.

Figure 7-13 show the estimation of the Pareto optimal front. As it can be observed, the prediction of the Pareto optimal front obtained via the metamodel presents a good correlation with respect to the Pareto front obtained via the original. Although the scattered points do not fall into exactly the same places, the trend is very similar. A maximum error of 1.5% has been calculated in the estimation of the Pareto front.

In addition to this, the computation times for optimisation via original and metamodels have been recorded. Table 7-5 summarises the total time required to obtain the solution to the optimisation problem shown in Figure 7-13. Although some time is required to build the surrogate models, the actual optimisation time has been highly reduced with respect to the original model. Hence, by the use of a Kriging surrogate model, the overall optimisation process runs over 15 times faster than the original model.

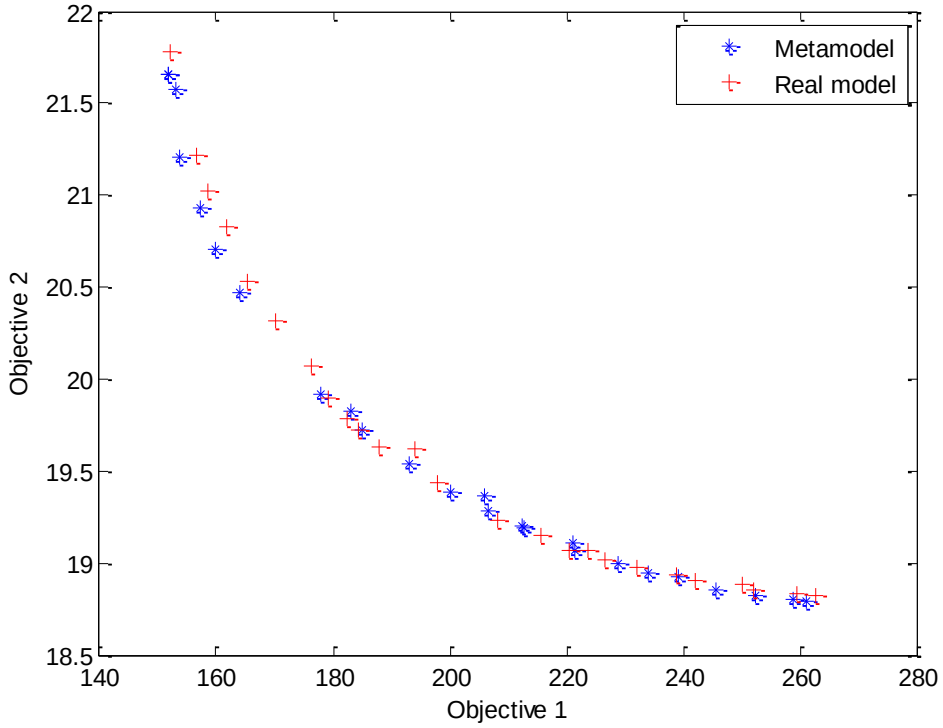

Figure 7-13: Cost function comparison between metamodel and original vehicle suspension model

Model	Construction Time	Optimisation Time	Total Time
Original	-	5988 secs	**5988 secs**
Kriging surrogate	362 secs	13 secs	**375 secs**

Table 7-5: Summary of computational time of original and metamodel for optimisation

7.5.2. Multi-Objective Algorithm

Racing car suspensions present an important role in the performance of the vehicle due to the interaction with tyres and aerodynamics. Furthermore, due to the multiple goals a racing car suspension must achieve in order to maximise the performance of the vehicle, in section 7.2, the suspension optimisation problem was defined as a Multi-Objective Optimisation problem (MOOP). In this section, an optimisation tool capable of solving suspension MOOP is presented.

This MOOP requires a solution method capable of optimising several conflicting objective functions simultaneously. Several optimisation methods have already been reviewed in Chapter 2. Multi-objective Evolutionary Algorithms (MOEAs) are well-suited for obtaining a set of solutions when several conflicting objectives are to be optimised. A vast variety of MOEAs can be found in literature. In this research work, an elitist non-dominated sorting

genetic algorithm (NSGA-II) has been selected as core optimisation method due to the increased computational efficiency and enhanced ability of finding the true Pareto optimal front over other MOEAs (Deb, et al., 2002).

Although it is outside the scope of this thesis to describe in detail the working principle of MOEAs, the main features of the NSGA-II optimisation tool used in this research work can be summarised as follows:

- It is a rank-based EA: individuals in the population are ranked according to the fitness score and sorted into non-dominated layers.
- It is an elitist EA: A sub-set of the best individuals of each generation is transferred to the following generation unaltered.
- It uses a crowded comparison operator in order to maintain diversity along the Pareto optimal line.
- A Tournament selection method has been used in the selection stage.
- A simulated binary crossover (SBX) operator has been used in the mating stage.
- A polynomial mutation technique has been used in the mutation stage.

Moreover, EAs are unlikely to find the true Pareto optimal solution due to the stochastic nature of their search engine. Hybrid techniques can therefore be used to overcome this problem (Deb & Goel, 2001). By using this hybrid technique, the results of the MOEA are fed into a local convergence search method, generally a gradient-based algorithm, so that true Pareto optimal solutions can be obtained. This hybrid algorithm combines the ability of finding a near true Pareto optimal front in only one optimisation run with the strong local convergence of gradient-based algorithms. In this research thesis, the NSGA-II has been coupled with a Sequential Quadratic Programming (SQP) algorithm.

As depicted in Figure 7-13, due to the conflicting nature of the objective functions, the outcome of this optimisation process is a set of non-dominated optimised suspension setups (Pareto Optimal front). This means that the suspension optimisation problem is underdetermined, i.e. there are several solutions to the problem. However, since current racing regulations do not allow any suspension tuning during racing events, a single solution must be selected among the Pareto front. In order to select an optimal solution from the Pareto front, additional information of the vehicle is required. This information can be obtained from different sources, from CAE simulation tools to race engineer´s experience.

The process of acquiring information and using it to find a single optimum is known as decision making process (Deb, 2001). In this research work, a novel decision making technique based of lap-time simulation has been developed. The following section describes the process by which a LTS can be used to objectively obtain a particular solution from the Pareto set.

7.5.3. Decision Making Process via the use of Lap-time simulation

The process described above provides a set of optimal non-dominated solutions. Each of the solutions contained in this optimal set offers no improvement in all objectives functions simultaneously. Thus, a decision making process must be enabled in order to select a single-point solution from the optimal set. The decision making process must be fed with additional information that has not been already contained in the mainstream of the optimisation process. This decision making process often contains a certain level of subjective information and it is not well defined and documented, e.g. a race engineer may use his experience and driver feedback to act as the decision maker of the suspension optimisation process.

The aim of the research process is to define an objective decision maker based in data obtained from simulation techniques. In order to account for all the additional information not contained in the suspension optimisation process, the LTS developed in Chapter 6 will be used as decision maker for the optimisation process.

The ultimate goal of any racing car is to complete a lap in shortest time possible. Hence, the decision maker must find a particular suspension setup within the Pareto set that optimises the final lap time. The approach in this research work is to cluster the solutions of the Pareto front into a number of finite solutions and a direct search algorithm is used to find the single optimal solution: each suspension setup from the clustered set is fed into the LTS and a lap time is obtained. The suspension setup that minimises lap time on a particular circuit will be the single optimal solution.

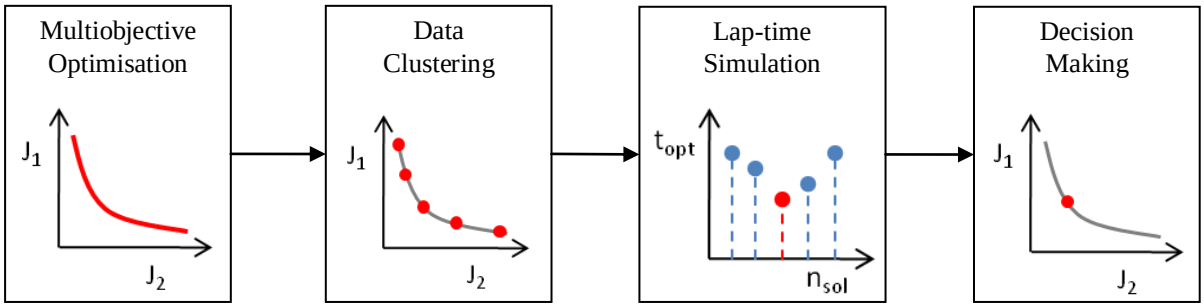

Figure 7-14: Decision Making Process

LTS compiles data from different systems that integrate the vehicle and environmental factors to analyse the ultimate performance of a race car on a particular car. Depending on the level of LTS complexity, more information not strictly contained in earlier stages of the optimisation process (track surface, track layout, aeromaps, tyre maps, suspension kinematics, etc.) could be used to find the final optimal solution. In addition to this, LTS allows the analysis of the impact of suspension dynamics in other vehicle subsystems such as steering, suspension kinematics, aerodynamics, etc.

The next section uses the optimisation process explained in this section in order to obtain an optimised suspension solution.

7.6. Case Study

In this section, the optimisation process depicted in Figure 7-8 and described in previous sections has been applied to a practical case study. Two vehicle suspension layouts have been analysed: a conventional suspension layout and a suspension featuring real inerters. In the first sub-section, the main parameters required to set up the optimisation process are defined; and in the second sub-section, results of the optimisation process for each suspension layout are presented and discussed.

7.6.1. Optimisation Process Set-up

Recalling Figure 7-8, the inputs of the optimisation process are:

- Vehicle suspension model
- Optimisation search space
- Performance cost functions

First, the validated vehicle suspension model developed in Chapter 5 has been used as input to the optimisation process (see Figure 5-21). This model can be featured to analyse both conventional suspensions and suspensions with inerters. In the case of a conventional layout, the inerter model branch can be eliminated by setting inerter and damper values to 0 (open-circuit) and stiffness values to 1 (short-circuit).

Secondly, the optimisation search space has been composed by front and rear axle damper and inerter values (see section 7.3). In the case of conventional suspension layout, the search space reduces only to 2 variables: front and rear damping coefficients. The range of the design space can be summarised in the following table:

	Lower Bound	**Upper Bound**
Front damping (Ns/m)	850	3500
Rear damping (Ns/m)	850	3500
Front inertance (kg)	1	40
Rear inertance (kg)	1	40

Table 7-6: Limits of the optimisation design space

The limits have been set so that a vast variety of suspension settings could be analysed by the optimiser. Damping limits cover from a lightly damped suspension setting ($\zeta \approx 0.25$) to a heavily damped suspension setting ($\zeta \approx 1.2$). Accordingly, inertance values have been set to range from an inertance-to-weight ratio of 0.01 to an inertance-to-weight ratio of about 0.75. Note that, in the case of conventional suspension layout, front and rear inertance will be set to 0 and front and rear damping limits will remain unchanged.

Thirdly, cost functions for mechanical grip, aerodynamic grip and mechanical balance (see section 7.4) have been used as target in the optimisation process for both suspension cases.

As explained in section 7.5, metamodels for all three performance cost functions have been built. These surrogate models can be effectively used in substitution for the original objective metrics. In order to improve the accuracy of the surrogate model within the range of the optimisation design space (see Table 7-6), larger limits have been defined to construct the DoE space. The limits of the DoE space can be summarised in Table 7-7.

	Lower Bound	Upper Bound
Front damping (Ns/m)	750	4000
Rear damping (Ns/m)	750	4000
Front inertance (kg)	0	45
Rear inertance (kg)	0	45

Table 7-7: Limits of the DoE space

Once metamodels for all cost functions have been successfully created, next step is to run the hybrid multi-objective optimiser described in section 7.5. Table 7-8 shows the main parameters required to set the MOEA.

Population size	100
Generations	100
Elite fraction	10 %
Crossover function	80 %

Table 7-8: MOEA setting parameters

Solutions of the multi-objective optimisation stage are then clustered into a limited number of discrete solutions. In this case study, it has been decided that, for each suspension layout, 10 solution points will be created and uniformly scattered across the Pareto Optimal surface. According to the level of detail the user is trying to achieve, more points could be selected. These solution points will then be fed into the decision making process where each suspension layout will be tested on the LTS developed in Chapter 6. The LTS has been determined according to the following points:

- Only suspension parameters will be tuned during the decision making process.
- The vehicle model presents the same parameterisation as in the case study presented in Chapter 6.
- The Bahrain International GP Circuit has been used as race track.
- The parameters required to set up the lap-time simulation remain unchanged (see Chapter 6).

The following section presents and discusses the results of the optimisation process.

7.6.2. Optimisation results and discussions

The first gateway of the optimisation process is the solution of the multi-objective stage. After the application of the MO optimiser, a set of non-dominated optimal solutions has been obtained for a conventional layout (L1) and for a suspension with inerter layout (L2). The results of the multi-objective optimisation stage are shown in Figure 7-15 and Figure 7-16. Figure 7-15 shows the 3D Pareto Optimal surface generated by the interaction of the three objective metrics. As can be observed, the shape and location of the optimised surface drawn for each suspension layout are quite different: on one hand, the cloud of optimal solutions is located in different regions within the objective space. Due to the way in which the objective functions have been defined (minimisation cost functions), solution points closer to the origin represent optimised solutions with respect to points further away for the origin. In this case study, L1 and L2 clouds intersect each other, which indicate that one layout will offer enhanced suspension performance on a particular objective with respect to the other layout. On the other hand, both layouts present a convex Pareto surface, which means that the performance functions are conflicting between each other. However, the Pareto surface for layout L2 is sparser than for L1. Although, the shape of the Pareto contour is similar in a J1-J2 2D view (see Figure 7-16), the sparsity is quite different in the other to views. This suggests the suspension layout could alter the interaction between objectives.

Figure 7-16 presents in more detail the particular one-to-one interactions between objectives for both suspension layouts. Arrows depict the principal direction of increasing damping and inertance values. As the graphs demonstrate, for both layouts, there is a principal conflicting interaction between mechanical grip J_1 and aerodynamic grip J_2 observable for both layouts. However, some differences can be noticed between suspension layout optimisation results: firstly, optimisation with suspension layout L1 offers improved mechanical grip solutions with respect to layout L2. The reason for this is that inerters induce an increase in dynamic tyre load variations at high frequencies due to a less controlled hub vibration mode, especially with low damping configurations. Secondly, as damping increases, the use of inerters represents an improvement over conventional suspensions: high damping coefficients can cause suspension locking-up (i.e. negligible relative motion between sprung and unsprung masses) and therefore this effect induces an uncontrolled tyre vibration mode. Inerters reduce the effective damping ratio (see Chapter 3) and enhance the control of the tyre mode. Furthermore, the combined use of high damping and inertance produces a sensible improvement in aerodynamic grip.

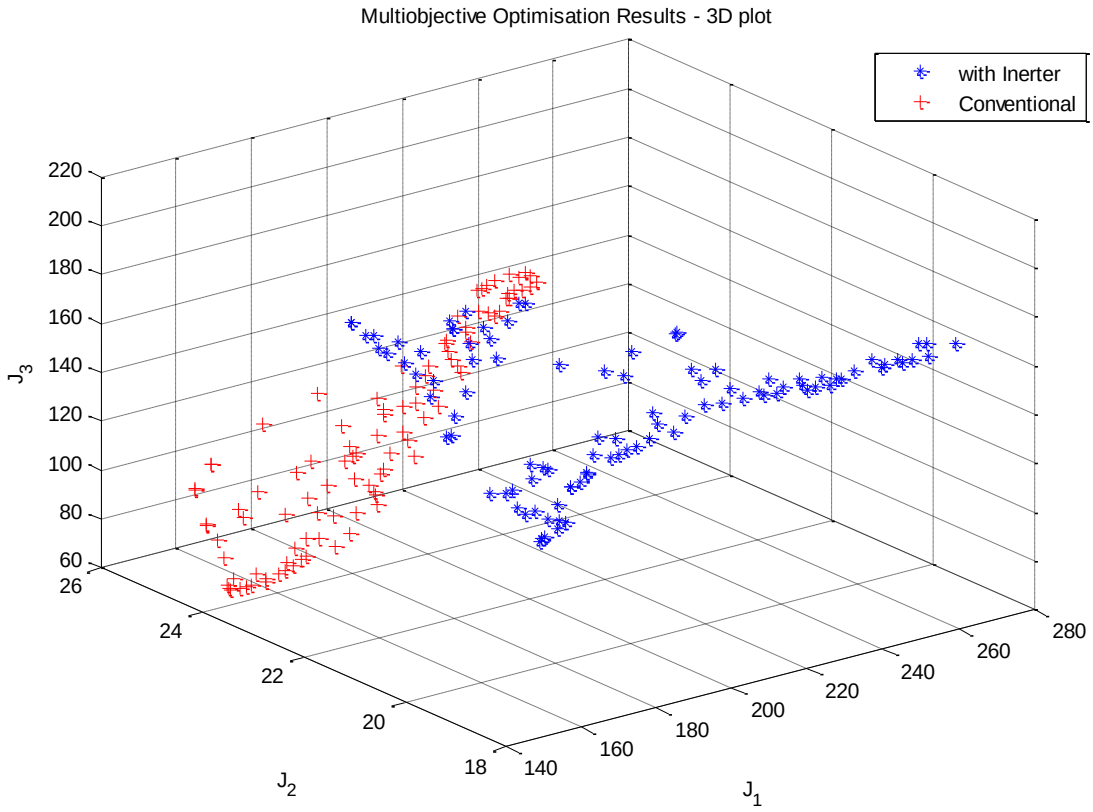

Figure 7-15: Suspension multiobjective optimisation results – 3D Plot

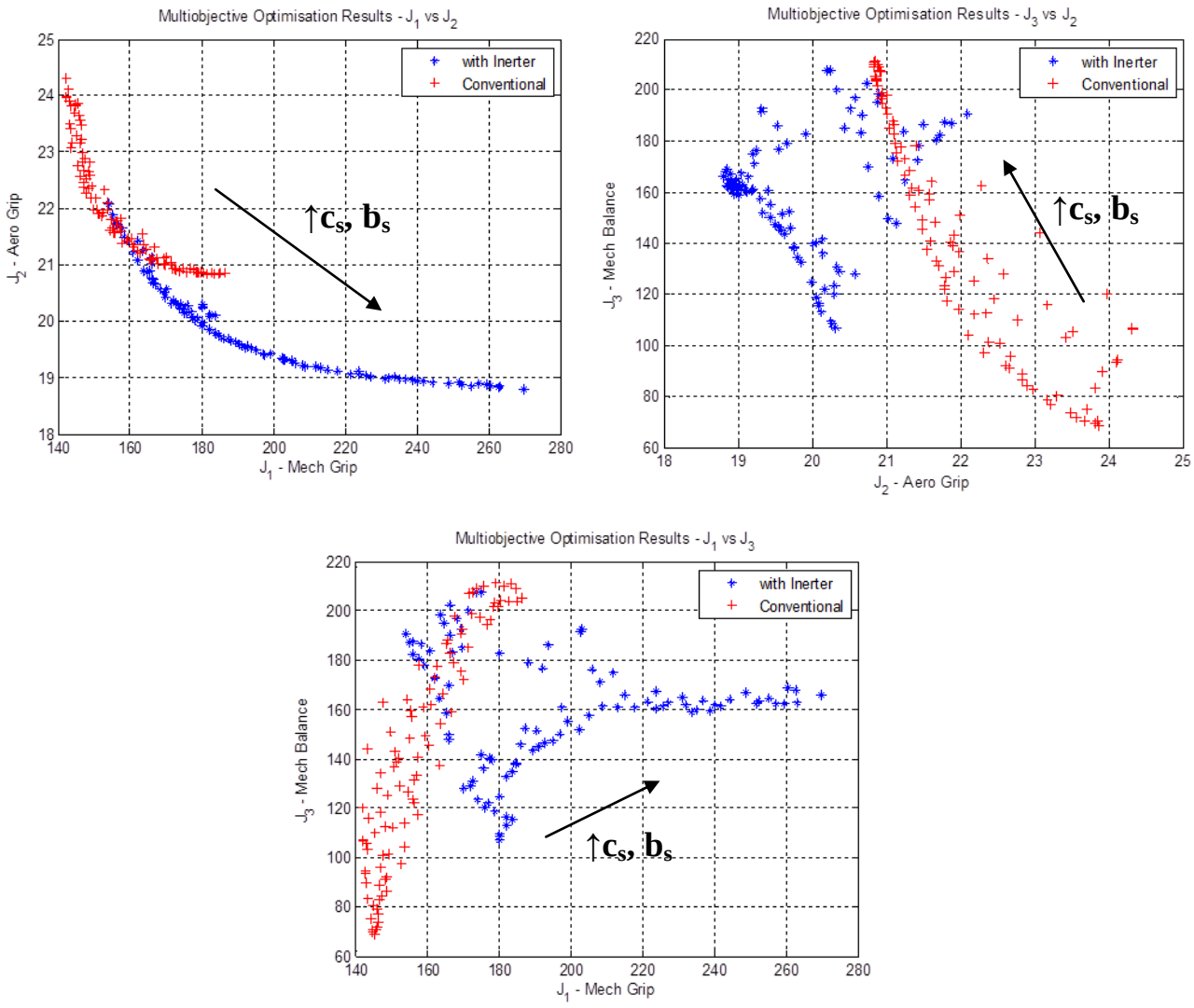

Figure 7-16: Suspension multiobjective optimisation results – 2D plots

The set of optimal suspension presented in the previous figures will be now used as input decision making process. As explained previously, the Pareto surface must be clustered into a reduced number solution points. In this particular case study, 10 uniformly distributed solution points have been selected for each layout. Figure 7-18 and Figure 7-17 show graphically the distribution of the selected solution points in the objective space for L1 and L2 suspension layouts respectively. Table 7-10 and Table 7-9 relate each solution point selected with a determined suspension setting.

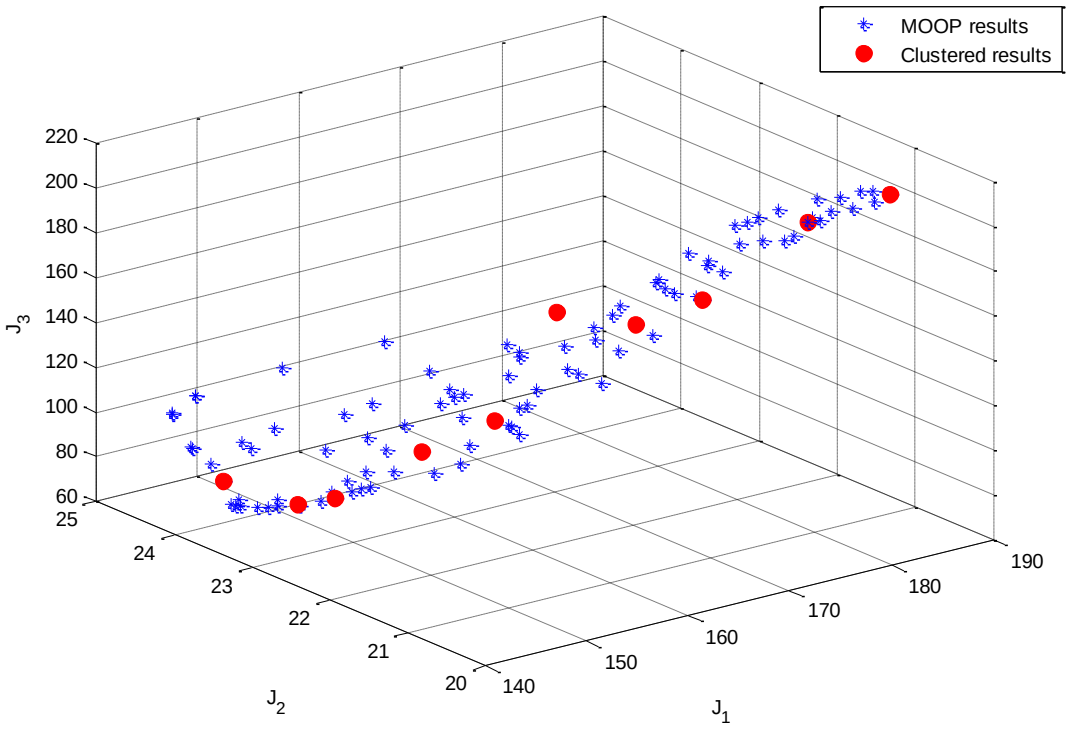

Figure 7-17: Clustered results for MO results – Conventional suspension

Solution point	Front damping (Ns/m)	Rear damping (Ns/m)
1	909	1208
2	1010	1420
3	1067	1516
4	1301	1581
5	1449	1741
6	1845	1523
7	1810	2008
8	1937	2251
9	2465	2218
10	2826	2345

Table 7-9: Summary of clustered optimised suspension settings – Conventional suspension

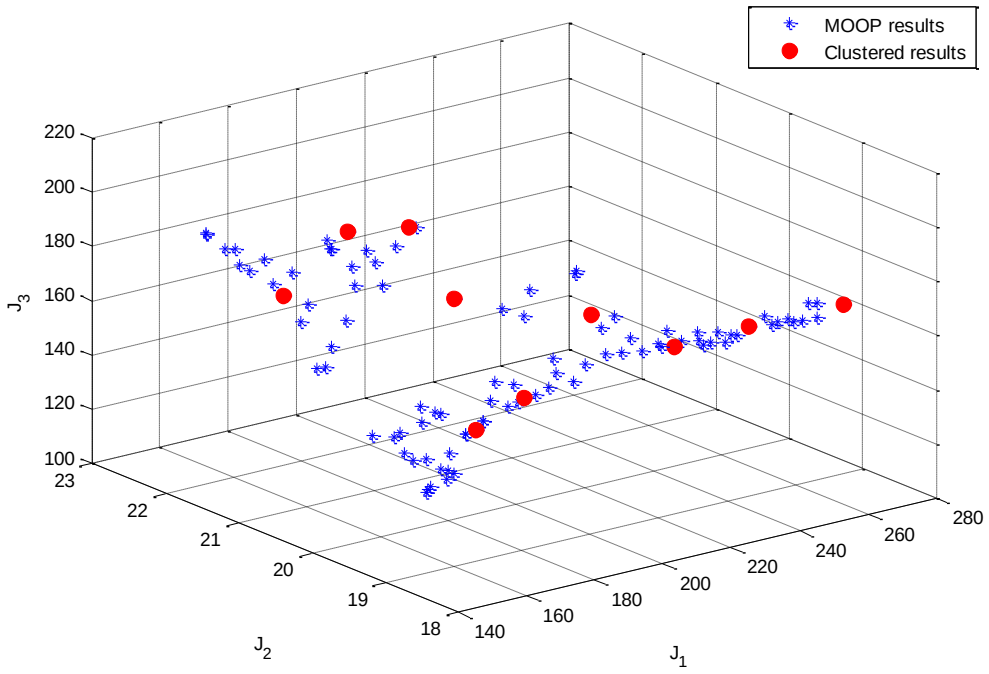

Figure 7-18: Clustered results for MO results – Suspension featuring inerters

Solution point	Front damping (Ns/m)	Rear damping (Ns/m)	Front inertance (kg)	Rear inertance (kg)
1	976	1272	3.8	4.7
2	1423	1228	6.6	1.3
3	1872	1229	9.8	1.5
4	2062	1489	10.5	4.4
5	2091	1687	7.6	10.2
6	2238	1730	10.8	13.1
7	2814	2009	16.6	13.6
8	2822	2307	18.1	23.8
9	2814	2353	22.1	28.9
10	2863	2752	26.6	36.3

Table 7-10: Summary of clustered optimised suspension settings – Suspension featuring inerters

Finally, the last stage in the optimisation process is to set each suspension variant in the virtual vehicle model and perform the lap-time simulation. The process has been repeated for both suspension layouts and optimal lap time has been recorded for each test run. Table 7-11 summarises the lap time recorded for each suspension variant.

Solution point	Optimal Lap time	
	Conventional	**With Inerters**
1	1’25’’856	1’25’’384
2	1’25’’691	1’25’’221
3	1’25’’687	1’25’’106
4	1’25’’442	1’24’’730
5	1’25’’354	1’24’’844
6	**1’25’’252**	1’24’’880
7	1’25’’340	1’24’’699
8	1’25’’481	1’24’’601
9	1’25’’559	**1’24’’573**
10	1’25’’703	1’24’’632

Table 7-11: Summary of lap times for both suspension layouts

As expected, suspension dynamics has an impact in the overall performance of the vehicle. Table 7-11 optimal suspension parameters for both suspension layouts are driven predominantly by the minimisation of objective J_2. This is due to the fact that the vehicle model represents a high aerodynamic performance racing car. Therefore maximising the aerodynamic performance of the vehicle is critical in the overall performance of the race car. Thus, minimisation of the dynamic ride height variation leads to a more stable aerodynamic platform which leads to a higher average downforce coefficient.

Furthermore, a crossing point between J_2 and J_1 can be found for both suspension layouts: solution point 6 for L1 and solution point 9 for L2. Beyond these crossing points, reductions in mechanical grip outweighs the improvements in aerodynamic grip. This is due to several factors: first, the differential improvement in aero grip due to higher damping and inertance settings tails off; secondly, the load sensitivity characteristic of the tyre changes with speed, i.e. the region around the nominal load for low vehicle speeds is more linear that the region around nominal loads at high vehicle speeds (see Figure 7-19). This means that the reduction on lateral and longitudinal force production due to dynamic load variation at high speeds will be higher than at low speeds the effect of load variation will cause a larger impact at higher speeds.

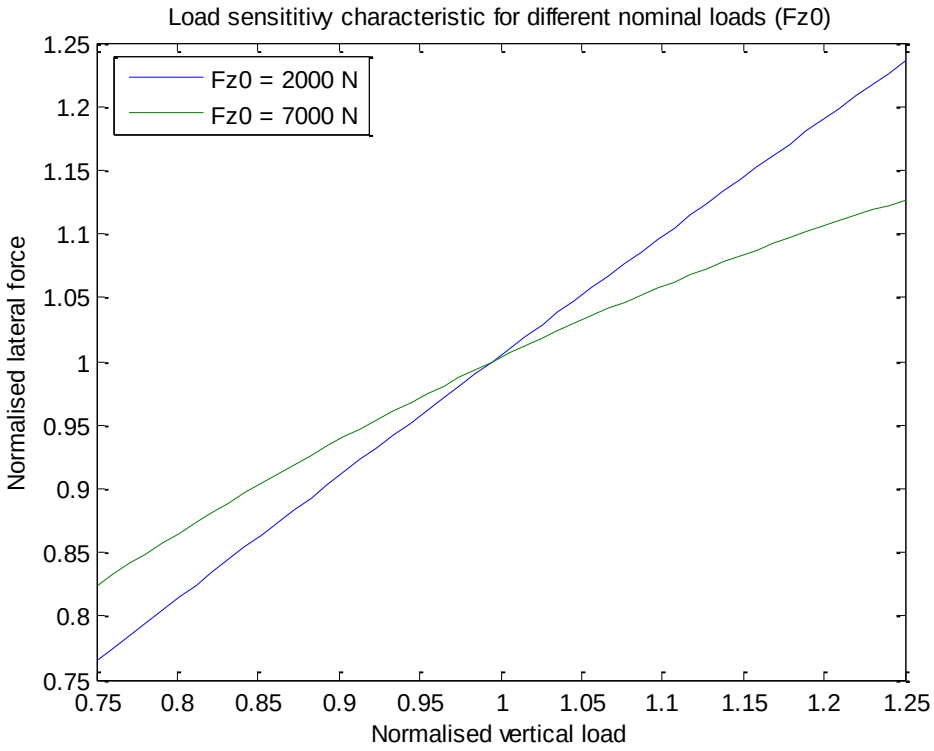

Figure 7-19: Difference in load sensitivity around

Moreover, the effects of mechanical balance can be noticed in lap times obtained for layout L2. Suspension settings 5 and 6 produce large values of J_3, i.e. poor balanced suspension. Even though, the aero grip has been improved with respect to previous suspension settings (3 and 4 suspension settings), this poorer mechanical balance between front and rear axle causes a slower lap times.

Finally, lap times obtained for layouts L1 and L2 must be compared. Table 7-11 shows that the suspension setting featuring inerters consistently achieves improvements in lap time with respect to the conventional suspension layout. This is due to the increased aerodynamic grip obtained by suspension layout 2 with respect to layout 1. Furthermore, in general suspension layout L2 achieves better mechanical balance than L1. Figure 7-20 and Figure 7-21 compare a section of the lap-time simulation carried out for the best L1 and L2 suspension configurations (see Table 7-11). Figure 7-20 shows that race car L2 can take a tighter racing line around turn 4 than L1 and the driver need not slow down so much to take the corner (see Figure 7-21) due to the increase in aerodynamic grip and mechanical balance provided by the suspension featuring inerters.

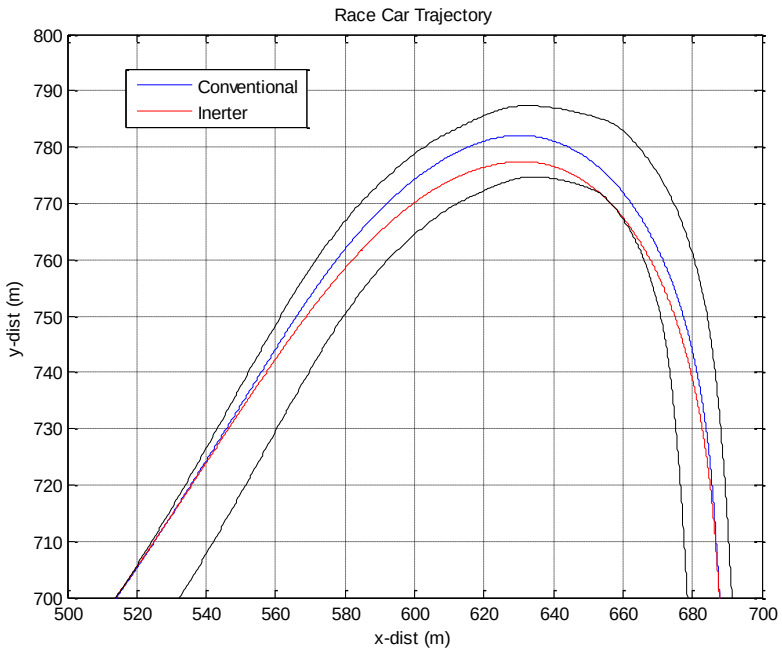

Figure 7-20: Race car trajectory for different suspension layouts at Turn 4

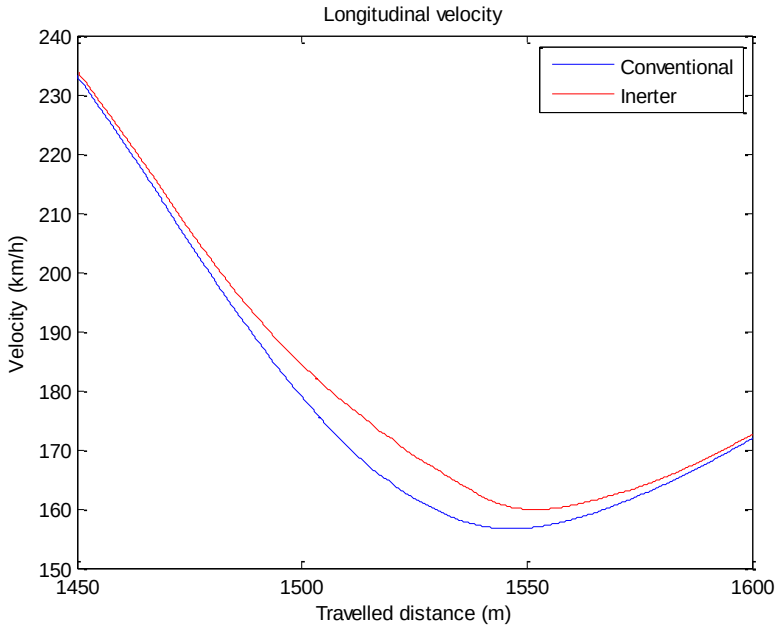

Figure 7-21: Race car speed trace for different suspension layouts at Turn 4

These suspension improvements translate into an overall gain of around 0.7 seconds on a single lap. In current Formula 1, this time gain could lead a race car from 9th position on the grip to pole position on a qualifying session. Hence, this improvement in lap time highlights the importance of optimising suspensions for performance and the benefits of integrating inerters within the suspension system.

7.7. Summary

In Chapter 7, the problem of suspension optimisation has been defined as a multi-objective optimisation problem. Definition and discussion of both search (design variables) and objective space (performance cost functions) have been carried out. A novel multi-stage suspension optimisation methodology based on a virtual environment has been developed. Finally, this method has been applied to obtain the optimal suspension setup of a race car for two suspension layouts. This optimisation method has successfully provided suspension solutions that maximises overall vehicle performance. Furthermore, results of the optimisation process have shown that the use of inerters leads to significant improvements in lap time (ultimate race car performance) with respect to conventional suspension layouts. The main reason for this improvement is the enhanced aerodynamic platform and the improved dynamic stability that can be achieved by the use of inerters.

It is also important to note that the main advantage of this optimisation methodology resides in that fact that, even though external factors such as race track layout or aerodynamic package will not affect the results obtained at the multi-objective stage, the selection of the final solution will be conditioned by these factors. It is therefore expected that, under different conditions such as a low-speed corner track layout and/or low downforce configuration, the optimal suspension obtained from the optimisation process would have been different from the one obtained in this case study. Hence, this methodology offers a multi-level suspension optimisation procedure in which suspension dynamics are analysed in isolation on a first level and then, complex interactions with the rest of vehicle systems are integrated to evaluate the overall performance of race car.

This novel optimisation procedure also provides enhancements in the design and development times of racing car suspension systems. Suspension solutions from the Pareto front obtained as a result of the multi-objective optimisation stage can be used to create a suspension setting database. Provided that no major changes are made in the fundamental design of the suspension throughout a season, suspension designers could use this database as baseline so that only final decision making process would be required in order to obtain the optimal suspension setting for each particular event.

The next chapter summarises the achievements and original work in this research thesis, and summarises some recommendations for future work.

8. Conclusions and Future Work

8.1. Summary of the Objectives Achieved

A formal method for optimising racing car suspension featuring inerters has been developed. The key features of this method are the use of an experimentally validated model of a race car suspension incorporating real mechanical inerters, the development of a robust and efficient optimisation methodology based on multi-objective optimisation, surrogate modelling and lap-time simulation and the definition of performance based suspension objective functions.

In Chapter 3, the dynamic behaviour of ideal inerters in a SDOF system has been characterised. The conclusions of this theoretical analysis enhanced the current understanding of the impact of the use of inerters on the dynamics of a vibratory system. The study also drew some suggestions on how inerters could be used to improve the ride dynamics of a vehicle suspension.

In Chapter 4, the design of a race car suspension fitted with real inerters has been carried out. A ball-screw-type inerter was decided as design solution due to its design simplicity. Moreover, the chassis frame and suspension system of a Formula Student car has been modified and re-designed in order to accommodate all new suspension components including the inerter devices. This vehicle has been used as test car in a 4-post rig test facility in order to estimate vehicle parameters and to validate the vehicle suspension model developed in Chapter 5. In order to properly acquire and estimate all the parameters of the test vehicle incorporating real inerters, the parameter estimation software developed by Bennett (2012) has been extended in order to account for the estimation of the vehicle suspension parameters including real inerters and the definition of additional to dynamic frequency responses such as front and rear ride height variation and dynamic longitudinal weight distribution variation.

In Chapter 5, a dynamic vehicle suspension model incorporating real inerters was developed. This novel vehicle suspension model accounted for linearised suspension parasitic effects such as suspension compliance, damper hysteresis and elastic and friction effects on the inerter. Moreover, in order to accurately represent the tyre dynamic behaviour experienced due to higher tyre deflections present with suspension systems incorporating inerters, a nonlinear tyre model was developed in relation to the measured data obtained from 4-post rig testing. Experimental data obtained from 4-post rig testing was used to evaluate the accuracy

of this model. A wide range of inerter settings were tested from light to heavy inertance characteristics. Results showed that the vehicle suspension model incorporating real inerters and a nonlinear vertical tyre model was capable of accurately replicating the dynamic behaviour of the real vehicle for all the test cases proposed. Moreover, this vehicle suspension model was used to perform a virtual optimisation in order to evaluate the predicting capabilities of the model. The predicted suspension settings obtained from the optimisation were used to set the suspension of the test car and experimental test was carried out on the 4-post rig. Results showed that the vehicle suspension model successfully predicted optimised suspension settings for two different performance objective functions.

In Chapter 6, a transient lap time simulation tool was developed. Based on work undertaken by other authors (Casanova, 2000; Kelly, 2008), the problem of minimising lap-time around a given track became one of calculating the minimum time for manoeuvring using Optimal Control. Issues and limitations of classical techniques of the previous research works (Casanova, 2000; Kelly, 2008) in the development of transient lap-time simulation tools were addressed, and a novel solution technique based on a multi-level optimisation algorithm and closed-loop driver steering has been developed. Furthermore, a full vehicle dynamic model that incorporates the suspension model developed in Chapter 5 has been formulated. A case study was carried out in order to evaluate the performance of this novel lap-time simulation tool. A racing car model was forced to produce the fastest lap time around Bahrain International GP Circuit. Results of the simulation demonstrated the efficiency and robustness of the LTS solver.

Chapter 7 dealt with development of a novel suspension optimisation methodology. In order to optimise the overall performance of a vehicle, suspension systems must successfully achieve a number of goals simultaneously. Hence, due to the multi-criteria nature of suspension design, the suspension optimisation problem was defined as a multi-objective optimisation problem (MOOP). In this research work, suspension objective functions were defined so that these functions express the impact of ride dynamics on the handling and overall performance of the vehicle. Objective functions representing mechanical grip, aerodynamic grip and understeer characteristic were developed. An NSGA-II evolutionary algorithm was selected as the core search engine for optimisation, due to its suitability to solve MOOPs. Computational efficiency and ability of finding the true optimal solution issues were addressed. Solutions to these issues were proposed. Firstly, it was identified that the numerical integration of the dynamic system every time the optimiser evaluates the

objective function caused the largest impact on the overall computational efficiency of the optimisation process. A Kriging metamodelling technique has been used so that the performance based objective functions are approximated to a more computationally efficient mathematical model than the original dynamic model. A good correlation was found between the results estimated by the metamodel and the actual results produced the original model. The use of this surrogate model based optimisation technique successfully reduced the computational time by over 90% of the optimisation time with the original vehicle model. A Sequential Quadratic Programming (SQP) algorithm was coupled with the Multi-Objective Evolutionary Algorithm (MOEA) to ensure that true optimal solutions were found. Two case studies were analysed in the chapter: a conventional suspension and a new suspension incorporating inerters. Results of this optimisation process showed that, due to conflicting interactions among objective functions, the solution of the optimisation problem was underdetermined, i.e. no single optimal solution was found. Instead of this, a trade-off of optimised solutions were found (Pareto Optimal front). In order to find a single optimal solution additional information was required. Hence, the lap-time simulation tool developed in Chapter 6 was used to transform the underdetermined suspension optimisation problem into a determined one. Solutions from the Pareto Optimal front obtained for both case studies from previous stages of the optimisation process were introduced into the LTS. Results showed that the suspension system incorporating inerters yielded important improvements in the overall performance of the race car. It was demonstrated that the use of inerters contributed to enhance the dynamic aerodynamic platform and to improve the overall stability of the race car (less front-to-rear dynamic balance variations).

Results from the optimisation process show that the use of mechanical inerters in a racing car suspension could theoretically produce performance gains of about 6 to 7 tenths of a second over one lap. Although this might look like a very small gain in comparison to the overall lap time (~ 85 secs), due to the competitive nature of the Motorsport industry, this gain could mean a jump of between 7 and 10 positions on a qualifying session according to current F1 standards.

8.2. Recommendations for future work

This research work has developed a formal method for optimisation of race car suspensions featuring inerters. The dynamic behaviour of inerters in mechanical systems has been investigated and an experimentally validated suspension model has been developed. While

this thesis has yielded a few significant conclusions and contributions to the field of suspension design and optimisation, further work would be highly desirable for improved suspension performance with the use of passive elements. The recommendations for future work are:

- Enhancement of inerter technology: the dynamic analysis carried out in this research thesis suggests that the use of complex inerters with nonlinear characteristics could bring further improvements to suspension performance. Complex design solutions could create an inerter that offers high inertance at low frequencies for optimal body control and lower inertance at high frequencies for improved vibration at higher frequencies. Moreover, a hydraulic inerter could be designed to create additional damping effects as well as inertial effects, thereby improving the packaging and the weight of the suspension.
- Development of a nonlinear suspension model incorporating real inerters: in this research work, the vehicle suspension was modelled as a transfer function *G(s)*, that accounts for linearised suspension component characteristics and linearised parasitic effects. Although it showed good correlation with experimental data, it could not replicate accurately enough highly nonlinear suspension properties such as bump stop characteristics or highly nonlinear damper characteristics. Comprehensive modelling of these characteristics would increase dramatically the complexity of the model and this would reduce its computational efficiency. Alternatively, the suspension could be modelled as a time-varying transfer function. In this way, the suspension is still defined as an instantaneous linear model and suspension nonlinear parameters could be passed as pre-calculated look-up tables.
- Inclusion of suspension kinematics into the vehicle model: a validated vehicle suspension model including kinematics could expand the range of analyses carried out with the methodology developed in the thesis. The impact in vehicle performance of kinematic variables such as tyre camber angle could be included as part of the optimisation process. The kinematic suspension variables could be used to expand the performance based objective functions in order to produce a complete optimisation of a race car suspension.
- Development of a more comprehensive nonlinear tyre model for ride analysis: although the nonlinear semi-empirical tyre model developed in Chapter 5 showed good correlation with experimental data, it cannot replicate nonlinear effects such as

hysteresis. A more comprehensive tyre model is expected to improve the correlation with the vehicle model. Furthermore, tyre thermal and wear effects could be introduced into this nonlinear tyre model. It is well known that tyre performance is subjected mainly to wear condition and temperature and pressure changes. A model that accounts for these effects could be used to develop a race simulator.

- Application of inerter technology into production vehicles. Although the main focus of this research work has been high performance racing applications, most of the work developed could be directly applied to road cars. The development of advanced passive suspensions featuring inerters could improve the comfort and safety capabilities of production road cars without the expense of complex active suspension systems.

References

Abdelhady, M. B. A., 2002. Aerodynamic Effects on Ride Comfort and Road Holding of Actively Suspensed Vehicles. *SAE Technical Paper 2002-01-2205.*

Abdelhady, M. B. A. & Crolla, D. A., 1989. Theoretical Analysis of Active Suspension Performance using a Four-Wheel Vehicle Model. *Journal of Automobile Engineering,* Volume 203, pp. 125-135.

Akcay, H. & Turkay, S., 2009. Influence of tire damping on mixed H-2/H-infinity synthesis of half-car active suspensions. *Journal of Sound and Vibration,* Volumen 322, pp. 15-28.

Al-Holou, N. et al., 2002. Sliding Mode Neural Network Inference Fuzzy Logic Control for Active Suspension Systems. *IEEE Transactions on Fuzzy Systems,* 10(2), pp. 234-246.

Alkhatib, R., Jazar, G. N. & Golnaraghi, M. F., 2004. Optimal Design of Passive Linear Suspension using Genetic Algorithm. *Journal of Sound and Vibration,* Volume 275, pp. 665-691.

Allen, P. J., Hameed, A. & Goyder, H., 2006. Automotive damper model for use in multi-body dynamic simulation. *Journal of Automobile Engineering,* Volume 220, pp. 1221-1233.

Allen, R. W. & Rosenthal, T. J., 1994. Requirements for Vehicle Dynamics Simulation Models. *SAE Technical Paper 940175.*

Andersen, E. R., 2007. *Multibody Dynamics Modeling and System Identification for a Quarter-Car Test Rig with McPherson Strut Suspension,* Virginia Polytechnic Institute: Master Thesis.

Antoniou, A. & Lu, W.-S., 2007. *Practical Optimization: Algorithms and Engineering Applications.* University of Victoria, Canada: Springer Science & Business Media, LLC.

Aschwanden, P., Müller, J. & Knörnschild, U., 2006. Experimental Study on the Influence of Model Motion on the Aerodynamic Performance of a Race Car. *SAE Technical Paper 2006-01-0803.*

Aschwanden, P., Müller, J., Travaglio, G. C. & Schöning, T., 2008. The Influence of Motion Aerodynamics on the Simulation of Vehicle Dynamics. *SAE Technical Paper 2008-01-0657.*

Balike, K. P., 2010. *Kineto-Dynamic Analysis Of Vehicle Suspension For Optimal Synthesis,* Concordia University: PhD thesis.

Barak, P., Panakanti, N. & Desai, T., 2004. Effect of Chassis Design Factors (CDF) on the Ride Quality using a Seven Degree of Freedom Vehicle Model. *SAE Technical Paper 2004-01-1555.*

Baumal, A., McPhee, J. & Calamai, P., 1998. Application of genetic algorithms to the design optimization of an active vehicle suspension system. *Computer Methods in Applied Mechanics and Engineering,* pp. 87-94.

Benedetti, A., Farina, M. & Gobbi, M., 2006. Evolutionary Multiobjective Industrial Design: The Case of a Racing Car Tire-Suspension System. *IEEE Transactions on Evolutionary Computation,* 10(3), pp. 230-244.

Bennett, L., 2012. *Ride and Handling Assessment of Vehicles Using Four-post Rig Testing and Simulation,* Oxford Brookes University: PhD thesis.

Benson, D., 2005. *A Gauss Pseudospectral transcription for Optimal Control,* Massachusetts Institute of Technology: PhD Thesis.

Betts, J. T., 2010. *Practical Methods for Optimal Control and Estimation using Nonlinear Programming.* 2nd edition ed. Philadelphia: SIAM.

Biegler, L. T. & Zavala, V. M., 2008. Large-Scale Nonlinear Programming Using IPOPT: An Integrating Framework for Enterprise-Wide Optimization. *Computers and Chemical Engineering,* 33(3), p. 575–582.

Blank, M. & Margolis, D., 1996. The Effect of Normal Force Variation on the Lateral Dynamics of Automobiles. *SAE Technical Paper 960484.*

Bleakney, W. M., Zielinski, L. F. & Ede, C. M., 1949. United States, Patent No. 2471857.

Boggs, C., Ahmadian, M. & Southward, S., 2008. Application of System Identification for Efficient Suspension Tuning in High-Performance Vehicles: Quarter-Car Study. *SAE International Journal of Passenger Car - Mechanical Systems,* 1(1), pp. 1298-1310.

Boggs, C., Ahmadian, M. & Southward, S., 2009. Application of System Identification for Efficient Suspension Tuning in High-Performance Vehicles: Full-Car Model Study. *SAE International Journal of Passenger Cars - Mechanical Systems,* pp. 622-635.

Bouazizi, M.-L., Ghanmi, S. & Bouhaddi, N., 2009. Multi-objective optimization in dynamics of the structures with nonlinear behaviour: Contributions of the metamodels. *Finite Elements in Analysis and Design,* 45(10), p. 612–623.

Braghin, F., Cheli, F., Melzi, S. & Sabbioni, E., 2008. Race Driver Model. *Computer and Structures,* Volume 86, pp. 1503-1516.

Bramanti, A., Di Barba, P., Farina, M. & Savini, A., 2001. Combining respense surfaces and evolutionary strategies for multiobjective pareto-optimization in electromagnetics. *International Journal of Applied Electromagnetics and Mechanics,* Volume 15, pp. 231-236.

Brayshaw, D., 2004. *The use of numerical optimisation to determine on-limit handling behaviour of race cars,* Cranfield University: PhD thesis.

Butz, T., Simeon, B. & Stadler, M., 2010. Optimal Design of Experiments for Estimating Parameters of a Vehicle Dynamics Simulation Model. *Journal of Computational and Nonlinear Dynamics,* 5(3), pp. 1011-1017.

Cambiaghi, D., Gadola, M. & D., V., 1998. Suspension System Testing and Tuning with the Use of a Four-Post Rig. *SAE Technical Paper 983023.*

Cane Creek, 2012. *Cane Creek Double Barrel Suspension.* [Online] Available at: http://www.canecreek.com/products/suspension/double-barrel [Accessed 2010].

Cappelleri, D. J., Frecker, M. I., Simpson, T. W. & Snyder, A., 2002. Design of a PZT Bimorph Actuator Using a Metamodel-Based Approach. *Journal of Mechanical Design,* Volume 129, pp. 354-357.

Captain, K., Boghani, A. & Wormley, D., 1979. Analytical Tire Models for Dynamic Vehicle Simulation. *Vehicle System Dynamics,* Volumen 8, pp. 1-32.

Casanova, D., 2000. *On minimum time vehicle manouvrering: the theoretical optimal lap,* Cranfield University: PhD thesis.

Casanova, D., Sharp, R. S. & Symonds, P., 2000. Minimum Time Manoeuvring: The Significance of Yaw Inertia. *Vehicle System Dynamics,* Volume 34, pp. 77-115.

Casanova, D., Sharp, R. S. & Symonds, P., 2001. Sensitivity to Mass Variations of the Fastest Possible Lap of a Formula One Car. *Vehicle System Dynamics,* Volume 35, pp. 119-134.

Casanova, D., Sharp, R. S. & Symonds, P., 2002. *On the Optimisation of the Longitudinal Location of the Mass Centre of a Formula One Car for two Circuits.* Hiroshima, Japan, 6th International Symposium on Advanced Vehicle Control.

Cheli, F., Dellachà, P. & Zorzutti, A., 2007. *Optimization and Potentiality Study of a Variable Kinematics Suspension.* Las Vegas, USA, Proceedings of the ASME 2007 International Design Engineering Technical Conferences & Computers and Information in Engineering Conference, pp. 1253-1260.

Chen, W., Garimella, R. & Michelena, N., 1999. *Robust Design for Improved Vehicle Handling under a Range of Maneuver Conditions.* Las Vegas, USA, Proceedings of the 1999 ASME Design Engineering Technical Conferences.

Chi, Z., He, Y. & Naterer, G. F., 2008. Design Optimization of Vehicle Suspensions with a Quarter-Vehicle Model. *Transactions of the CSME,* 32(2), pp. 297-312.

Chung, H.-S. & Alonso, J. J., 2004. *Multiobjective optimization using approximation model-based genetic algorithms.* Albany, USA, 10th AIAA/ISSMO Symposium on Multidisciplinary Analysis and Optimization.

Close, C. M. & K., F. D., 1995. *Modeling and Analysis of Dynamic Systems.* 2nd ed. New York: John Wiley and Sons, Inc.

Cooke, R., Crolla, D. A. & Abe, M., 1997. Modelling Combined Ride and Handing Manoeuvres for a Vehicle with slow-Active Suspension. *Vehicle System Dynamics,* Volume 27, pp. 457-476.

Dassault Systems Solidworks Corp., 2012. *Solidworks.* [Online] Available at: http://www.solidworks.com/

Davis, B. R. & Thompson, A. G., 2001. Power Spectral Density of Road Profiles. *Vehicle System Dynamics,* 35(6), pp. 409-415.

Deb, K., 2001. *Multi-Objective Optimization using Evolutionary Algorithms.* New York: John Wiley & Sons, Ltd.

Deb, K. & Goel, T., 2001. *A Hybrid Multi-Objective Evolutionary Approach to Engineering Shape Design.* Zurich, Switzerland, Proceedings of the First International Conference on Evolutionary Multi-Criterion Optimization, pp. 385-399.

Deb, K., Pratap, A., Agarwal, S. & Meyarivan, T., 2002. A Fast and Elitist Multiobjective Genetic Algorithm. *IEEE Transactions on Evolutionary Computation,* 6(2), pp. 182-197.

Del Castillo, J. M., Pintado, P. & Benitez, F. G., 1990. Optimization for Vehicle Suspension II: Frequency Domain. *Vehicle System Dynamics,* Volume 19, pp. 331-352.

Deshpande, S., Mehta, S. & Jazar, G. N., 2006. Optimization of Secondary Suspension of Piecewise Linear Vibration Isolation Systems. *International Journal of Mechanical Sciences,* Volume 48, pp. 341-377.

Dominy, J. A. & Dominy, R. G., 1984. Aerodynamic Influences on the Performance of the Grand Prix Racing Car. *Journal of Automobile Engineering,* 198(7), pp. 87-93.

Dominy, J. & Bullman, D. N., 1995. An Active Suspension for a Formula One Grand Prix Racing Car. *Journal of Dynamic Systems, Measurement, and Control,* 107(1), pp. 73-79.

Dominy, R. G., 1992. Aerodynamics of Grand Prix Cars. *Journal of Automobile Engineering,* Volume 206, pp. 267-274.

Els, P., Uys, P., Snyman, J. & Thoresson, M., 2006. Gradient-based approximation methods applied to the optimal design of vehicle suspension systems using computational models with severe inherent noise. *Mathematical and Computer Modelling,* Volume 43, p. 787–801.

Evangelou, S., Limebeer, D. J. N., Sharp, R. S. & Smith, M. C., 2007. Mechanical Steering Compensators for High-Performance Motorcycles. *Journal of Applied Mechanics,* Volumen 74, pp. 332-346.

Fang, H., Rais-Rohani, M., Liu, Z. & Horstemeyer, M. F., 2005. A comparative study of metamodeling methods for multiobjective crashwirthiness optimization. *Computers and Structures,* Volume 83, pp. 2121-2136.

Floyd, S. & Law, E. H., 1994. Simulation and Analysis of Suspension and Aerodynamic Interactions of Race Cars. *SAE Technical Paper 942537.*

Fonseca, C. M. & Fleming, P. J., 1995. An Overview of Evolutionary Algorithms in Multiobjective Optimization. *Evolutionary Computation,* 3(1), pp. 1-16.

Forrester, A., Sobester, A. & Keane, A., 2008. *Engineering Design Via Surrogate Modelling: A practical guide.* New York: John Wiley & Sons, Ltd.

Fricke, D. & Hogg, S., 2010. Implementation and Validation of Active Aerodynamic Force Control During Race Vehicle 7-Post Testing. *SAE International Journal of Materials and Menufacturing,* 3(1), pp. 550-558.

Fujioka, T. & Kimura, T., 1992. Numerical simulation of minimum-time cornering behaviour. *JSAE Review,* 13(1), pp. 44-51.

Genta, G. & Morello, L., 2009. *The Automotive Chassis.* Berlin: Springer.

Georgiou, G. & Natsiavas, S., 2009. Optimal Selection of Suspension Parameters in Large Scale Vehicle Models. *Vehicle System Dynamics,* 47(9), pp. 1147-1166.

Georgiou, G., Verros, G. & Natsiavas, S., 2007. Multi-Objective Optimization of Quarter-Car Models with Passive or Semi-Active Suspension System. *Vehicle System Dynamics,* 45(1), pp. 77-92.

Ghike, C. & Shim, T., 2008. *Development of Integrated Chassis Control System for Vehicle Handling Enhancement.* Ann Arbor, USA, 2008 ASME Dynamic Systems and Control Conference, pp. 1375-1382.

Gies, P. E. & Rumsey, R. D., 1962. United States, Patent No. 3018854.

Gillespie, T. D., 1992. *Fundamentals of Vehicle Dynamics.* Warrendale: SAE International.

Gill, P. E., Murray, W. & Saunders, M. A., 2002. SNOPT: An SQP Algorithm for Large-Scale Constrained Optimization. *SIAM Review,* 47(1), p. 99–131.

Gobbi, M., Levi, F. & Mastinu, G., 2006. Multi-objective stochastic optimisation of the suspension system of road vehicles. *Journal of Sound and Vibration,* Volume 298, pp. 1055-1072.

Gobbi, M., Mastinu, G. & Doniselli, C., 1999. Optimising a Car Chassis. *Vehicle System Dynamics,* Volumen 32, p. 149–170.

Goel, T. et al., 2007. Response surface approximation of Pareto optimal front in multi-objective optimization. *Computer Methods in Applied Mechanics and Engineering,* Volume 196, pp. 879-893.

Graf, M. & Kosuch, S., 2008. Simulation with a Vertical Oscillationg Race Car Model. *SAE Technical Paper 2008-01-2963.*

Hegazy, S. & Sandy, C., 2009. Vehicle Ride Comfort and Stability Performance Evaluation. *SAE Technical Paper 2009-01-2859.*

Hendrikx, J. P. M., Meijlink, T. J. J. & Kriens, R. F. C., 1996. Application of optimal control theory to inverse simulation of car handling. *Vehicle System Dynamics,* Volume 12, pp. 449-462.

Hrovat, D., 1997. Survey of Advanced Suspension Developments and Related Optimal Control Applications. *Automatica,* 33(10), pp. 1781-1817.

Huntington, G. T., 2007. *Advancement and Analysis of a Gauss Pseudospectral Transcription for Optimal Control Problems,* Massachusetts Institute of Technology: PhD thesis.

Jazar, G. N., Alkhatib, R. & Golnaraghi, M. F., 2006. Root Mean Square Optimization Criterion for Vibration Behaviour of Linear Quarter Car using Analytical Methods. *Vehicle System Dynamics,* 44(5), pp. 477-512.

Jin, R., Chen, W. & Simpson, T. W., 2000. Comparative Studies of Metamodeling Techniques under Multiple Modeling Criteria. *American Institute of Aeronautics and Astronautics.*

Jin, Y., 2005. A Comprehensive Survey of Fitness Approximation in Evolutionary Computation. *Journal of Soft Computing,* 9(1), pp. 3-12.

Johnston, M., Rieveley, R., Johrendt, J. & Minaker, B., 2010. Metrics for Evaluating the Ride Handling Compromise. *SAE Technical Paper 2010-01-1139.*

Kelly, D. P., 2008. *Lap time simulation with transient vehicle and tyre dynamics,* Cranfield University: PhD thesis.

Kelly, J., Kowalczyk, H. & Oral, H. A., 2002. Track Simulation and Vehicle Characterization with 7 Post Testing. *SAE Technical Paper 2002-01-3307.*

King, W. J., 1912. United States, Patent No. 1044188.

Kirk, D. E., 2004. *Optimal Control Theory: An Introduction.* Mineola: Dover Publications, Inc.

Konak, A., Coit, D. W. & Smith, A. E., 2006. Multi-objective optimization using genetic algorithms: A tutorial. *Genetic Algorithms and Reliability,* 91(9), pp. 992-1007.

Kowalczyk, H., 2002. Damper Tuning with the use of a Seven Post Shaker Rig. *SAE Technical Paper 2002-01-0804.*

Kropác, O. & Múcka, P., 2008. Effect of obstacles in the road profile on the dynamic response of a vehicle. *Journal of Automobile Engineering,* Volume 222, pp. 353-370.

Kuo, Y.-P., Pai, N.-S., Lin, J.-S. & Yang, C.-Y., 2008. *Passive Vehicle Suspension System Design Using Evolutionary Algorithm.* Wuhan, China, IEEE International Symposium on Knowledge Acquisition and Modeling Workshop, pp. 292 - 295.

Li, T.-H. S.-. & Kuo, Y.-P., 2000. Evolutionary Algorithms for Passive Suspension Systems. *International Journal of Mechanical Systems,Machine Elements and Manufacturing,* 43(3), pp. 537-544.

Loyer, B. & Jézéquel, L., 2009. Robust design of a passive linerar quarter car suspension system using a multi-objective evolutionary algorithm and analytical robustness indexes. *Vehicle System Dynamics,* 47(10), pp. 1253-1270.

Lu, J. & DePoyster, M., 2002. Multiobjective Optimal Suspension Control to Achieve Integrated Ride and Handling Performance. *IEEE Transactions on Control Systems Technology,* 10(6), pp. 807-821.

Lyu, N. et al., 2006. *Design of automotive torsion beam suspension using lumped-compliance linkage model.* Chicago, USA, ASME 2006 International Mechanical Engineering Congress and Exposition, pp. 219-228.

Maher, D., 2011. *Combined Time and Frequency Domain Approaches to the Operational Identification of Vehicle Suspension Systems,* Dublin City University: PhD thesis.

Man, K. F., Tang, K. S. & Kwong, S., 1996. Genetic Algorithms: Concepts and Applications. *IEEE Transactions on Industrial Electronics,* 43(5), pp. 519-534.

March, C. & Shim, T., 2007. Integrated control of suspension and front steering to enhance vehicle handling. *Journal of Automobile Engineering,* Volume 221, pp. 377-391.

Mashadi, B. & Crolla, D. A., 2005. Influence of Ride Motions on the Handling Behaviour of a Passenger Vehicle. *Journal of Automobile Engineering,* Volume 219, pp. 1047-1058.

MathWorks, 2010. *Optimisation Toolbox User's Guide.* Release 5.1 ed.

MathWorks, 2012. *MathWorks - SimMechanics.* [Online] Available at: http://www.mathworks.co.uk/products/simmechanics/

MathWorks, 2012. *MathWorks - Simulink.* [Online] Available at: http://www.mathworks.co.uk/products/simulink/

Metwalli, S. M., 1986. Optimum Nonlinear Suspension Systems. *ASME Journal of Mechanisms, Transmissions, and Automation in Design,* 48(2), pp. 197-203.

Metz, D. & Williams, D., 1989. Near Time-Optimal Control of Racing Vehicles. *Automatica,* 25(6), pp. 841-857.

Miller, A., 2002. Testing a Formula SAE Racecar on a Seven-Poster Vehicle Dynamics Simulator. *SAE Technical Paper 2002-01-3309.*

Milliken, W. F. & Milliken, D. L., 1995. *Race Car Vehicle Dynamics.* Warrendale: SAE International.

Miura, Y., Tokutake, H. & Okubo, H., 2004. Cornering Time Estimation with Transient Dynamics under Bump Disturbance. *SAE Technical Paper 2004-01-3519.*

Molina-Cristobal, A. y otros, 2007. Multi-Objective Controller Design: Evolutionary Algorithms and Bilinear Matrix Inequalities for a Passive Suspension. *International Journal of Tmography and Stadistics,* 7(F07), pp. 31-36.

MscSoftware, 2012. *Msc Software - Adams.* [Online] Available at: http://www.mscsoftware.com/uk/Products/CAE-Tools/Adams.aspx

MÜhlmeier, M. & Müller, N., 2002. Optimization of the Driving Line on a Race Track. *SAE Technical Paper 2002-01-3339.*

Multimatic Technical Centre, E., 2011. *Multimatic Four Post Technical Specification and Operating Manual,* Thetford: Multimatic Technical Centre Europe.

Nocedal, J. & Wright, S. J., 2006. *Numerical Optimization.* 2 ed. Berlin: Springer Verlag.

Orlando, S., Peeters, B. & Coppotelli, G., 2008. *Improved FRF estimators for MIMO Sine Sweep data.* Leuven, Belgium, Proceedings of ISMA 08 International Conference of Noise and Vibration.

Pacjeka, H. B., 2006. *Tire and Vehicle Dynamics.* 2 ed. Oxford: BUTTERWORTH HEINEMANN.

Papageorgiou, C., Lockwood, O. G., Houghton, N. E. & Smith, M. C., 2007. *Experimental testing and modelling of a passive mechanical steering compensator for high-performance motorcycles.* Kos, Greece, s.n., pp. 3592-3599.

Papageorgiou, C. & Smith, M., 2006. Positive Real Synthesis Using Matrix Inequalities for Mechanical Networks: Application to Vehicle Suspension. *IEEE Transactions on Control Systems Technology,* 14(3), pp. 423-435.

Papageorgiou, C. & Smith, M. C., 2005. *Laboratory experimental testing of inerters.* Seville, Spain, Proceedings of the 44th IEEE Conference on Decision and Control.

Prokop, G., 2001. Modeling Human Vehicle Driving by Model Predictive Online Optimization. *Vehicle System Dynamics,* 35(1), pp. 19-53.

Purdy, D. J. & Bullman, D. N., 1997. An experimental and theoretical investigation into the design of an active suspension system for a racing car. *Journal of Automobile Engineering,* 211(3), pp. 161-173.

Queipo, N. V. et al., 2005. Surrogate based analysis and optimization. *Journal of Progress in Aerospace Sciences,* Volume 41, pp. 1-28.

Rakheja, S. & Ahmed, A. K. W., 1991. simulation of Nonlinear Variable Dampers using Energy Similary. *Engineering Computations,* Volume 8, pp. 333-344.

Sbalzarini, I. F., Müller, S. & Koumoutsakos, P., 2000. *Multiobjective optimization using Evolutionary Algorithms.* Stanford, USA, s.n., pp. 63-74.

Scheibe, F. & Smith, M. C., 2009. Analytical solutions for optimal ride comfort and tyre grip for passive vehicle suspensions. *Vehicle System Dynamics,* 47(10), pp. 1229-1252.

Schmitt, K., Madsen, J., Anitescu, M. & Negrut, D., 2008. *A Gaussian Process Based Approach for Handling uncertainity in Vehicle Dynamics Simulation.* Boston, USA, ASME 2008 International Mechanical Engineering Congress and Exposition, pp. 617-628.

Seqveland, I. E., 1933. United States, Patent No. 1933768.

Shannan, J. E. & Vanderploeg, M. J., 1989. A Vehicle Handling Model with Active Suspensions. *Journal of Mechanisms, Transmissions and Automation in Design,* Volume 111, pp. 375-380.

Sharp, R. S., Hassan & A., S., 1987. The Relative Performance Capabilities of Passive, Active and Semi-Active Car Suspension Systems. *Journal of Automobile Engineering,* 200(3), pp. 219-228.

Shihani, N., Kumbhar, B. K. & Kulshreshtha, M., 2006. Modeling of Extrusion Process using Response Surface Methodology and Artificial Neural Networks. *Journal of Engineering Science and Technology,* 1(1), pp. 31-40.

Shim, T. & Ghike, C., 2007. Understanding the limitations of different vehicle models for roll dynamics studies. *Vehicle System Dynamics,* 45(3), pp. 191-216.

Shim, T. & Margolis, D., 2005. Dynamic Normal Force Control for Vehicle Stability Enhancement. *International Journal of Vehicle Autonomous Systems,* 3(1), pp. 1-14.

Shirahatt, A., Prasad, P., Panzade, P. & Kulkarni, M., 2008. Optimal design of passenger car suspension for ride and road holding. *Journal of the Brazilian Society of Mechanical Sciences and Engineering,* 30(1), pp. 66-76.

Siegler, B., Deakin, A. & Crolla, D. A., 2000. Lap Time Simulation: Comparison of Steady State, Quasi- Static and Transient Racing Car Cornering Strategies. *SAE Technical Paper 2000-01-3563.*

Simpson, T. W., 1998. Comparison of Response Surface and Kriging Models in the Multidisciplinary Design of an Aerospike Nozzle. *Institute for Computer Applications in Science and Engineering (ICASE) Report 98-16.*

Simpson, T. W., Korte, J. J., Mauery, T. M. & Mistree, F., 2001. Kriging Models for Global Approximation in Simulation-Based Multidisciplinary Design Optimization. *American Institute of Aeronautics and Astronautics,* 39(12), pp. 2233-2241.

Simpson, T. W., Peplinski, J., Koch, P. N. & Allen, J. K., 2001. Metamodels for computer-based engineering design: survey and recommendations. *Engineering with Computers,* Volume 17, pp. 129-150.

Smith, M. C., 2002. Synthesis of Mechanical Networks: The Inerter. *IEEE Transactions on Automatic Control,* 46(10), pp. 1648-1662.

Smith, M. C., 2003. *The Inerter Concept and Its Application.* Fukui, Japan, Society of Instrument and Control Engineers (SICE) Annual Conference.

Smith, M. C., 2006. *Passive Network Synthesis Revisited.* Kyoto, Japan, 17th International Symposium on Mathematical Theory of Networks and Systems.

Smith, M. C. & Wang, F.-C., 2004. Performance Benefits in Passive Vehicle Suspension employing Inerters. *Vehicle System Dynamics,* pp. 235-257.

Soliman, A. M. A., Abd Allah, S. A., El-Beter, A. A. & Hamid, M. S., 2001. Effect of Suspension Spring Stiffness on Vehicle Dynamics. *International Journal of Vehicle Design,* 8(3/4), pp. 316-334.

Soliman, A. M. A., Moustafa, S. M. & Shogae, A. O. M., 2008. Parameters Affecting Vehicle Ride Comfort using Half Vehicle Model. *SAE Technical Paper 2008-01-1146.*

Southward, S. C. & Boggs, M. B., 2008. Comparison of the Performance of 7-Post and 8-Post Dynamic Shaker Rigs for Vehicle Dynamics Studies. *SAE Technical Paper 2008-01-2966.*

Stamatov, S., Krishnan, M. & Yost, S. A., 2007. Using Quasi-linearization for Real Time Dynamic Simulation of a Quarter Vehicle Suspension. *SAE Technical Paper 2007-01-0833.*

Stone, M. R. & Demetriou, M. A., 2000. *Modeling and Simulation of Vehicle Ride and Handling Performance.* Rio, Greece, Proceedings of the 15th lEEE lntemational Symposium on Intelligent Control, pp. 85-89.

Storey, I., Bourmistrova, A. & Subic, A., 2006. *Multiobjective Optimisation of Control of Active and Semi-Active Suspension Systems using Jerk as a measure of Comfort.* Yokohama, Japan, Fisita 2006.

Sun, P.-Y. & Chen, H., 2003. *Multiobjective output-feedback suspension control on a half-car model.* Istanbul, Turkey, Proceedings of 2003 IEEE Conference on Control Applications, pp. 290-295.

Sun, T., Zhang, Y. & Barak, P., 2002. 4-DOF Vehicle Ride Model. *SAE Technical Paper 2002-01-1580.*

Sun, W. et al., 2010. Ride-comfort-oriented suspension optimization using the pseudo-excitation method. *Journal of Automobile Engineering,* Volume 224, pp. 1357-1367.

Tauscher, H., 1928. United States, Patent No. 1654763.

THK Co., Ltd., 2012. *THK - Precision Ball Screw Product Descriptions.* [Online] Available at: https://tech.thk.com/en/products/thk_cat_main.php?id=359 [Accessed 2010].

THK Co., Ltd., 2012. *THK Global.* [Online] Available at: http://www.thk.com/

Thompson, A. G., 1973. Quadratic Performance Indices and Optimum Suspension Design. *Proceedings of the Institution of Mechanical Engineers,* 187(1), pp. 129-139.

Thompson, A. G., 1983. Suspension Design for Optimum Road-Holding. *SAE Technical Paper 830663.*

Thoresson, M., Uys, P., Els, P. & Snyman, J., 2009. Efficient optimisation of a vehicle suspension system, using a gradient-based approximation method, Part 1: Mathematical modelling. *Mathematical and Computer Modelling,* Volume 50, pp. 1421-1436.

Thoresson, M., Uys, P., Els, P. & Snyman, J., 2009. Efficient optimisation of a vehicle suspension system, using a gradient-based approximation method, Part 2: Optimisation results. *Mathematical and Computer Modelling,* Volume 50, pp. 1437-1447.

Timings, J. & Cole, D., 2011. *Efficient minimum manoeuvre time optimisation of an oversteering vehicle at constant forward speed.* San Francisco, USA, American Control Conference (ACC), pp. 5267 - 5272.

Timings, J. P. & Cole, D. J., 2010. *Minimum manoeuvre time of a nonlinear vehicle at constant forward speed using convex optimisation.* Loughborough, UK, Proceedings of the 10th International Symposium on Advanced Vehicle Control.

Todd, K. B. & Kulakowski, B. T., 1990. *Handling Performance of Road Vehicles with different Active Suspensions.* Dallas, USA, Winter Annual Meeting of the American Society of Mechanical Engineers, pp. 19-26.

Ullman, D. G., 1997. *The Mechanical Design Process.* New York: McGraw-Hill.

Vaidyanathan, R., Tucker, P. K., Papila, N. & Shyy, W., 2004. Computational-fluid-dynamics-based design optimization for single-element rocket injector. *Journal of Prpulsion and Power,* 20(4), pp. 705-717.

Velenis, E. & Tsiotras, P., 2005. *Minimum Time vs. Maximum Exit Velocity Path Optimization During Cornering.* Dubrovnik, Croatia, Proceedings of the IEEE International Symposium on Industrial Electronics, pp. 355 - 360.

Velenis, E. & Tsiotras, P., 2005. *Optimal velocity profile generation for given acceleration limits: receding horizon implementation.* Atlanta, USA, Proceedings of the 2005 American Control Conference, pp. 2147 - 2152.

Velenis, E. & Tsiotras, P., 2005. *Optimal velocity profile generation for given acceleration limits: theoretical analysis.* Atlanta, USA, Proceedings of the 2005 American Control Conference, pp. 1478 - 1483.

Venkatamaran, P., 2002. *Applied Optimization with MATLAB programming.* New York: John Wiley & Sons, Inc.

Verros, G., Natsiavas, S. & Papadimitriou, C., 2005. Design Optimization of Quarter-car Models with Passive and Semi-active Suspensions under Random Road Excitation. *Journal of Vibration and Control,* Volumen 11, p. 581–606.

Wang, F.-. C., Chen, C.-. W., Liao, M.-. K. & Hong, M.-. F., 2007. *Performance Analyses of Building Suspension Control with Inerters.* New Orleand, USA, Proceedings of the 46th IEEE Conference on Decision and Control, pp. 3786-3791.

Wang, F.-C. & Chan, H.-A., 2008. *Mechatronic Suspension Design and Its Applications to Vehicle Suspension Control.* Cancun, Mexico, Proceedings of the 47th IEEE Conference on Decision and Control, pp. 3769-3774.

Wang, F.-. C., Hong, M.-. F. & Chen, C.-. W., 2010. Building suspensions with inerters. *Journal of Mechanical Engineering Science,* 224(8), pp. 1605-1616.

Wang, F.-. C. & Su, W.-J., 2008. *Inerter Nonlinearities and the Impact on Suspension Control.* Seattle, USA, American Control Conference, pp. 3245-3250.

Wang, F.-C., Hong, M.-F. & Lin, T.-C., 2011. Designing and testing a hydraulic inerter. *Journal of Mechanical Engineering Science,* 225(1), pp. 66-72.

Wang, F.-C., Hsu, M.-S., Su, W.-J. & Lin, T.-C., 2009. s.l. Patent No. US 2009/0108510.

Wang, F.-C., Yu, C.-H., Chang, M.-L. & Hsu, M., 2006. *The performance Improvements of Train Suspension Systems with Inerters.* San Diego, USA, Proceedings of the 45th IEEE Conference on Decision and Control, pp. 1472-1477.

Wang, G. G. & Shan, S., 2007. Review of Metamodelling Techniques in Support of Engineering Design Optimisation. *Journal of Mechanical design,* 129(4), pp. 370-380.

Wang, J., Wilson, D. A., Xu, W. & Crolla, D. A., 2006. Integrated Vehicle Ride and Steady-State Handling Control via Active Suspensions. *International Journal of Vehicle Design,* 42(3/4), pp. 306-326.

Watres, L. S., 1908. United States, Patent No. 893680.

Weise, T., 2011. *Global Optimization Algorithms: Theory and Application.* 3 ed. E-book: http://www.it-weise.de/.

Wentao, X., Tongchen, M. & Zheng, L., 2011. An Efficient Multi-objective Optimization Method for Complicated Vehicle Random Vibration. *Applied Mechanics and Materials,* Volume 94-96, pp. 1694-1700.

Whitehead, R., Travis, W., Bevly, D. M. & Flowers, G., 2004. A Study of the Effect of Various Vehicle Properties on Rollover Propensity. *SAE Technical Paper 2004-01-2094.*

Williams, D. E. & Haddad, W. M., 1997. Active Suspension Control to improve Vehicle Ride and Handling. *Vehicle System Dynamics,* Volumen 28, pp. 1-24.

Williams, R. A., 1997. Automotive Active Suspensions. Part 1: Basic Principles. *Journal of Automobile Engineering,* Volumen 211, pp. 415-426.

Wilson, B., Cappelleri, D., Simpson, T. W. & Frecker, M., 2001. Efficient Pareto Frontier Exploration using Surrogate Approximations. *Optimization and Engineering,* Volume 2, p. 31–50.

Wright, P. G., 1982. The Influence of Aerodynamics on the Design of Formula One Racing Cars. *International Journal of Vehicle Design,* 3(4), pp. 383-397.

Yang, R. S. & Huang, X. D., 2009. *Multi-Objective Optimization of Vehicle Handling and Ride Comfort by Approximation Model.* Manchester, UK, Proceedings of 2nd International Conference on Modelling and Simulation, pp. 242-246.

Yildirim, S. & Eski, I., 2009. Vibration Analysis of an Experimental Suspension System using Artificial Neural Networks. *SAE Technical Paper 2009-01-0734.*

Ziegenmeyer, J. D., 2007. *Estimation of Disturbance Inputs to a Tire Coupled Quarter-car Suspension Test Rig,* Virginia Polytechnic Institute: Master thesis.

Zitzler, E., Thiele, L. & Deb, K., 2000. Comparison of Multiobjective Evolutionary Algorithms: Empirical Results. *Evolutionary Computation,* Volume 8, pp. 173-195.

Appendix A: OBU Four-post rig Calibration Certificate

Appendix B: Derivation of Vehicle Equations of Motion

Appendix B derives the equations of motion of the vehicle model used in Chapter 6 for its use into lap-time simulation. Figure B- 1 and Figure B- 2 show a schematic diagram of the vehicle model in plan and lateral views.

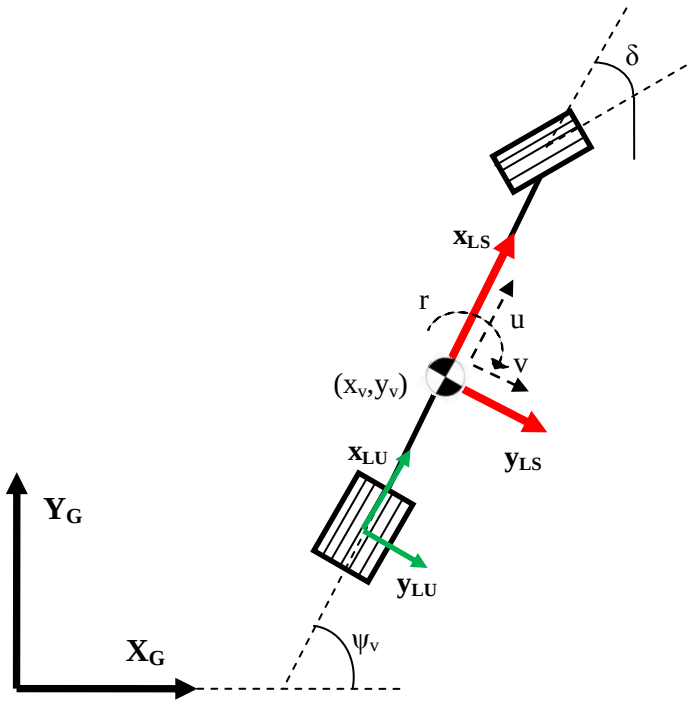

Figure B- 1: Schematic plan view of vehicle model for lap-time simulation

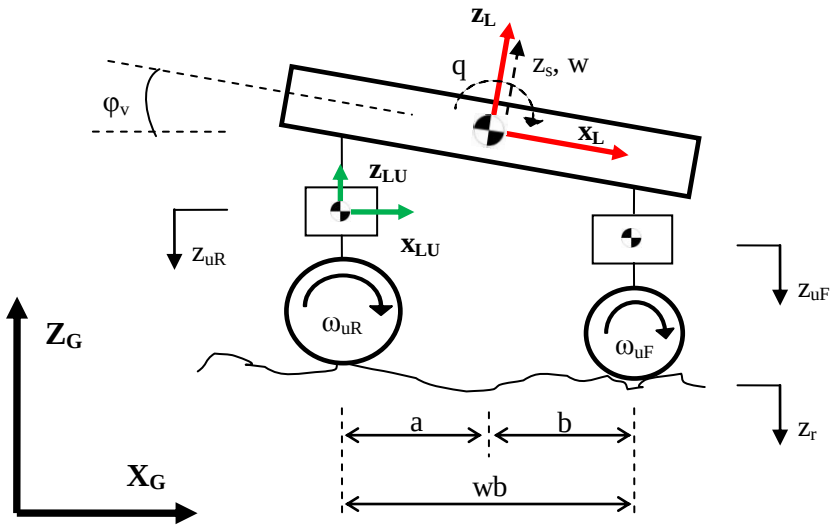

Figure B- 2: Schematic lateral view of vehicle model for lap-time simulation

Definition of DOFs of the vehicle model and reference frame

First, considering the vehicle model shown in Figure B- 1 and Figure B- 2, three reference frames have been defined: firstly, a global inertial frame $X_GY_GZ_G$ (black coloured reference frame), a non-inertial sprung mass fixed reference frame $x_Sy_Sz_S$ (red coloured reference frame) and a local frame moving with the CoG of the unsprung mass of the vehicle $x_Uy_Uz_U$ (green coloured reference frame).

As introduced in Chapter 6, a lumped parameter single-track vehicle model has been used in this thesis to evaluate the impact of ride dynamics on the performance of the race car. The model consists of three bodies: one solid-rigid body that represents sprung mass m_s and two more bodies that represent front and rear wheels m_{uf} and m_{ur} respectively. This model presents 9 DOFs. The model allows translational motion of the vehicle in all three dimensions in space (longitudinal, lateral and vertical motions) and rotations around two axes (yaw and pitch motion). Front and rear unsprung wheels are connected to the main body via a suspension system. Unsprung masses are assumed to have motion only in vertical direction. Moreover, wheels are allowed to rotate only about the spin axis. According to this, the vector of generalised displacement (linear and angular) coordinates $\boldsymbol{q}$ that includes these motions can be defined as:

$$\boldsymbol{q} = [x_v \;\; y_v \;\; z_s \;\; \varphi_v \;\; \Psi_v \;\; z_{uF} \;\; z_{uR} \;\; \theta_{uF} \;\; \theta_{uR}]^T \qquad (B.1)$$

Moreover, for vehicle modelling is more appropriate to express these motions in terms of velocities rather than displacements. Therefore, a vector of velocities $\boldsymbol{w}$ related to generalised displacements q can be defined as:

$$\boldsymbol{w} = [u \;\; v \;\; w \;\; q \;\; r \;\; v_{zuF} \;\; v_{zuR} \;\; \omega_{uF} \;\; \omega_{uR}]^T \qquad (B.2)$$

Where $v_{zuj} = \dot{z}_{uj}$ for j=*F,R*

Note that, the velocities expressed in vector $\boldsymbol{w}$ are related to non-inertial reference frames. In order to express these variables with respect to an inertial reference frame, rotation matrices between references frames must be defined. According to this, the sprung mass reference frame $x_Sy_Sz_S$ moves and rotates with the CoG of the sprung mass. Since the vehicle model presents rotations in two axis (yaw and pitch motions), two rotation matrices R_1 (yaw rotation) and R_2 (pitch rotation) can be defined:

$$R_1 = \begin{bmatrix} \cos(\Psi_v) & -\sin(\Psi_v) & 0 \\ \sin(\Psi_v) & \cos(\Psi_v) & 0 \\ 0 & 0 & 1 \end{bmatrix} \quad (B.3)$$

$$R_2 = \begin{bmatrix} \cos(\varphi_v) & 0 & \sin(\varphi_v) \\ 0 & 1 & 0 \\ -\sin(\varphi_v) & 0 & \cos(\varphi_v) \end{bmatrix} \quad (B.4)$$

These two rotations can be then combined so that translational motions in a local reference frame can be expressed in a global inertial reference frame. A general transformation matrix for translational motion R_{trans} can be obtained by multiplying matrices (B.3) and (B.4):

$$R_{trans} = R_1 R_2 = \begin{bmatrix} \cos(\Psi_v)\cos(\varphi_v) & -\sin(\Psi_v) & \cos(\Psi_v)\sin(\varphi_v) \\ \sin(\Psi_v)\cos(\varphi_v) & \cos(\Psi_v) & \sin(\Psi_v)\sin(\varphi_v) \\ -\sin(\varphi_v) & 0 & \cos(\varphi_v) \end{bmatrix} \quad (B.5)$$

In addition to this, a rotation matrix for rotational motions R_{rot} can be also defined as:

$$R_{rot} = \begin{bmatrix} 1 & 0 \\ 0 & \cos(\varphi_v) \end{bmatrix} \quad (B.6)$$

Since, the unsprung mass reference frame $x_U y_U z_U$ does not rotate with respect to respect to the global inertial reference frame $X_G Y_G Z_G$, the transformation matrix for unsprung mass motions R_u can be expressed as an identity matrix:

$$R_u = I_{4x4} \quad (B.7)$$

Transformation of Lagrange Energy Method for quasi-velocities

The general Lagrange Energy Method must be re-arranged into a Lagrange Energy Method for quasi-velocities when velocities related to non-inertial reference frames are used as generalised coordinates (Genta & Morello, 2009). Therefore, the modified expression for the Lagrange method can be defined as follows:

$$\frac{d}{dt}\left(\frac{\partial L}{\partial w}\right) + B^T \Gamma \left(\frac{\partial L}{\partial w}\right) - B^T \left(\frac{\partial L}{\partial q}\right) + \frac{\partial D}{\partial w} = B^T \mathrm{Q} \quad (B.8)$$

Where $L = T - U$ represents the Lagrangian of the system

T represents the total kinetic energy of the system

U represents the total potential energy of the system

D represents the total energy dissipation term

$w = [w_i]^T$ represents the vector of *n* quasi-velocities w_i expressed with respect to a moving frame reference frame

$q = [q_i]^T$ represents the vector of *n* generalised coordinates q_i expressed with respect to a global frame reference frame

$Q = [Q_i]^T$ represents the vector of generalised forces Q_i

B represents the rotation matrix from quasi-velocities w_i to generalised velocities $\dot{q}_i$ so that $[\dot{q}_i] = B[w_i]$

$\Gamma = \dot{A} - \left[w^T B^T \frac{\partial A}{\partial q_k}\right]$ represents the gamma operator with $A = B^{-T}$

$for\ i = [1,..,n]$

In this thesis, all forces generated from engine/brake, suspension, aerodynamic and tyre systems have been considered as external generalised forces Q_i.

The total kinetic energy of the system *T* can be obtained as follows:

$$T = T_s + \sum T_{ui} \qquad (B.9)$$

Where $T_s = T_{strans} + T_{srot}$: Total kinetic energy carried by the sprung mass

$T_{strans} = \frac{1}{2} m_s \boldsymbol{V^T V}$: Kinetic energy due to translational motion of the sprung mass

$T_{srot} = \frac{1}{2} \boldsymbol{\Omega^T I_s \Omega}$: Kinetic energy due to rotational motion of the sprung mass

$\boldsymbol{V} = [u \quad v \quad w]^T$: Translational velocity vector of the sprung mass

$\boldsymbol{\Omega} = [0 \quad q \quad r]^T$: Rotational velocity vector of the sprung mass

$\boldsymbol{I_s} = \begin{bmatrix} I_{xx} & 0 & 0 \\ 0 & I_{yy} & 0 \\ 0 & 0 & I_{zz} \end{bmatrix}$: Inertia tensor of sprung mass

$T_{uj} = T_{utransj} + T_{urotj}$: Total kinetic energy carried by the unsprung mass *j*

$T_{utransj} = \frac{1}{2} m_{uj} \boldsymbol{V_{uj}}^{\boldsymbol{T}} \boldsymbol{V_{uj}}$: Kinetic energy due to translational motion of the unsprung mass *j*

$T_{uroti} = \frac{1}{2}\boldsymbol{\Omega_{uj}}^{\boldsymbol{T}}\boldsymbol{J_{uj}}\boldsymbol{\Omega_{uj}}$: Kinetic energy due to rotational motion of the unsprung mass

$\boldsymbol{V_{uF}} = [u \quad v + ar \quad v_{zuF}]^T$: Translational velocity vector of the front sprung mass

$\boldsymbol{V_{uR}} = [u \quad v - br \quad v_{zuR}]^T$: Translational velocity vector of the rear sprung mass

$\boldsymbol{\Omega_{uj}} = \begin{bmatrix} 0 & 0 & \omega_{uj} \end{bmatrix}^T$: Rotational velocity vector of the unsprung mass *j*

$\boldsymbol{J_{uj}} = \begin{bmatrix} J_{ux} & 0 & 0 \\ 0 & J_{uy} & 0 \\ 0 & 0 & J_{\omega j} \end{bmatrix}$: Inertia tensor of unsprung mass *j*

For *j=F, R*

Accordingly, the total potential energy of the system *U* can be calculated as:

$$U = U_s + \sum U_{uj} \qquad (B.10)$$

Where $U_s = mgz_s$: Potential energy of the sprung mass

$U_{uj} = m_{uj}gz_{uj}$: Potential energy of the unsprung mass *j*

Moreover, the rotation matrix A can be composed of rotation matrices (B.5) to (B.7) as follows:

$$A^T = \begin{bmatrix} {R_{trans}}^T & 0_{3x2} & 0_{3x4} \\ 0_{2x3} & R_{rot} & 0_{2x4} \\ 0_{4x3} & 0_{4x2} & I_{4x4} \end{bmatrix} \qquad (B.11)$$

In this thesis, *D=0* because all forces generated from suspension and tyre systems have been considered as external generalised forces Q_i.

Derivation of EOMs

Assuming small angle approximation, the EOMs describing the dynamic behaviour of the vehicle can be derived from the Lagrange Method for quasi-velocities (see equation (B.9)):

$$[Q_{local}] = \begin{bmatrix} M_t \cdot \dot{u} - M_t \cdot r \cdot v + m_s \cdot q \cdot w + (m_{uR} \cdot b - m_{uF} \cdot a) \cdot r^2 \\ M_t \cdot \dot{v} - M_t \cdot r \cdot u + (m_{uF} \cdot a - m_{uR} \cdot b) \cdot \dot{r} \\ m_s \cdot g + m_s \cdot \dot{w} - M_t \cdot q \cdot u \\ I_{yy} \cdot \dot{q} + (m_{uF} + m_{uR}) \cdot u \cdot w \\ (I_{zzT} + m_{uF} \cdot a^2 + m_{uR} \cdot b^2) \cdot \dot{r} + (m_{uF} \cdot a - m_{uR} \cdot b) \cdot (\dot{v} + r \cdot u) \\ m_{uF} \cdot g + m_{uF} \cdot \ddot{z}_{uF} \\ m_{uR} \cdot g + m_{uR} \cdot \ddot{z}_{uR} \\ J_{\omega F} \cdot \dot{\omega}_{uF} \\ J_{\omega R} \cdot \dot{\omega}_{uR} \end{bmatrix} \quad (B.12)$$

Moreover, the generalised forces ***Q*** can be obtained as follows:

$$[Q_{local}] = \begin{bmatrix} \Sigma F_x \\ \Sigma F_y \\ \Sigma F_z \\ \Sigma M_y \\ \Sigma M_z \\ \Sigma F_{zuF} \\ \Sigma F_{zuR} \\ \Sigma M_{\omega uF} \\ \Sigma M_{\omega uR} \end{bmatrix} = \begin{bmatrix} F_{xF} + F_{xR} - F_{Drag} \\ F_{yF} + F_{yR} \\ F_{SuspF} + F_{SuspR} - F_{LiftT} \\ F_{SuspF} \cdot a - F_{SuspR} \cdot b - F_{LiftF} \cdot a + F_{LiftF} \cdot b \\ F_{yF} \cdot a - F_{yR} \cdot b \\ F_{TyreF} - F_{SuspF} \\ F_{TyreR} - F_{SuspR} \\ T_{\omega F} - F_{xF} \cdot R_{\omega F} \\ T_{\omega R} - F_{xR} \cdot R_{\omega R} \end{bmatrix} \quad (B.13)$$

State-Space Model Representation

Recalling the definition of a dynamic system in state-space representation:

$$\dot{\boldsymbol{x}} = f(\boldsymbol{x}(t), \boldsymbol{u}(t), t) \qquad x(t=0) = x_0$$

Where ***x(t)*** represents the vector of states of the system

u(t) represents the vector of inputs

t represents the independent variable time

According to this, the vector of states ***x(t)*** can be defined as a combination of vectors ***w*** and ***q***:

$$\boldsymbol{x}(t) = [\Psi_v \ r \ u \ v \ x_v \ y_v \ \varphi_v \ p \ z_s \ \dot{z}_s \ \omega_F \ \omega_R \ z_{uF} \ \dot{z}_{uF} \ z_{uR} \ \dot{z}_{uR}]^T \quad (B.14)$$

Equations (B.12) and (B.13) can then be combined and re-arranged to produce the final state-space representation:

$$\begin{bmatrix} \dot{\Psi}_v \\ \dot{r} \\ \dot{u} \\ \dot{v} \\ \dot{x}_v \\ \dot{y}_v \\ \dot{\varphi}_v \\ \dot{q} \\ \dot{z}_s \\ \dot{w} \\ \dot{\omega}_{uF} \\ \dot{\omega}_{uR} \\ \dot{z}_{uF} \\ \ddot{z}_{uF} \\ \dot{z}_{uR} \\ \ddot{z}_{uR} \end{bmatrix} = \begin{bmatrix} r \\ \frac{1}{(I_{zzT} + m_{uF} \cdot a^2 + m_{uR} \cdot b^2)} \cdot \{\Sigma M_z - (m_{uF} \cdot a - m_{uR} \cdot b) \cdot (\dot{v} + r \cdot u)\} \\ \frac{1}{M_T} \cdot \{\Sigma F_x + M_t \cdot r \cdot v - m_s \cdot q \cdot w - (m_{uR} \cdot b - m_{uF} \cdot a) \cdot r^2\} \\ \frac{1}{M_T} \cdot \{\Sigma F_y + M_t \cdot r \cdot u - (m_{uF} \cdot a - m_{uR} \cdot b) \cdot \dot{r}\} \\ u \cdot cos(\Psi_v) + v \cdot sin(\Psi_v) \\ u \cdot sin(\Psi_v) - v \cdot cos(\Psi_v) \\ q \\ \frac{1}{I_{yy}} \cdot \{\Sigma M_y - (m_{uF} + m_{uR}) \cdot u \cdot w\} \\ w \\ \frac{1}{m_s} \cdot \{\Sigma F_z - m_s \cdot g + M_t \cdot q \cdot u\} \\ \frac{1}{J_{\omega F}} \cdot \Sigma M_{\omega uF} \\ \frac{1}{J_{\omega R}} \cdot \Sigma M_{\omega uR} \\ v_{zuF} \\ \frac{1}{m_{uF}} \cdot \{\Sigma F_{zuF} - g\} \\ v_{zuR} \\ \frac{1}{m_{uR}} \cdot \{\Sigma F_{zuR} - g\} \end{bmatrix} \quad (B.15)$$